.....contributing to man's understanding of the environment world

PRELIMINARY EVALUATION OF THE ALASKAN LONG-PERIOD ARRAY

D. M. CLARK
R. P. MASSE'
J. E. DUNAVANT
SEISMIC DATA LABORATORY

19 JANUARY 1972

Prepared for
AIR FORCE TECHNICAL APPLICATIONS CENTER
Washington, D.C.

Under
Project VELA UNIFORM

Sponsored by
ADVANCED RESEARCH PROJECTS AGENCY
Nuclear Monitoring Research Office
ARPA Order No. 1714

TELEDYNE GEOTECH
ALEXANDRIA LABORATORIES

158

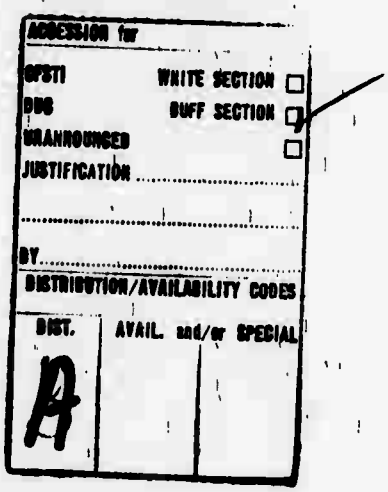

Unclassified

Security Classification

DOCUMENT CONTROL DATA - R&D

(Security classification of title, body of abstract and indexing annotation must be entered when the overall report is classified)

1. ORIGINATING ACTIVITY (Corporate author)	2a. REPORT SECURITY CLASSIFICATION
TELEDYNE GEOTECH ALEXANDRIA, VIRGINIA	Unclassified
	2b. GROUP

3. REPORT TITLE

PRELIMINARY EVALUATION OF THE ALASKAN LONG-PERIOD ARRAY

4. DESCRIPTIVE NOTES (Type of report and inclusive dates)

Scientific

5. AUTHOR(S) (Last name, first name, initial)

Clark, D.M.; Massé, R.P.; Dunavant, J.E.

6. REPORT DATE	7a. TOTAL NO. OF PAGES	7b. NO OF REFS
19 January 1972	156	10

8a. CONTRACT OR GRANT NO.	9a. ORIGINATOR'S REPORT NUMBER(S)
F33657-72-C-0009 b. PROJECT NO. VELA T/2706 ARPA Order No. 1714 ARPA Program Code No. 2F-10	281 9b. OTHER REPORT NO(S) (Any other numbers that may be assigned this report)

10. AVAILABILITY/LIMITATION NOTICES

APPROVED FOR PUBLIC RELEASE; DISTRIBUTION UNLIMITED.

11. SUPPLEMENTARY NOTES	12. SPONSORING MILITARY ACTIVITY
	Advanced Research Projects Agency Nuclear Monitoring Research Office Washington, D.C.

13. ABSTRACT

The object of this study was to determine the characteristics of signals and noise as recorded at the Alaska Long Period Array (ALPA), and to evaluate the performance of signal processing techniques using data from this array. Only a partial array of five to eight sites was available for analysis. The following results were obtained:

1. Beams were calculated using an average of seven sites, and the noise reduction was found to approach $N^{1/2}$. The signal-to-noise ratio improvement was only slightly less.
2. Spectra of the signals indicated the peak power (uncorrected for system response) to be about .05 Hz.
3. Noise spectra were calculated for two successive days at FB2AK (ALPA site 33) and on another day for all available sites at ALPA. Spectral peaks occurred at frequencies of .01, .07 and .14 Hz.
4. Match filtering was performed on several events. The results are inconclusive due to the small number of events processed.
5. Based on the average noise RMS, and using a seven element array, it is estimated that surface waves from earthquakes of $m_b = 4.6 \pm .2$ depending upon the distance, can be detected.
6. M_S/m_b points for nine earthquakes fall on the Gutenberg and Richter curve of $M_S = 1.59\ m_b - 3.9$ and form a cluster distinct from the positions of the LONG SHOT and MILROW M_S/m_b points.

14. KEY WORDS

Long-Period Array
Signal to Noise Improvement
Surface Wave Spectra

Unclassified

Security Classification

I

PRELIMINARY EVALUATION OF THE ALASKAN LONG-PERIOD ARRAY

SEISMIC DATA LABORATORY REPORT No. 281

AFTAC Project No.:	VELA T/2706
Project Title:	Seismic Data Laboratory
ARPA Order No.:	1714
ARPA Program Code No.:	2F-10
Name of Contractor:	TELEDYNE GEOTECH
Contract No.:	F33657-72-C-0009
Date of Contract:	01 July 1971
Amount of Contract:	$ 1,314,000
Contract Expiration Date:	30 June 1972
Project Manager:	Royal A. Hartenberger (703) 836-7647

P. O. Box 334, Alexandria, Virginia

II

ABSTRACT

The object of this study was to determine the characteristics of signals and noise as recorded at the Alaska Long Period Array (ALPA), and to evaluate the performance of signal processing techniques using data from this array. Only a partial array of five to eight sites was available for analysis. The following results were obtained:

1. Beams were calculated using an average of seven sites, and the noise reduction was found to approach $N^{1/2}$. The signal-to-noise ratio improvement was only slightly less.

2. Spectra of the signals indicated the peak power (uncorrected for system response) to be at about .05 Hz.

3. Noise spectra were calculated for two successive days at FB2AK (ALPA site 33) and on another day for all available sites at ALPA. Spectral peaks occurred at frequencies of .01, .07 and about .14 Hz.

4. Match filtering was performed on several events. The results are inconclusive due to the small number of events processed.

5. Based on the average noise RMS, and using a seven element array, it is estimated that surface waves from earthquakes of $m_b = 4.6 \pm .2$ depending upon the distance, can be detected.

6. M_s/m_b points for nine earthquakes fall on the Gutenberg and Richter curve of $M_s = 1.59\ m_b - 3.97$ and form a cluster distinct from the positions of the LONG SHOT and MILROW M_s/m_b points.

TABLE OF CONTENTS

LIST OF FIGURES

LIST OF FIGURES (Cont'd.)

LIST OF TABLES

INTRODUCTION

The purpose of this study is to determine the basic capabilities of the Alaska Long Period Array (ALPA). Included in the study are the determination of the characteristics of seismic noise and signals recorded at ALPA, the evaluation of beamforming and matched filtering processing, the estimation of detection levels, and the investigation of discrimination techniques applied to ALPA data.

The geology of the array is very complex. Reference is made to Teledyne Geotech Report No. 70-39 which includes a comprehensive geologic report of the surface and subsurface.

The ALPA array consists of 19 three-component long-period sensors. For the time period from which data was selected for this preliminary study, no more than nine sensors were providing usable data, and these sensors were , in general, located in the southern half of the array. Events processed were selected from the PDE cards supplied by NOAA and were located in Russia and China. Events with good signal-to-noise ratios were generally selected so that accurate signal spectra and phase velocities across the array could be computed and accurate determinations of the signal-to-noise improvement obtained from beaming could be made.

It should be emphasized that this report is preliminary and may be subject to later modification. For the most part the results are based on a small data

sample which was recorded at less than 50% of the sites. It is intended that this report cover briefly many topics which will later become the subjects of more intensive investigations.

CONFIGURATION AND INSTRUMENTATION

The Alaska Long-Period Array consists of 19 three-component sensors arranged hexagonally with a diameter of about 80 km and an intersensor spacing of 20 km. Figure 1 shows the geometric configuration of the array and Table I contains information concerning site identification, geographic coordinates, elevation, depth of burial and X, Y coordinates.

Each site contains a three component triaxial bore-hole instrument with each component having a free period of 20 seconds and a mass of 10 kilograms. The system response for these components is shown in Figure 2 and correction factors are listed in Table II. The three seismometer components (modules) are installed as a single unit resting on a concrete slab at the bottom of a 50 foot bore-hole and firmly attached against the bore-hole casing. The modules axes are inclined 35° 16' from the horizontal and oriented along azimuths of 180°, 60° and 300°.

TABLE I

Map Location Data for ALPA

Map Location Data, 19-Site Alaskan Long-Period Array

Site Code		N. Latitude (+10 sec)	W. Longitude (+20 sec)	Elev. Feet	Instr. Depth Feet	Coordinates (Km) X	Y
	1-1	65° 14' 00"	147° 44' 36"	2100	45	0	0
	2-1	65° 22' 25"	147° 24' 04"	1850	50	15.9	15.6
	2-2	65° 11' 40"	147° 18' 58"	2250	47	19.9	- 4.3
	2-3	65° 03' 55"	147° 33' 50"	1300	49	8.4	-18.7
	2-4	65° 05' 52"	148° 00' 05"	1400	50	-12.0	-15.0
	2-5	65° 16' 01"	148° 08' 11"	1450	51	-18.3	3.7
	2-6	65° 24' 02"	147° 53' 57"	1800	50	- 7.3	18.6
	3-1	65° 30' 10"	147° 07' 03"	2350	48	29.2	30.0
A1	(3-12)	65° 20' 02"	147° 00' 27"	2200	45	34.3	11.2
	3-2	65° 08' 53"	146° 52' 45"	2100	45	40.3	- 9.5
A2	(3-23)	65° 01' 43"	147° 11' 46"	1850	48	25.5	-22.8
	3-3	64° 54' 36"	147° 26' 47"	1125	46	13.8	-36.0
A3	(3-34)	64° 56' 41"	147° 51' 34"	1500	46	- 5.4	-32.1
	3-4	64° 57' 07"	148° 17' 03"	2350	175	-25.2	-31.3
A4	(3-45)	65° 07' 42"	148° 24' 05"	1800	44	-30.7	-11.7
	3-5	65° 18' 55"	148° 35' 10"	1500	50	-39.3	9.1
A5	(3-56)	65° 26' 09"	148° 18' 56"	1400	55	-26.7	22.5
	3-6	65° 33' 24"	148° 00' 00"	1900	50	-12.0	36.0
A6	(3-16)	65° 32' 23"	147° 35' 31"	2050	51	7.1	34.1

TABLE II

Response Correction Factors

Correction Factors for

ALPA SYSTEM RESPONSE

T	G_t	$1/G_t$	$1/G_{tT}$
10	.17	5.88	.588
11	.22	4.55	.414
12	.29	3.45	.288
13	.36	2.78	.214
14	.45	2.22	.159
15	.56	1.79	.119
16	.65	1.54	.096
17	.74	1.35	.079
18	.80	1.25	.069
19	.87	1.15	.061
20	.92	1.09	.054
21	.95	1.05	.050
22	.97	1.03	.047
23	.99	1.01	.044
24	1.00	1.00	.042
25	1.00	1.00	.040
26	.99	1.01	.039
27	.97	1.03	.038
28	.95	1.05	.038
29	.92	1.09	.038
30	.89	1.12	.037
31	.83	1.20	.039
32	.79	1.27	.040
33	.75	1.33	.040
34	.71	1.41	.041
35	.67	1.49	.043
36	.65	1.54	.043
37	.61	1.64	.044
38	.58	1.73	.045
39	.56	1.79	.046
40	.53	1.89	.047

PREPARATION OF DATA

The following is a brief description of the processing required before ALPA data is in a form suitable for analysis. The digital data for the dates and time periods of interest are requested from the Seismic Array Analysis Center (SAAC), and this data is then processed by demultiplexing the 16-bit ALPA words into 48-bit words in the standard Seismic Data Laboratory (SDL) library format. The demultiplexed data is then processed through a program that removes the simple instrumental and transmission spikes. Following this, event information such as the epicentral distance, back-azimuth and Δt's for a given velocity are calculated. The ALPA data is then processed with a digital program which transforms the data obtained from the original inclined orthogonal triaxial recording system to equivalent data which would be obtained from a three-component system consisting of vertical, radial and transverse instruments -- all relative to the true location of the event. This rotation is accomplished by means of the following equations:

$$R_1 = (T_1 + T_2 + T_3) \cos (90° - 35°16')$$

$$R_2 = [\cos(\alpha - \beta)T_1 + \cos(\alpha - \gamma)T_2 + \cos(\alpha - \delta)T_3] \sin(90° - 35°16')$$

$$R_3 = [\cos(\alpha + 90° - \beta)T_1 + \cos(\alpha + 90° - \gamma)T_2 + \cos(\alpha - 90° - \delta)T_3] \sin(90° - 35°16')$$

where T_1, T_2 and T_3 are the original data recorded by the triaxial seismometers, R_1, R_2 and R_3 represent the true motion in the vertical, radial and transverse directions respectively and α = event azimuth, $\beta = 180°$, $\gamma = 60°$ and $\delta = 300°$. Figures 3 through 5 are sample rotated seismograms of the Kamchatka event of 03 October 1970 and indicate arrival times of various phases.

BEAMFORMING OF LONG PERIOD ENERGY

Events with good signal-to-noise ratios were selected to evaluate the performance of beamforming both vertical and horizontal components of ALPA. These events are listed in Table III. They occurred during the months of September through November 1970 and have body wave magnitudes between 4.7 and 5.3 (NOAA). The events are all of shallow focus (less than 70 km depth) and the distances range between 2900 km and 8000 km, with all epicenters lying in China or Russia. Event No. 3 is located within a few degrees of Russia's major test site and produced an excellent signal (Figure 9) which is suitable for use as a matched filter.

Beaming of the long period energy was accomplished through the use of a digital program which can perform the following functions:

1. Detrend
2. Phaseless Filter
3. Form an unphased sum of all selected data channels.
4. Form a phased sum for any desired velocity.
5. Compute RMS of the noise in mμ for any specified time sample for the individual channels as well as the phased and unphased sums.
6. Compute the (peak-to-peak)/2 amplitude of the signal in mμ.
7. Compute the ratio of signal-to-noise in db.

All data was processed unfiltered (to determine the effect of the array on noise reduction) and filtered (15-50 sec). The RMS noise was calculated over a window

TABLE III

Events Beamed

ALPA - Events Beamed

Event No.	Location	Date	Origin Time (GMT)	Latitude	Longitude	Approximate Distance(Km)	Depth (Km)	Magnitude
1	Kamchatka	24Sep70	16:44:39.9	54.7N	162.8E	2900	34	5.3
2	Kamchatka	03Oct70	00:16:25.9	55.2N	163.2E	2900	31	5.2
3	Kazakh/ Sinkiang	24Nov70	11:45:59.2	47.5N	84.3E	6750	33	4.9
4	Kurils	14Sep70	19:44:31.5	43.5N	147.9E	4575	30	5.1
5	Kurils	19Oct70	08:08:38.6	43.3N	147.5E	4575	47	4.9
6	Kurils	25Nov70	09:39:58.9	43.2N	146.7E	4650	67	4.7
7	Sinkiang	17Oct70	05:33:15.2	41.4N	79.2E	7500	33	5.0
8	Sinkiang	16Nov70	04:57:32.9	43.2N	81.2E	7300	24	5.2
9	Tadzhik	09Oct70	13:48:52.6	39.1N	71.7E	7975	46	5.2

length of about 600 seconds chosen in a time interval before the expected "P" arrival time. This eliminates the possiblity of any part of the signal effecting the noise estimate. Care was also taken to assure, as much as possible, the absence of any other registered event that might have energy arriving close enough to the "P" arrival time so that contamination of either the noise or signal samples could occur.

The signal window for amplitude calculation varied in length from 150 to 300 seconds depending upon the signal shape and length. Amplitude measurements and beaming were thus performed over approximately six to twelve cycles of the signal. A phase velocity of 3.6 km/sec was determined to be appropriate for beaming the Rayleigh signals. Figure 6 shows the delay times (relative to the sensor first receiving the signal) as a function of the distance between sites for three events. Signal arrivals recorded at several of the sites differ by one or two seconds from the times calculated for a phase velocity of 3.6 km/sec; these time differences may or may not be real, and additional study is necessary to determine if "anomalies" exist. There are inconclusive indications that site 36 would be delayed as much as two seconds.

Table IV and V list the results of beamforming the Rayleigh signals four of nine events. The table shows the largest amplitude (O-P), the RMS value and the signal-to-noise ratios for both the mean levels and phased sums unfiltered and filtered. It also contains the signal loss (db) and the RMS noise reduction (db)

TABLE IV

Unfiltered Beamforming Results

UNFILTERED

Event	Mean(mμ) P-P/2	rms	S/rms	P-sum(mμ) P-P/2	rms	S/rms	P-sum(db) P-P/2	rms	S/rms
1	2956	38.0	85.1	2848	17.1	167.0	-0-	-7	6
2	1324	19.1	74.4	1305	7.9	164.0	-0-	-8	7
3	328	33.9	10.1	307	12.5	24.6	-1	-8	8
4	144	30.0	5.0	119	12.0	9.9	-2	-8	6
5	283	34.8	8.7	262	14.8	17.7	-1	-7	6
6	146	32.6	4.6	116	13.0	8.9	-2	-8	6
7	85	22.1	4.3	67	8.3	8.1	-2	-9	5
8	496	72.7	6.9	479	31.1	15.4	-0-	-7	7
9	84	18.3	5.3	66	6.2	10.5	-2	-9	6
Average		≈35			≈14				

Unfiltered beamforming results

TABLE V

Filtered Beamforming Results

FILTERED (15-50 sec)

Event	Mean(mμ) P-P/2	rms	S/rms	P-sum(mμ) P-P/2	rms	S/rms	P-sum(db) P-P/2	rms	S/rms	No. of Sensors	$\sqrt{N}$ db
1	1968	21.9	101	1933	10.6	183.0	-0-	-6	5	6	8
2	1263	12.7	119	1238	5.4	229.0	-0-	-7	6	7	8
3	319	18.1	18.1	304	6.6	46.0	-0-	-9	8	7	8
4	139	21.0	6.7	117	8.9	13.2	-2	-8	6	7	8
5	272	20.2	14.5	250	8.8	28.5	-1	-7	6	6	8
6	129	17.8	7.4	107	7.6	14.0	-2	-7	6	7	8
7	76	12.2	7.2	67	4.9	13.7	-1	-8	6	8	9
8	488	43.0	12.1	484	19.8	24.4	-0-	-7	6	5	7
9	79	12.0	7.3	65	4.6	14.3	-2	-8	6	8	9
Average		~20			≈ 9						

from beaming. Figures 7 through 15 illustrate the filtered signals for the nine events and Figures 16 and 24 show the corresponding filtered noise. The RMS for the phased noise traces are presented in Table VI.

Referring again to Table IV, the S/N improvement actually achieved through beaming the signals can be seen to range from 5 to 8 db, and to average 6-7 db for unfiltered data. The average number of sensors used in forming the beam is 7 with the expected theoretical S/N improvement of about 8 db. Since the RMS noise reduction does approach the expected $N^{1/2}$ on an average the approximate 1 or 2 db difference can be contributed to signal loss through beaming. Therefore, based on the above, it can be stated that the effect of beaming 7 elements of the array is to produce approximately 6 db gain in S/N over that of a single sensor. The loss of signal for a few of the events analyzed is not directly related to misalignment. Within the time window used the wave form and maximum amplitude from site to site can and does vary. The maximum amplitude, as calculated from the phased sum, will not necessarily correspond to the same time as the peak amplitude on the individual channels. Therefore, the computed "mean", in some instances, will be higher than it would be if computed within a narrower time window corresponding to the phased sum maximum. Texas Instruments (1971) have found an average signal loss of -.15 db from beamforming. This is considerably lower than our findings but can be explained by the fact that Texas Instruments employes a much smaller signal window and compares the amplitude of the single

TABLE VI

Three Component Noise Levels

ALPA - Three Component Noise Levels

Event	Component	UNFILTERED Mean rms(mμ)	UNFILTERED P-Sum rms(mμ)	UNFILTERED P-Sum(db) rms	FILTERED (15-50 sec) Mean rms(mμ)	FILTERED (15-50 sec) P-Sum rms(mμ)	FILTERED (15-50 sec) P-Sum(db) rms	No. of Sensors	$\sqrt{N}$ dB
	Z	19.1	7.9	-8	12.7	5.4	-7	7	8
2	R	25.2	11.6	-7	13.7	5.8	-8	6	8
	T	25.4	12.7	-6	16.5	6.8	-8	7	8
	Z	22.1	8.3	-9	12.2	4.9	-8	8	9
7	R	33.1	14.4	-7	16.6	6.6	-8	8	9
	T	24.5	10.6	-7	12.8	5.5	-7	7	8

sensors to the same cycle on the beam.

The average improvement in the S/N ratios due to filtering the data, with a 15 to 50 second bandpass, can be obtained by comparing the RMS (filtered) with the RMS (unfiltered). The improvement due to filtering alone was thus determined to average 4 $\pm$ 1 db. The average total gain, due to beaming and filtering, is the S/N of the beam over the S/N of the average single sensor or 10 db for seven ALPA sensors.

The unfiltered individual site mean RMS noise levels (Table IV) for the nine events range from 19 to 73 mμ with an average of about 35 mμ. After beaming, this level drops to an average of 14 mμ. The filtered data mean RMS ranges from 12 to 43 mμ and averages about 20 mμ. This value is similar to that found at TFO but more than that computed for UBO and LASA (Massé, Clark and Mecklenberg, 1970). The 20 mμ average single sensor RMS noise level was also found by von Seggern (1970). However, Texas Instruments (1971) report a value closer to 10 mμ, possibly a result of processing the data with a narrower bandpass filter (20 to 40 seconds). The average of the filtered ALPA beams is about 9 mμ. This again equals TFO but is greater than UBO and LASA by 3 and 5 db respectively.

The relative noise level on the vertical components for some of the ALPA sites is illustrated in Figure 25 which presents the ratio of the individual channel unfiltered RMS to the mean RMS for each event. This figure indicates that sites 36, 34 and possibly 24 and 33 may have lower noise levels than the other sites.

Noise on the horizontal components was examined for events 2 and 7 and was found to be slightly larger (2 db) than the noise measured on the vertical components. Table VI shows the values calculated for three components for the two events.

Event No. 2 was beamed for the P, SV, Love and Rayleigh phases. The vertical component was used in beaming for the P and Rayleigh phases, the radial component for the SV phase and the transverse component for beaming the Love phase. The results for each are given in Table VII.

A finite velocity array response for only the sensors used in beaming this event is shown in Figure 26. The broad lobe shows the low resolution or ineffectiveness of such an "array" in separating, for example, two events originating west of ALPA. A maximum of 4 db separation is expected for any event occurring up to 40° either side of the 0 db back azimuth which, in this case, is 270°.

TABLE VII

Beaming of Different Phases of 3 October 1970 Event

ALPA - Beaming of different phases

Kamchatka, 3 October 1970

Filtered 15-50 sec

Phase	Mean(mμ) P-P/2	rms	S/rms	P-sum(mμ) P-P/2	rms	S/rms	P-sum(db) P-P/2	rms	S/rms	No. of Sensors	√N db
P	32	10.9	3.3	31	5.6	5.5	-0-	-6	5	6	8
S	323	13.7	30.2	322	6.0	53.3	-0-	-7	5	6	8
LQ	2642	14.3	273	2563	7.0	364	-0-	-6	3	6	8
LR	1263	12.7	119	1238	5.4	229	-0-	-7	6	7	8

LONG PERIOD NOISE

Spectra of the noise recorded at FB2AK (ALPA site 33) were computed for time samples recorded on September 17 and 18, 1970. Recordings of these time periods are shown in Figures 27 and 28. Station FB2AK includes a standard surface long period system of three seismometers with the horizontal instruments oriented N-S and E-W. Spectra (over 1024 seconds) of the microbarograph (MKB), surface instruments (LPZ, LPN, LPE), triaxial components (TR1, TR2, TR3) and triaxial components rotated to the same orientation as the surface componnts (ZCT, NCT, ECT) are shown in Figures 29 through 38 for noise recorded on both September 17 and 18, 1970. Prominent spectral peaks occur at frequencies of about .01, .04 and .14 Hz. The time sample of September 17, 1970 represents a fairly quiet MKB time, while the time sample of September 18, 1970 corresponds to the arrival of a storm front which marked the beginning of the winter period for which the mean daily temperature was below 0° C. The spectra for the two days in September show more low frequency noise on the surface instruments for the time period with higher MKB levels. Coherency and phase between the different components was computed for both days and is shown in Figures 39 to 58. As expected, there is high coherency between the surface components and the rotated triaxial components. The coherency between the MKB and the seismometers components is small.

Figures 59 through 79 show spectra for September 5, 1970 of noise computed for seven ALPA sites.

The spectra of the vertical transform show power peak at .01, .024 and .06 Hz. The power levels are approximately the same at all sites analyzed with the one exception of site 31 which has about ten times more noise power at .01 to .025 Hz than do the either sites. Spectra of the horizontal transforms show a broad peak centered around .015 Hz, and in general reveal more variation between sites (as much as a factor of 100) than do the vertical transforms.

Zero lag cross correlations were calculated over a bandpass filtered noise sample (15-50 sec) of 1000 sec recorded on 5 September 1970. Seven sites were available and the calculations were made between all possible pairs representing distances of 20 km to 70 km. Almost all coefficients were less than $\pm$ 0.1. Two methods were used to compute these correlation coefficients. The methods (which yielded near equivalent results) are:

$$R(x_i y_j) = \frac{2C_c}{C_{ai} + C_{aj}} \qquad \text{and}$$

$$\text{Rho}(x_i y_j) = \frac{C_c}{\sqrt{C_{ai} \times C_{aj}}} \qquad \text{where}$$

C_c = cross correlation function.

C_a = auto correlation function.

These results suggest that simple beamforming will yield $N^{1/2}$ improvement in signal-to-noise.

LONG PERIOD SIGNALS

The spectral content of some long period signals as recorded at ALPA was determined for a set of events occurring in the Kuril-Kamchatka and Continental Asian regions. Table VIII lists the source parameters for these events and Figures 80 and 81 show the recorded signals from each event. Rayleigh wave spectra are shown in Figures 82 to 91. The spectra were computed with a 128 second time window and were not corrected for the system response. The peak frequencies range from 0.04 to 0.06 Hz with the maximum commonly occurring at 0.05 Hz. Love, P and S wave spectra were computed for three of the events listed in Table VIII, also using a time window of 128 seconds, and these spectra are shown in Figures 92 to 100. For all spectra calculations the mean and linear trend were removed from the full noise and signal data of from 2500 to 4000 seconds.

Employing the technique given by Dziewonski et al., 1969, Love and Rayleigh wave group velocity dispersion for the fundamental mode was determined for paths to ALPA from some seismic regions within Continental Asia and for the Kuril-Kamchatka region. These group velocity dispersion curves are shown in Figures 101 to 105 for Rayleigh waves and Figures 106 to 110 for Love waves.

TABLE VIII

Events Used in Matched Filter Processing

ALPA - Events Spectral Estimated

Event No.	Location	Date	Origin Time (GMT)	Latitude	Longitude	Approximate Distance (Km)	Depth (Km)	Magnitude
1	Kamchatka	24Sep70	16:44:39.9	54.7N	162.8E	2900	34	5.2
2	Kamchatka	03Oct70	00:16:25.9	55.2N	163.2E	2900	31	5.2
3	Kazakh/ Sinkiang	24Nov70	11:45:59.2	47.5N	84.3E	6750	33	4.9
4	Kurils	14Sep70	19:44:31.5	43.5N	147.9E	4575	30	5.1
5	Kurils	19Oct70	08:08:38.6	43.3N	147.5E	4575	47	4.9
6	Kurils	25Nov70	09:39:58.9	43.2N	146.7E	4650	67	4.7
7	Sinkiang	17Oct70	05:33:15.2	41.4N	79.2E	7500	33	5.0
8	Sinkiang	16Nov70	04:57:32.9	43.2N	81.2E	7300	24	5.2
9	Tadzhik	09Oct70	13:48:52.6	39.1N	71.7E	7975	46	5.2
10	Kurils	08Oct70	23:36:09.7	43.8N	147.4E	4550	15	5.8

MATCHED FILTERING OF SOME SIGNALS

Figures 111 to 113 show the vertical component recordings at ALPA for three events from the Sinkiang region. Rayleigh energy is visible from the earthquakes which occurred on 17 October 1970 and 16 November 1970, but is not visible from the earthquake which occurred on 29 November 1970. Epicenter information for these events is given in Table IX. Using the Rayleigh signal from the Sinkiang event of 17 October 1970 as a matched filter, signals from the 29 November 1970 Sinkiang event were processed. Table X summarizes the sites used. Figure 111 indicates the portion of the signal used as a matched filter and Figure 114 presents the matched filter results for each site as well as the beam of these matched filter traces. The results are weak on the individual traces, but are fairly good on the sum trace. The recording made at site 11 of the Sinkiang event of 16 November 1970 was also used as a matched filter for the 29 November 1970 event. As may be seen from Figure 115, the results are poor. The reason may in part be explained by the wave form at one site having been used as a matched filter for all the sites. Figure 116 shows the results of using the 16 November 1970 event as a filter for the 17 October 1970 event.

An earthquake which occurred on 14 December 1970 in Kamchatka and did not produce a visible recorded signal at ALPA (Figure 117) was processed using a Kamchatka event which occurred on 3 October 1970 (Figure 3). The results as shown in Figure 118 are poor, although

TABLE IX

Events Used in Matched Filter Processing

Event No.	Location	Date	Origin Time (GMT)	Latitude	Longitude	Approximate Distance(Km)	Depth (Km)	Magnitude
1	Kamchatka	03Oct70	00:16:25.9	55.2N	163.2E	2900	31	5.2
2	Kamchatka	14Dec70	13:59:36.3	52.2N	156.4E	3400	208	4.6
3	Sinkiang	17Oct70	05:33:15.2	41.4N	79.2E	7500	33	5.0
4	Sinkiang	16Nov70	04:57:32.9	43.2N	81.2E	7300	24	5.2
5	Sinkiang	29Nov70	02:03:37.4	41.6N	81.8E	7425	33	5.1

TABLE X

Sites Used in Matched Filter Processing

Event	Matched Filter Trace	Event	Processed (Filtered) Trace
17Oct70	33	29Nov70	33
	34		34
	23		23
	11		11
	24		24
16Nov70	11	29Nov70	33
	11		A3
	11		34
	11		23
	11		11
	11		24
16Nov70	A2	17Oct70	A2
	32		32
	A2		33
	A2		34
	A2		23
	11		11
	24		24
03Oct70	A2	14Dec70	A2
	32		32
	34		34
	23		23
	24		24

the body wave magnitudes of the two events are fairly close. In general, it is not possible to make any conclusions concerning matched filtering of signals recorded at ALPA because the number of processed events is too small.

DETECTION LEVEL

Using the average noise levels for filtered beams of seven sensors, it is possible to arrive at an estimate of detection level at ALPA. Assuming that a well dispersed surface wave can be detected with a p-p signal-to-RMS noise ratio of 6 to 1 (twice the maximum amplitude expected in a noise sample) then surface wave magnitudes (M_s) of 3.1 could be detected from filtered beam data from the Kuril Islands region at .04 Hz, and 3.5 from Sinkiang. These correspond to approximate m_b magnitudes of 4.5 and 4.7 using the Gutenberg and Richter (1956) equation : $M_s = 1.59\ m_b - 3.97$.

Again based on the average calculated RMS values for single sites, it is theoretically possible to detect 3.6 and 4.0 surface wave magnitude events from the Kurils and Sinkiang regions respectively, or 5.4 and 5.6 m_b events. Match filter processing could conceivably improve the detection level by several tenths magnitude.

Of the relatively few events examined at ALPA to date, no events below about 4.6 m_b could be detected on the individual channels from either of these source areas. This is in fair agreement with the estimate given above.

No attempt was made at this time to relate these approximations to a detection level of confidence or false alarm rate.

M_s VERSUS m_b

Figure 119 is a plot of M_s versus m_b for the nine events listed in Table III. The M_s values were computed from signals recorded at ALPA using the equation log A/T (25 sec) + (1.66 logΔ°) - .18, and the m_b values were obtained from data published by NOAA. Since this study is concerned primarily with large events, the range of magnitudes for the events processed is insufficient to determine a slope. However, the lines from three other investigations are presented as a reference to this data. The Gutenberg and Richter (1956) line for earthquakes is shown along with those of Capon (1967) and Liebermann and Pomeroy (1967) for two Algerian explosions. The M_s - m_b values for the explosions MILROW and LONG SHOT are also shown. The mean for the events measured from ALPA recordings agrees well with Gutenberg's line and falls above the other lines by less than one order of M_s magnitude. Gutenberg derived his slope from numerous events in the western pacific region as recorded in California (Gutenberg 1945). With a few exceptions, the nine events measured at ALPA occurred in the same region as those measured by Gutenberg, and all had mainly oceanic or mixed continental-oceanic paths. It may also be noted, as stated by Basham (1969), that wave impingement on oceanic/continental boundaries can, due to scattering, reduce the amplitude by up to a factor of 4 or 0.6 magnitude.

CONCLUSIONS

From this preliminary study of a partial ALPA array, the following results are indicated:

1. The noise is reduced by approximately $N^{1/2}$ through beamforming.

2. The S/N ratio improvement from beamforming is about 2 db less than $N^{1/2}$.

3. The average filtered (15 to 50 second) RMS noise level from individual sensors is about 20 mμ while the RMS noise level of the beam is 9 mμ. These noise levels are similar to those computed for TFO but are higher than those calculated for UBO and LASA (Massé, Clark and Mecklenburg, 1970).

4. Peaks occur at frequencies of .01, .07 and .14 Hz in the noise spectra and at .05 Hz for signal spectra, with all spectra uncorrected for system response.

5. Since the events processed were of approximately the same body wave magnitude, the calculated M_s values were clustered. These values fall on the Gutenberg and Richter slope of $M_s = 1.59\ m_b - 3.97$.

6. No conclusion can be reached relative to matched-filtering at this time since only a few events were processed.

REFERENCES

Basham, P.W., 1969, Canadian magnitudes of earthquakes and nuclear explosions in south-western North America: J.R. Geophys. Astr. Soc., v. 17, p. 1-13.

Capon, J., Greenfield, R.J. and Lacoss, R.T., 1967, Semiannual technical summary: Lincoln Labs, MIT, June.

Dziewonski, A., Bloch, S. and Landisman, M., 1969, A technique of the analysis of transient seismic signals: BSSA, v. 59, p. 427-444.

Gutenberg, B., 1954, Amplitudes of surface waves and magnitudes of shallow earthquakes: BSSA, v. 35.

Gutenberg, B. and Richter, C.F., 1956, Magnitude and energy of earthquakes: Annali, Geofis., v. 9.

Liebermann, R.C. and Pomeroy, P.W., 1967, Excitation of surface waves by events in southern Algeria: Science, v. 156.

Massé, R.P., Clark, D.M. and Mecklenberg, H.J., 1970, Analysis of long period seismic signals and noise at LASA, TFO and UBO: Seismic Data Laboratory Report No. 254, Teledyne Geotech, Alexandria, Virginia.

Teledyne Geotech, 1970, Technical Report No. 70-39, Final Report Project VT/8707, Alaskan long period array: Garland, Texas.

Texas Instruments, Inc., Final Report Project VT/9707, Long period array processing development: Dallas, Texas.

von Seggern, D.H., 1970, A long-period noise study at Murphy Dome, Alaska: Seismic Data Laboratory Report No. 247, Teledyne Geotech, Alexandria, Virginia.

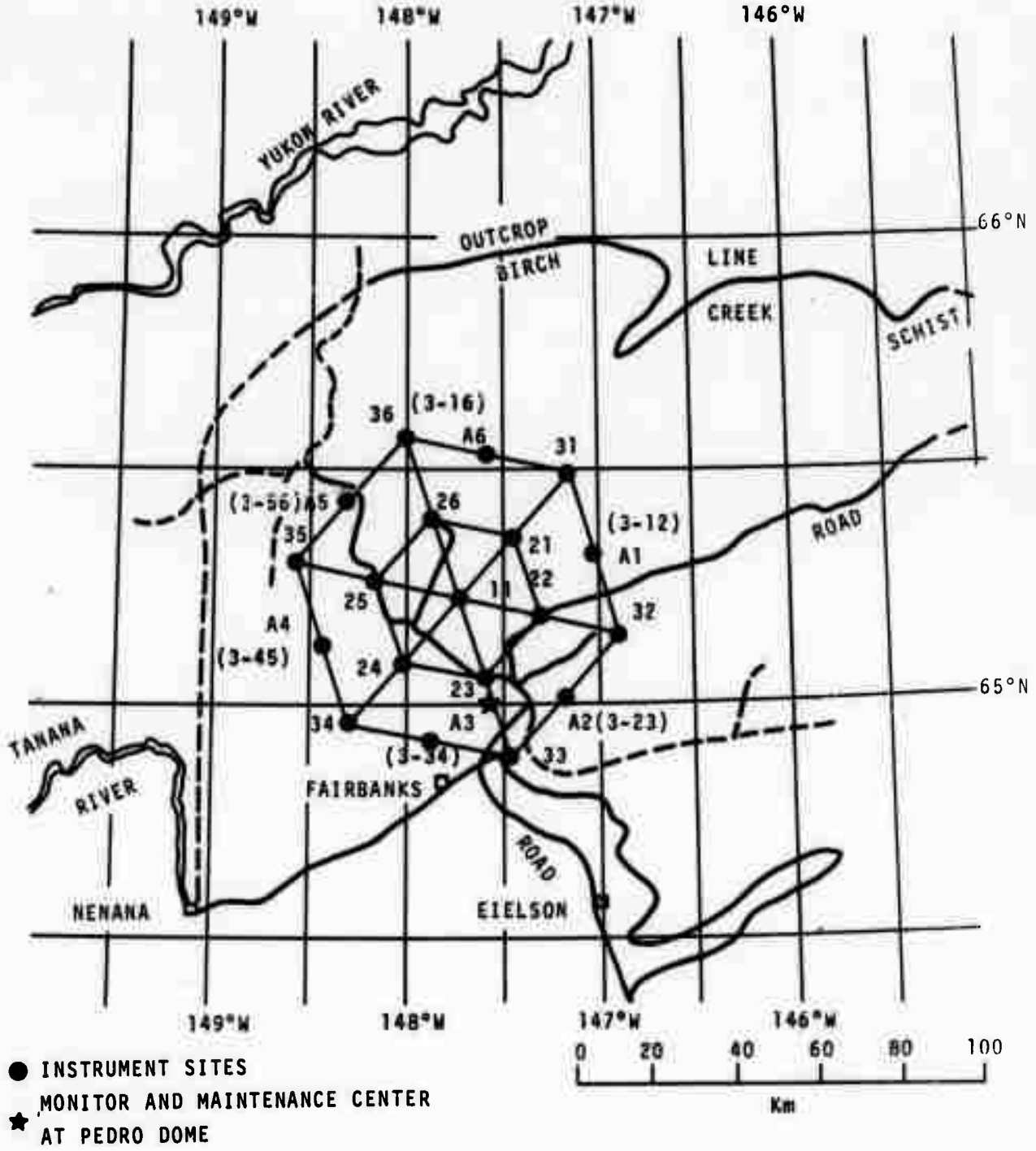

Figure 1. Map of ALPA array.

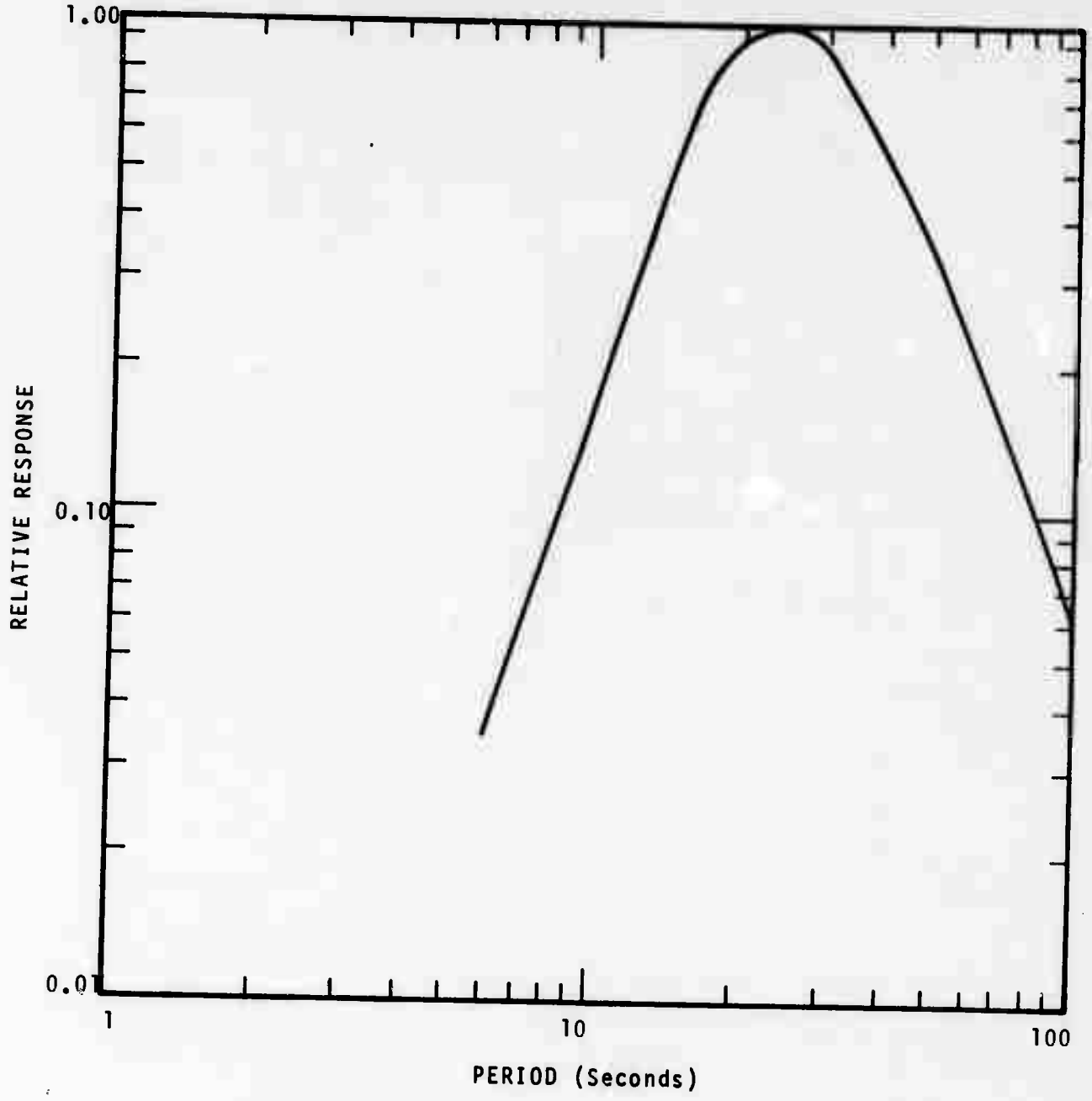

Figure 2. ALPA system response.

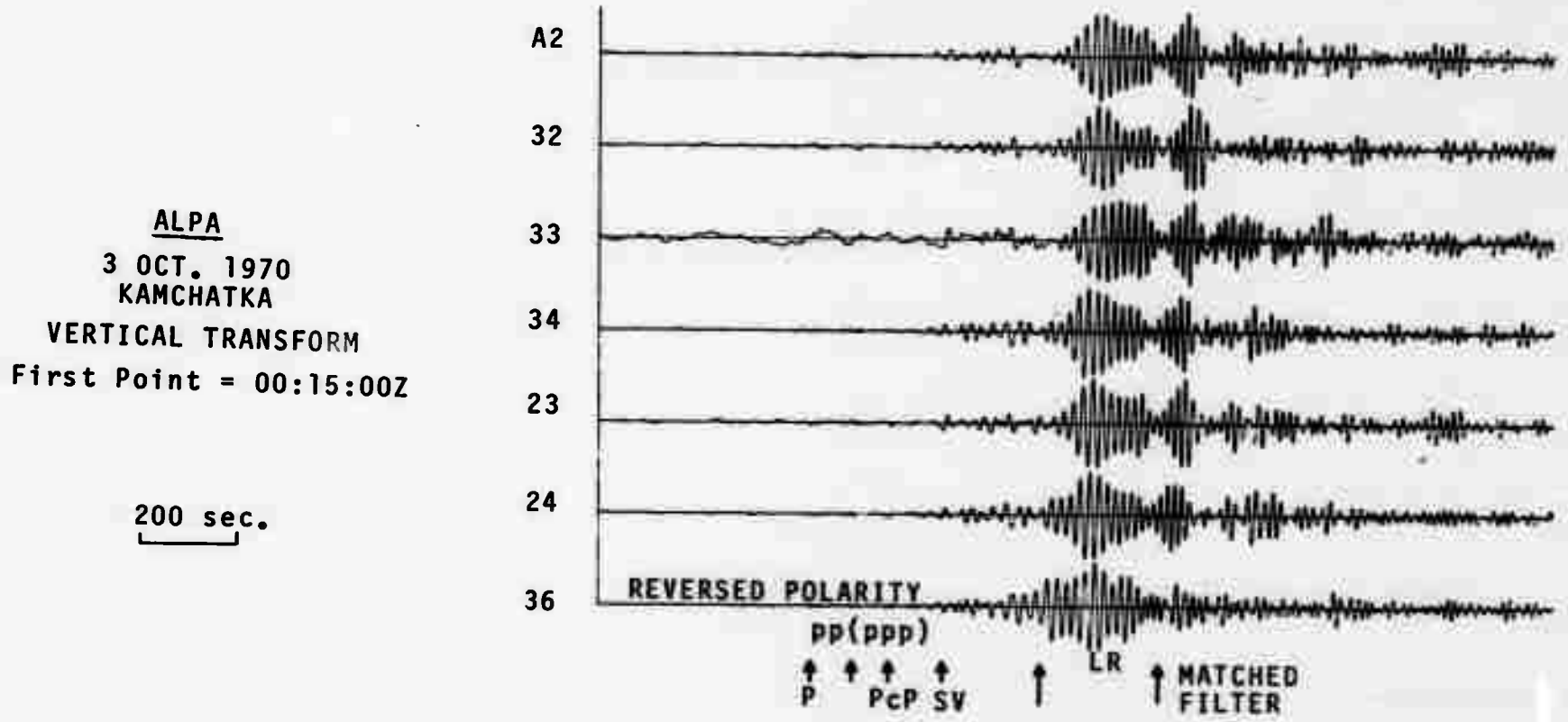

Figure 3. 03 October 1970 three component rotated seismograms.

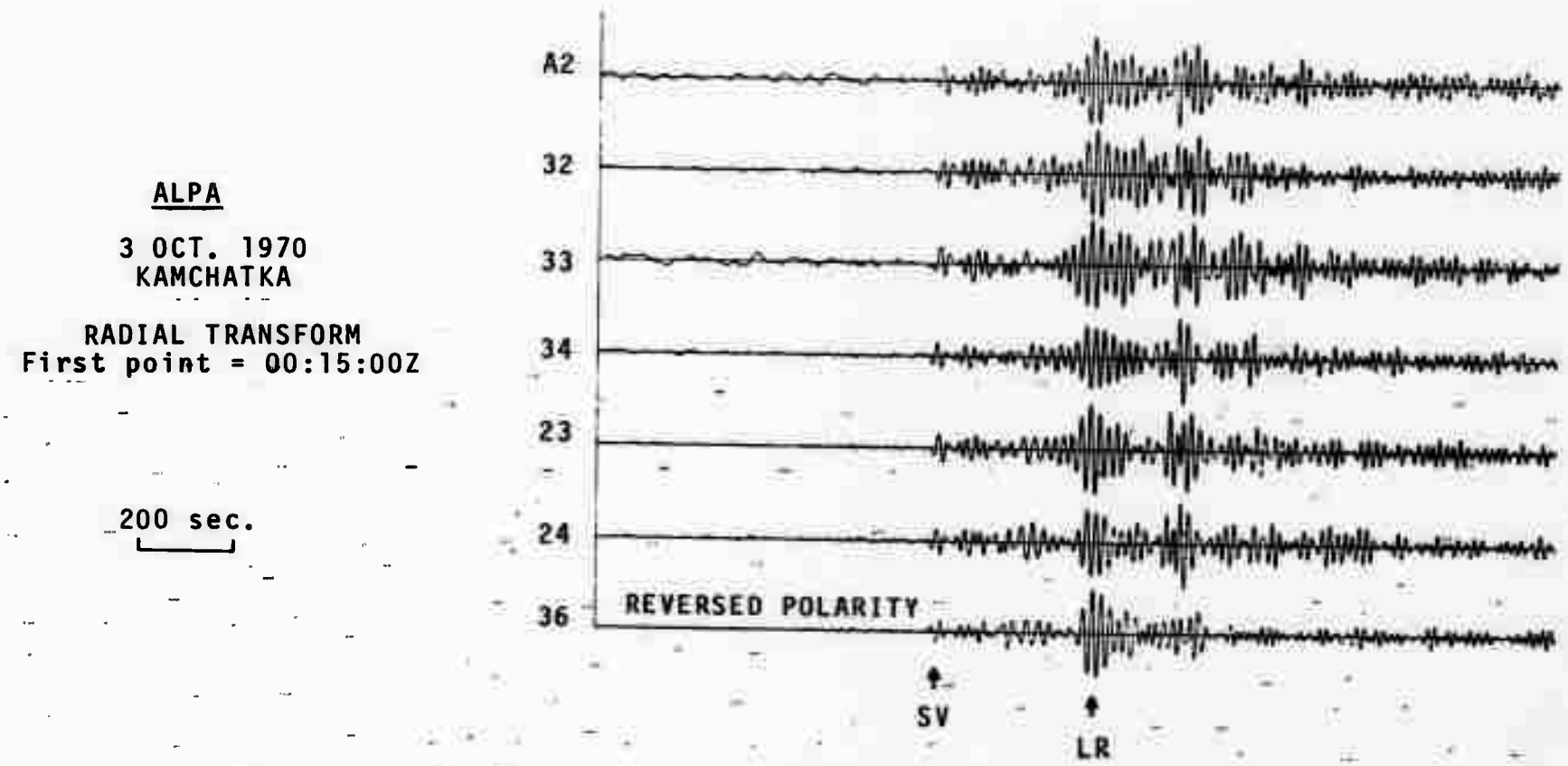

Figure 4. 03 October 1970 three component rotated seismograms.

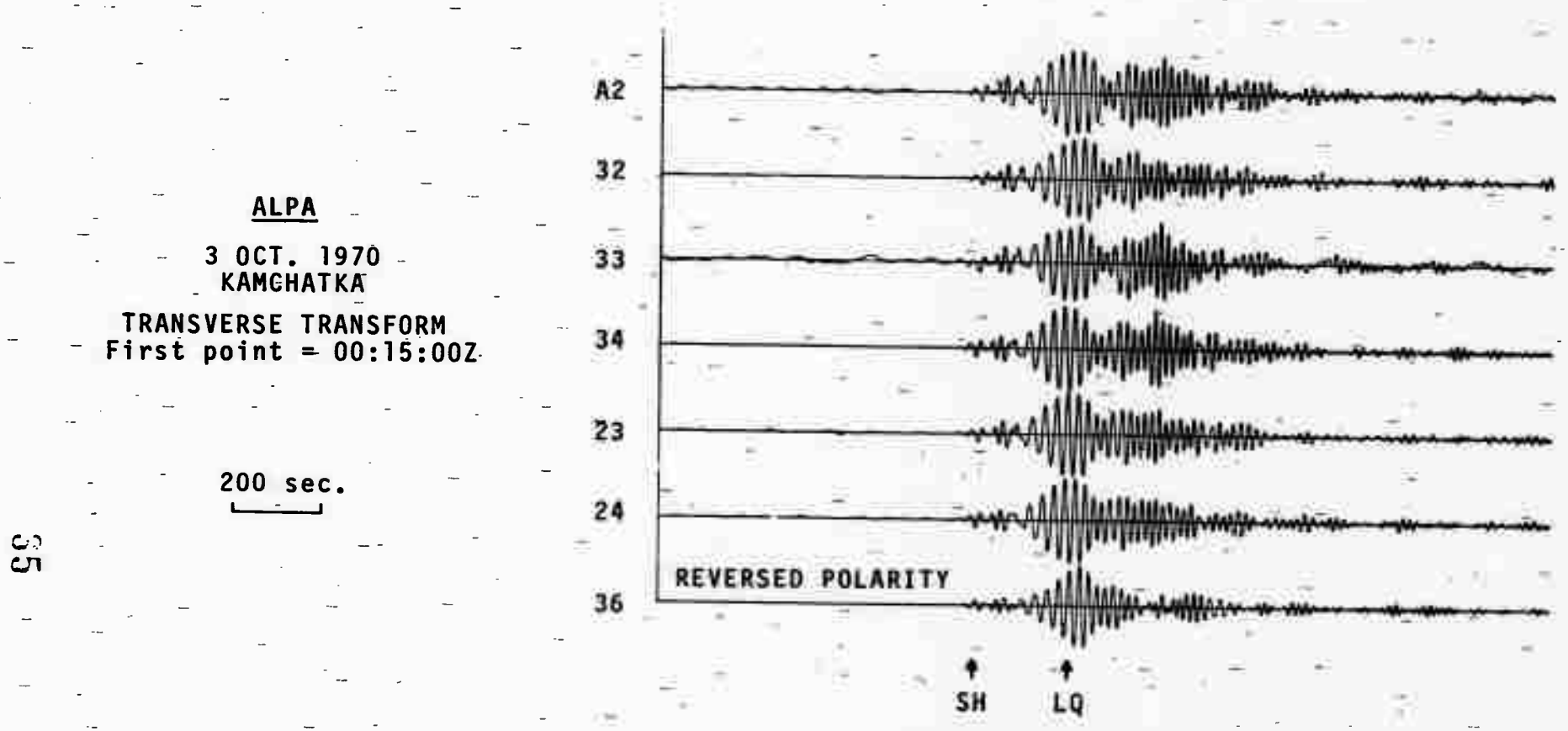

Figure 5. 03 October 1970 three component rotated seismograms.

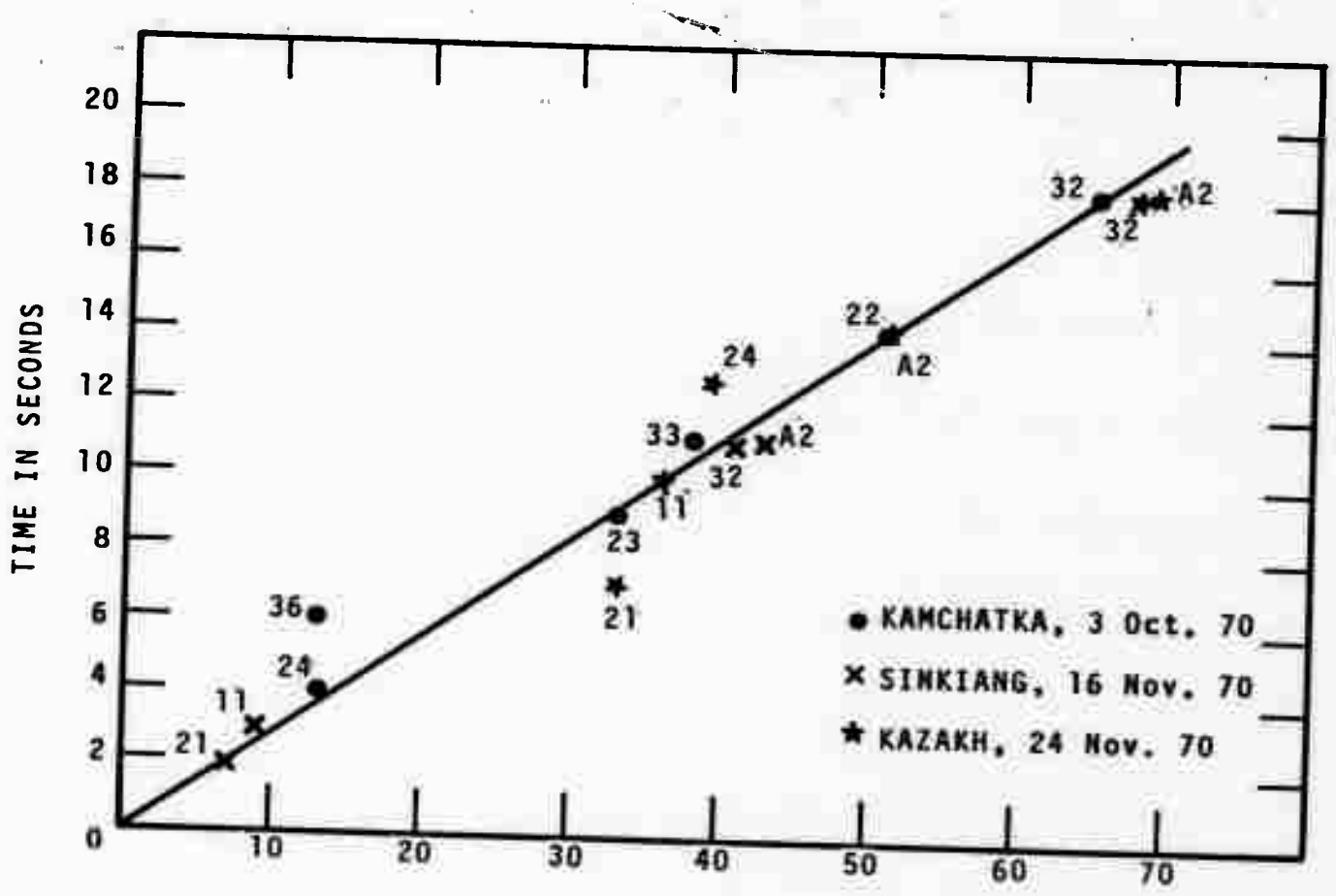

Figure 6. Delay times for three events.

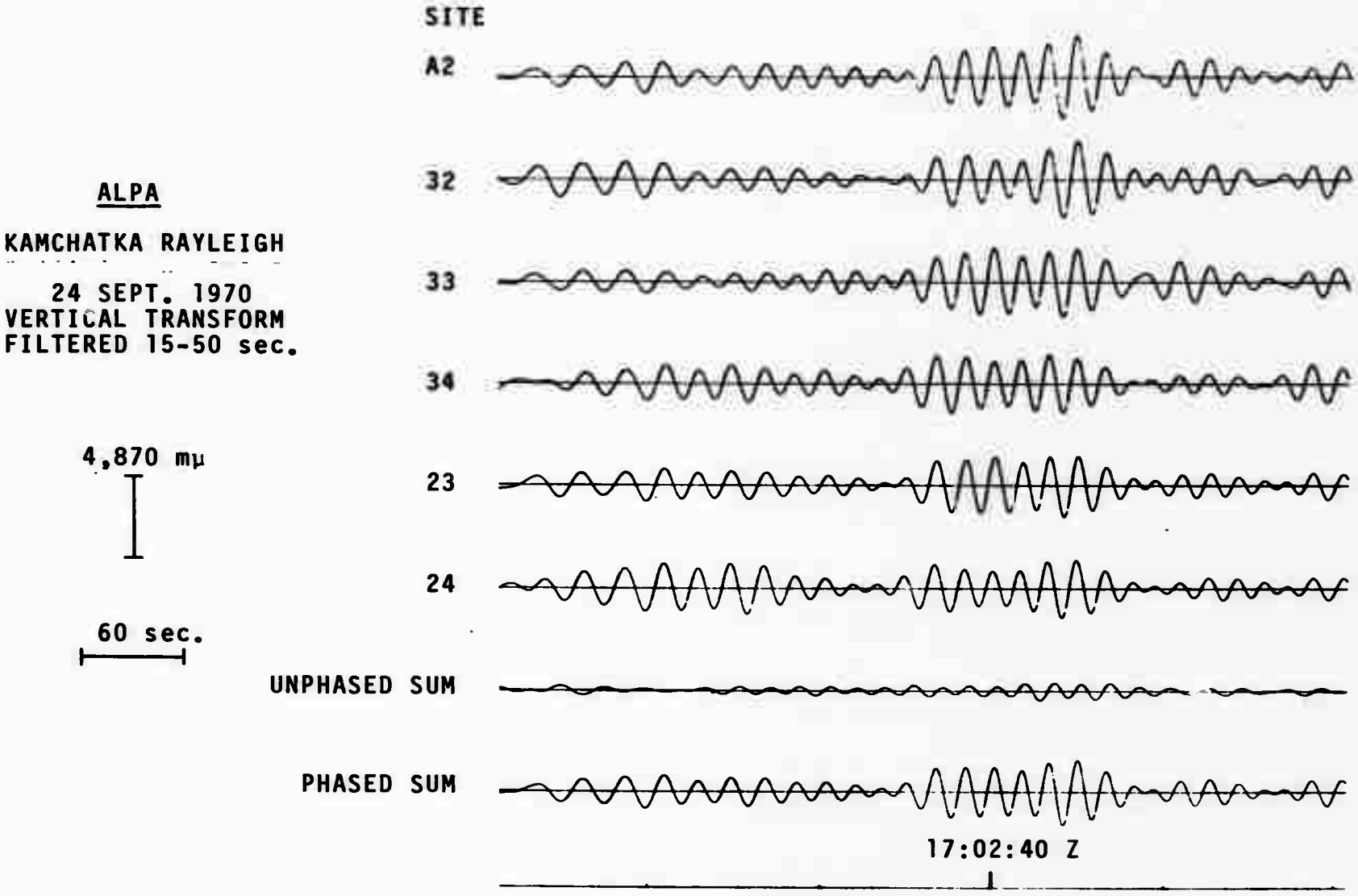

Figure 7. Processed Rayleigh signals from nine events.

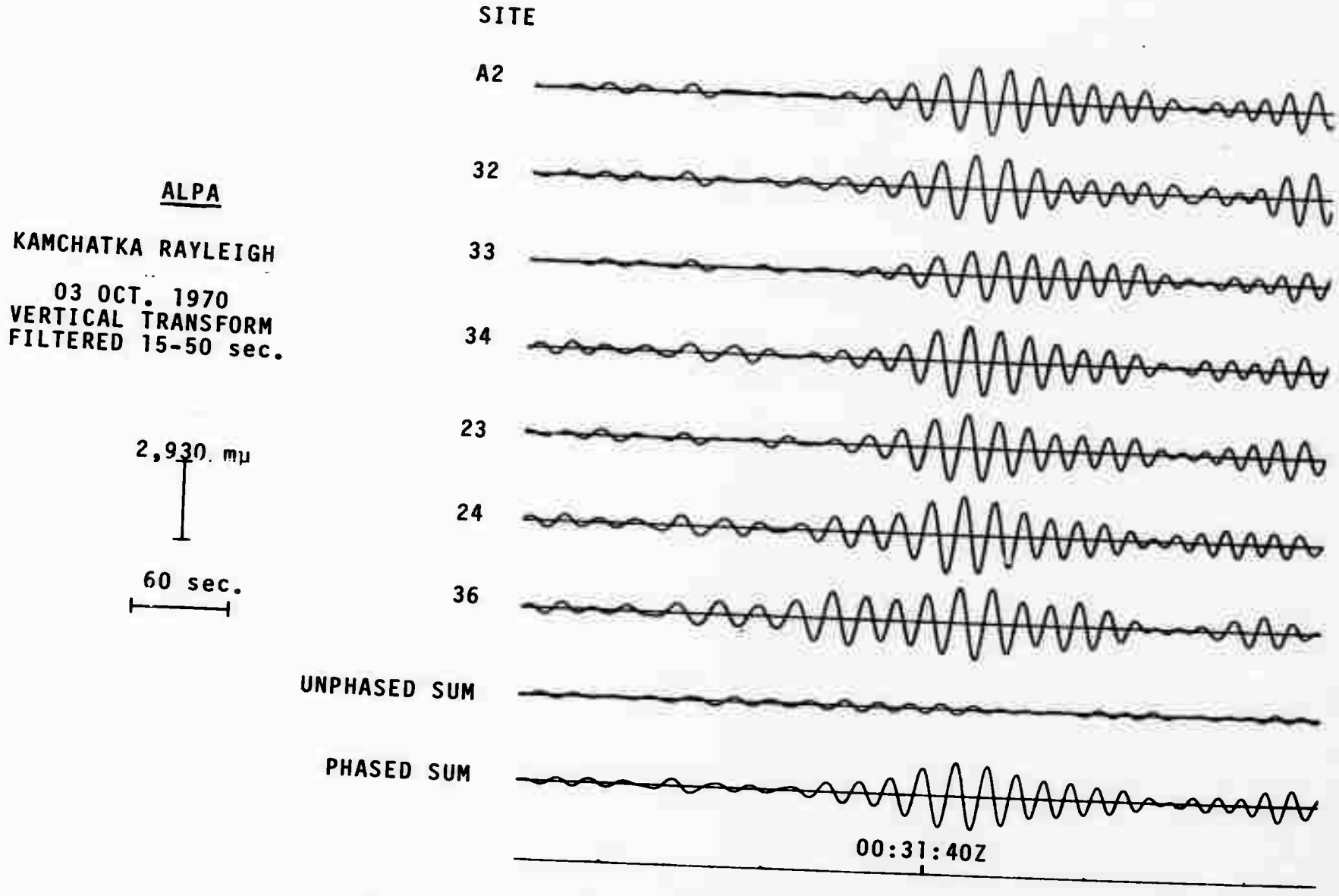

Figure 8. Processed Rayleigh signals from nine events.

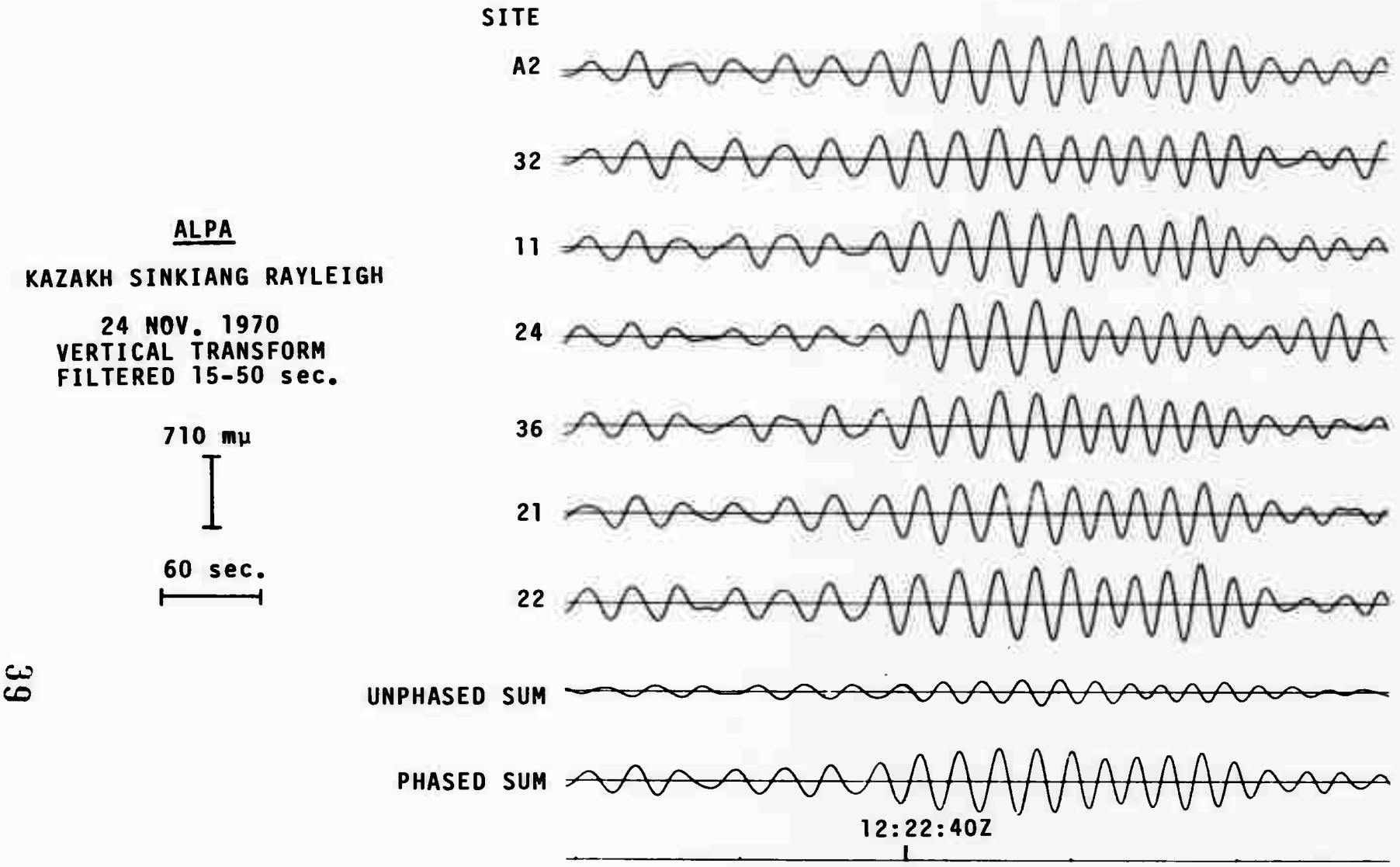

Figure 9. Processed Rayleigh signals from nine events.

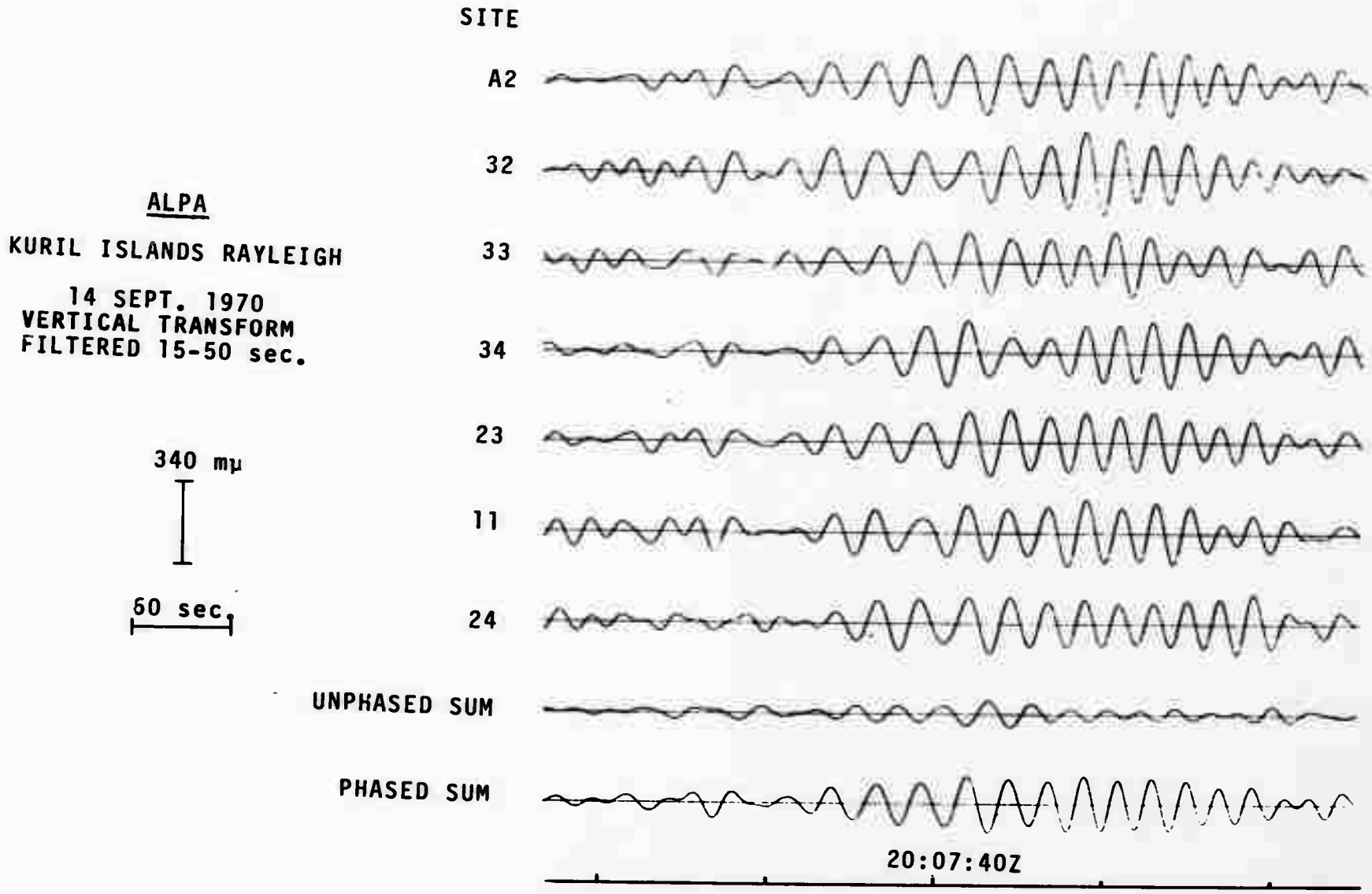

Figure 10. Processed Rayleigh signals from nine events.

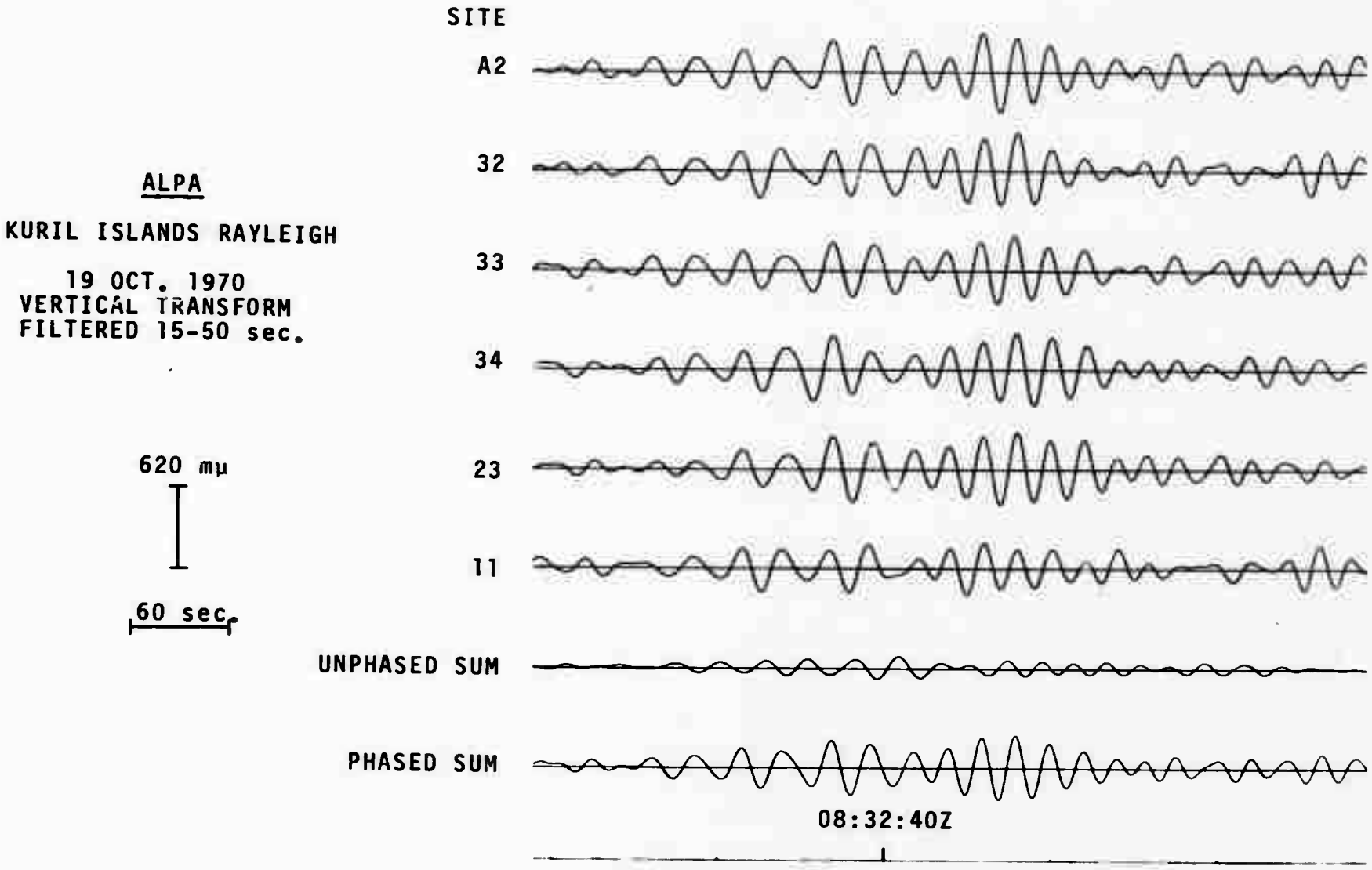

Figure 11. Processed Rayleigh signals from nine events.

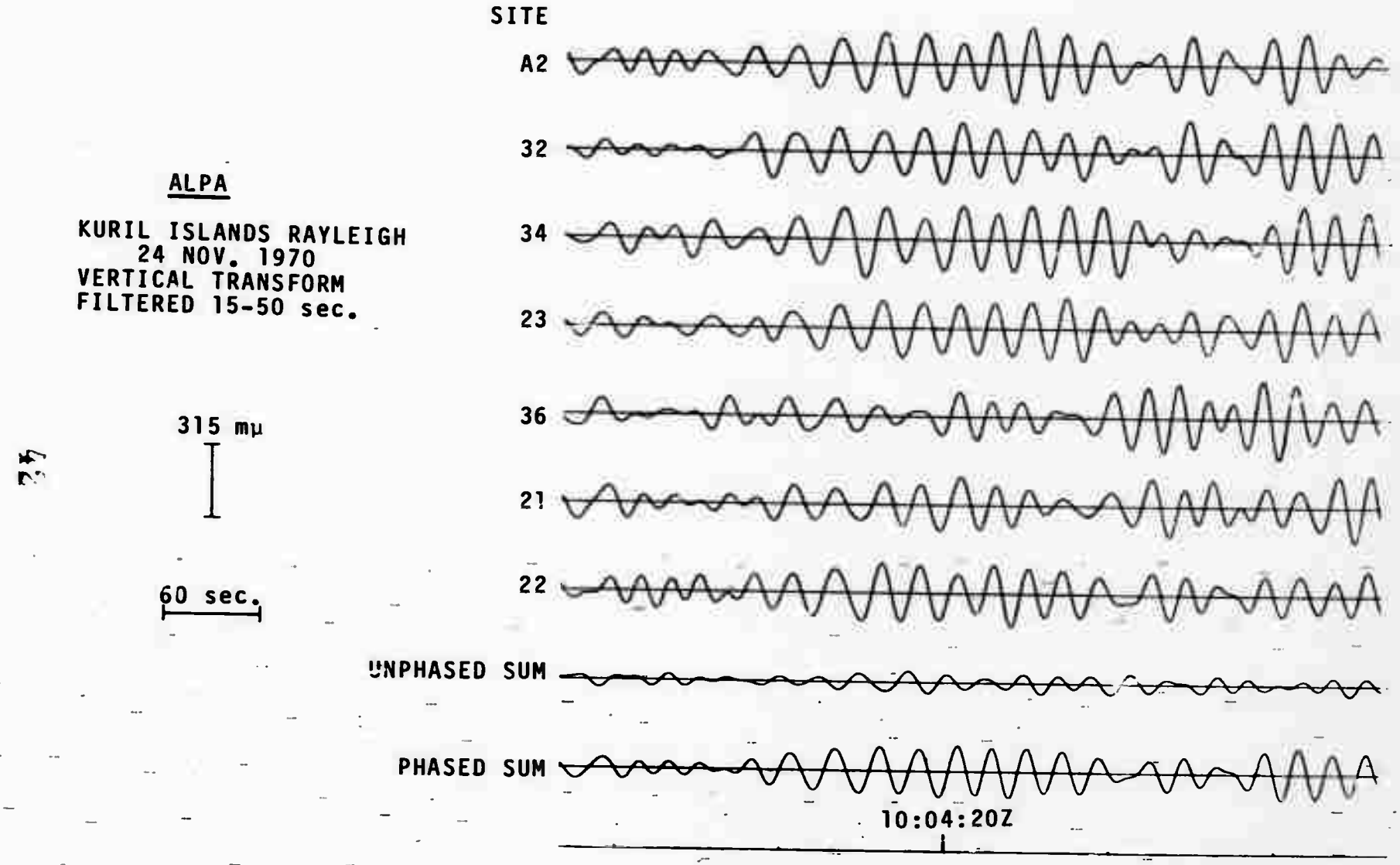

Figure 12. Processed Rayleigh signals from nine events.

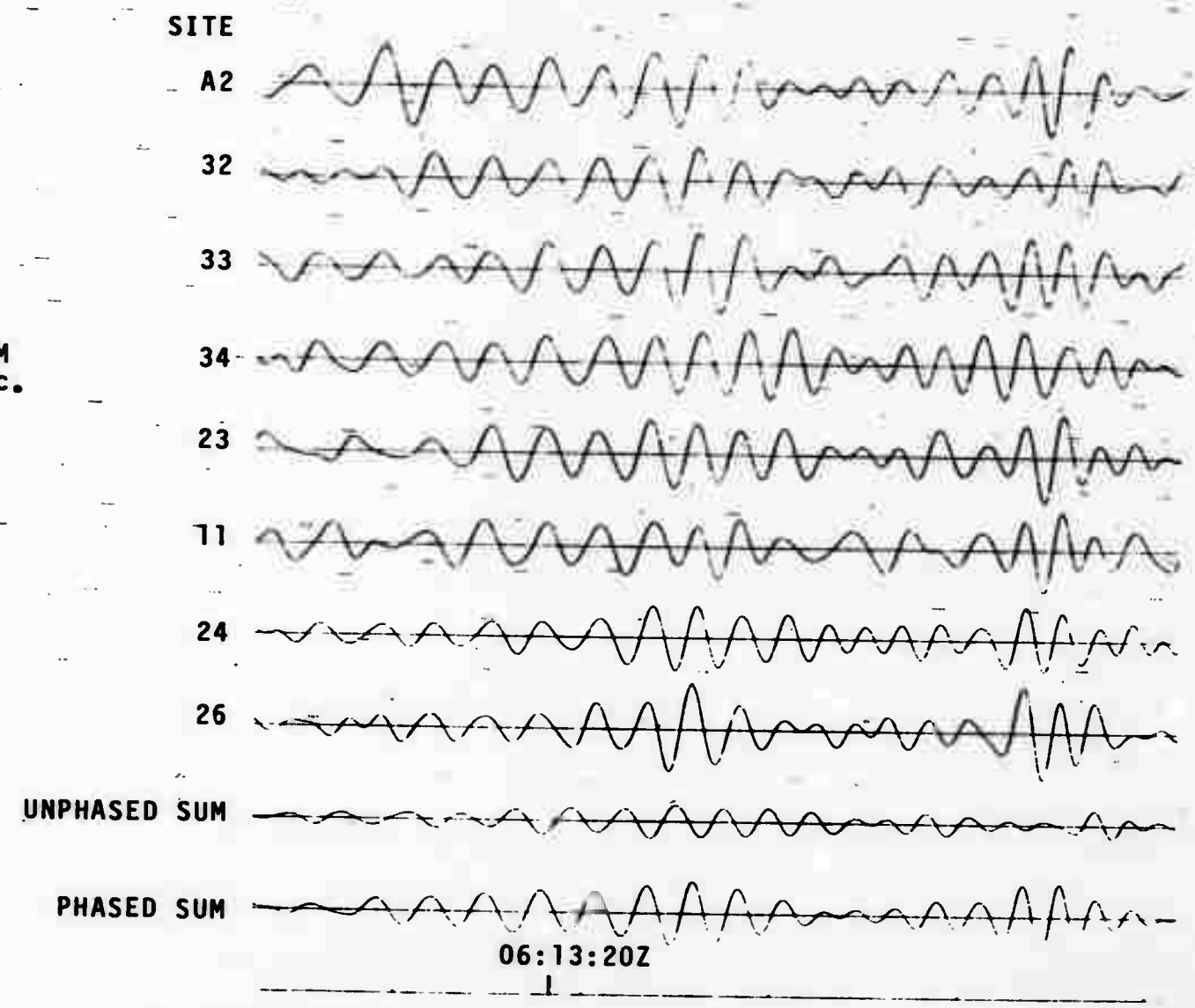

Figure 13. Processed Rayleigh signals from nine events.

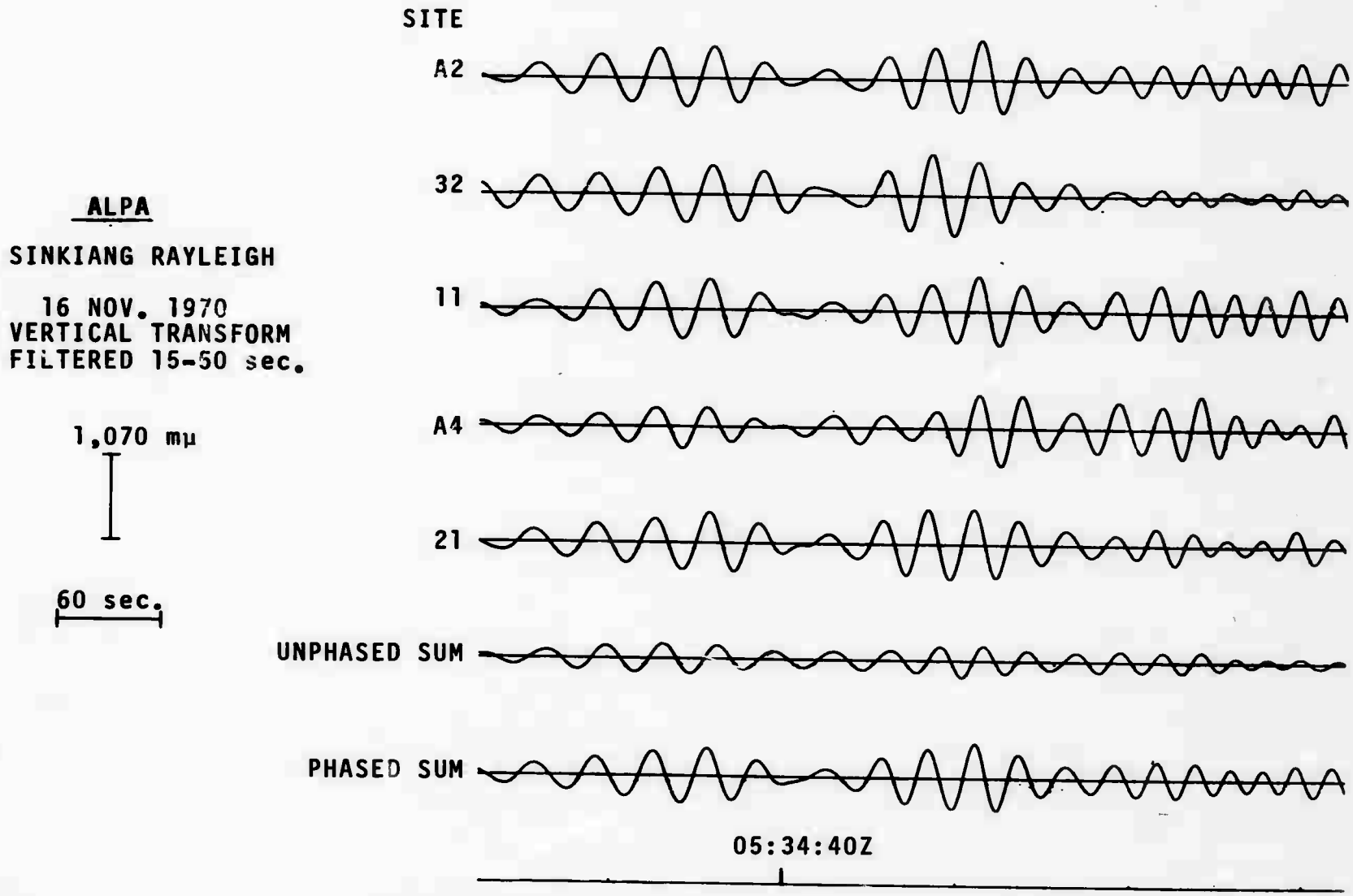

Figure 14. Processed Rayleigh signals from nine events.

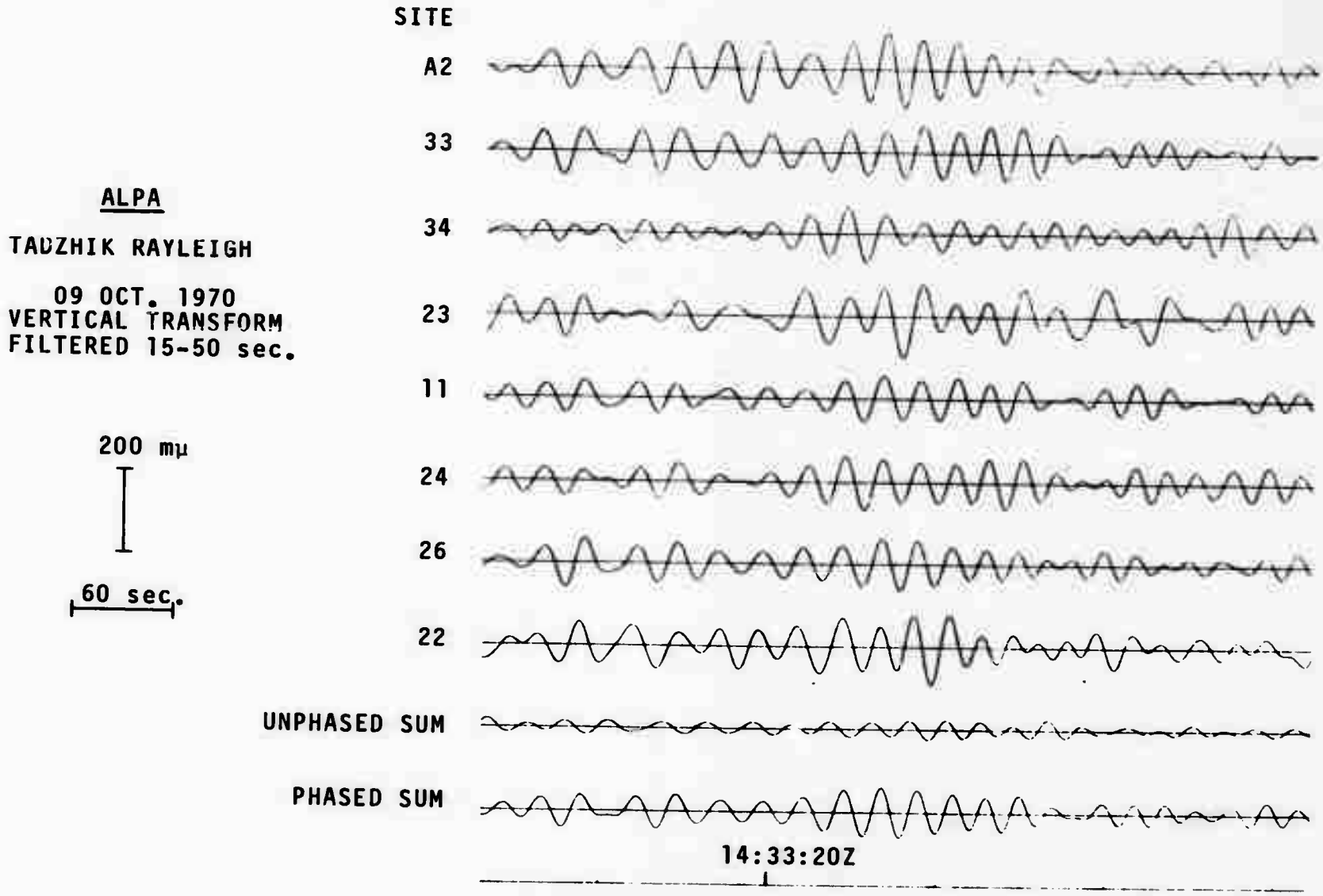

Figure 15. Processed Rayleigh signals from nine events.

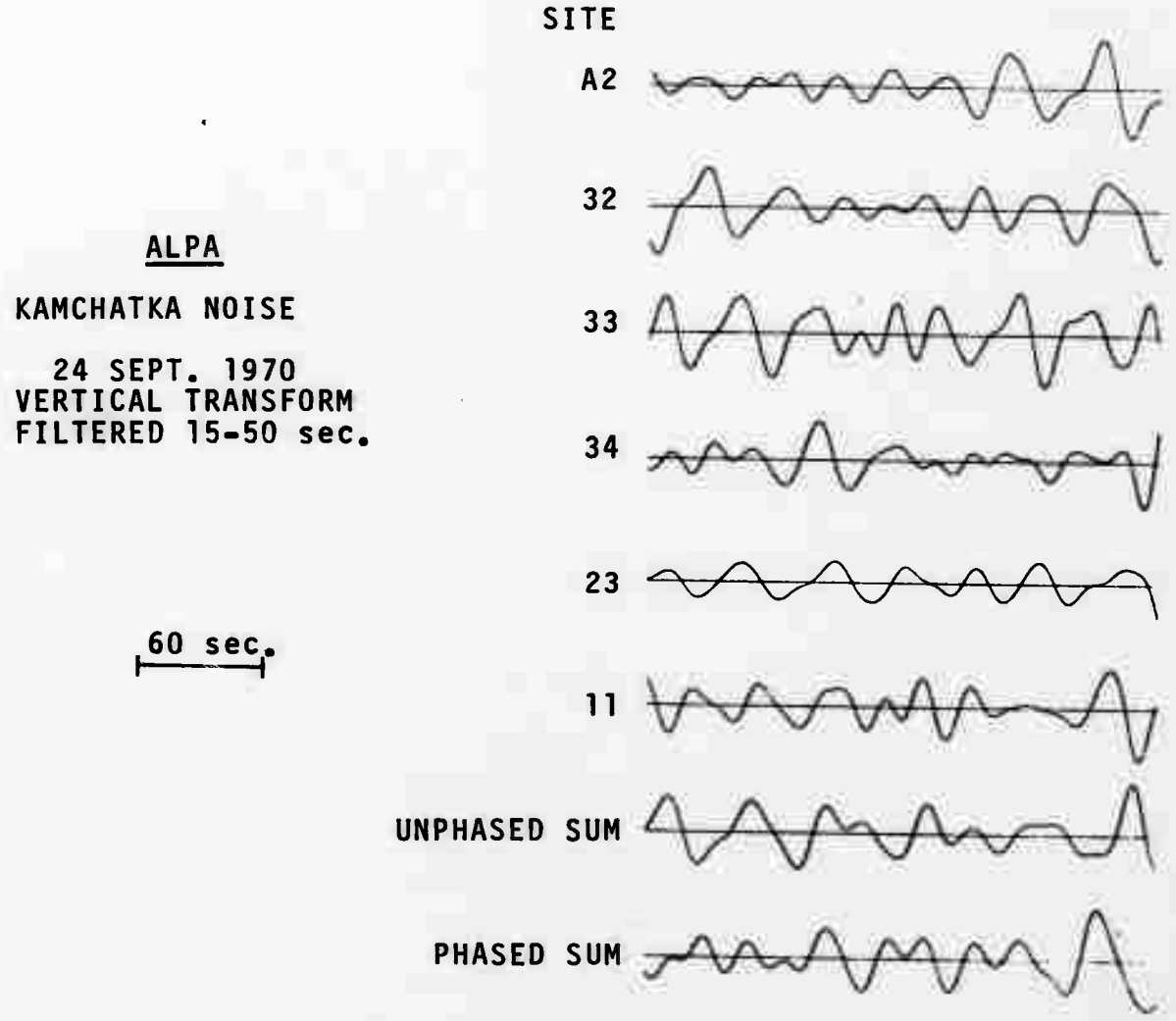

Figure 16. Processed noise before nine events.

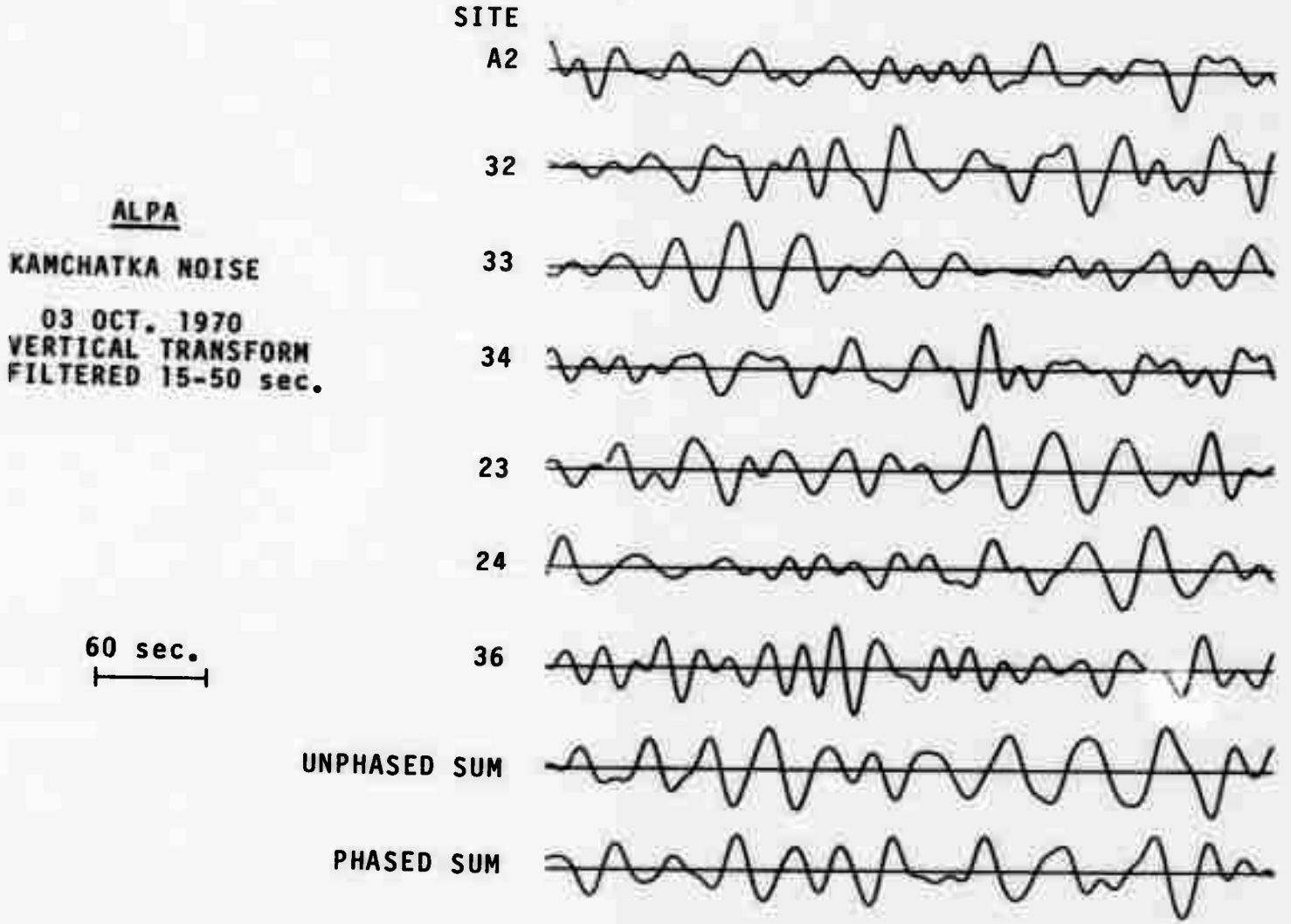

Figure 17. Processed noise before nine events.

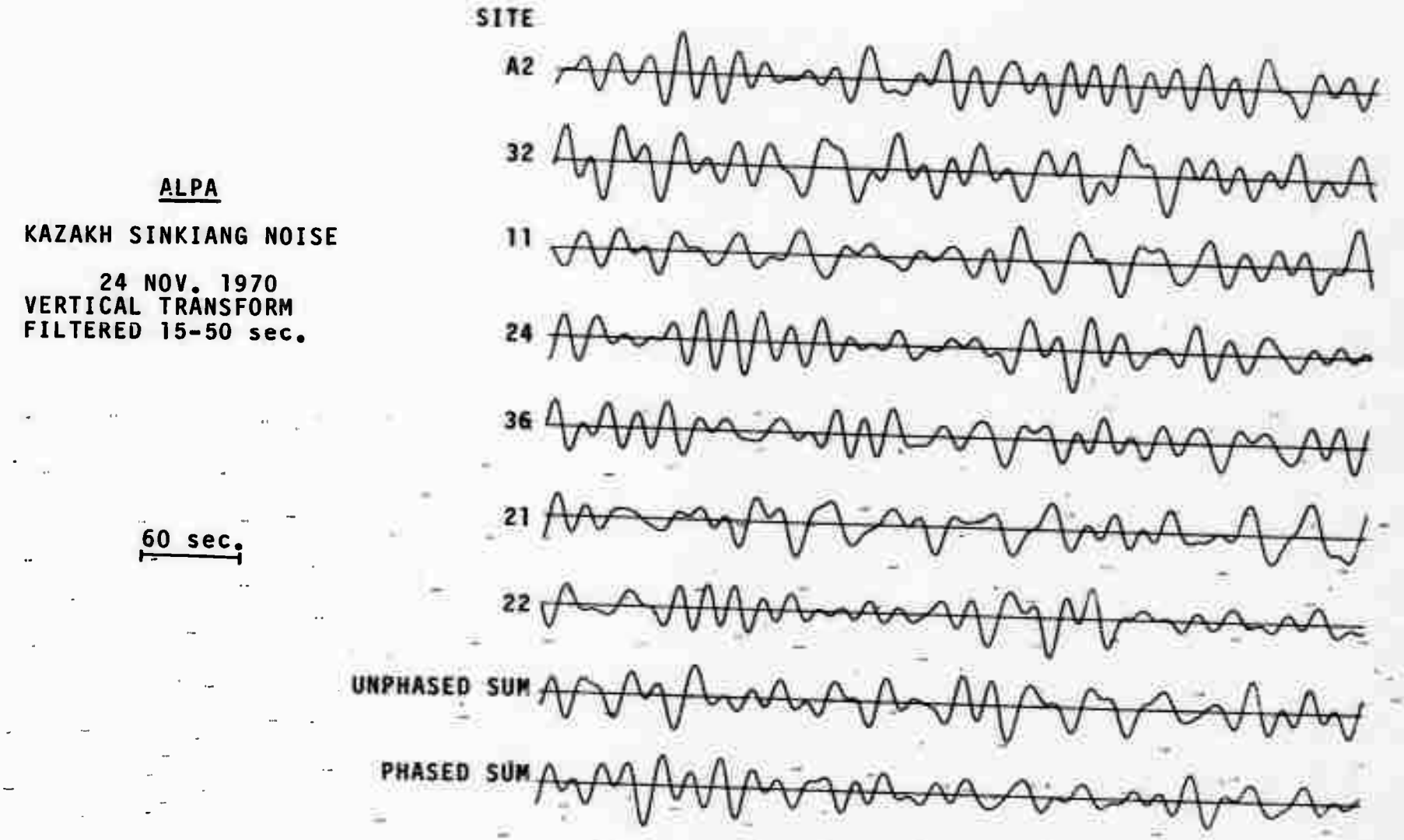

Figure 18. Processed noise before nine events.

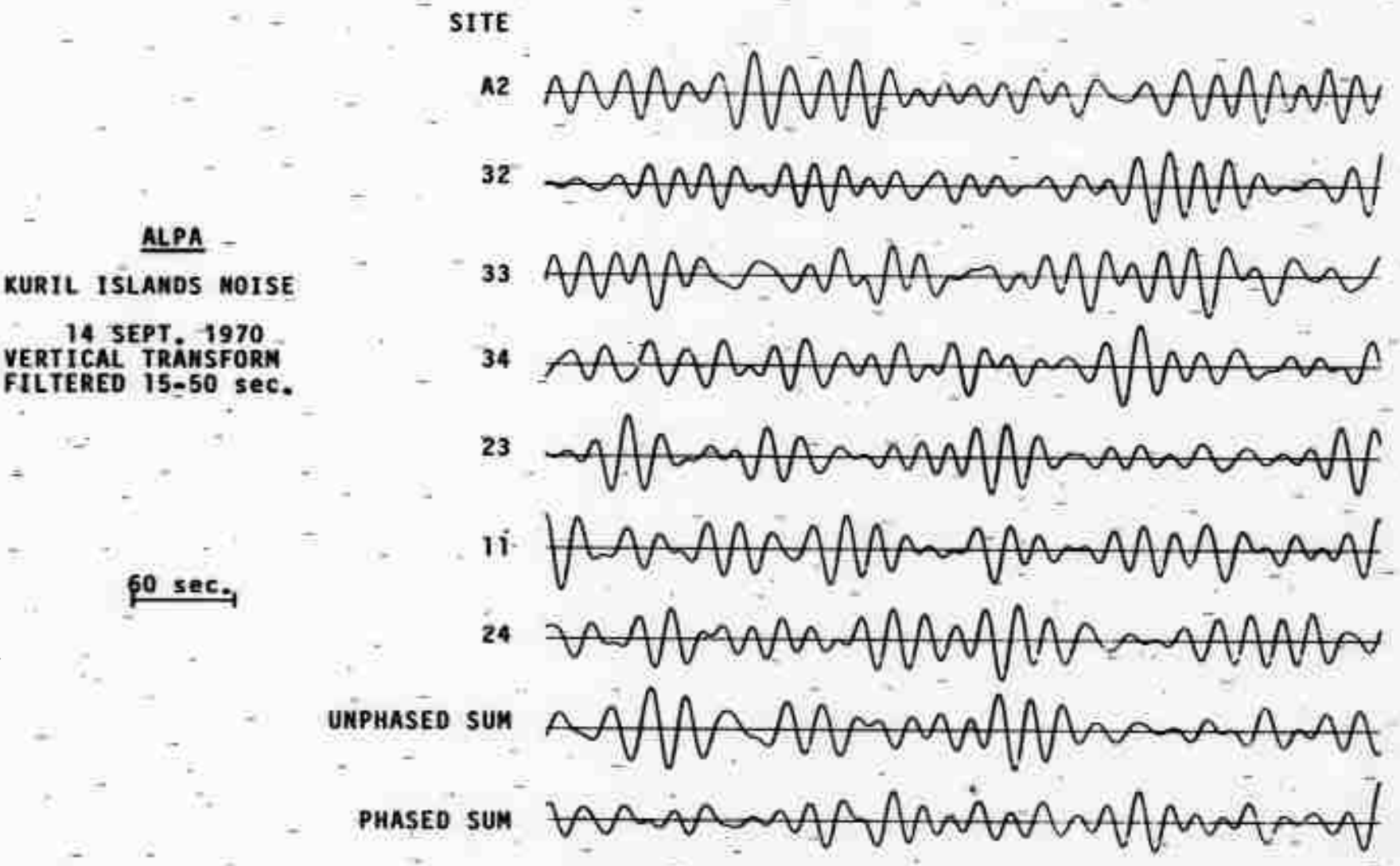

Figure 19. Processed noise before nine events.

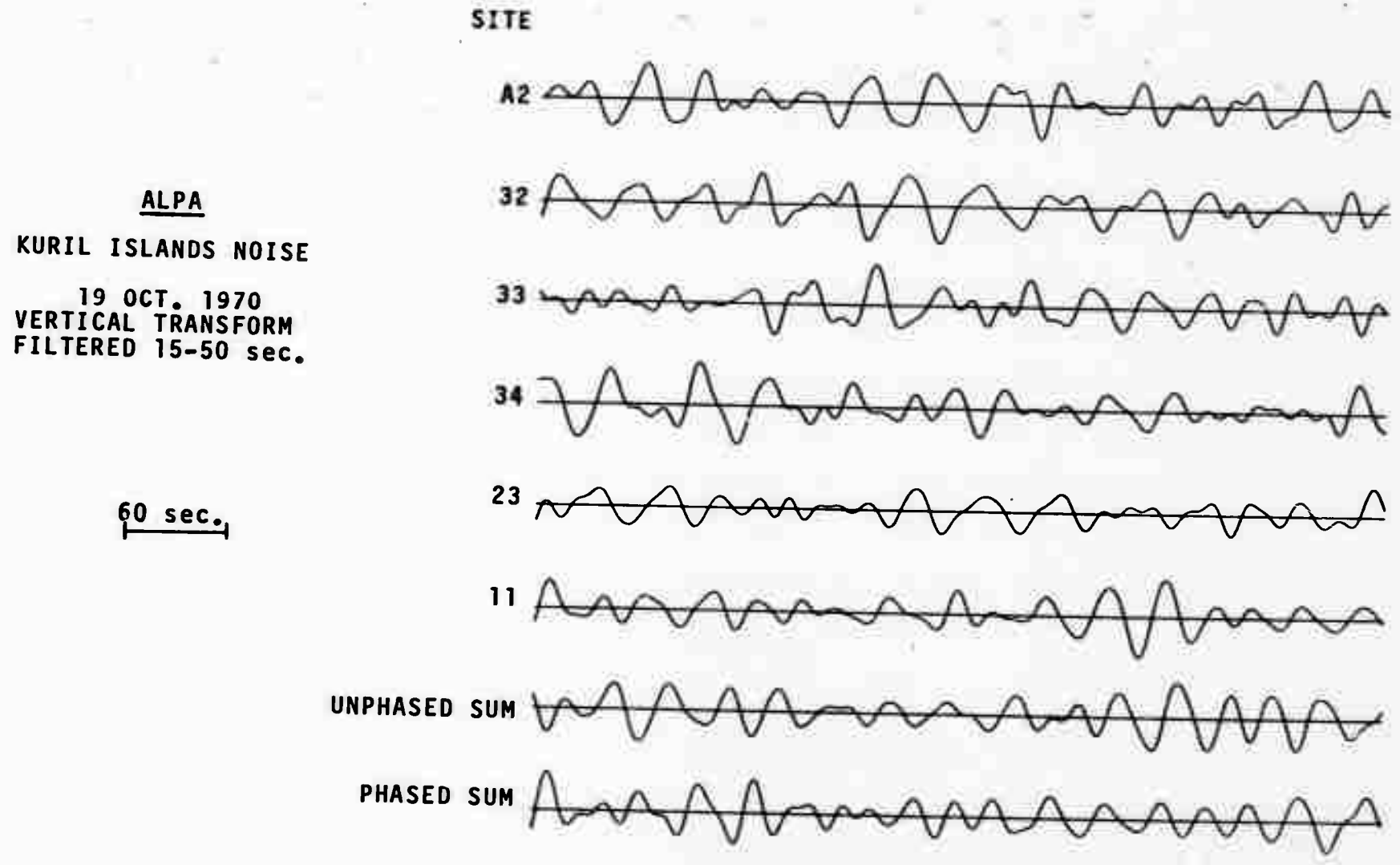

Figure 20. Processed noise before nine events.

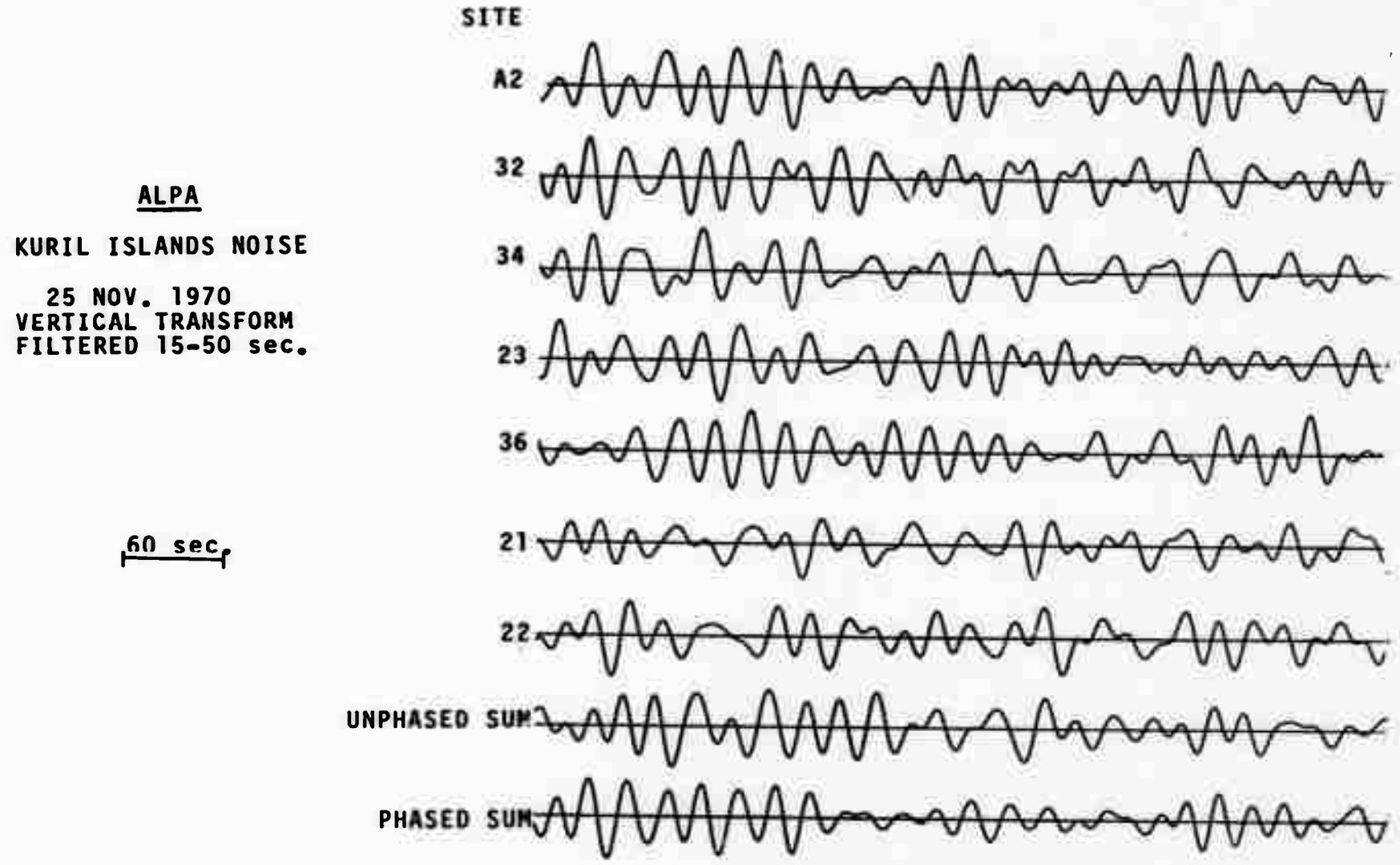

Figure 21. Processed noise before nine events.

ALPA

SINKIANG NOISE

17 OCT. 1970
VERTICAL TRANSFORM
FILTERED 15-50 sec.

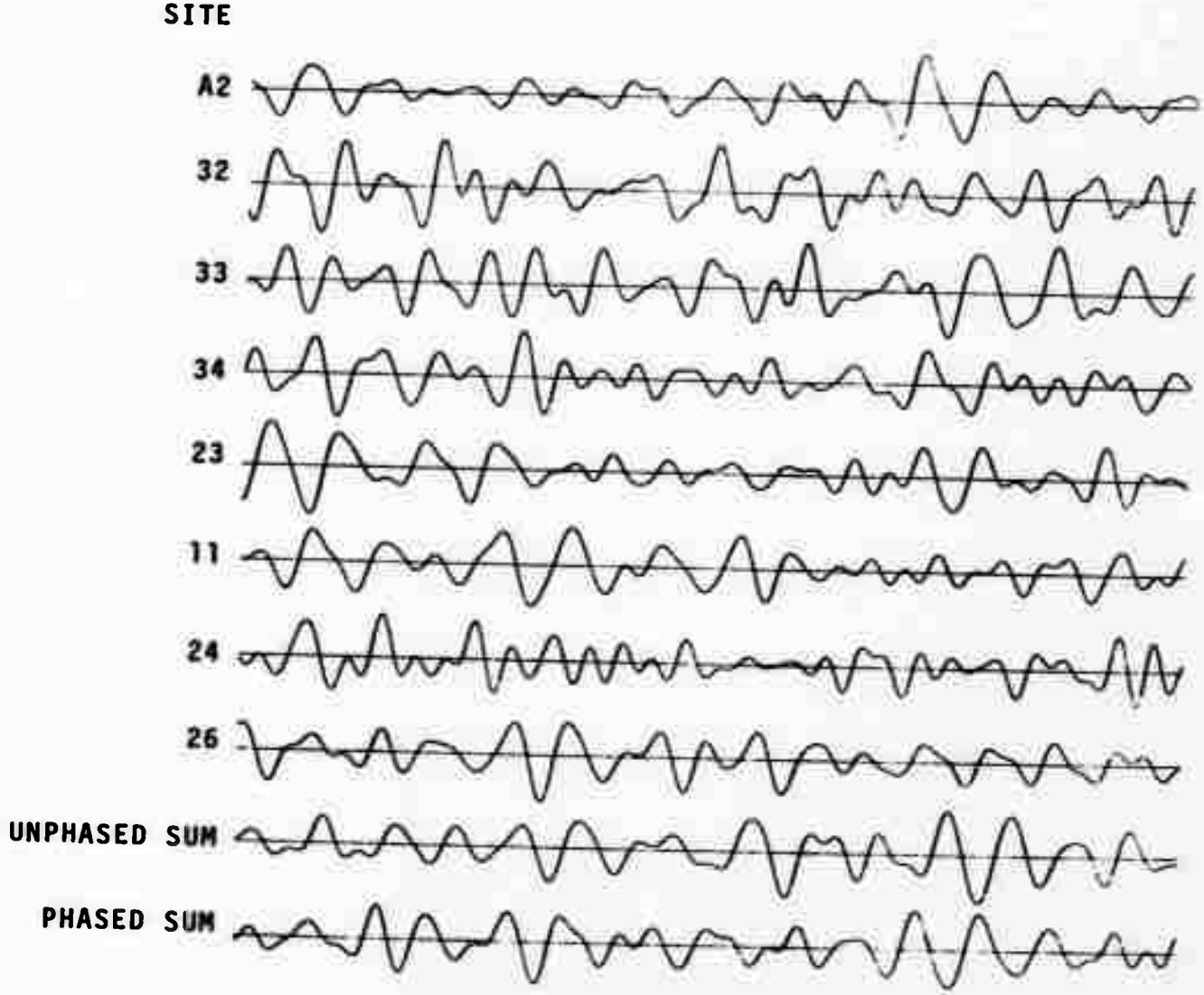

Figure 22. Processed noise before nine events.

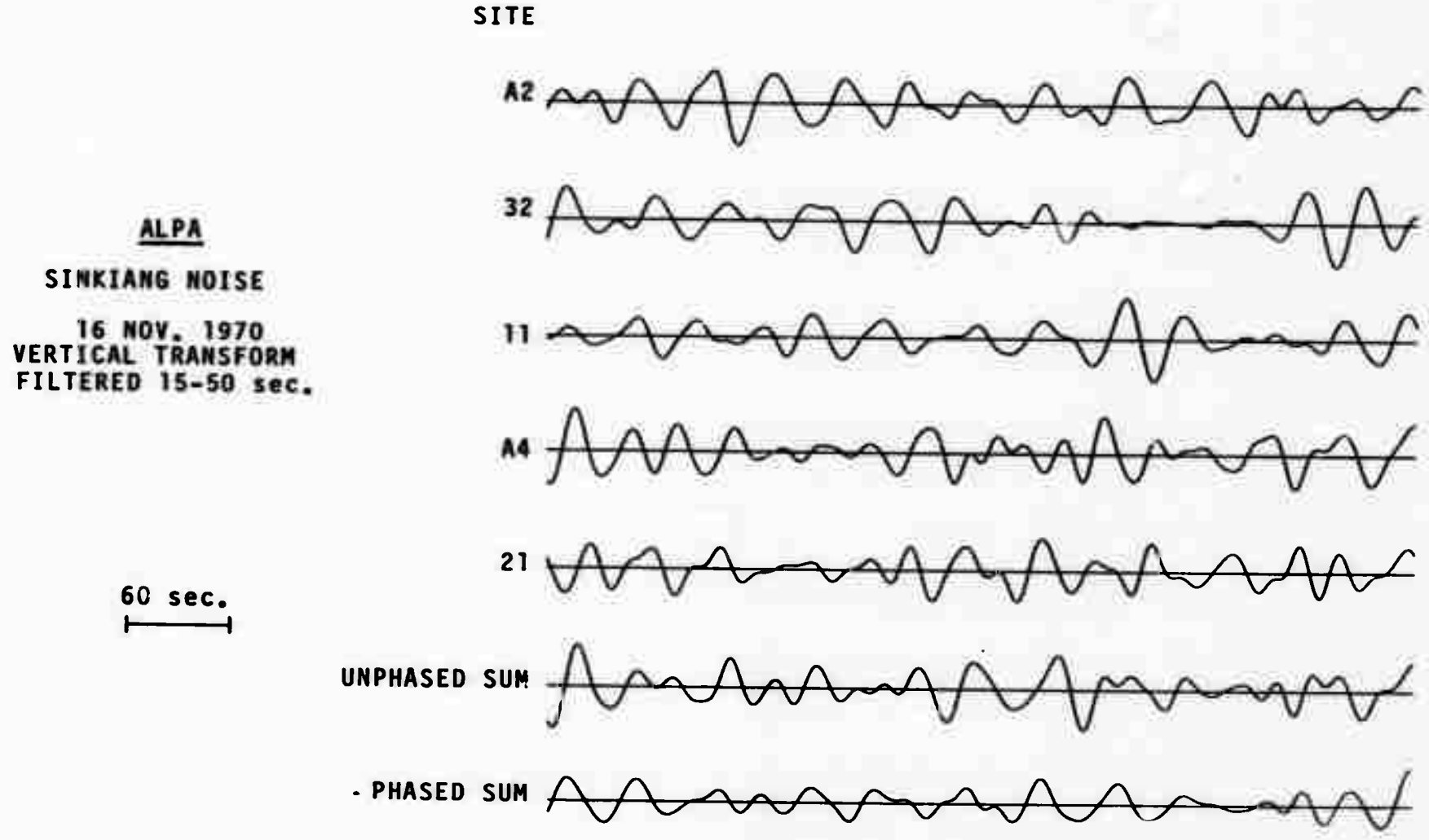

Figure 23. Processed noise before nine events.

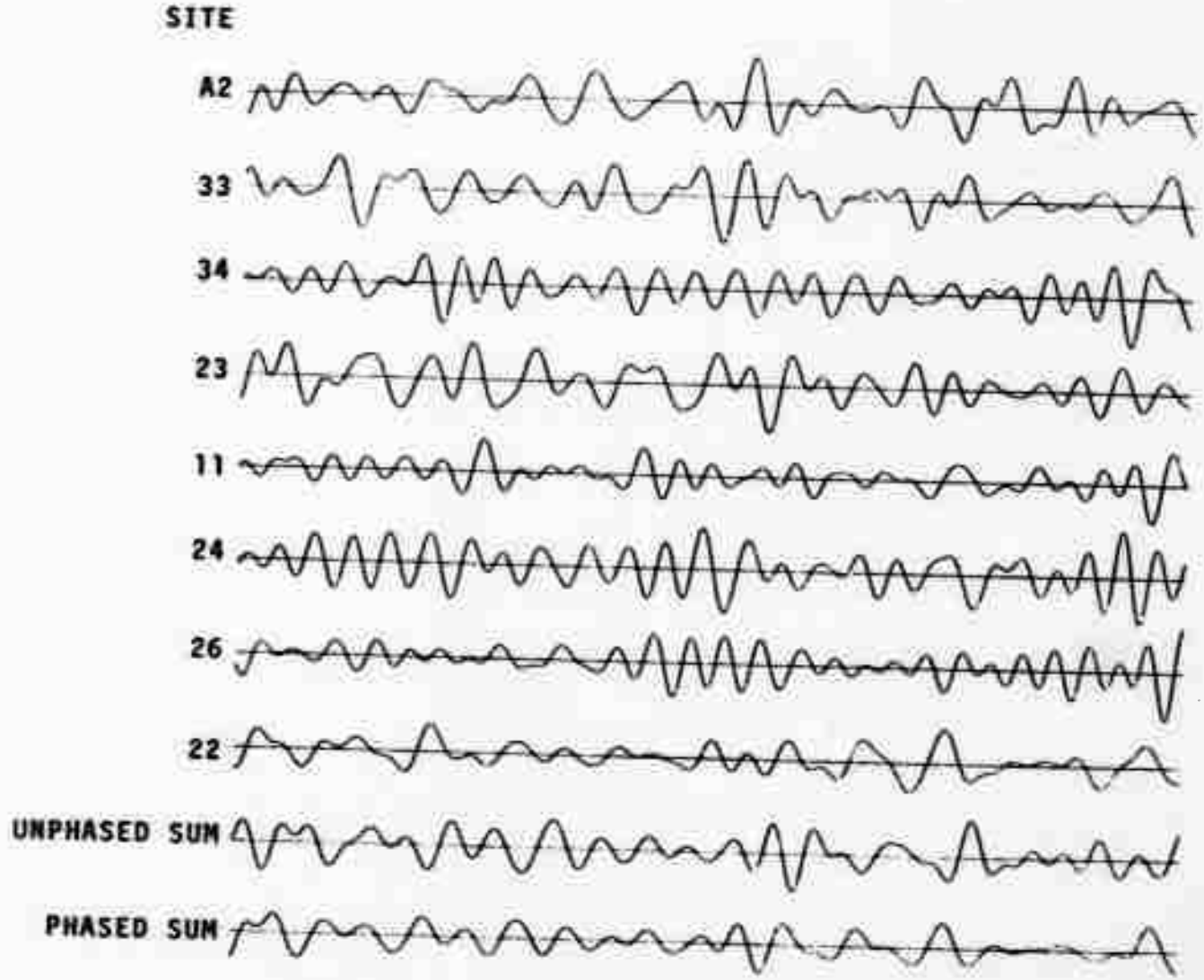

Figure 24. Processed noise before nine events.

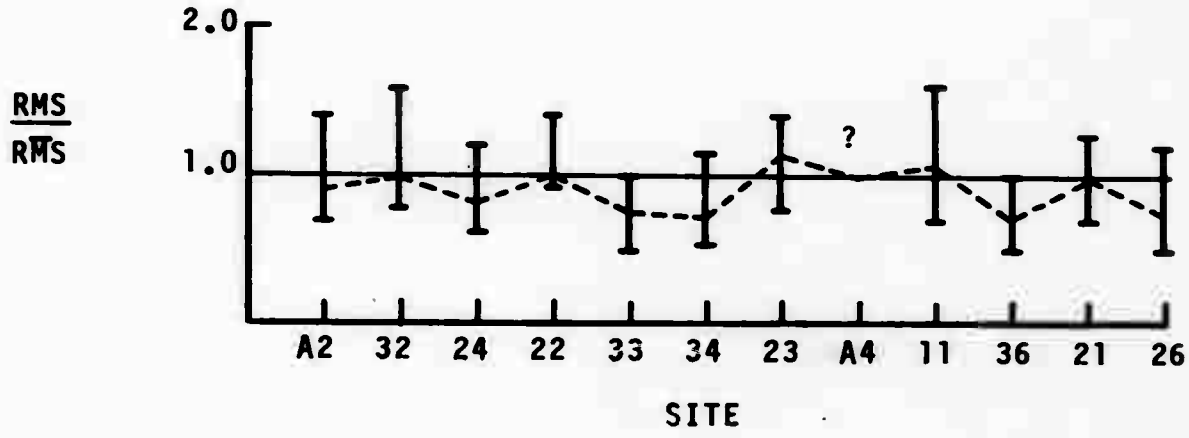

RANGE (SOLID LINES) AND MEAN (DASHED LINES) $\frac{RMS}{\bar{RMS}}$
NOISE LEVEL FOR ALPA SITES

Figure 25. Range and mean noise levels for ALPA sites.

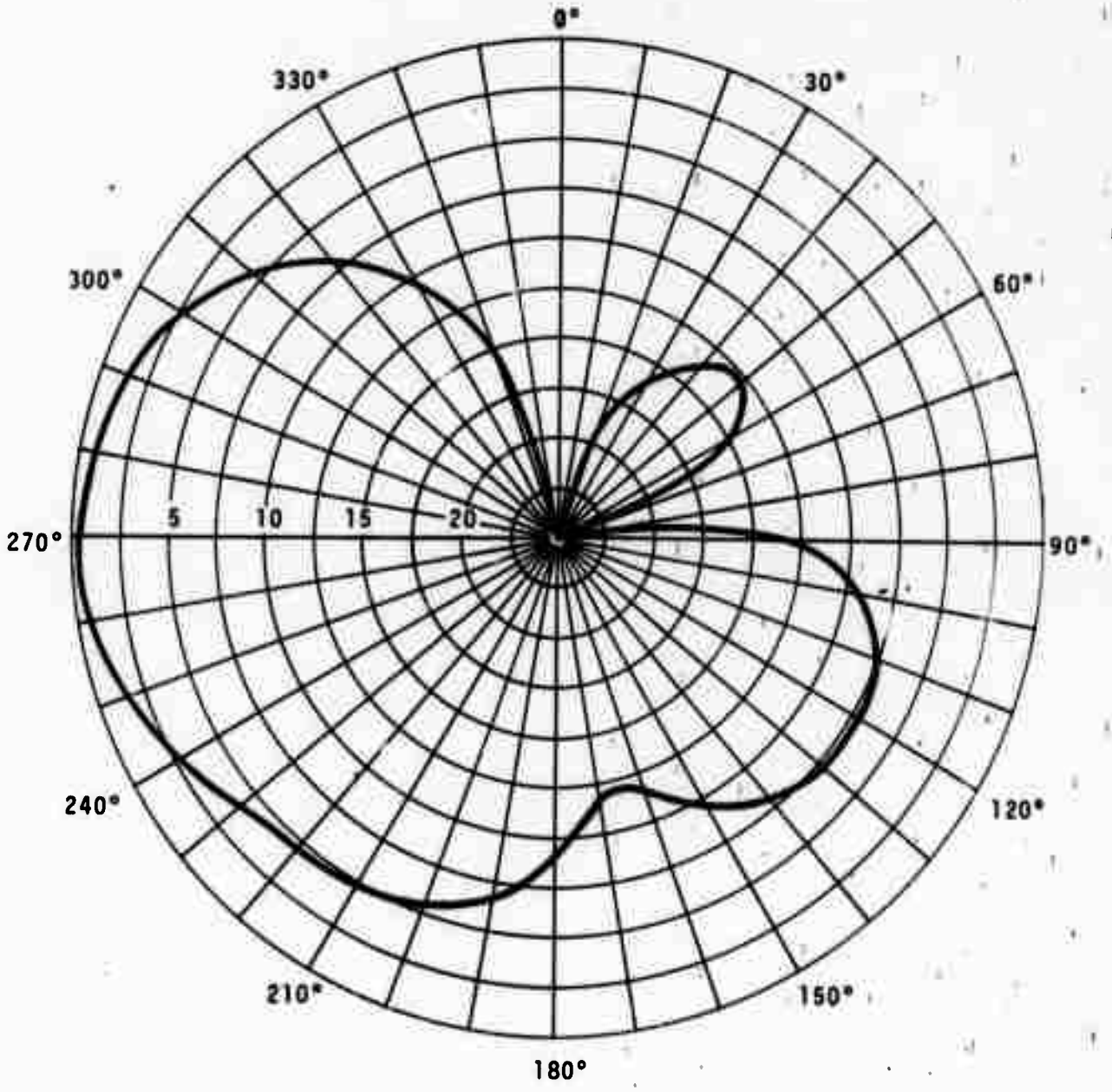

Figure 26. Array response of seven sites beamed toward Kamchatka.

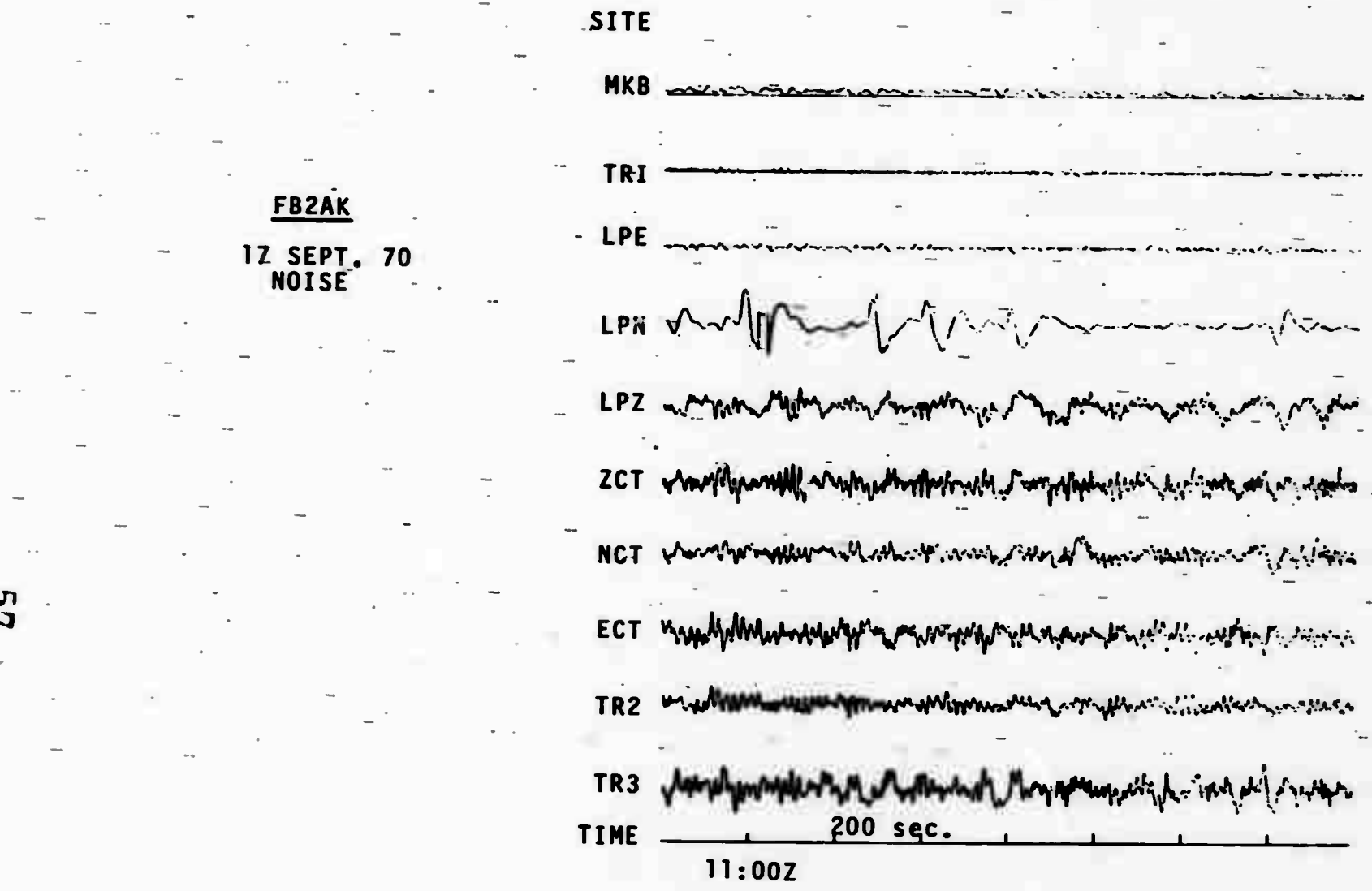

Figure 27. FBAK noise samples.

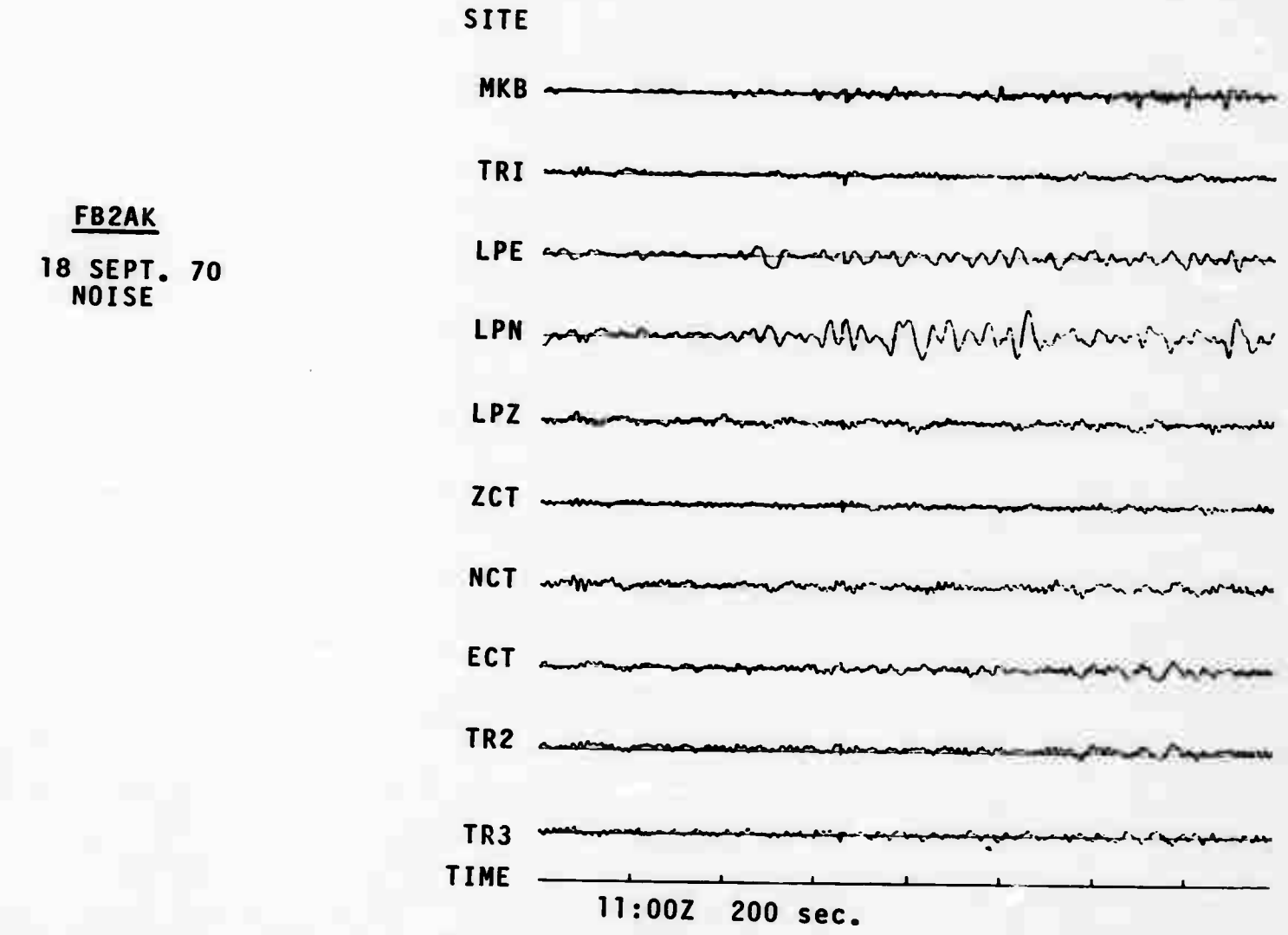

Figure 28. FBAK noise samples.

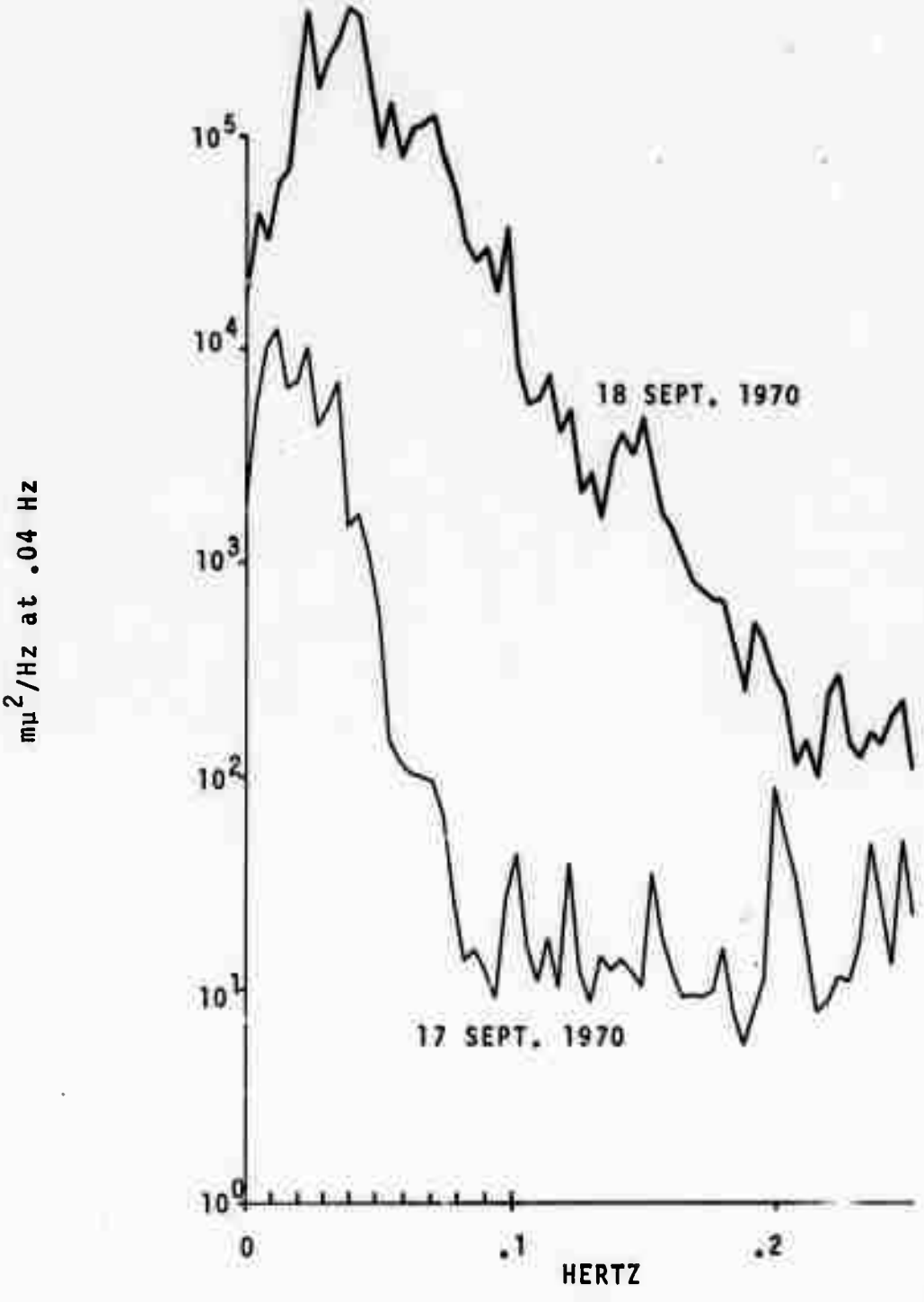

Figure 29. FBAK noise spectra of 17 and 18 September 1970 by channel.

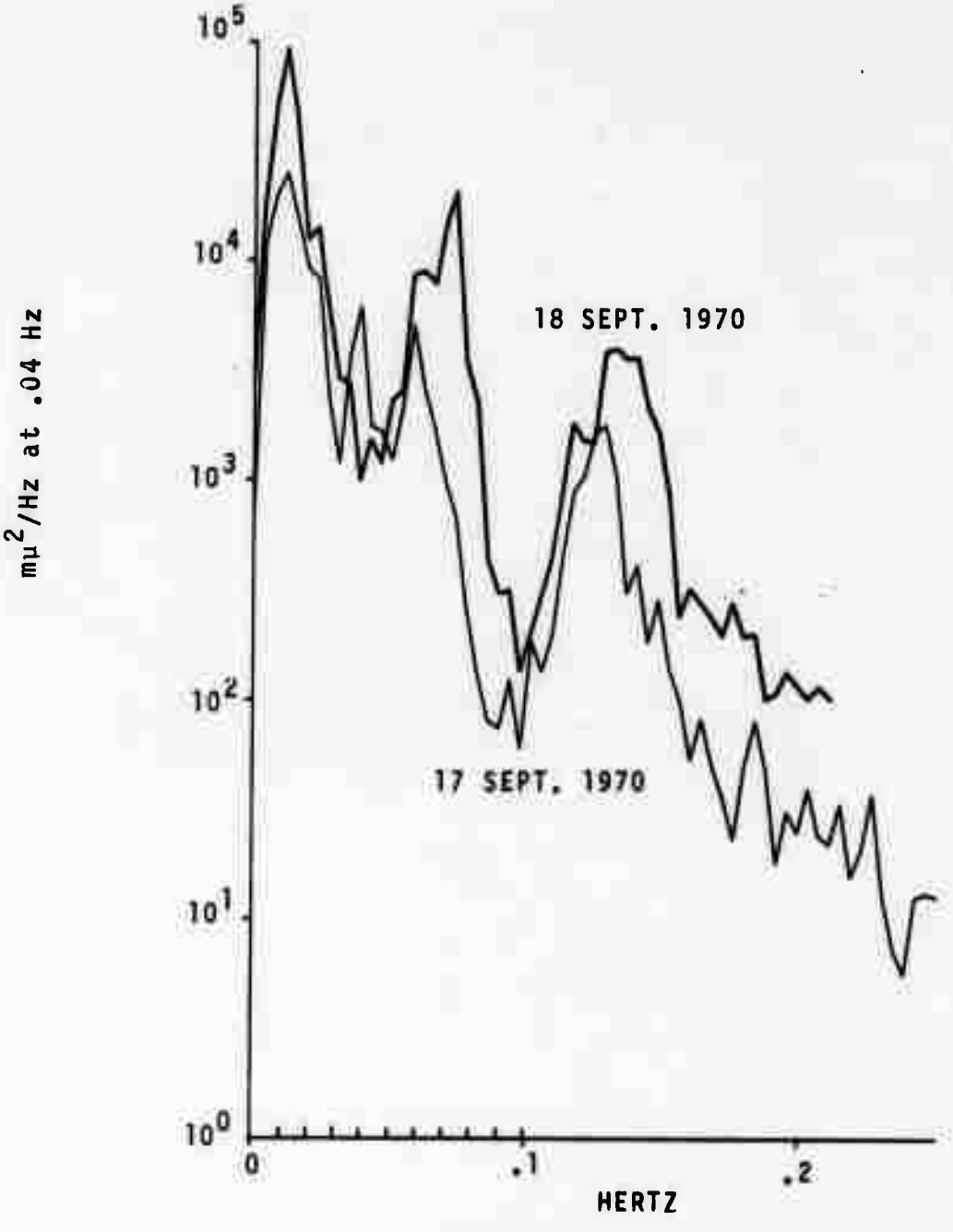

Figure 30. FBAK noise spectra of 17 and 18 September 1970 by channel.

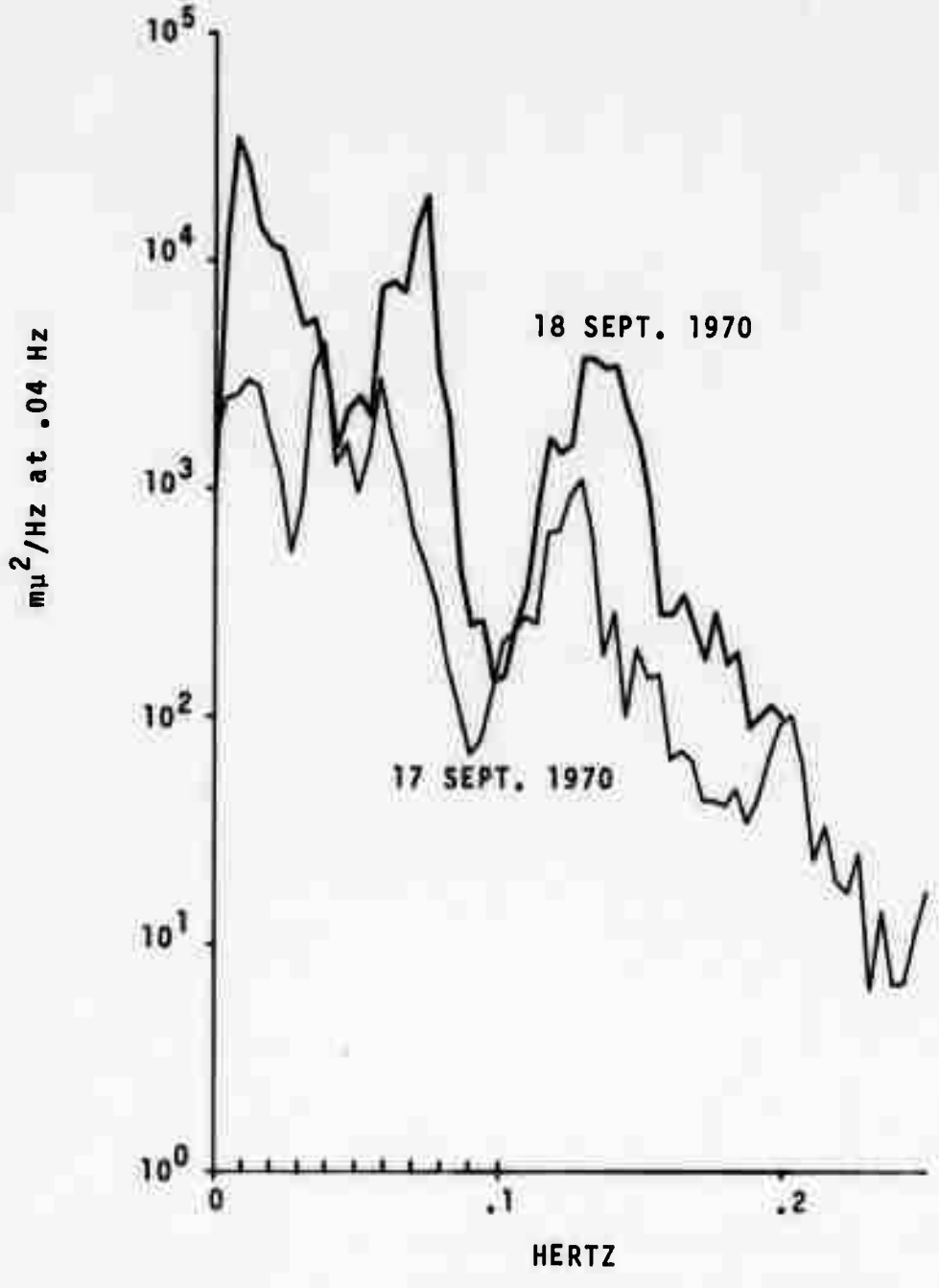

Figure 31. FBAK noise spectra of 17 and 18 September 1970 by channel.

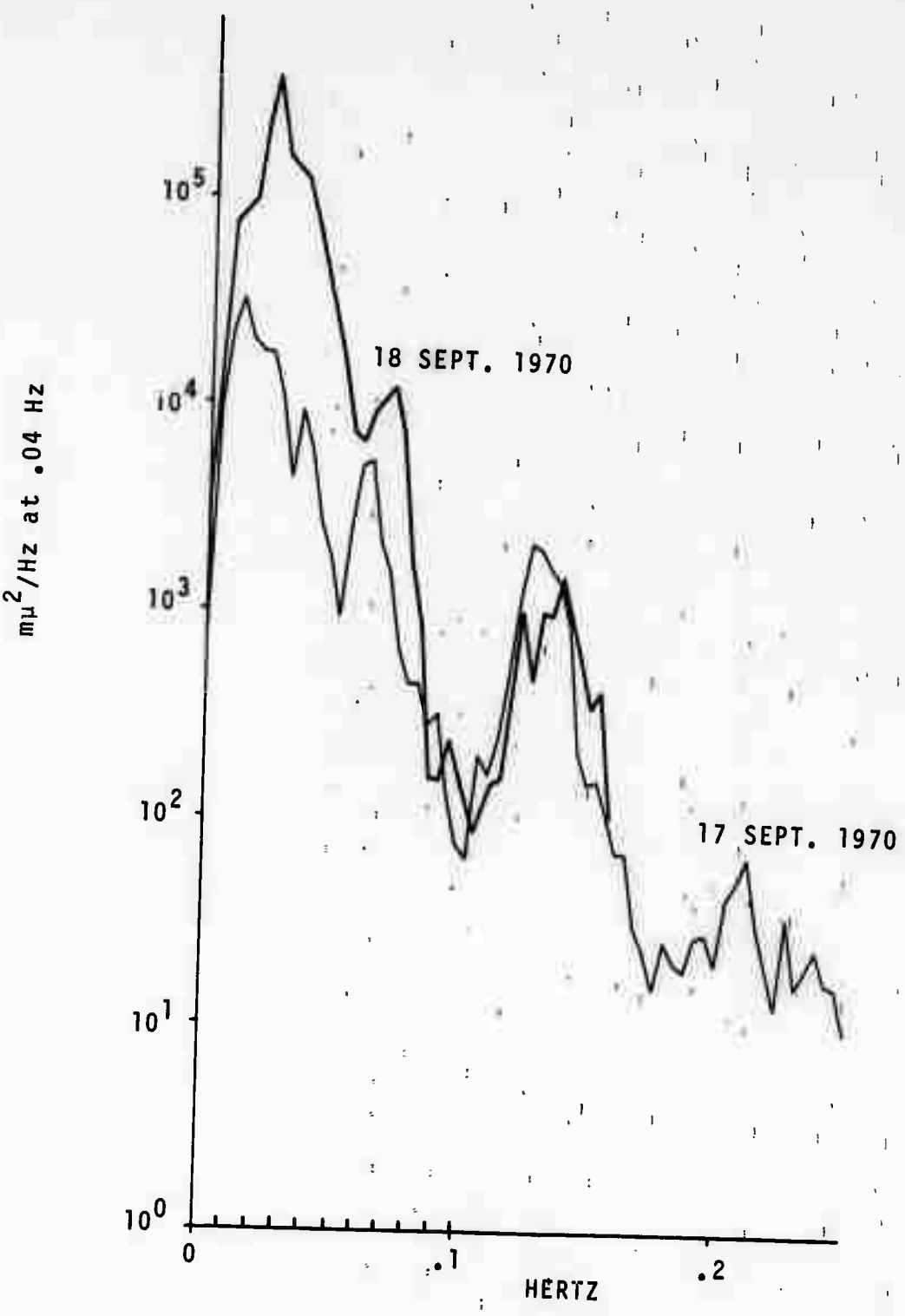

Figure 32. FBAK noise spectra of 17 and 18 September 1970 by channel.

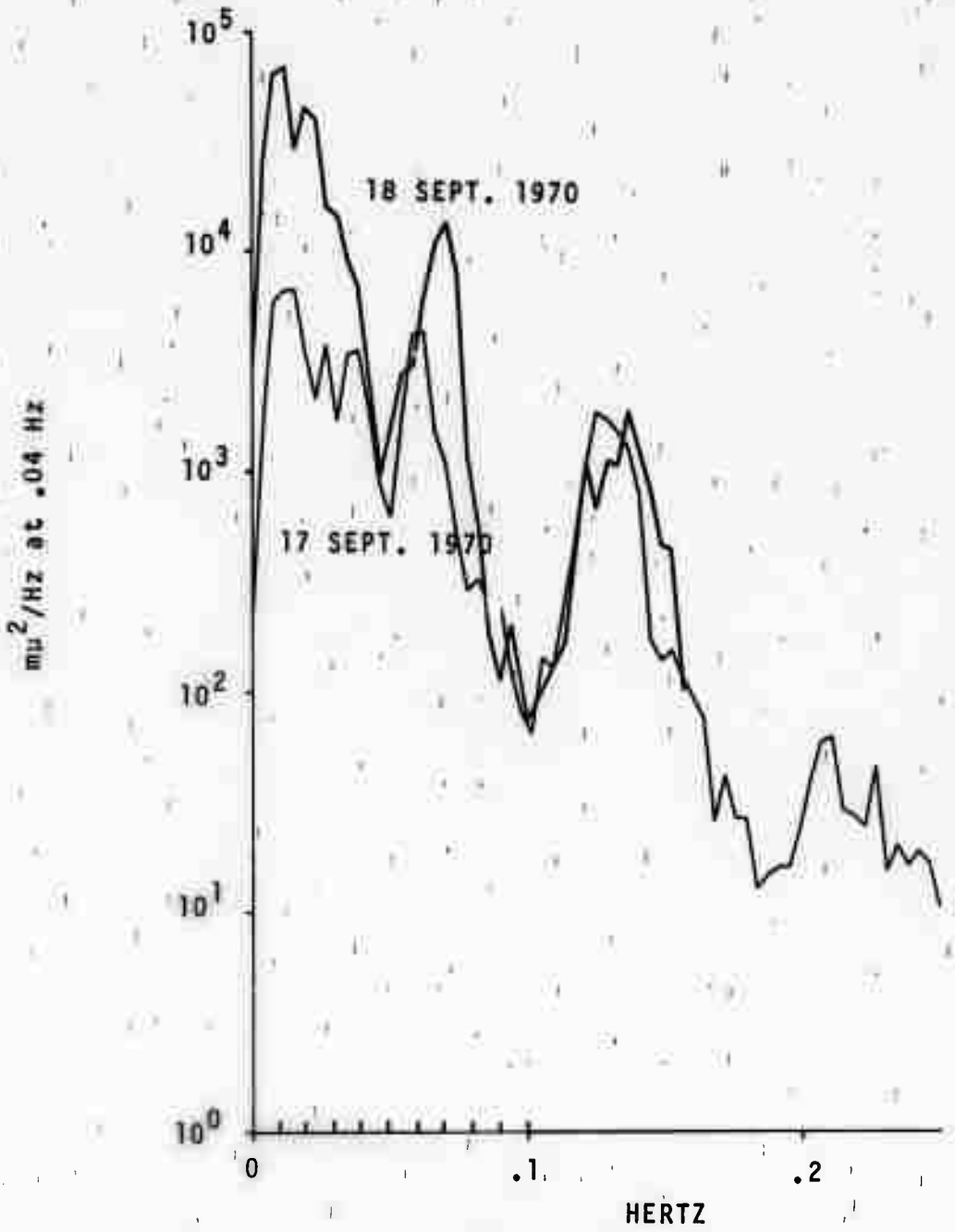

Figure 33. FBAK noise spectra of 17 and 18 September 1970 by channel.

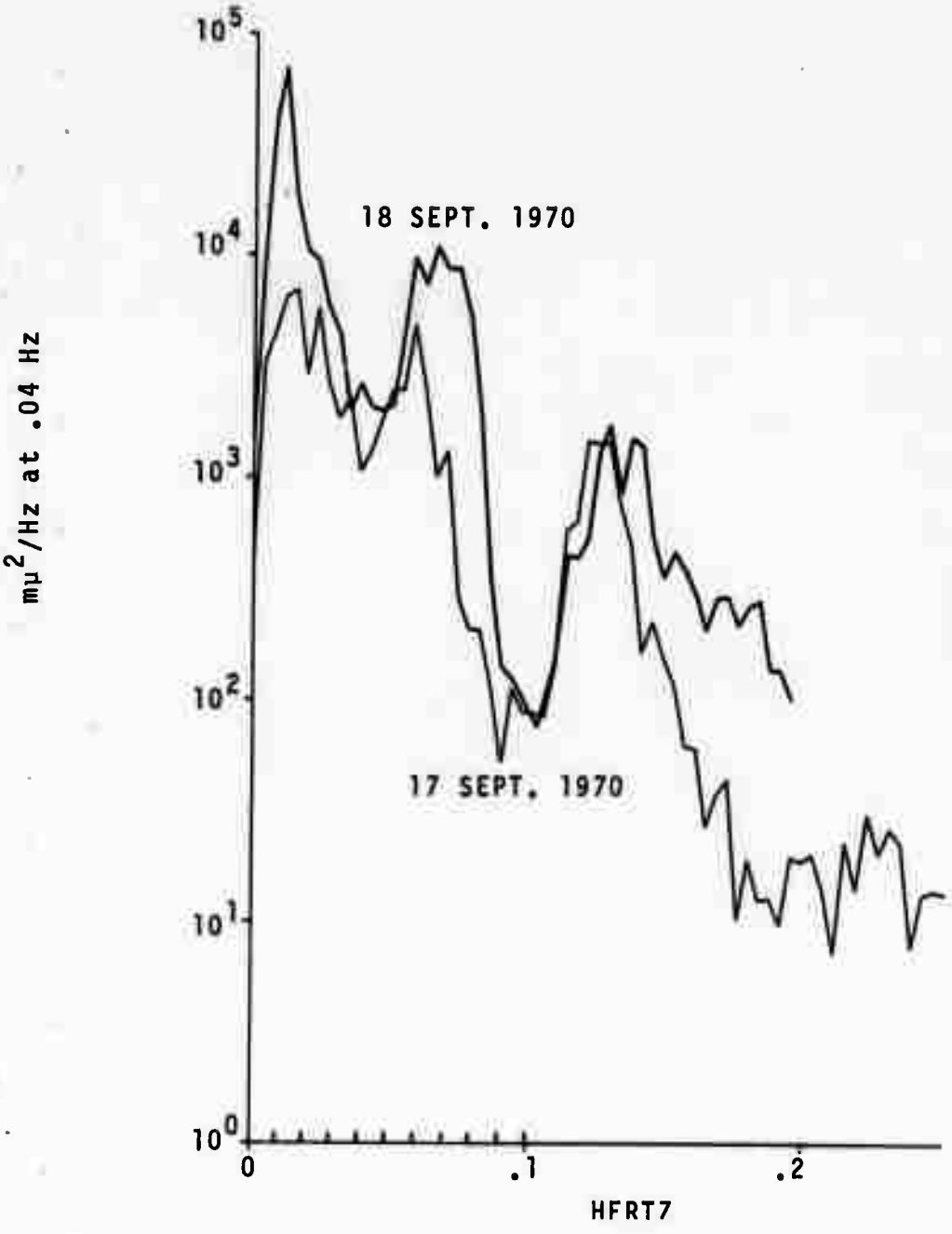

Figure 34. FBAK noise spectra of 17 and 18 September 1970 by channel.

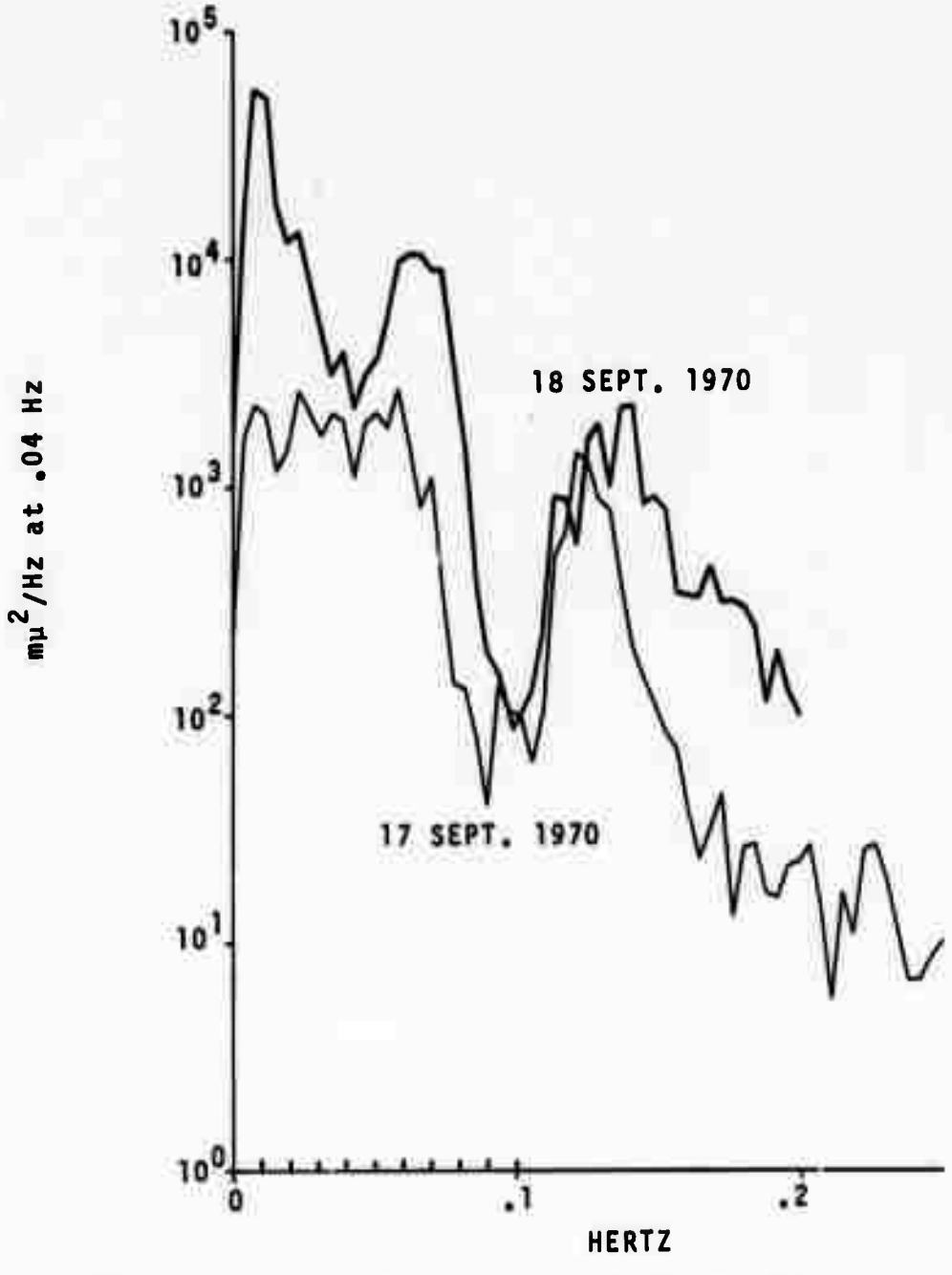

Figure 35. FBAK noise spectra of 17 and 18 September 1970 by channel.

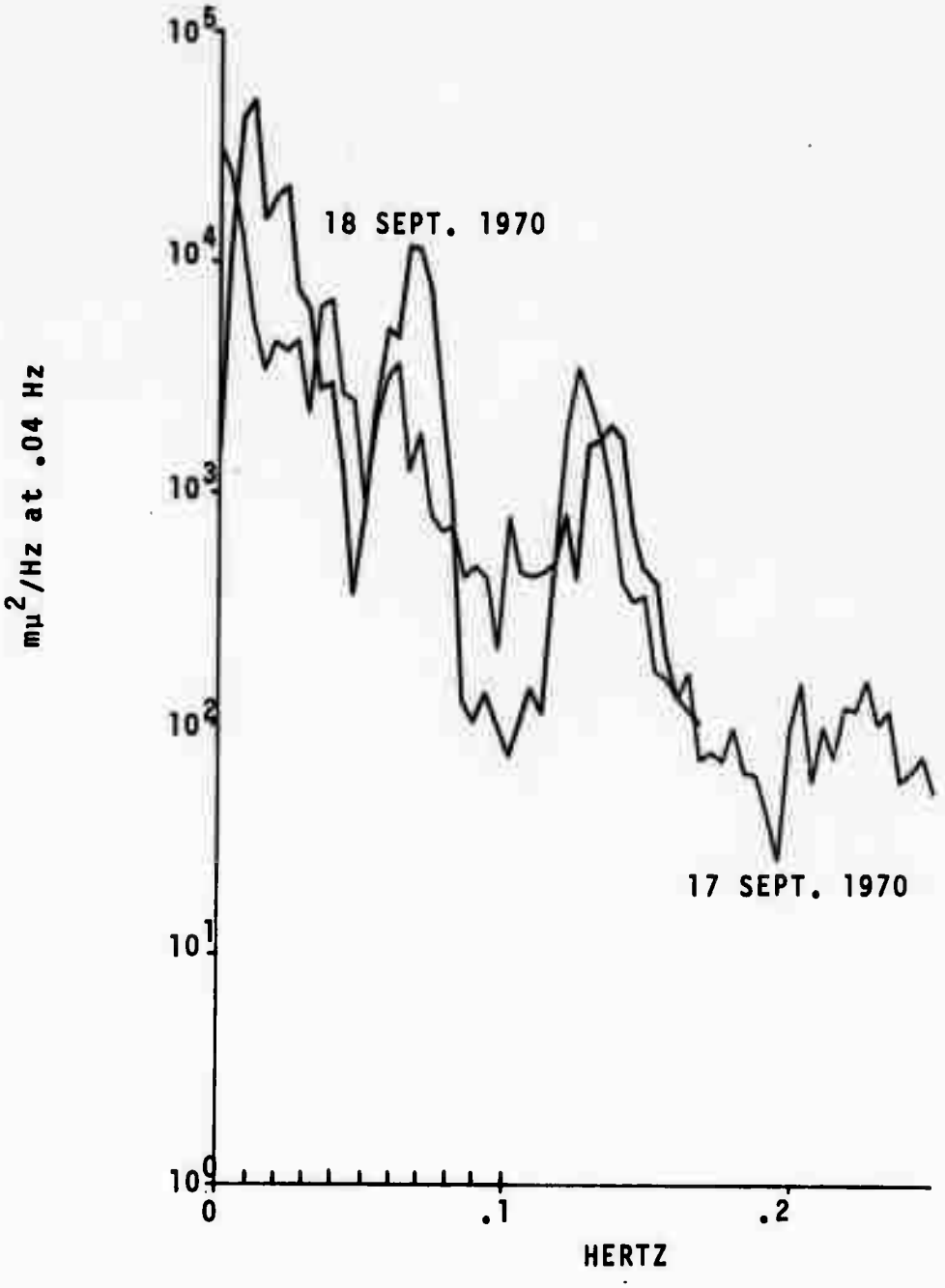

Figure 36. FBAK noise spectra of 17 and 18 September 1970 by channel.

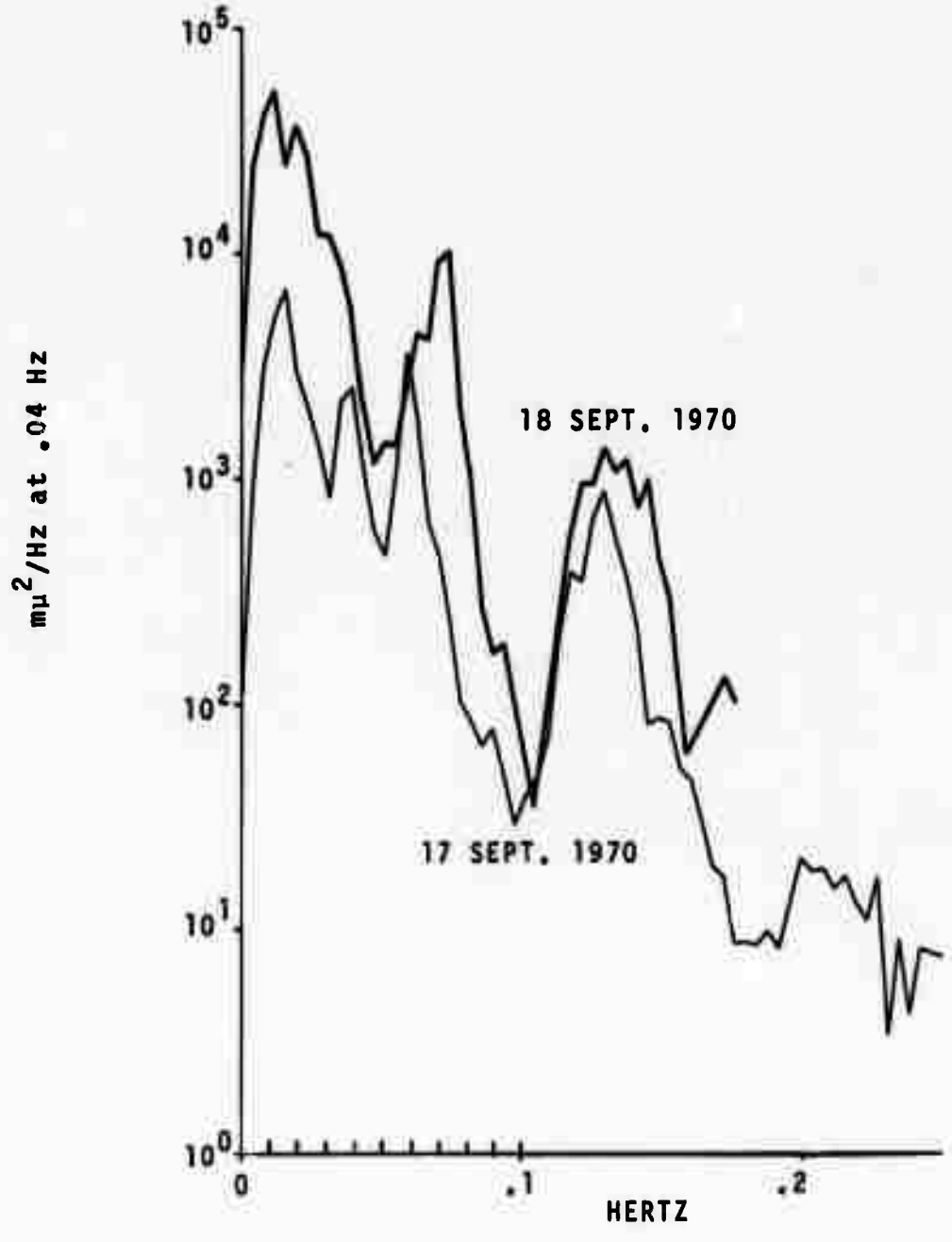

Figure 37. FBAK noise spectra of 17 and 18 September 1970 by channel.

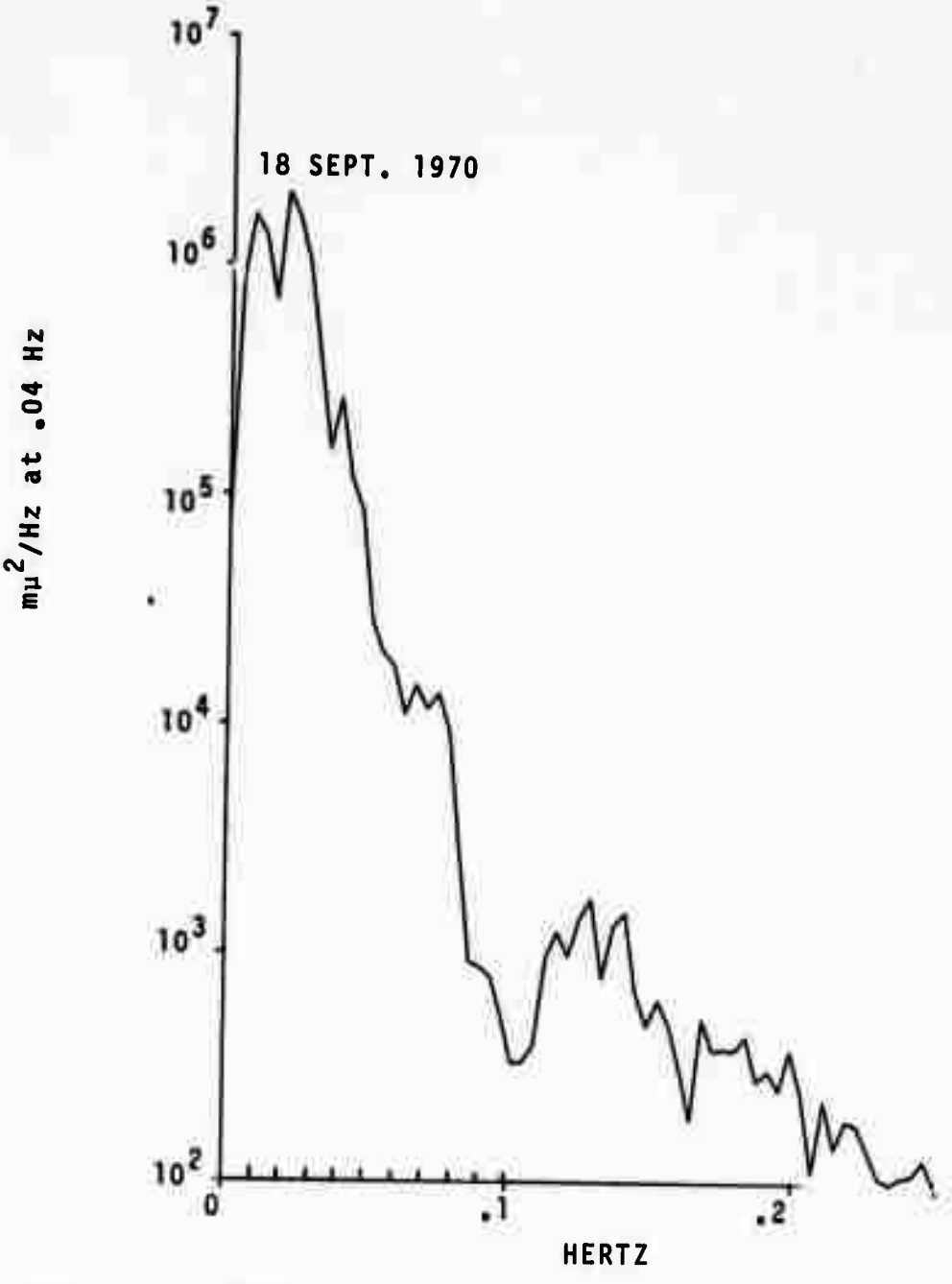

Figure 38. FBAK noise spectra of 17 and 18 September 1970 by channel.

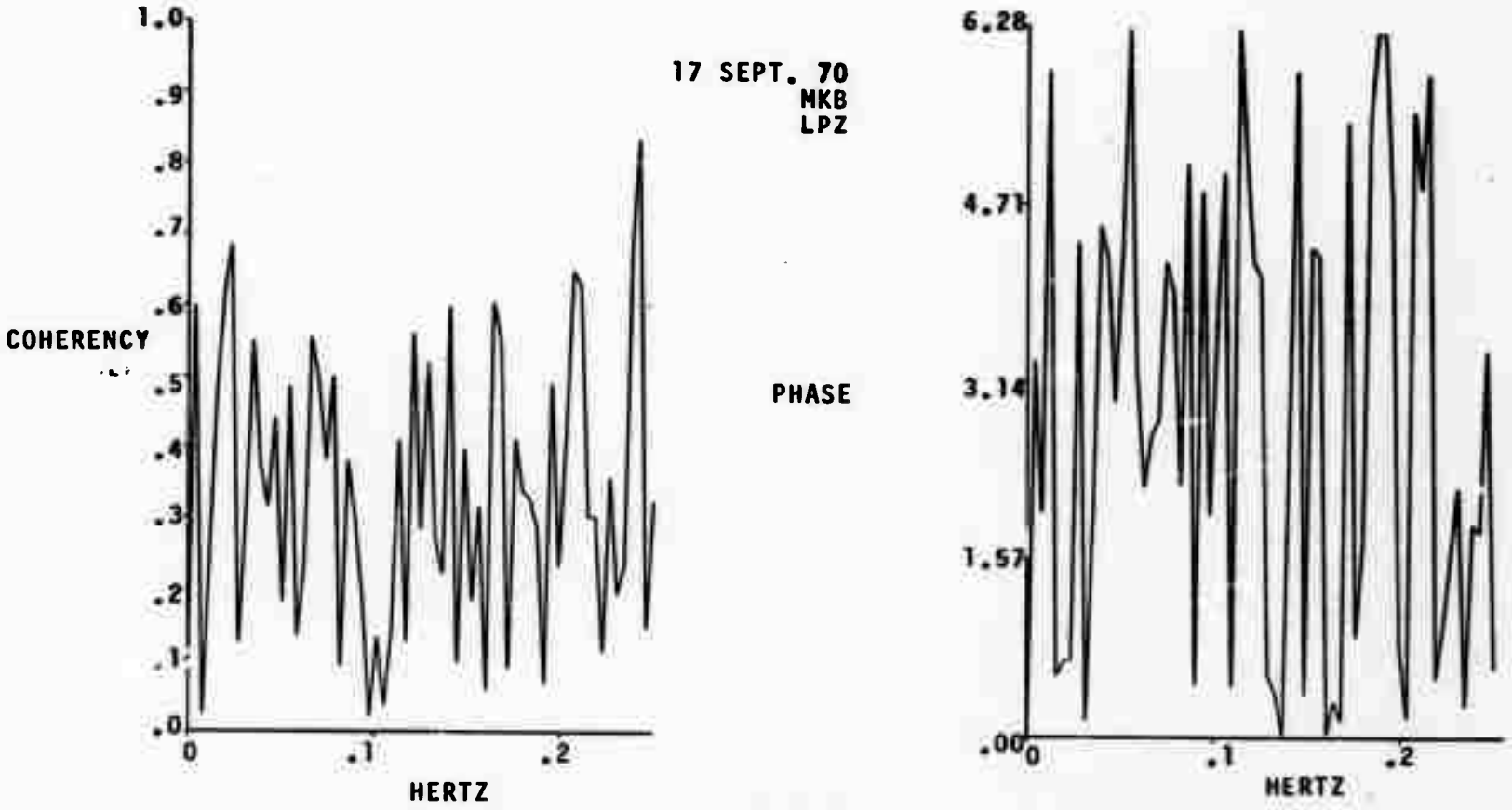

Figure 39. Coherencey and phase of 17 and 18 September 1970 noise by channel.

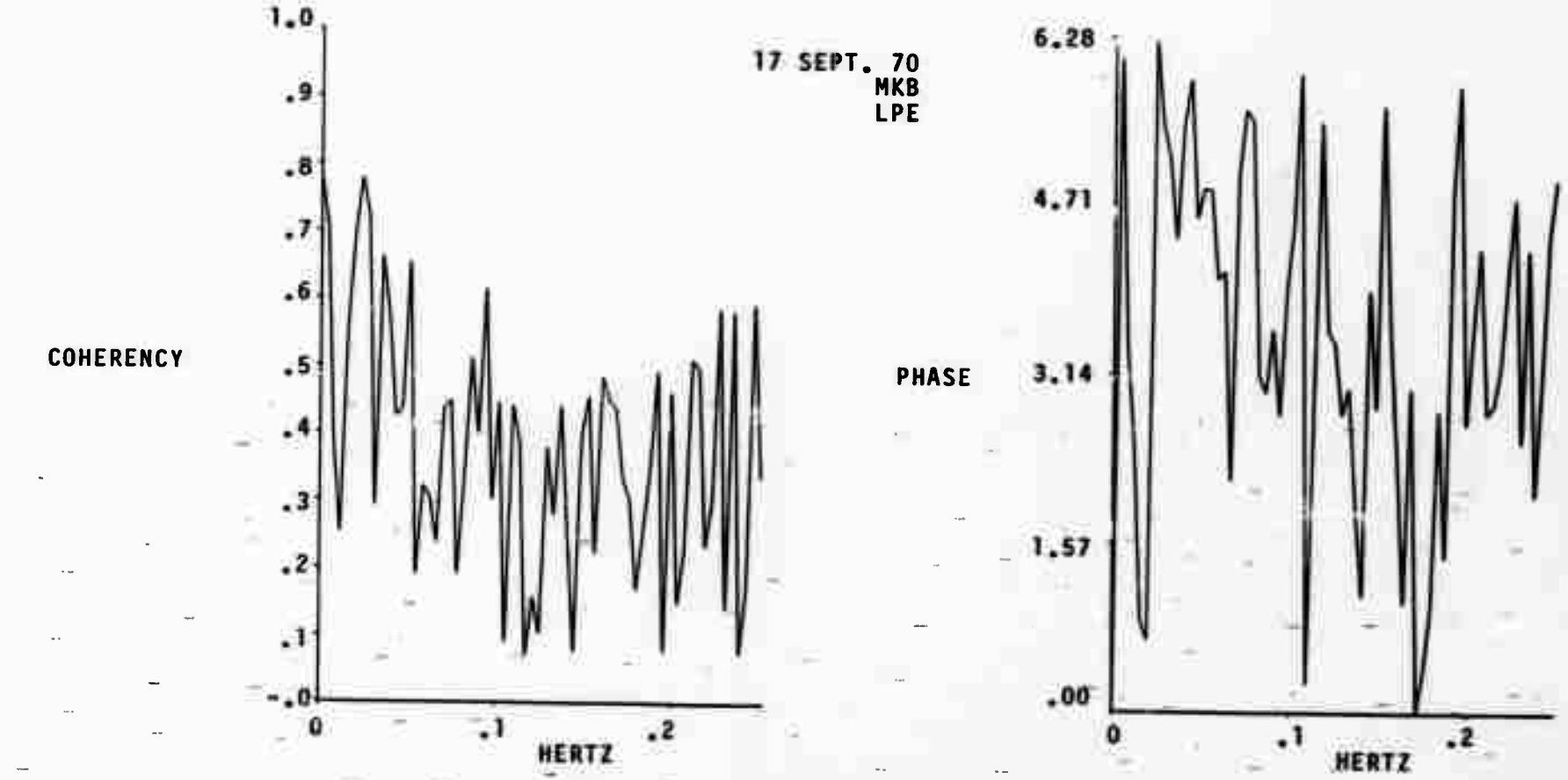

Figure 40. Coherency and phase of 17 and 18 September 1970 noise by channel.

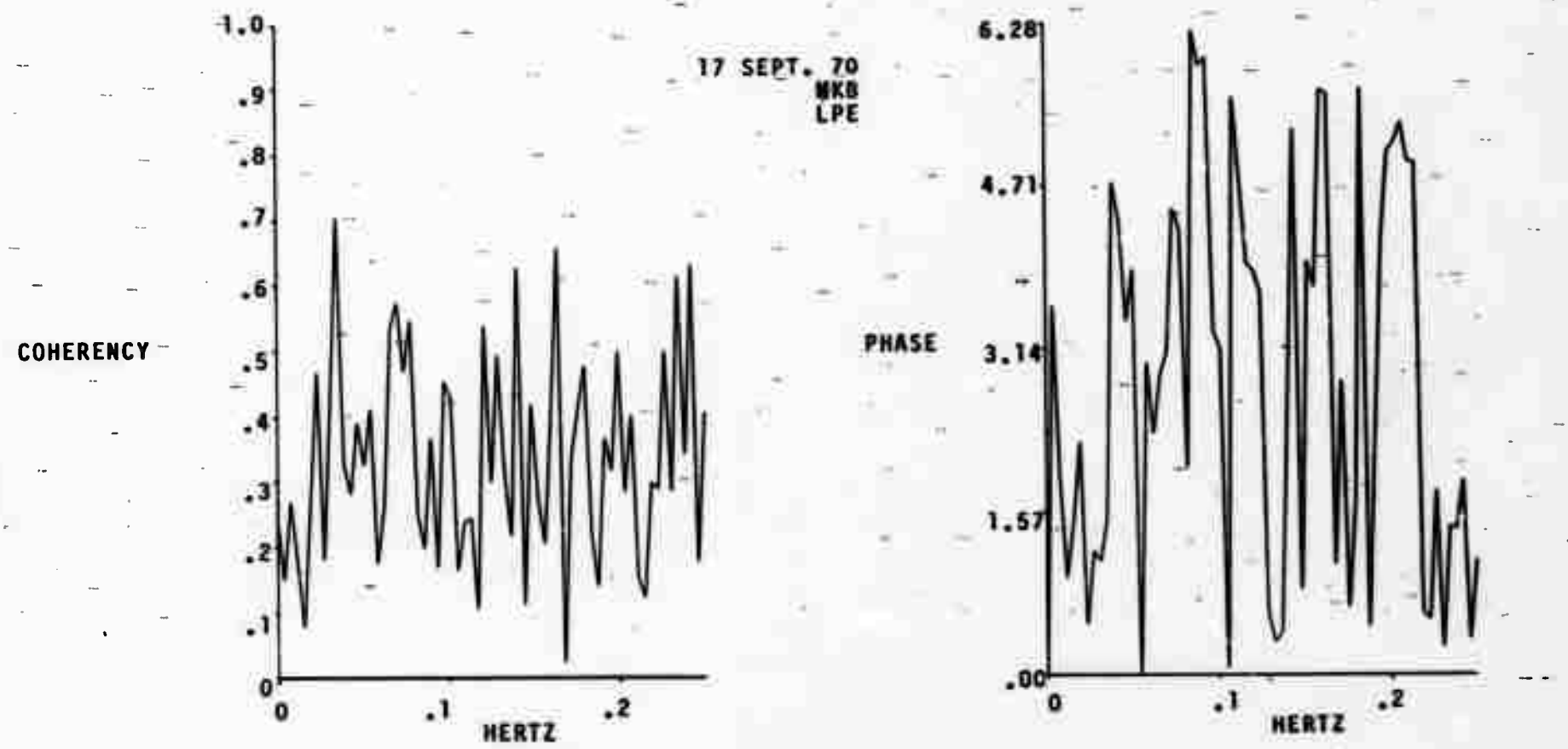

Figure 41. Coherency and phase of 17 and 18 September 1970 noise by channel.

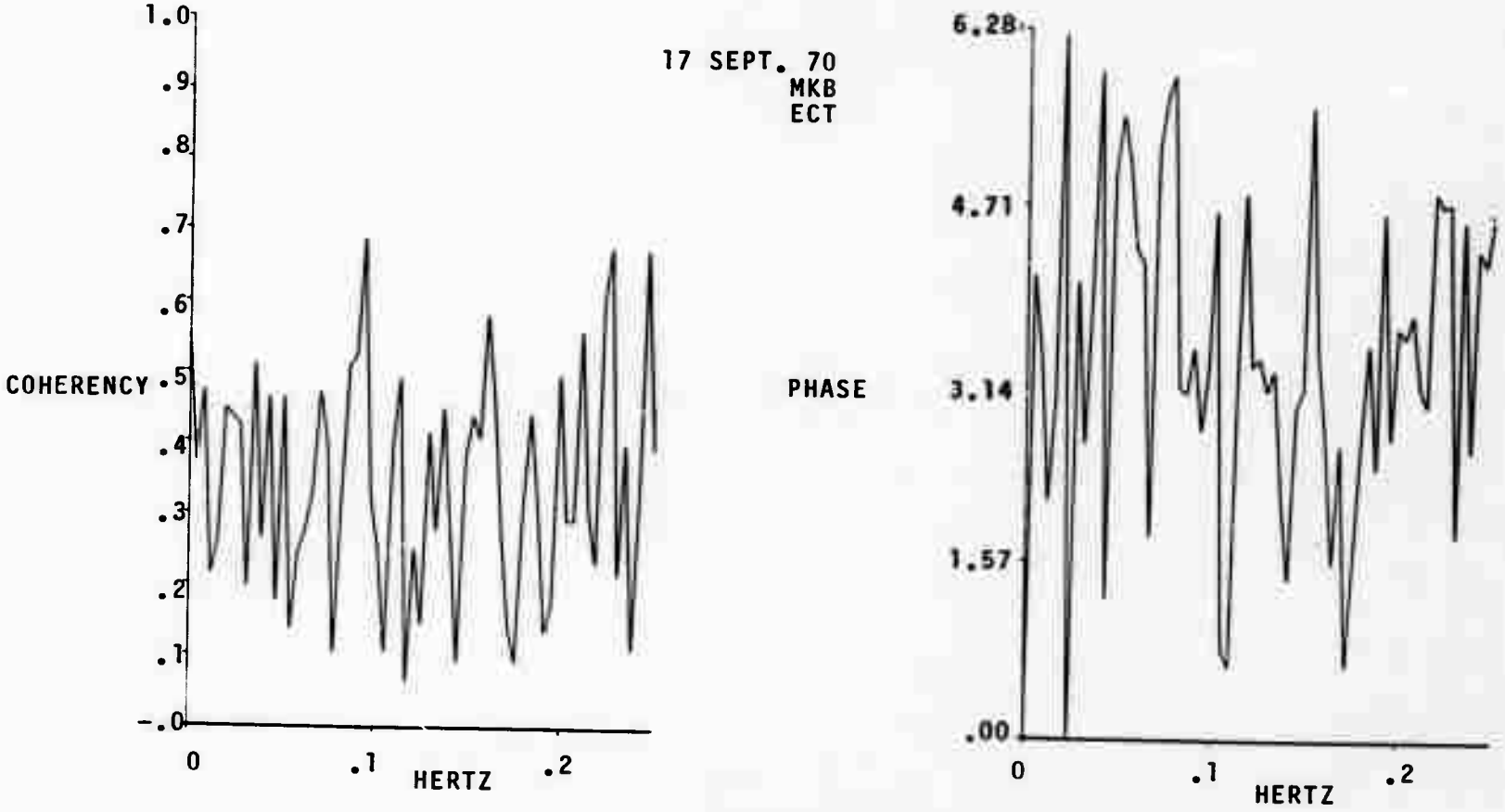

Figure 42. Coherency and phase of 17 and 18 September 1970 noise by channel.

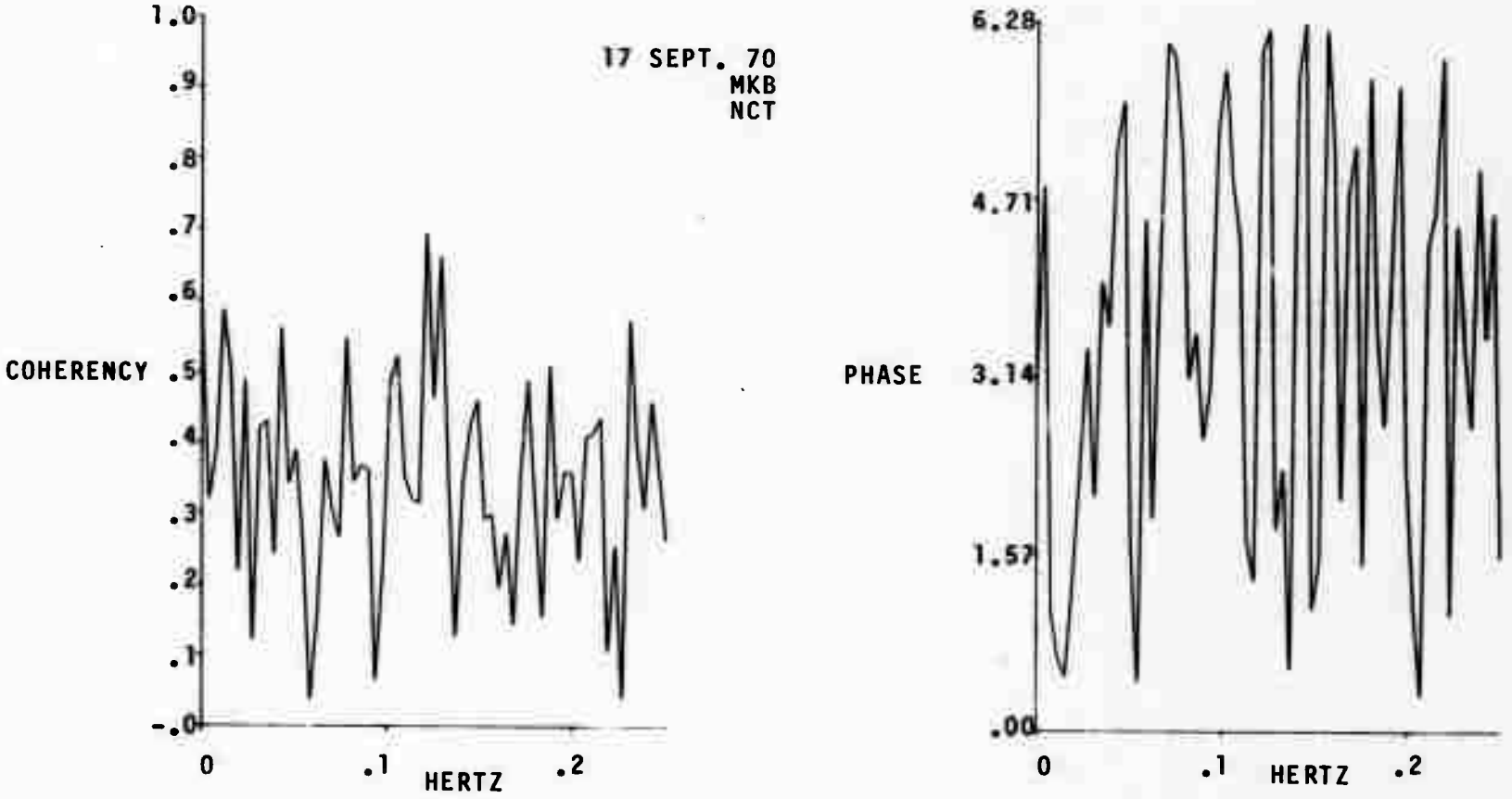

Figure 43. Coherency and phase of 17 and 18 September 1970 noise by channel.

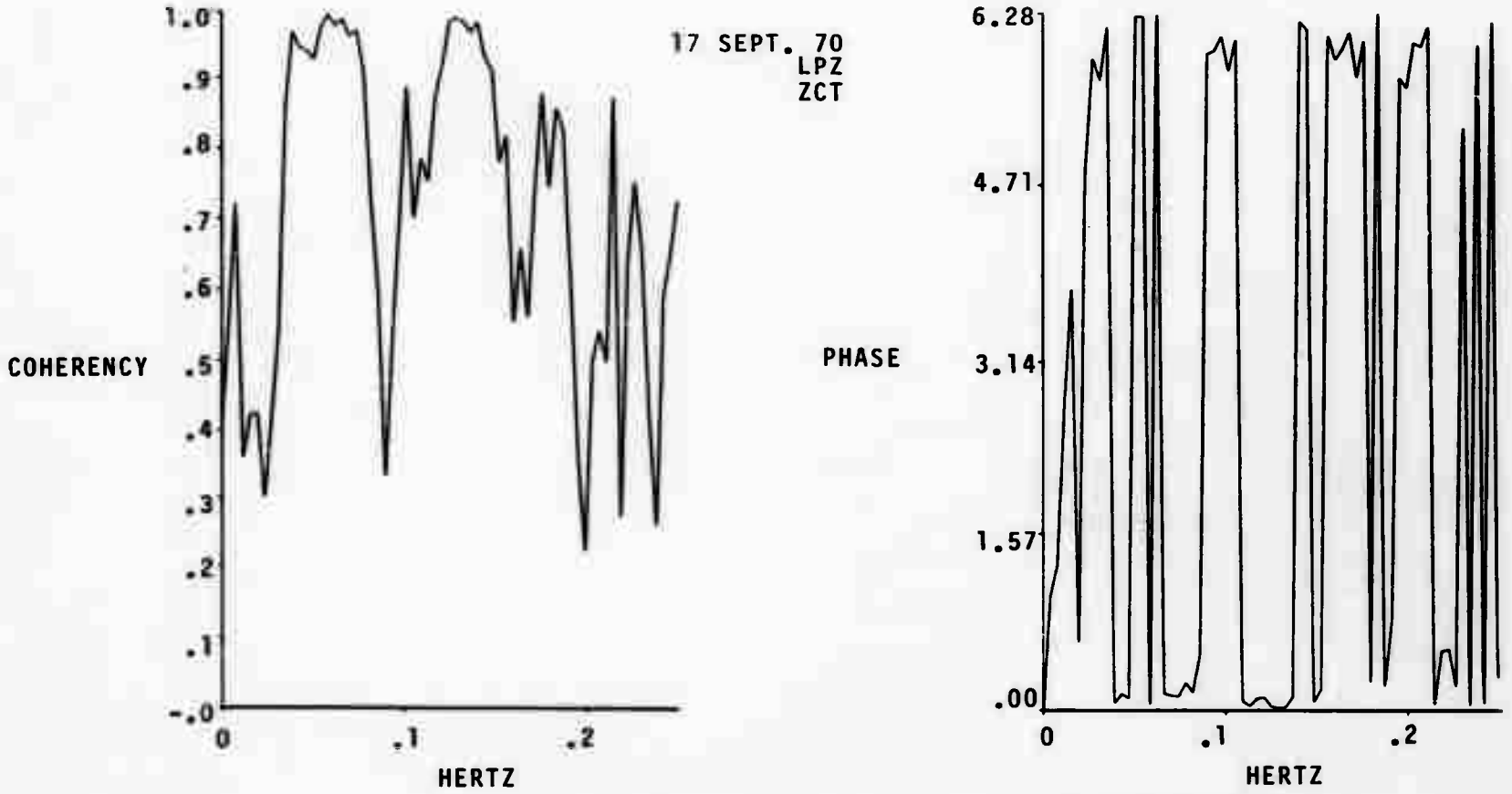

Figure 44. Coherency and phase of 17 and 18 September 1970 noise by channel.

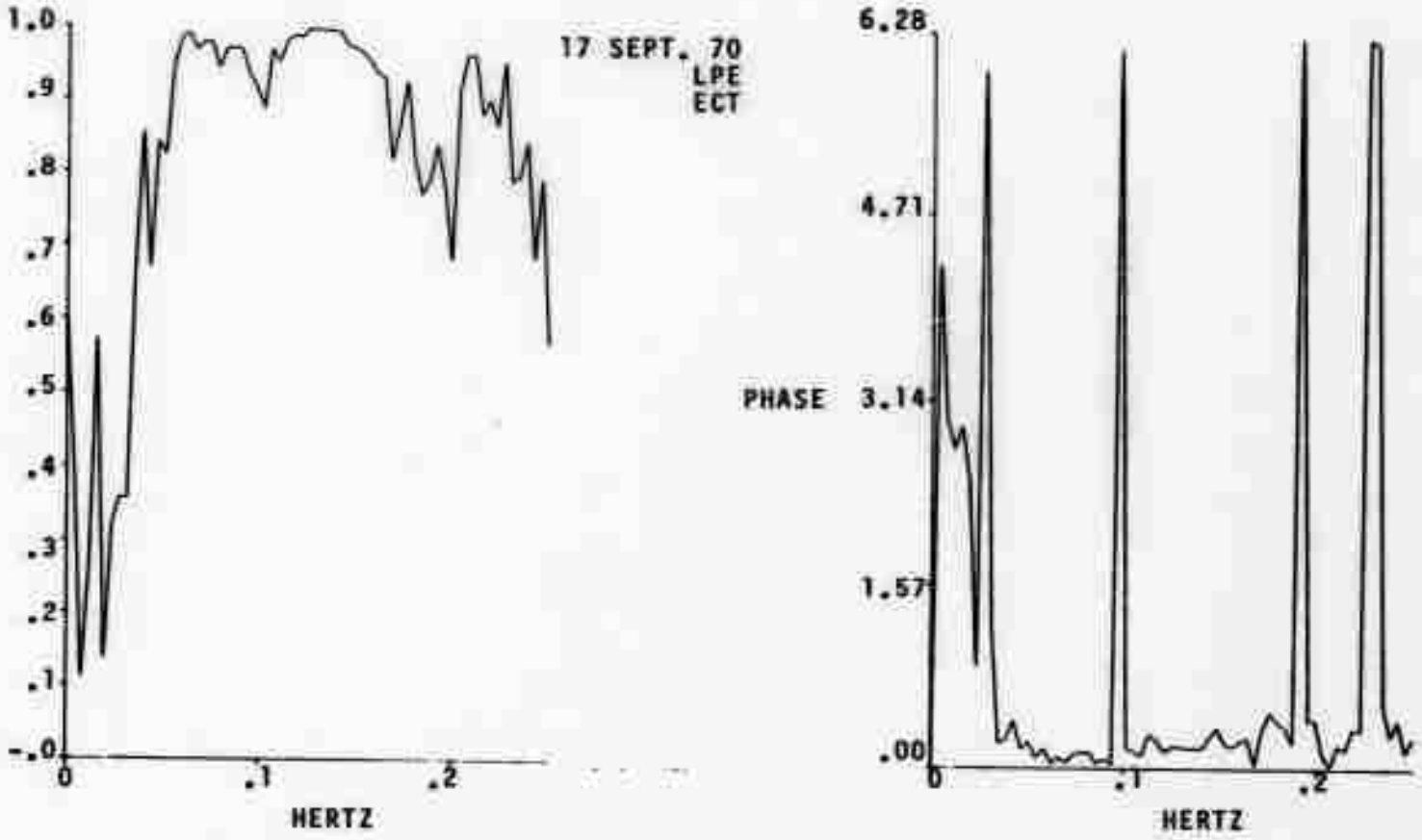

Figure 45. Coherency and phase of 17 and 18 September 1970 noise by channel.

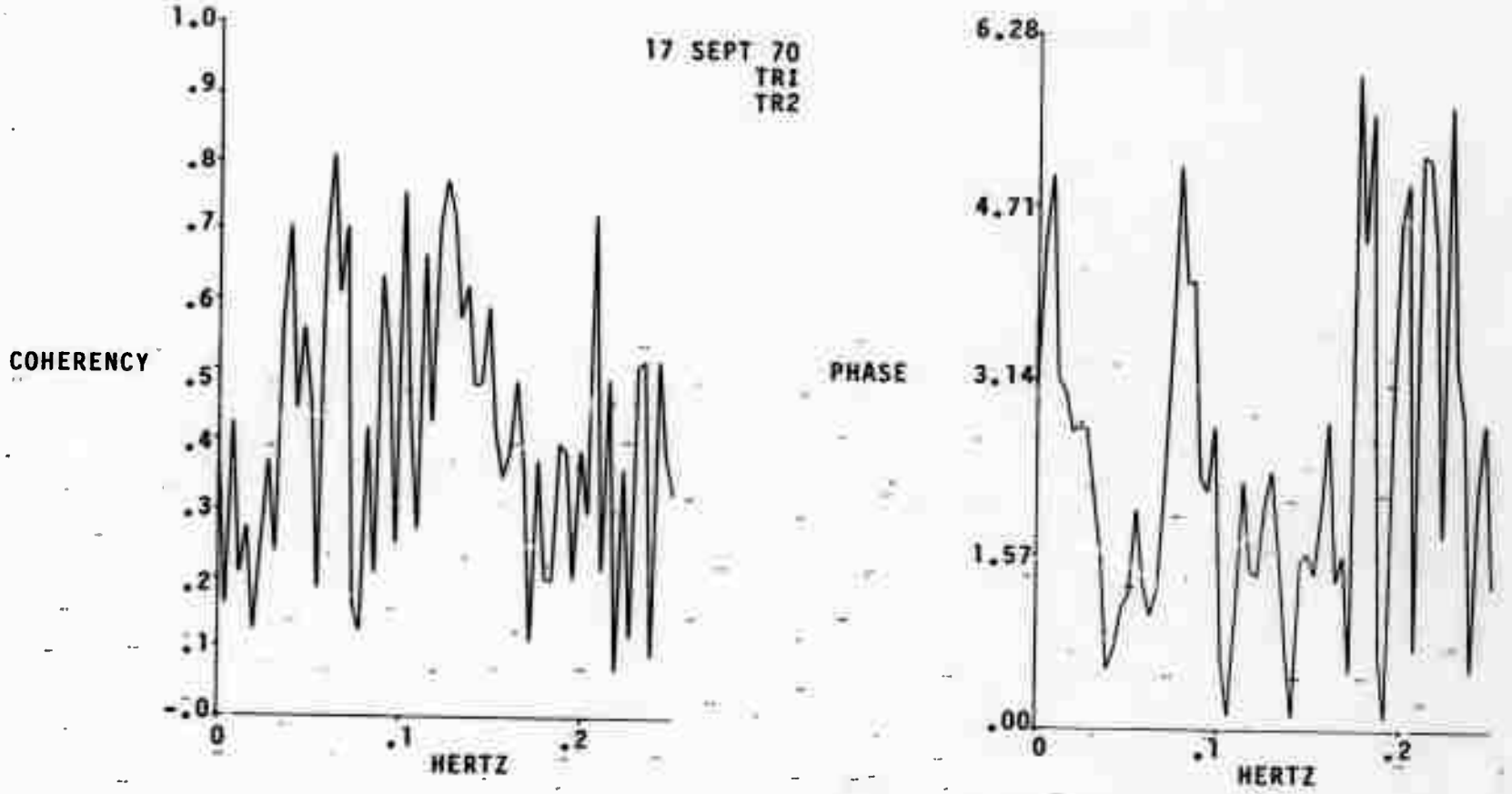

Figure 46. Coherency and phase of 17 and 18 September 1970 noise by channel.

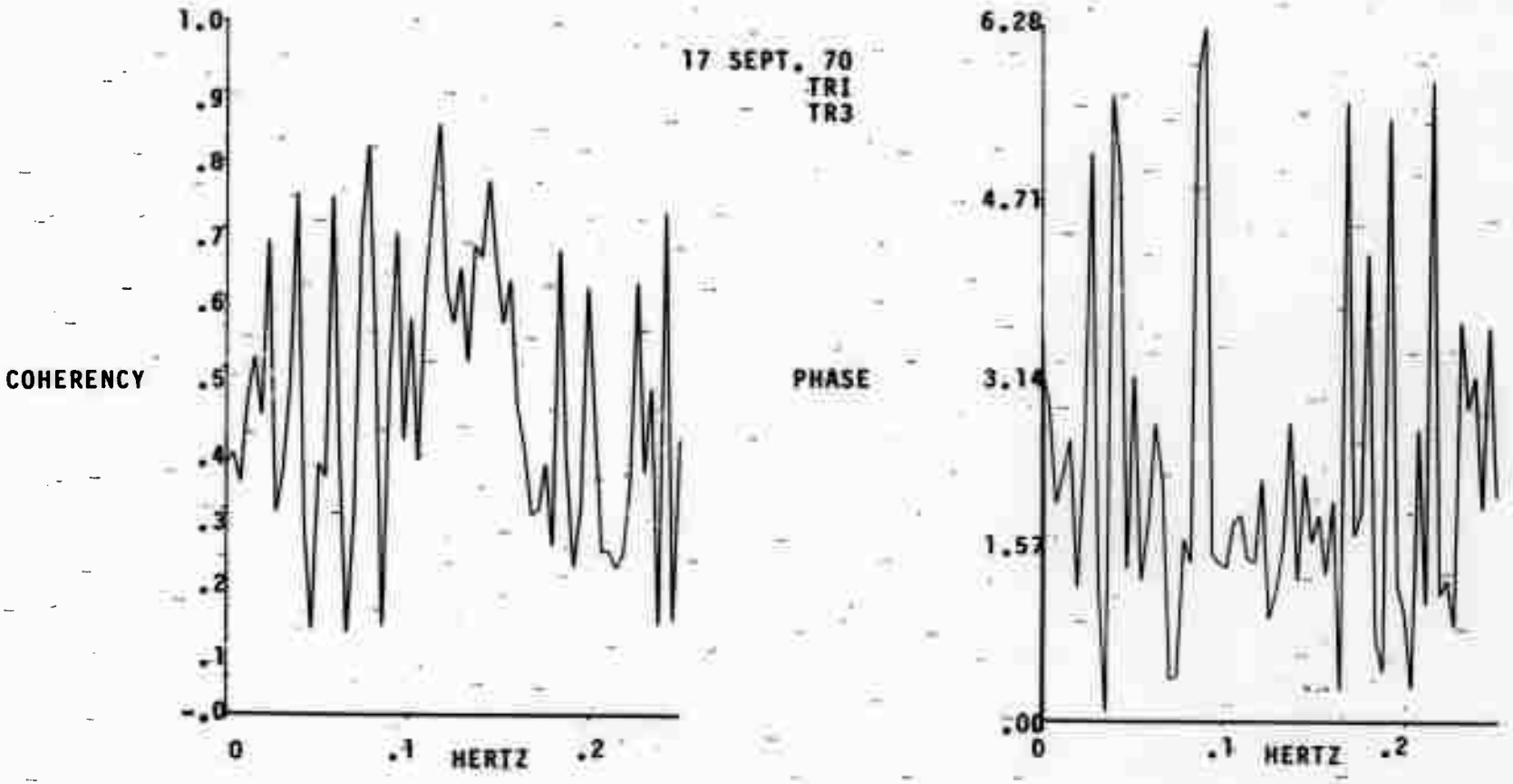

Figure 47. Coherency and phase of 17 and 18 September 1970 noise by channel.

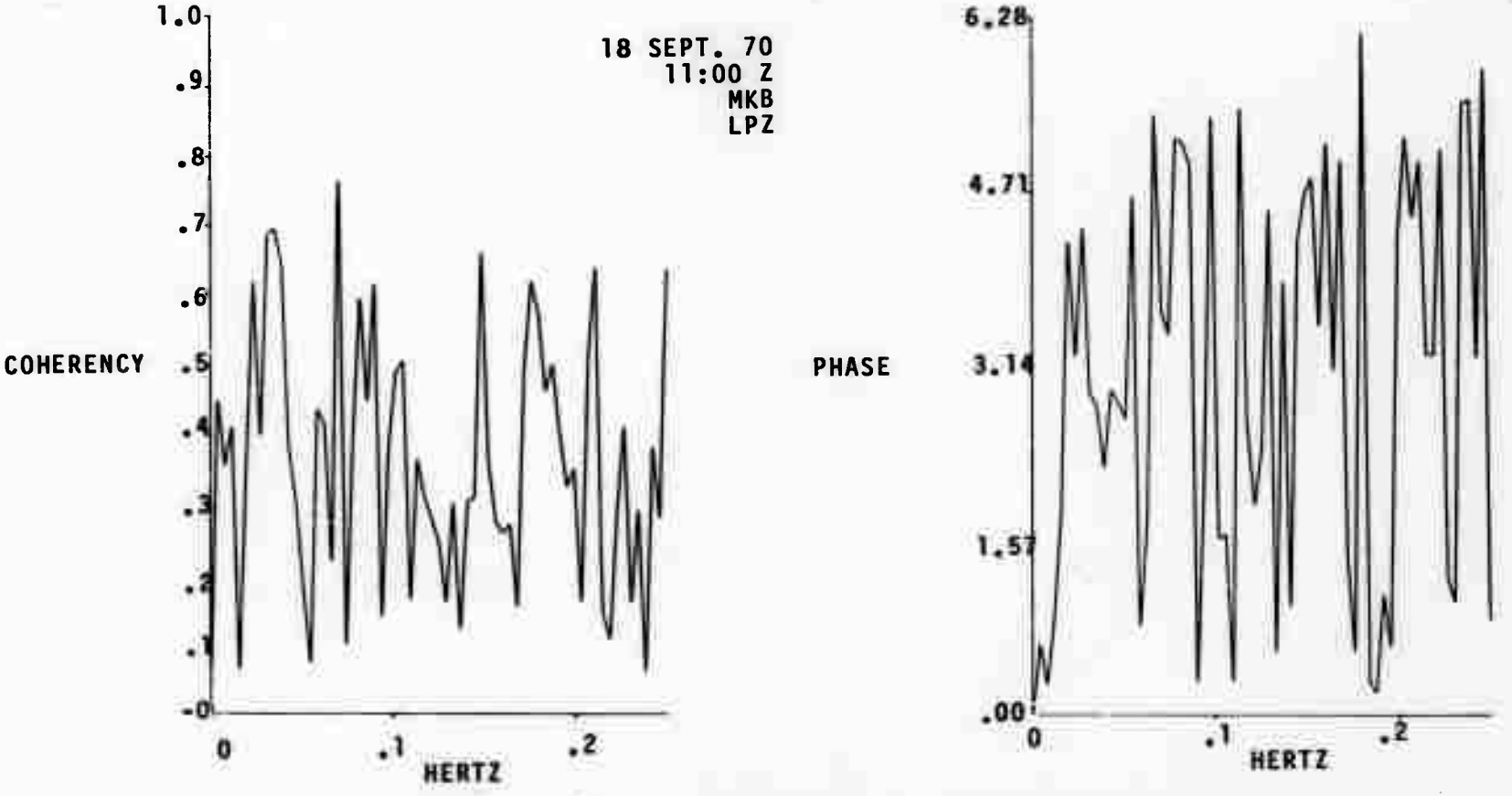

Figure 48. Coherency and phase of 17 and 18 September 1970 noise by channel.

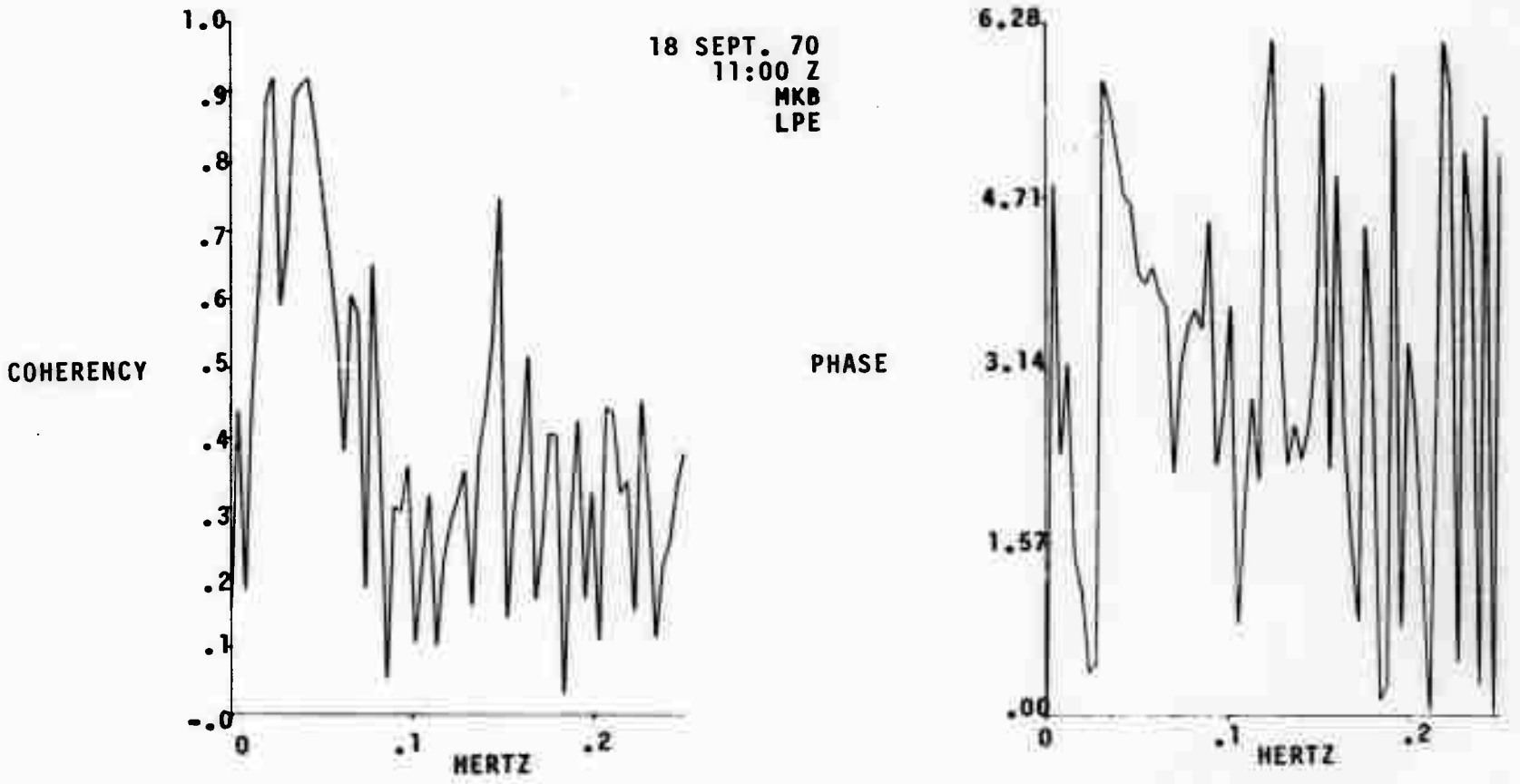

Figure 49. Coherency and phase of 17 and 18 September 1970 noise by channel.

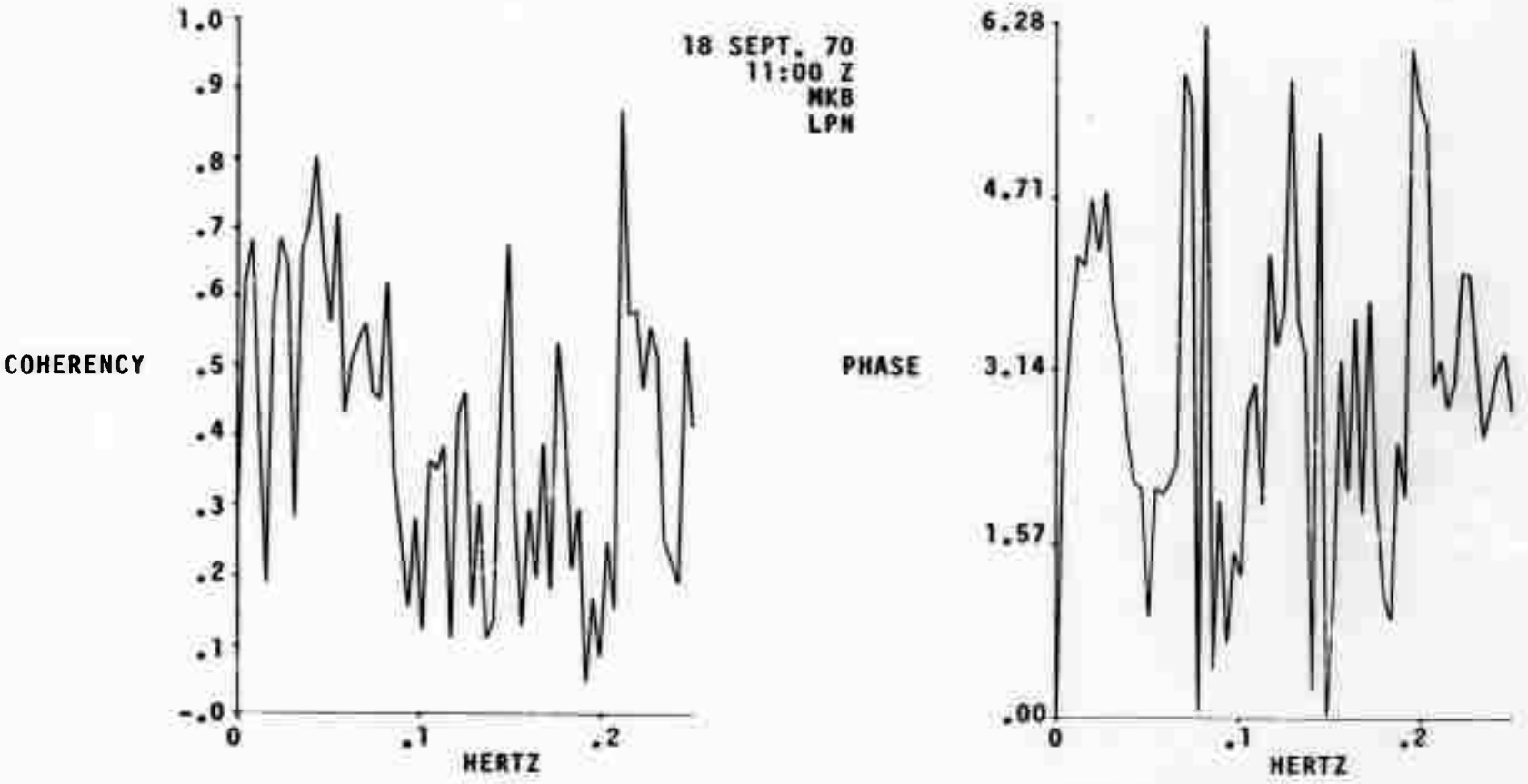

Figure 50. Coherency and phase of 17 and 18 September 1970 noise by channel.

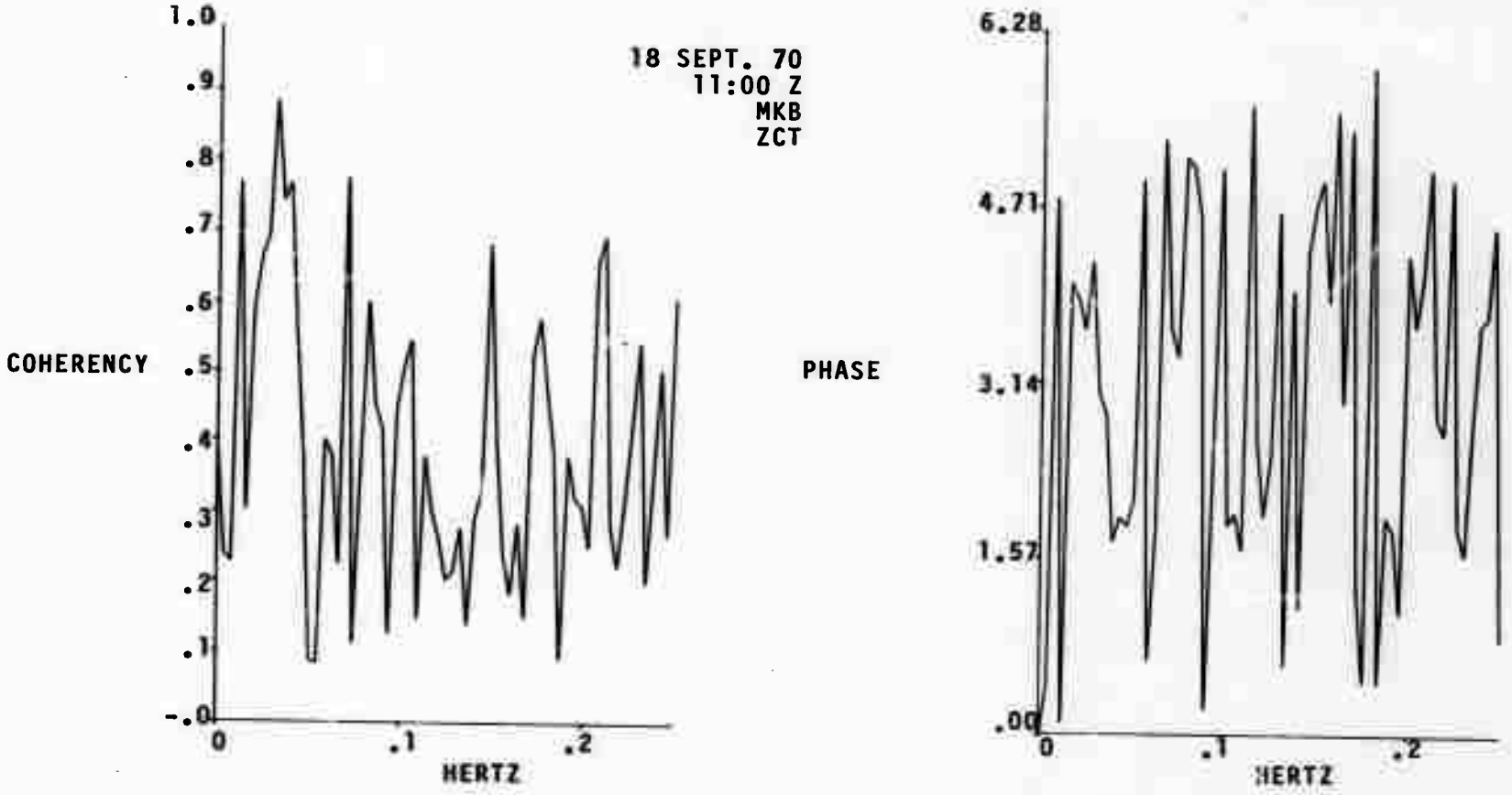

Figure 51. Coherency and phase of 17 and 18 September 1970 noise by channel.

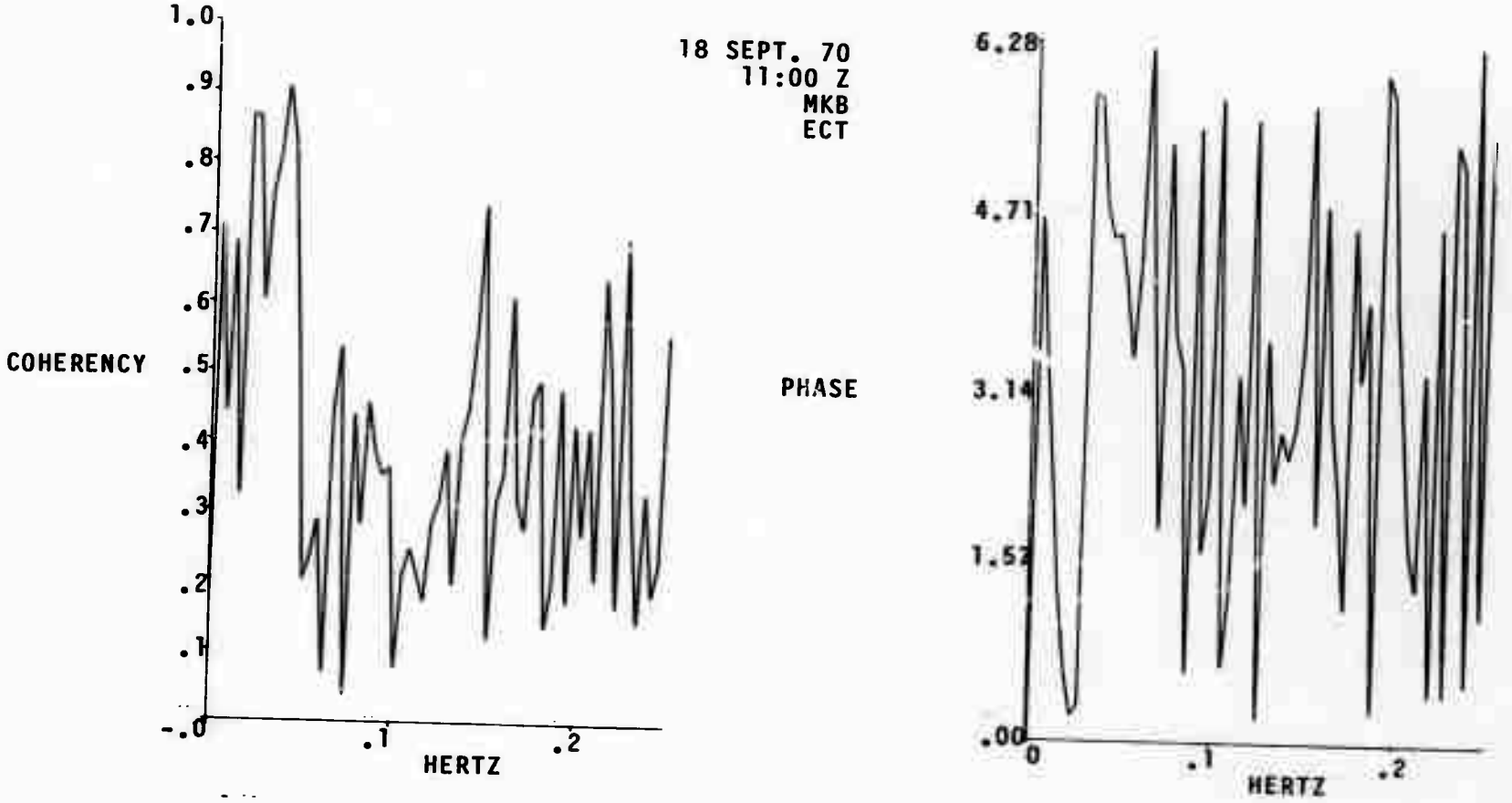

Figure 52. Coherency and phase of 17 and 18 September 1970 noise by channel.

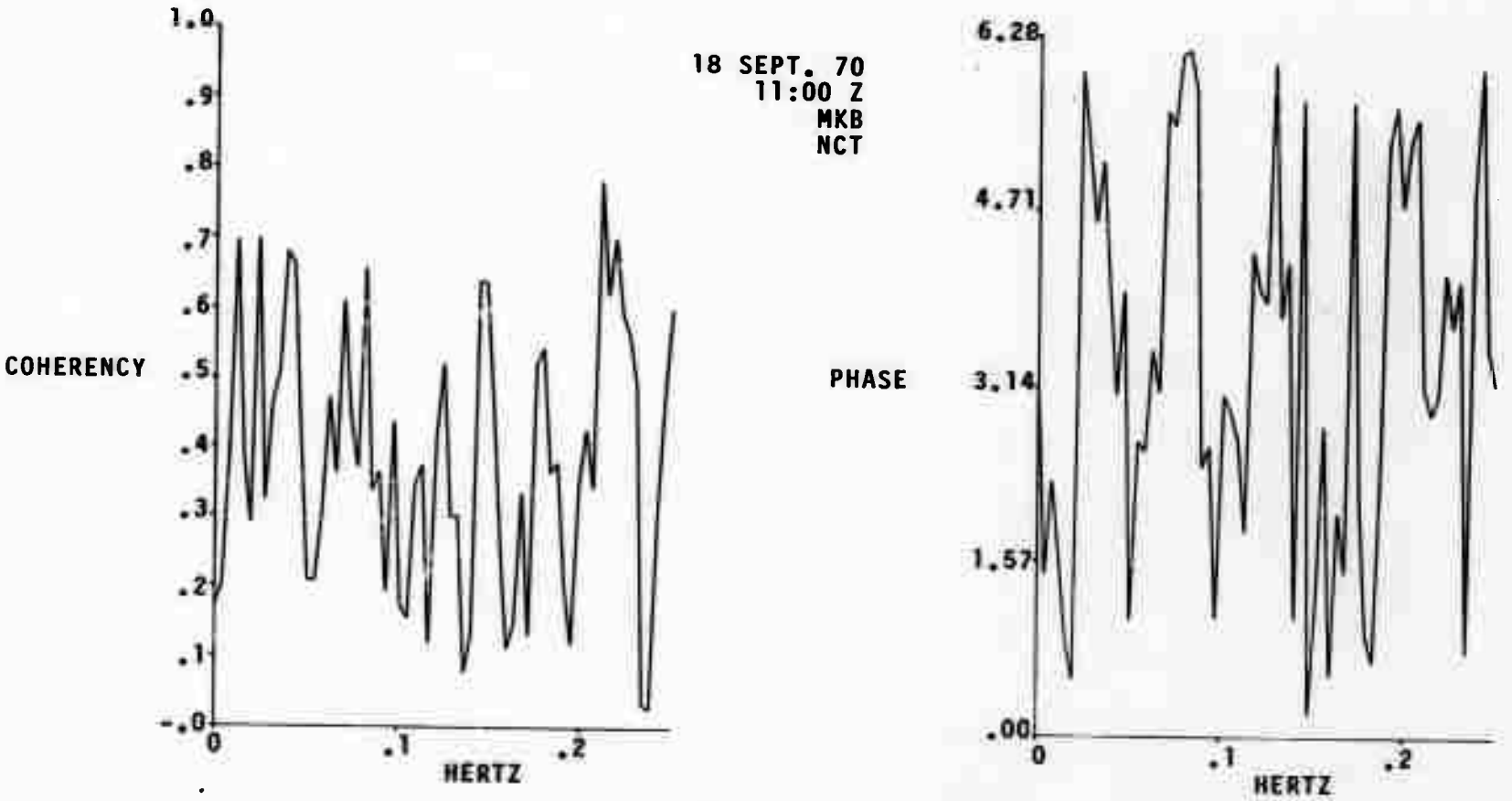

Figure 53. Coherency and phase of 17 and 18 September 1970 noise by channel.

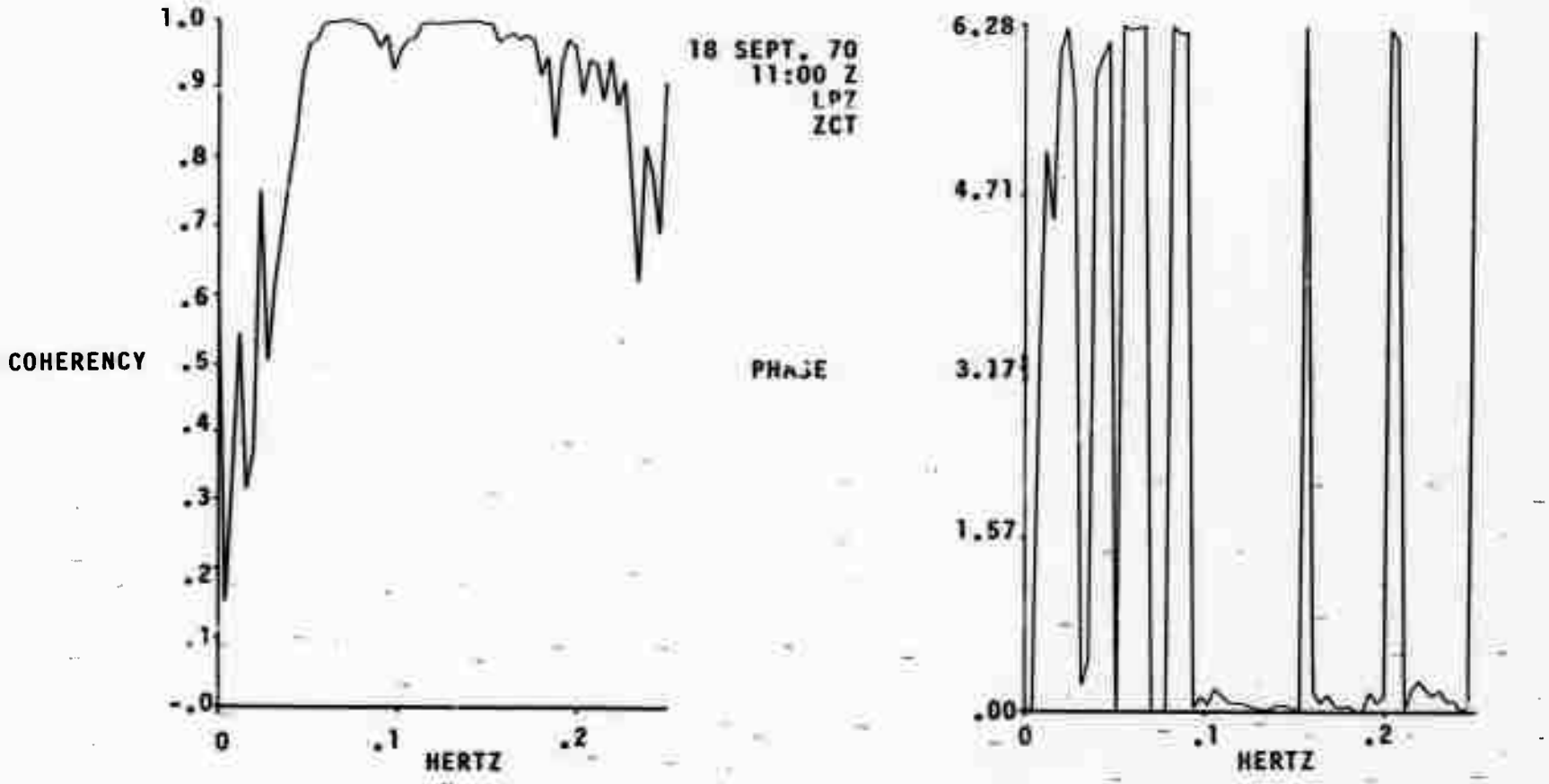

Figure 54. Coherency and phase of 17 and 18 September 1970 noise by channel.

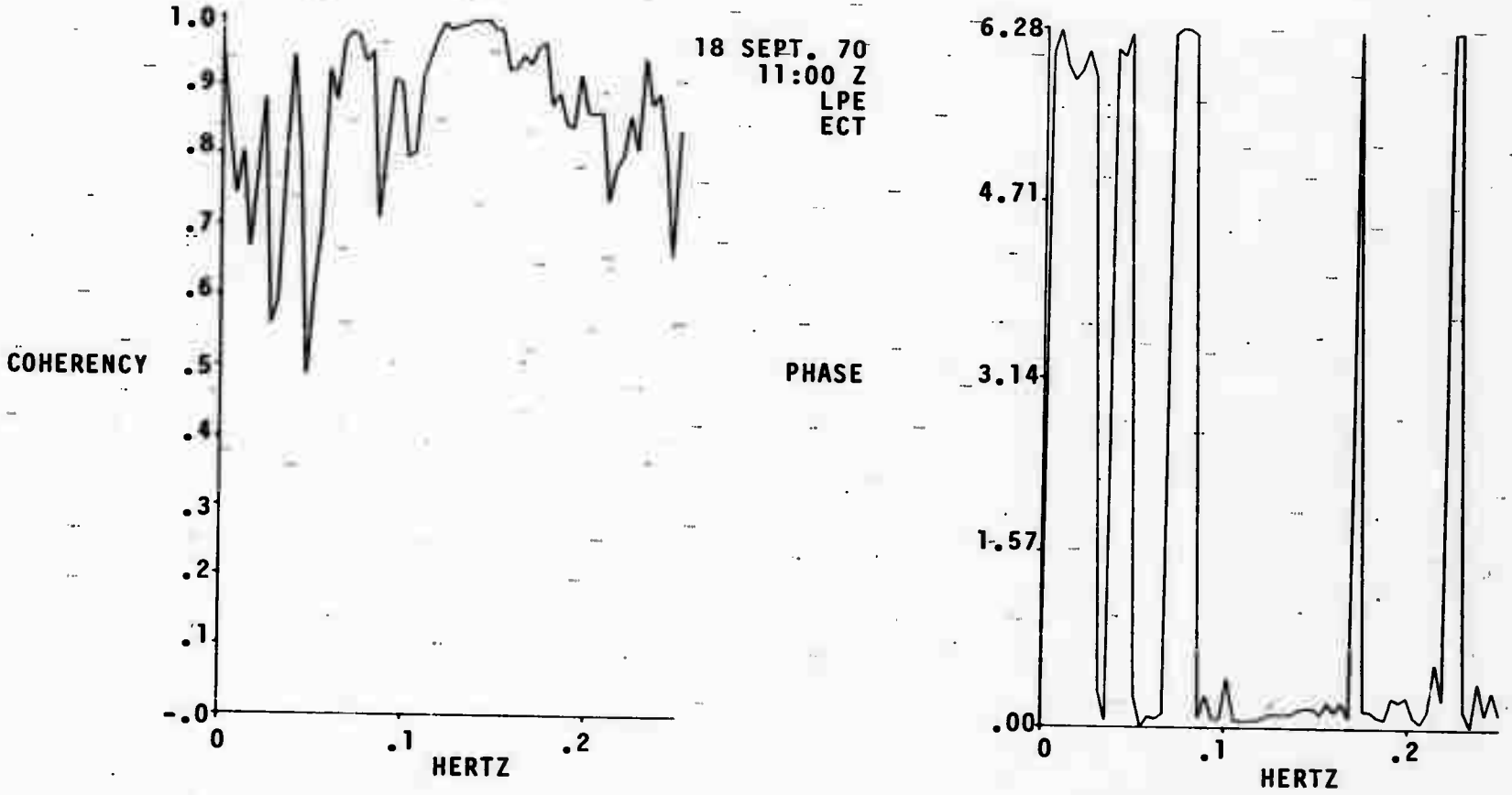

Figure 55. Coherency and phase of 17 and 18 September 1970 noise by channel.

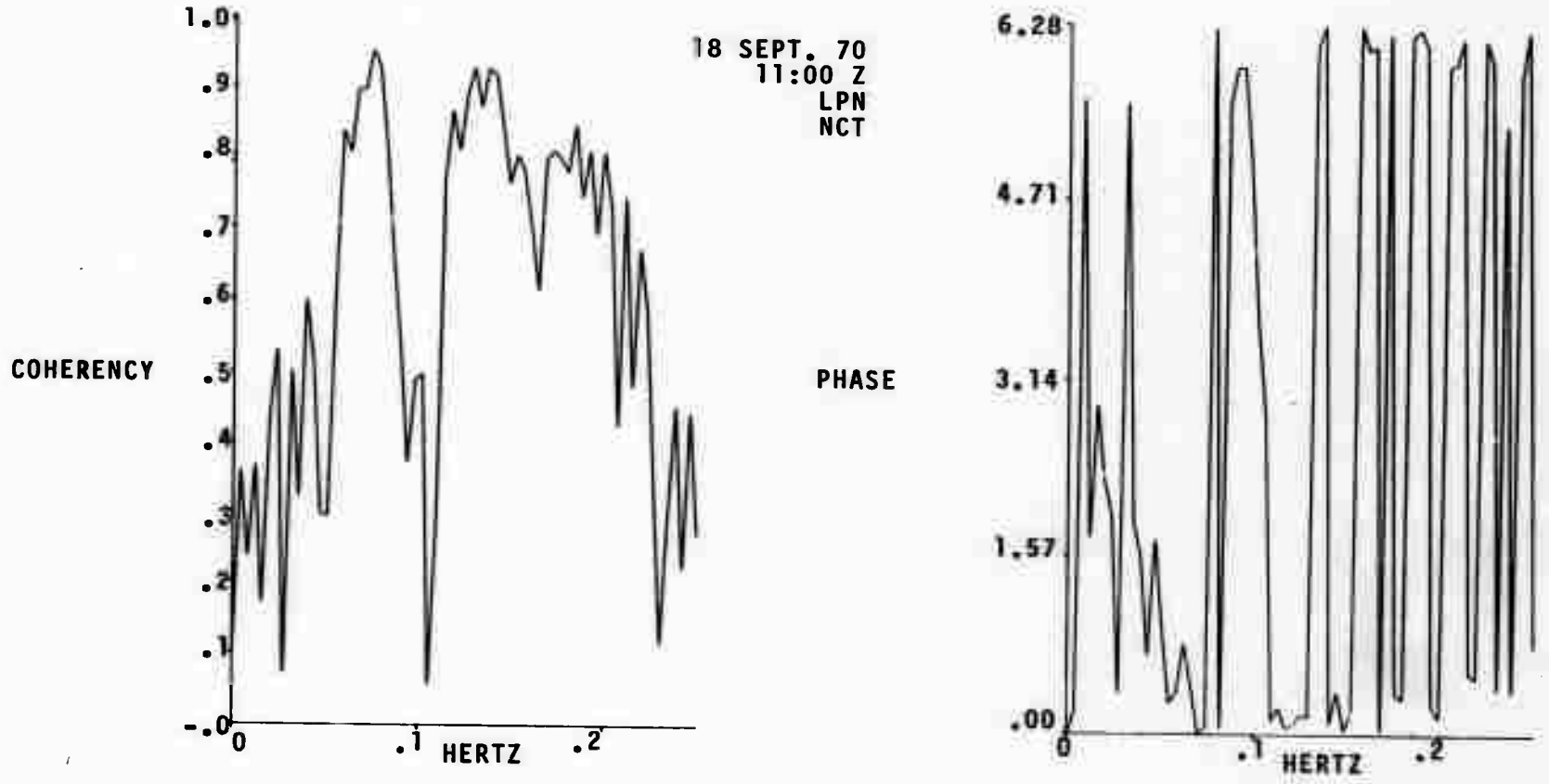

Figure 56. Coherency and phase of 17 and 18 September 1970 noise by channel.

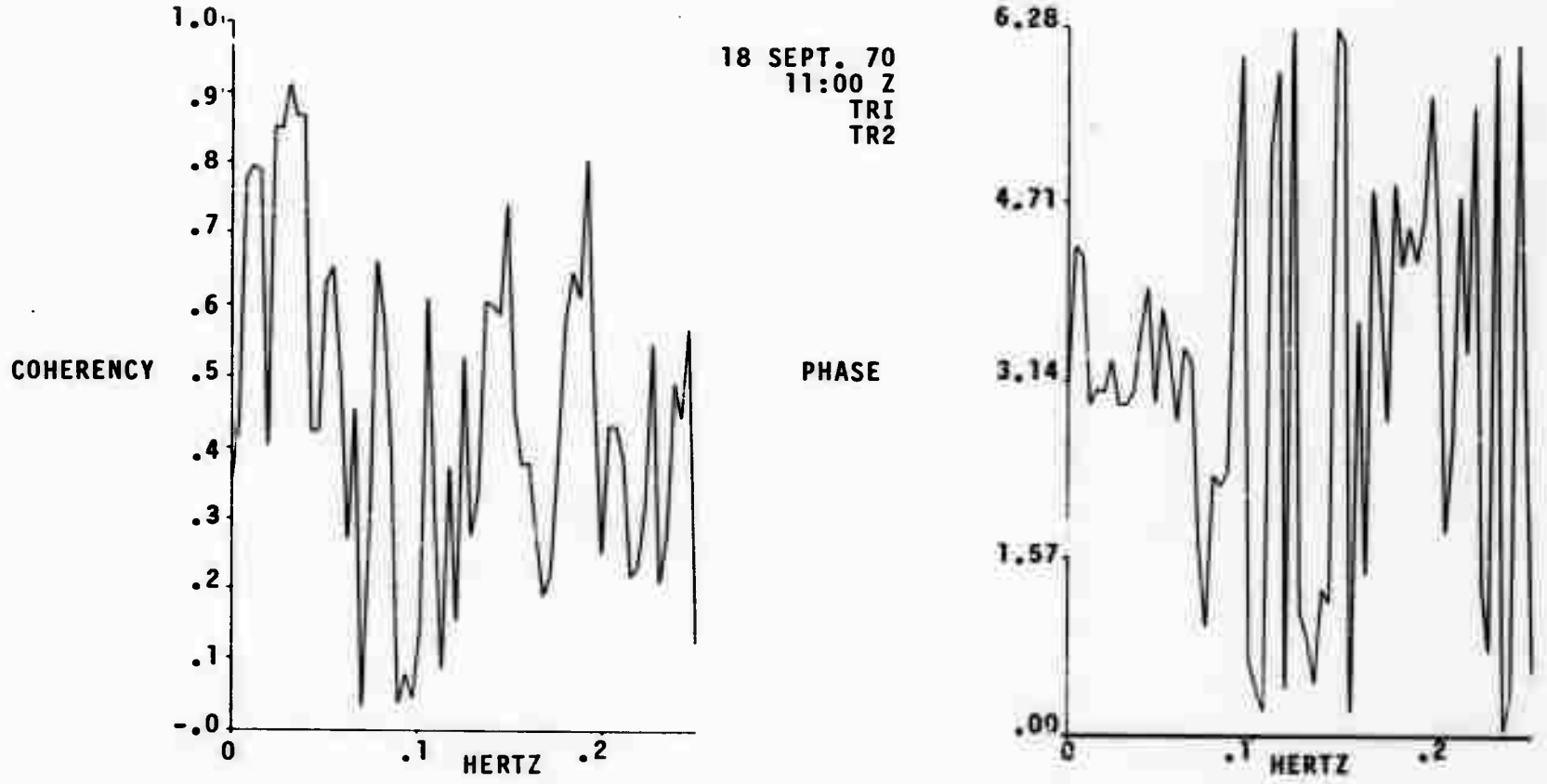

Figure 57. Coherency and phase of 17 and 18 September 1970 noise by channel.

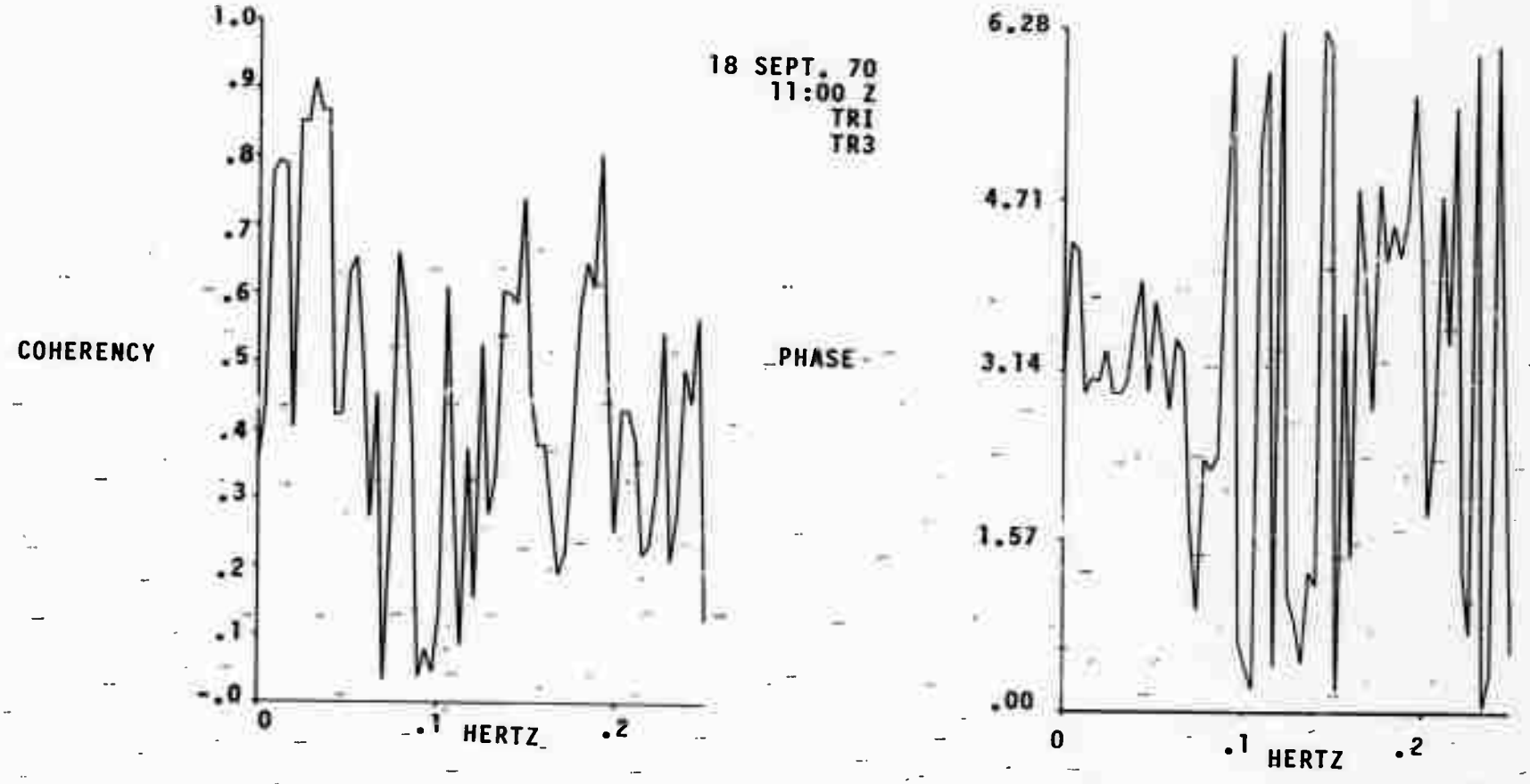

Figure 58. Coherency and phase of 17 and 18 September 1970 noise by channel.

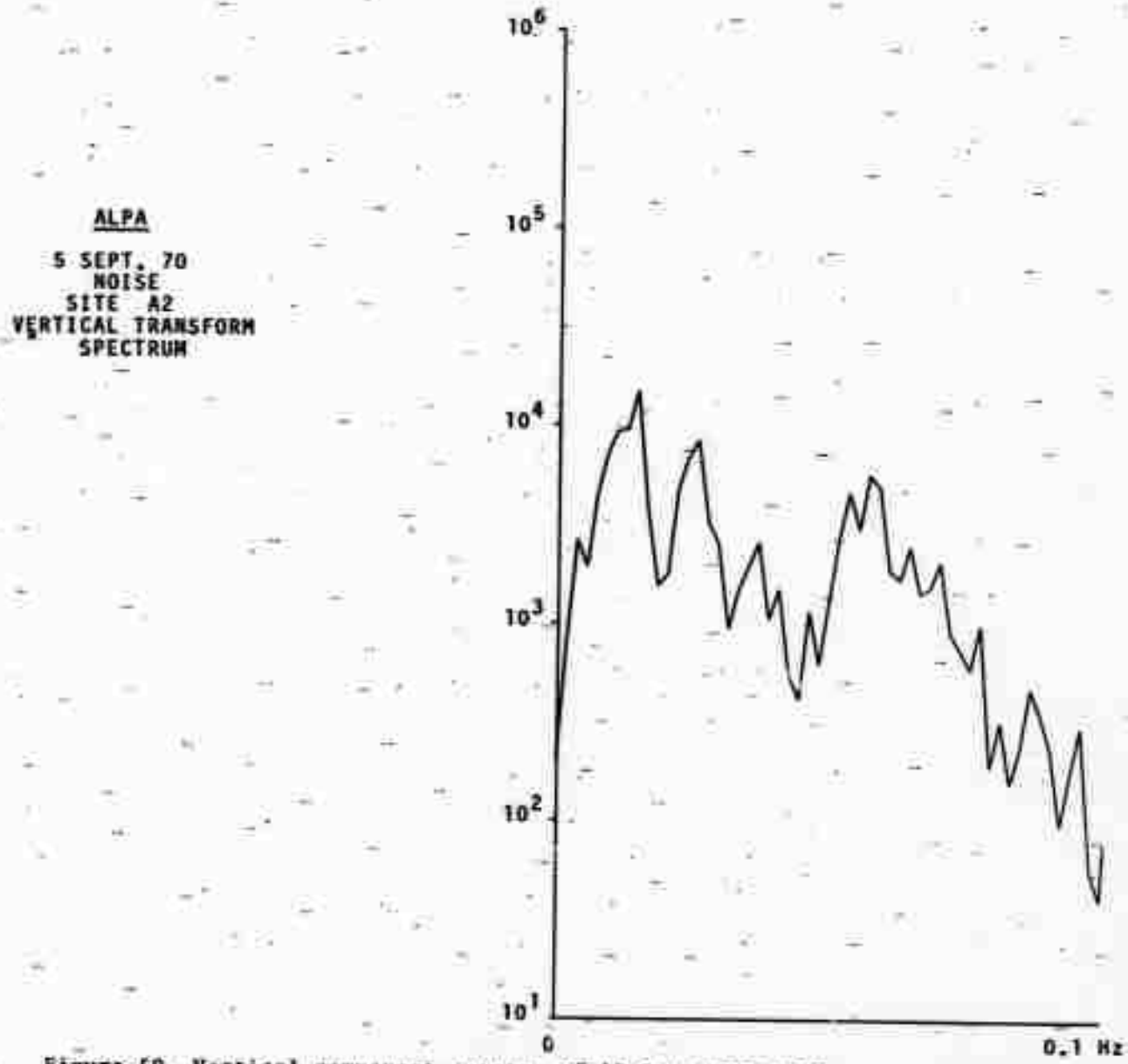

Figure 59. Vertical component spectra of 05 September 1970 noise by site.

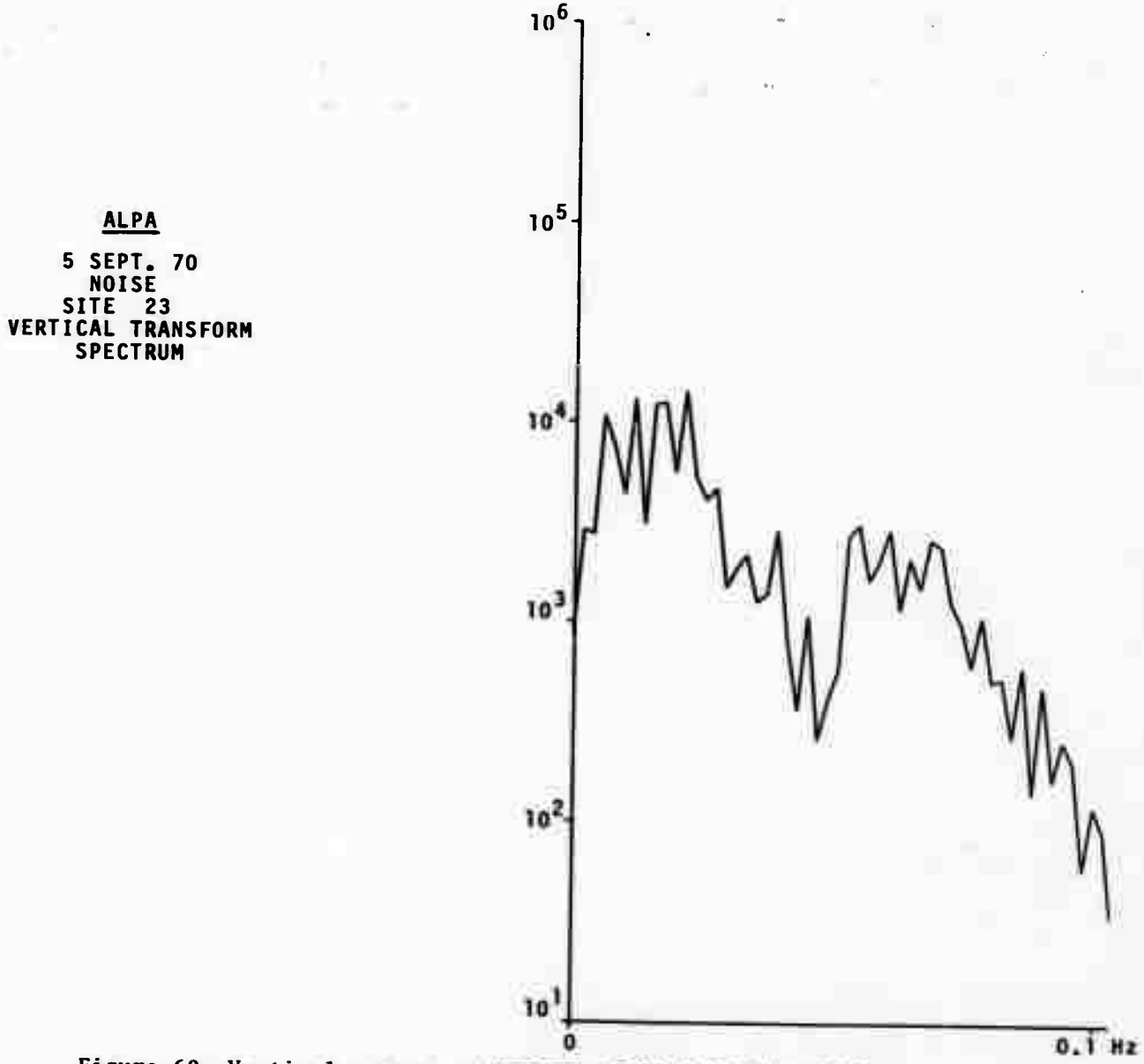

Figure 60. Vertical component spectra of 05 September 1970 noise by site.

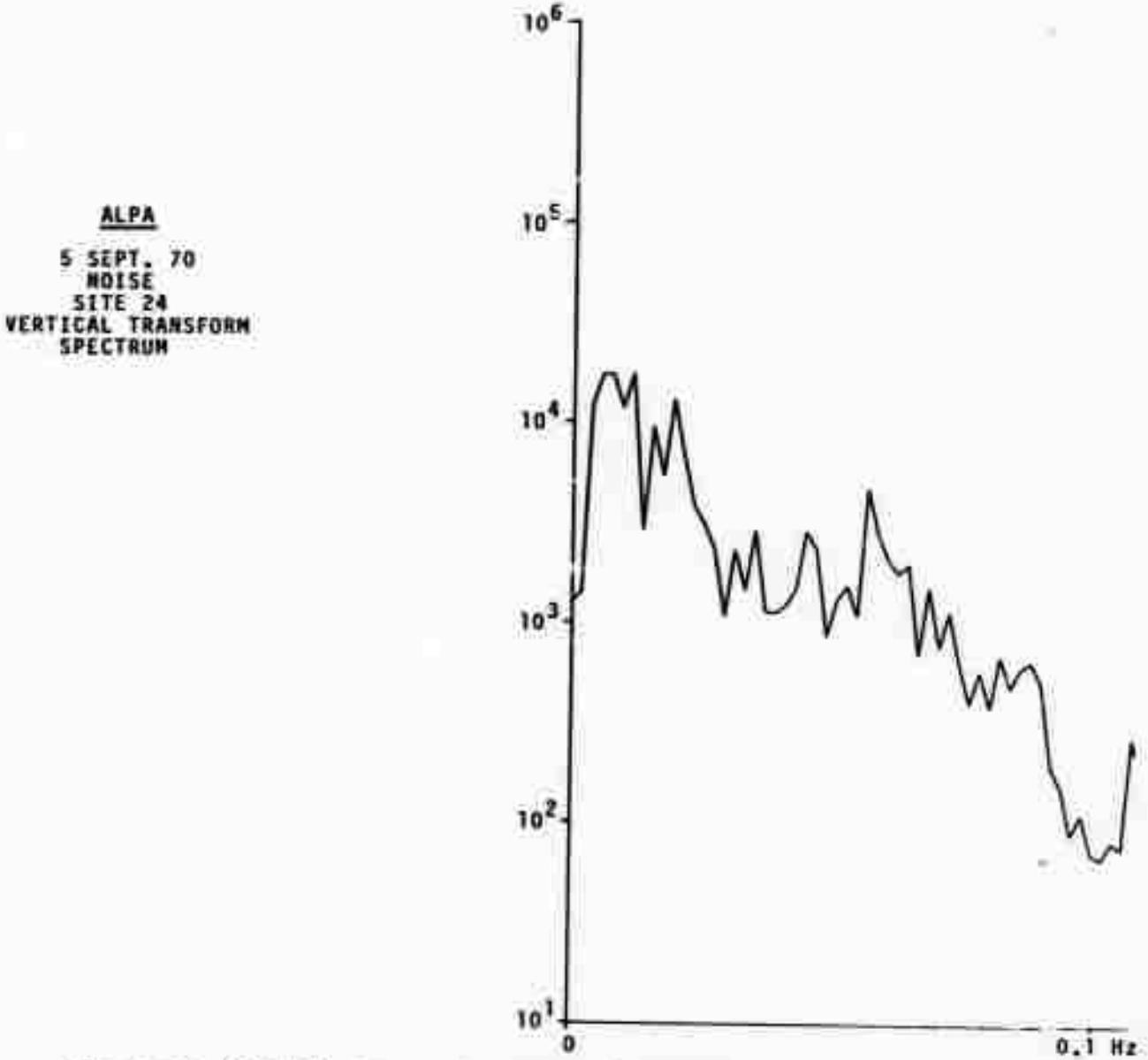

Figure 61. Vertical component spectra of 05 September 1970 noise by site.

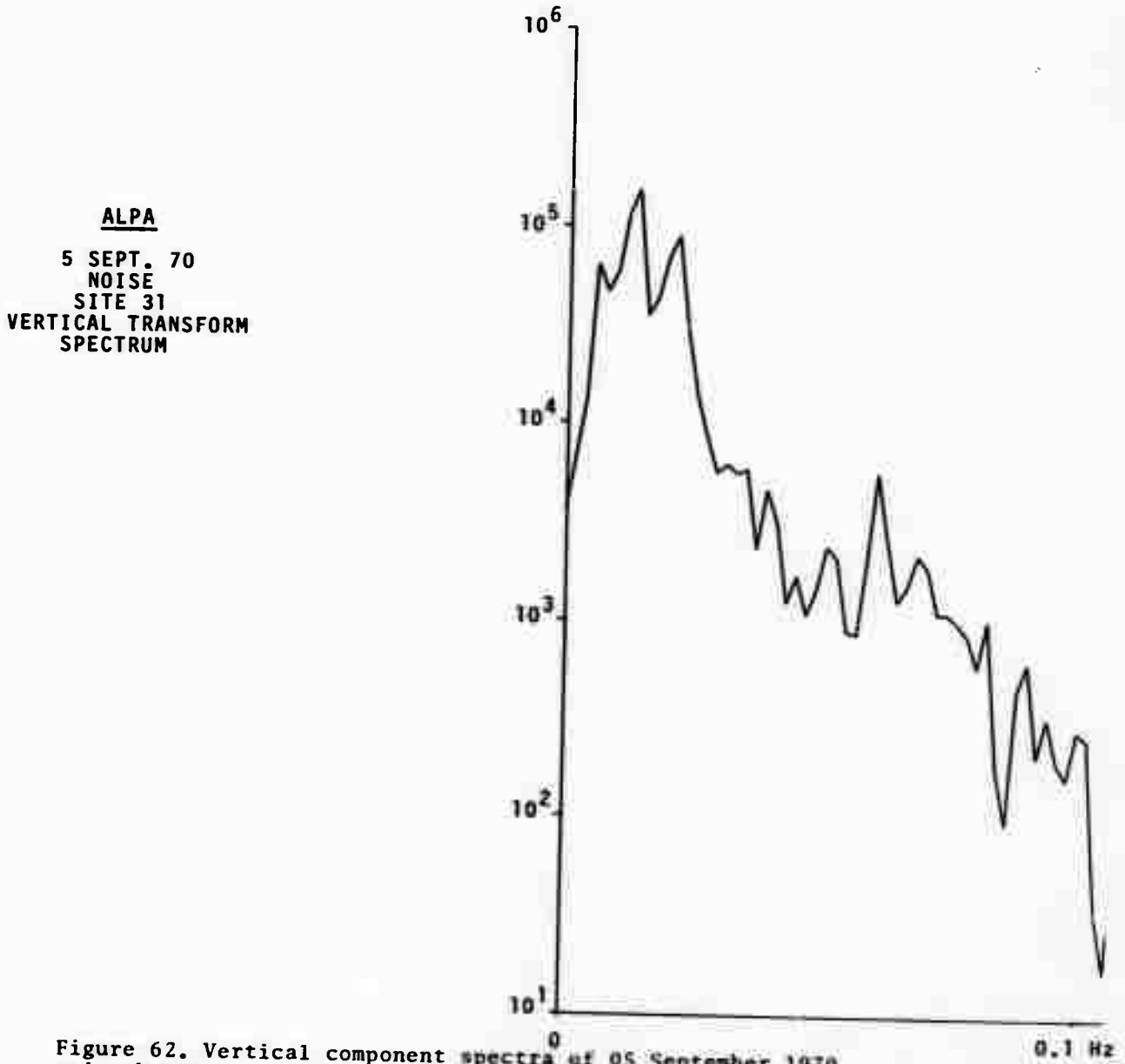

Figure 62. Vertical component spectra of 05 September 1970 noise by site.

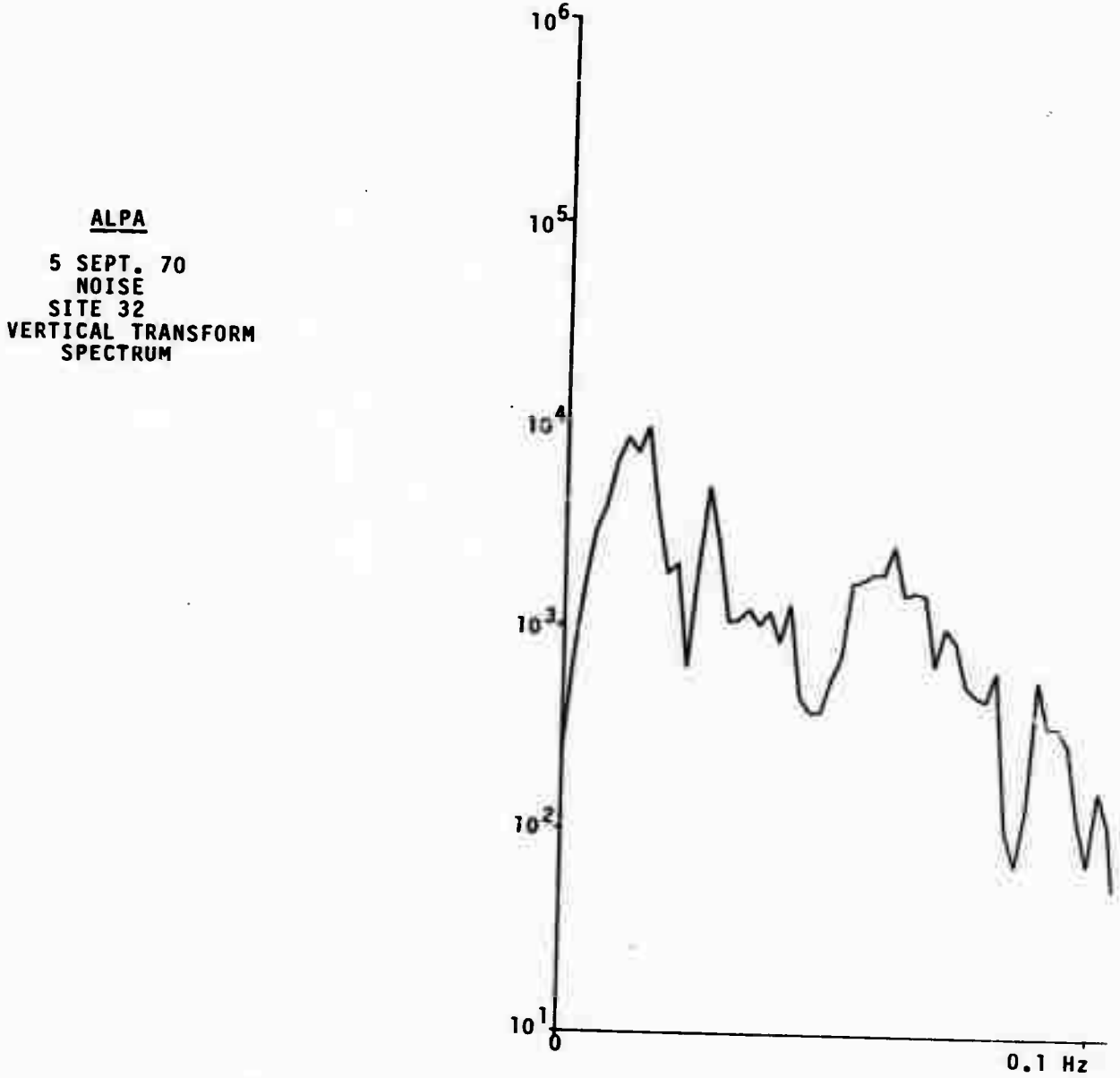

Figure 63. Vertical component spectra of 05 September 1970 noise by site.

ALPA

5 SEPT. 70
NOISE
SITE 33
VERTICAL TRANSFORM
SPECTRUM

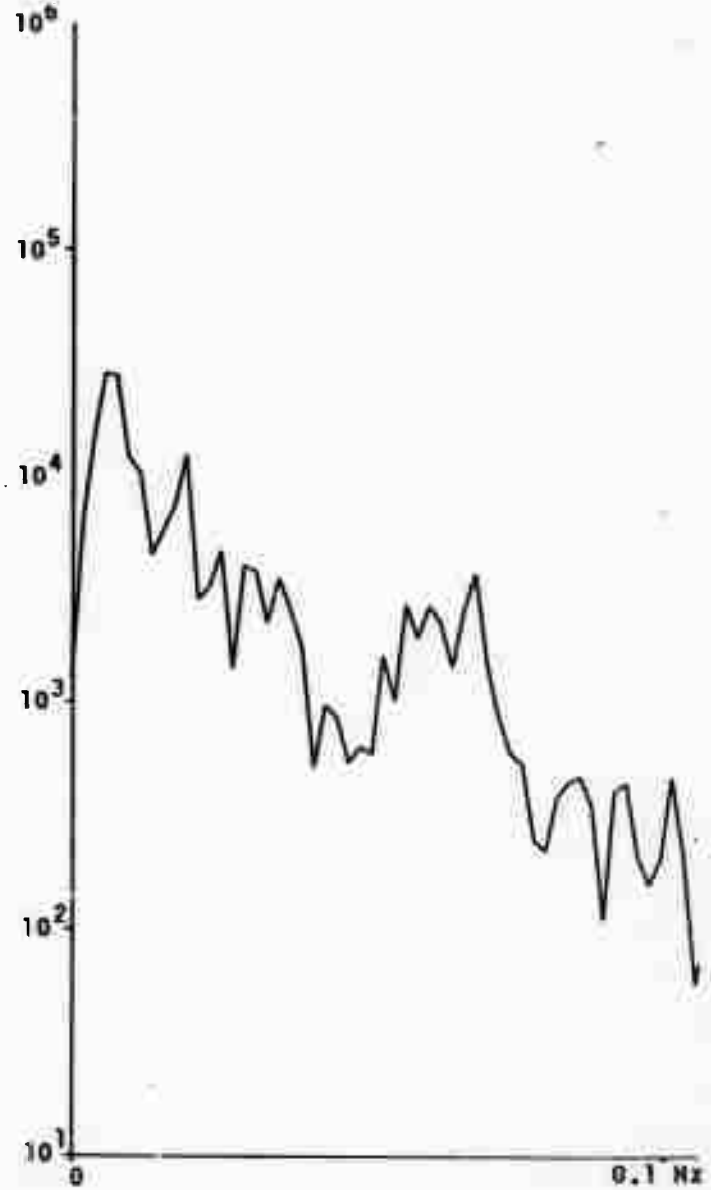

Figure 64. Vertical component spectra of 05 September 1970 noise by site.

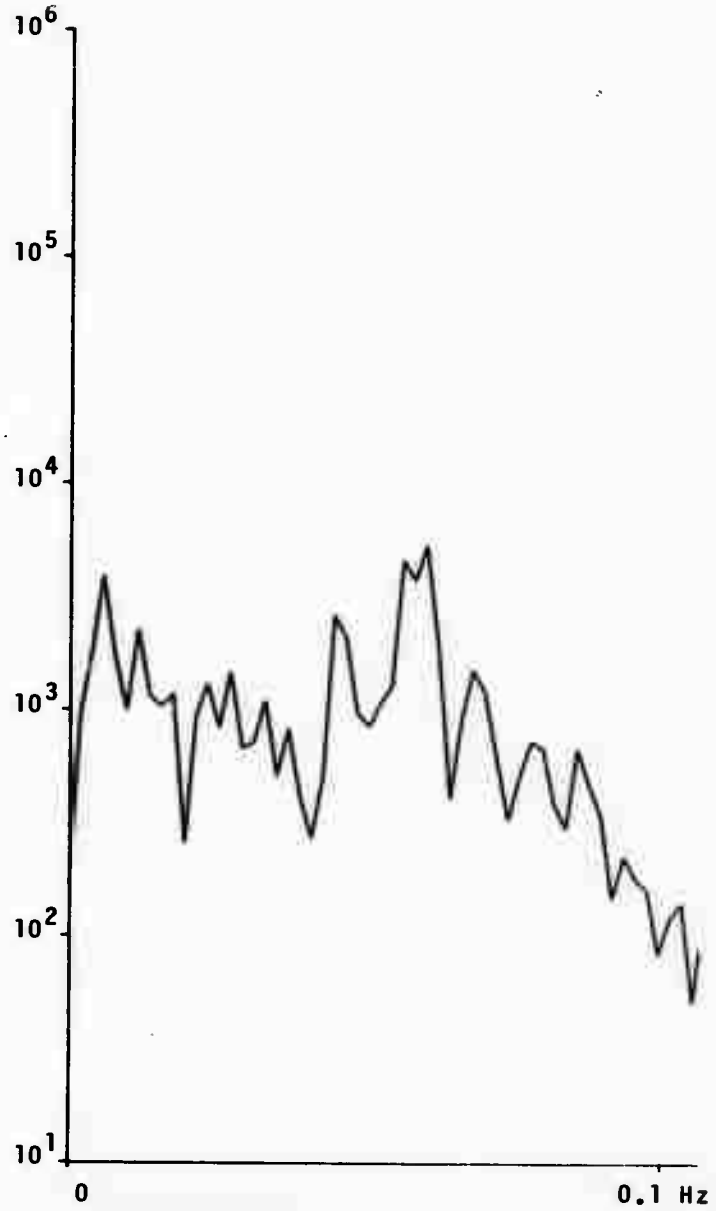

Figure 65. Vertical component spectra of 05 September 1970 noise by site.

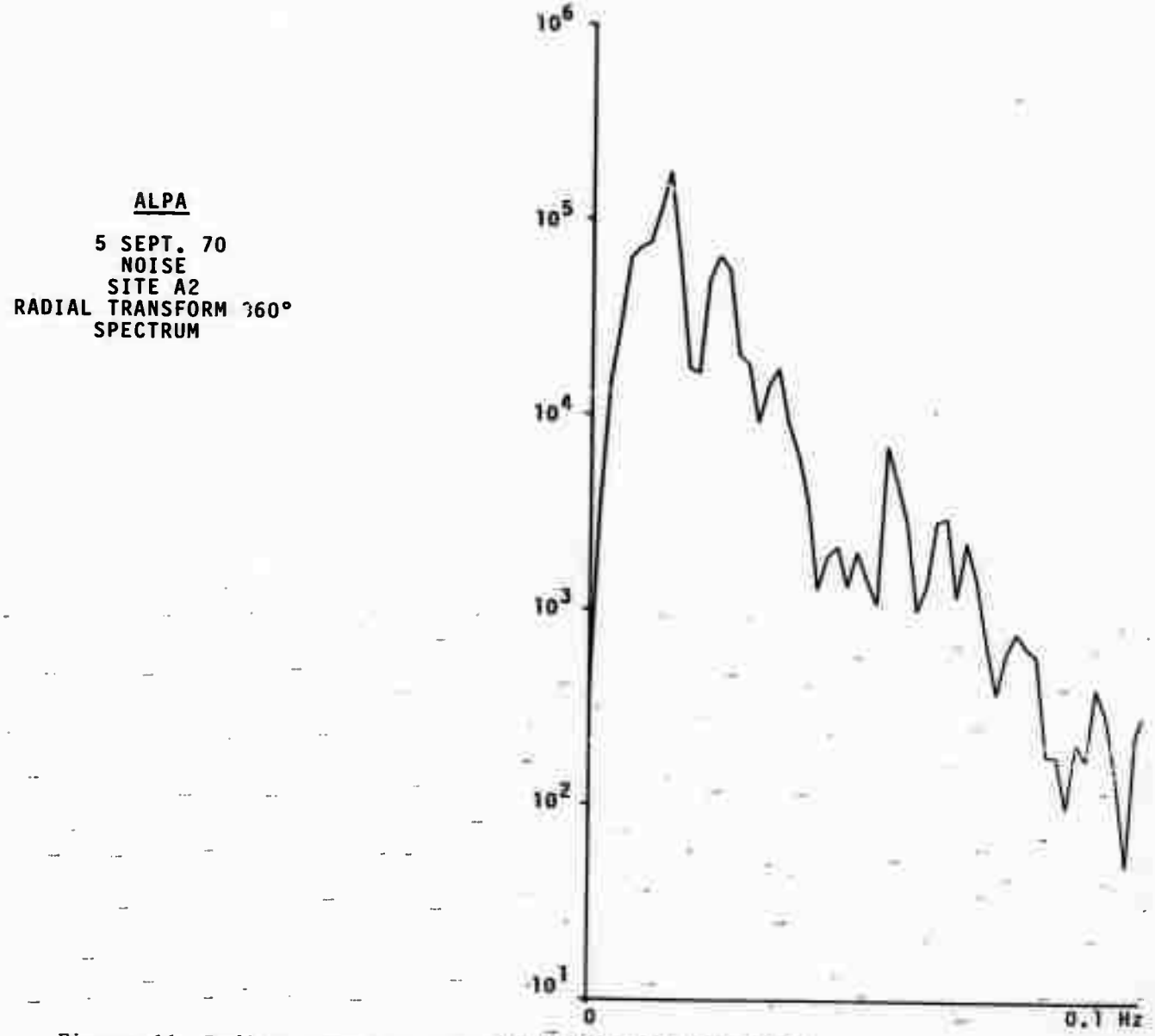

Figure 66. Radial component spectra of 05 September 1970 noise by site.

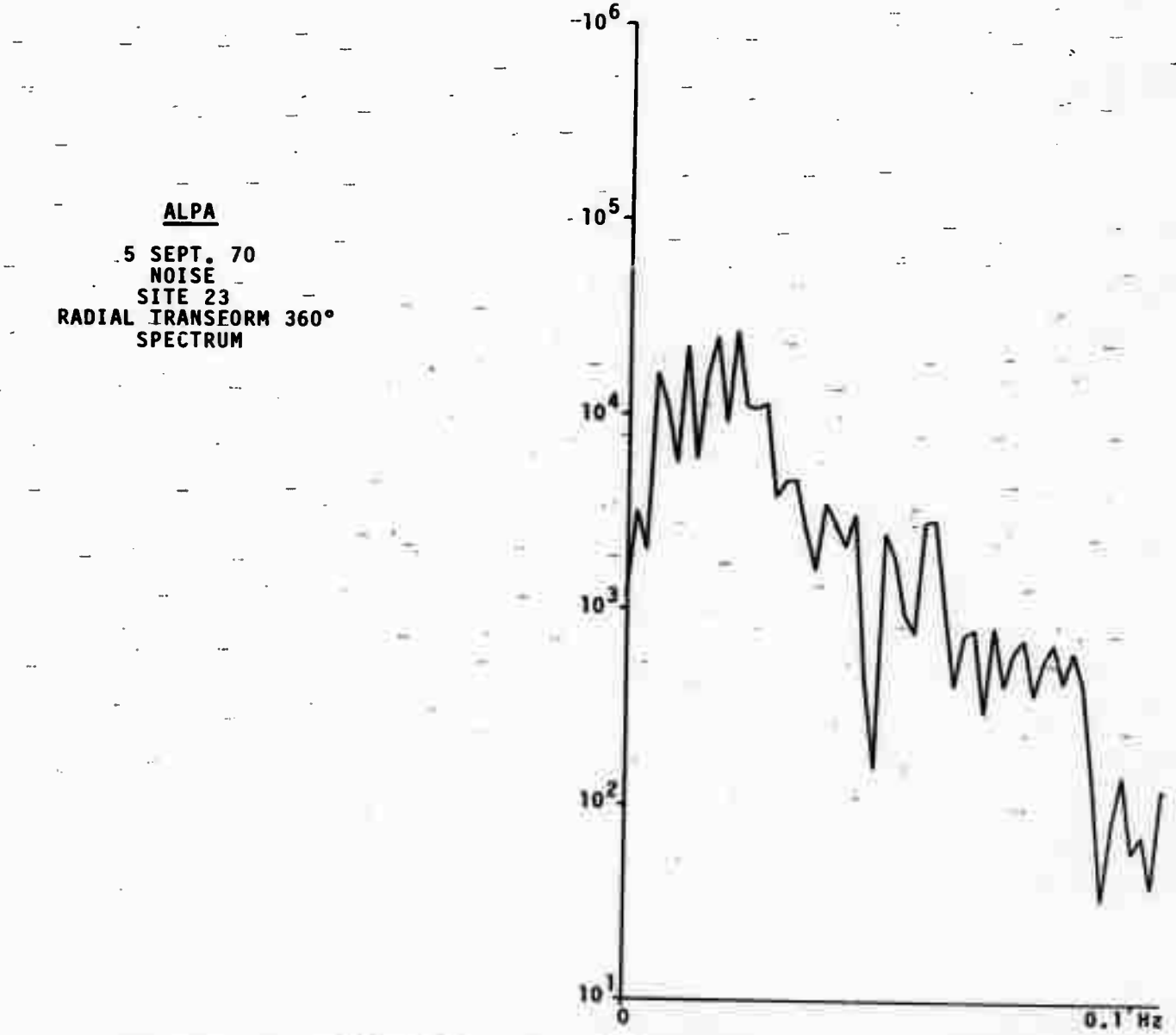

Figure 67. Radial component spectra of 05 September 1970 noise by site.

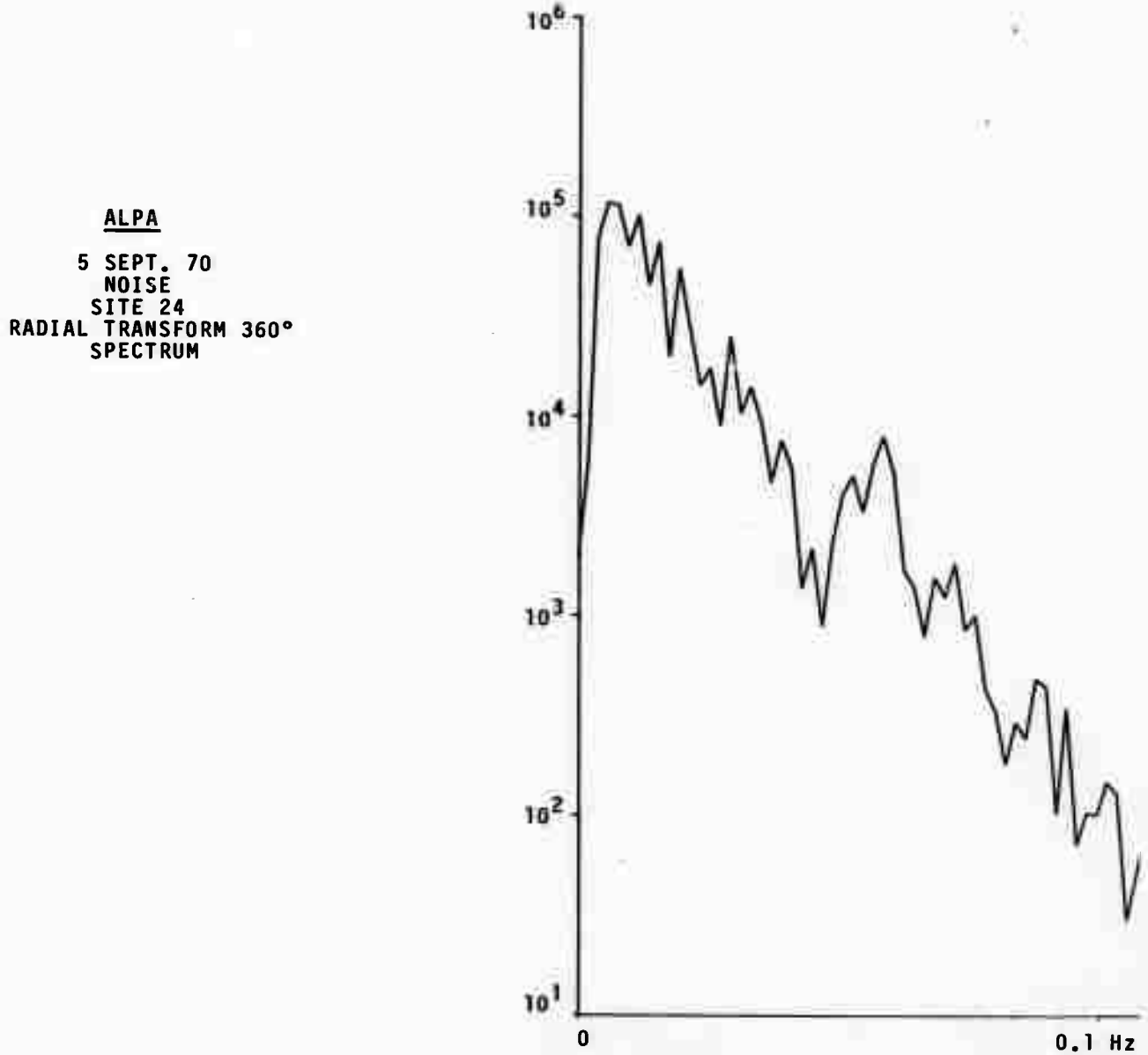

Figure 68. Radial component spectra of 05 September 1970 noise by site.

ALPA

5 SEPT. 70
NOISE
SITE 31
RADIAL TRANSFORM 360°
SPECTRUM

Figure 69. Radial component spectra of 05 September 1970 noise by site.

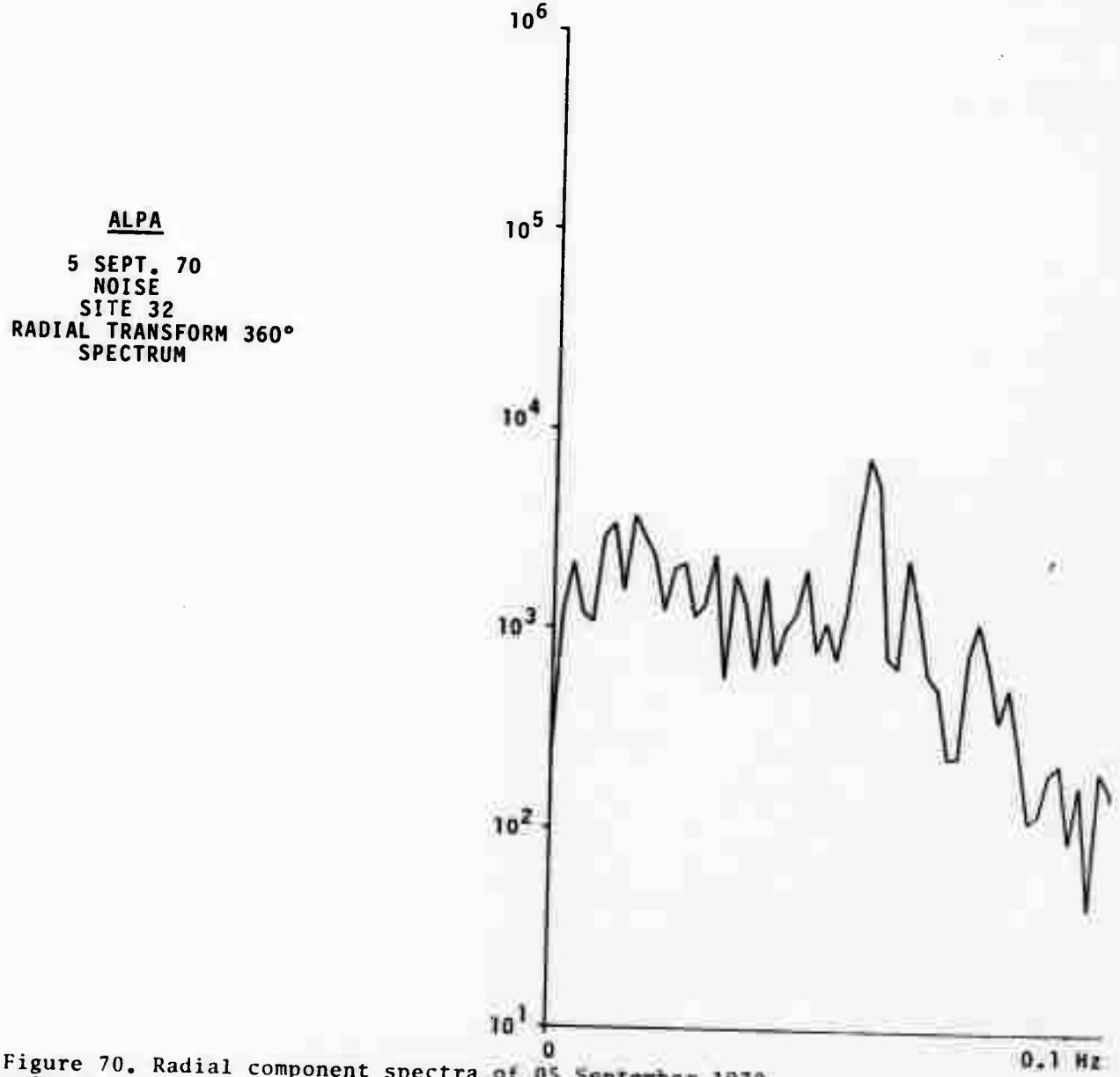

Figure 70. Radial component spectra of 05 September 1970 noise by site.

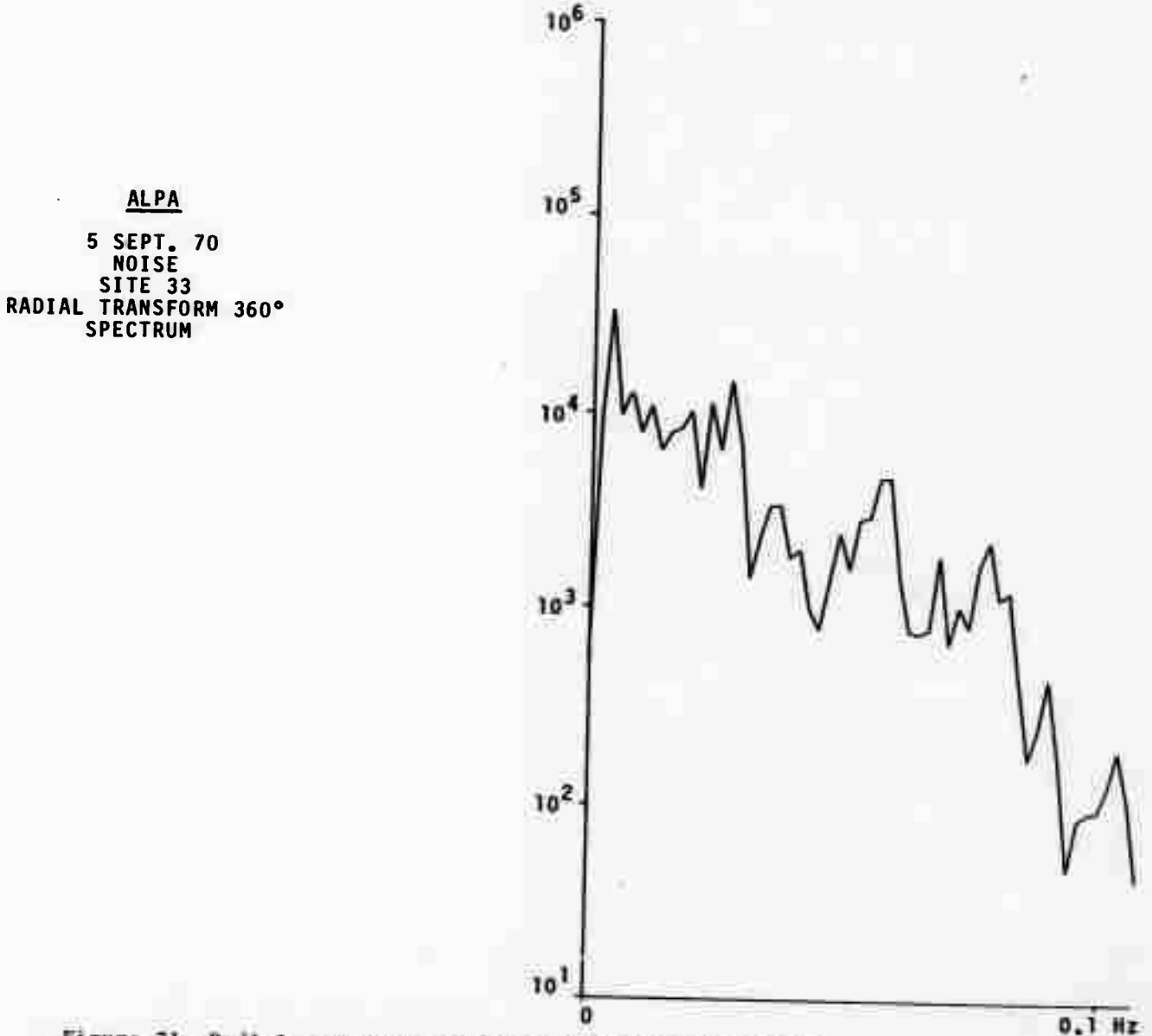

Figure 71. Radial component spectra of 05 September 1970 noise by site.

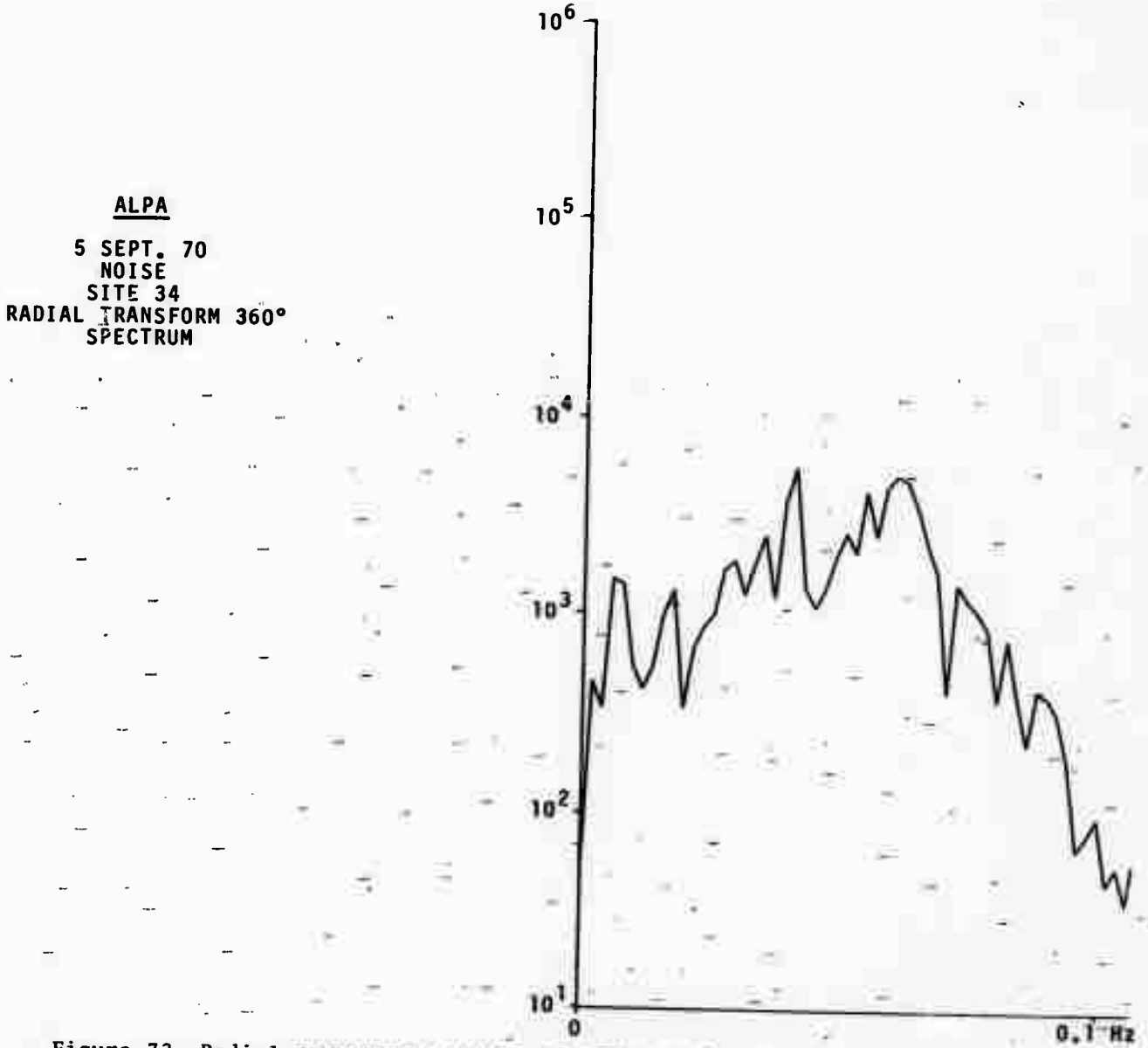

Figure 72. Radial component spectra of 05 September 1970 noise by site.

ALPA

5 SEPT. 70
NOISE
SITE A2
TRANSVERSE TRANSFORM 90°
SPECTRUM

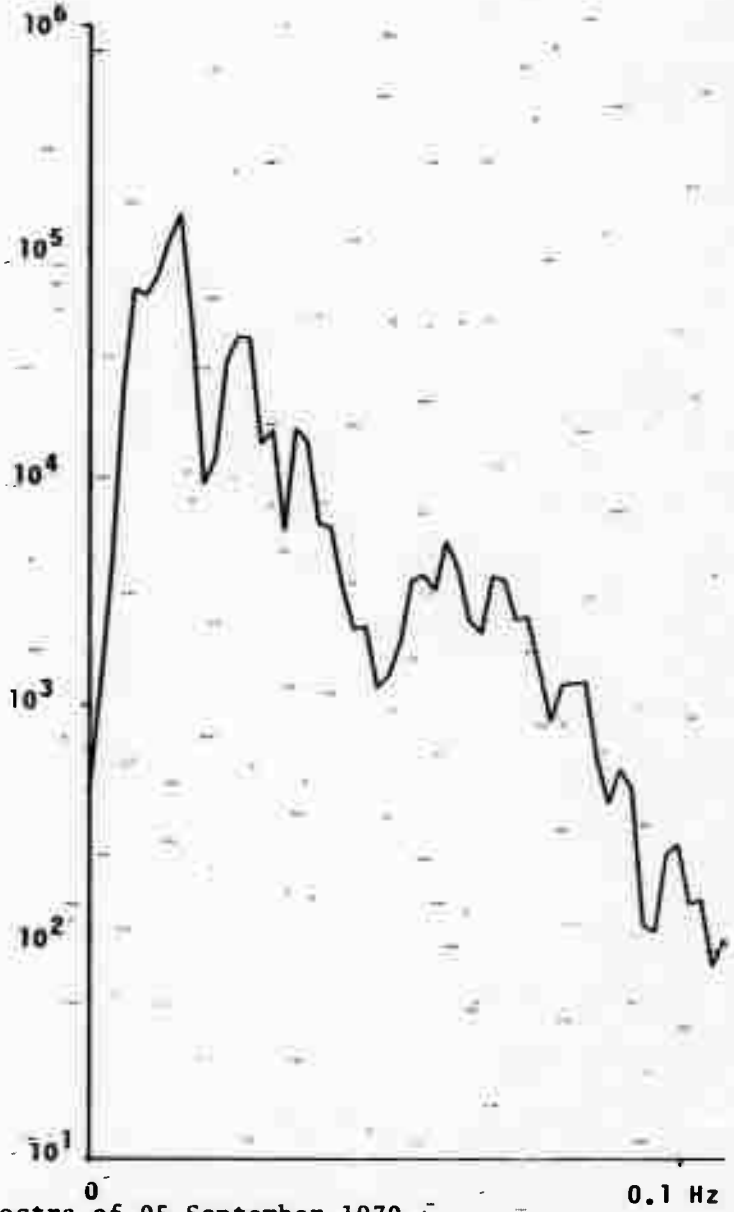

Figure 73. Transverse component spectra of 05 September 1970 noise by site.

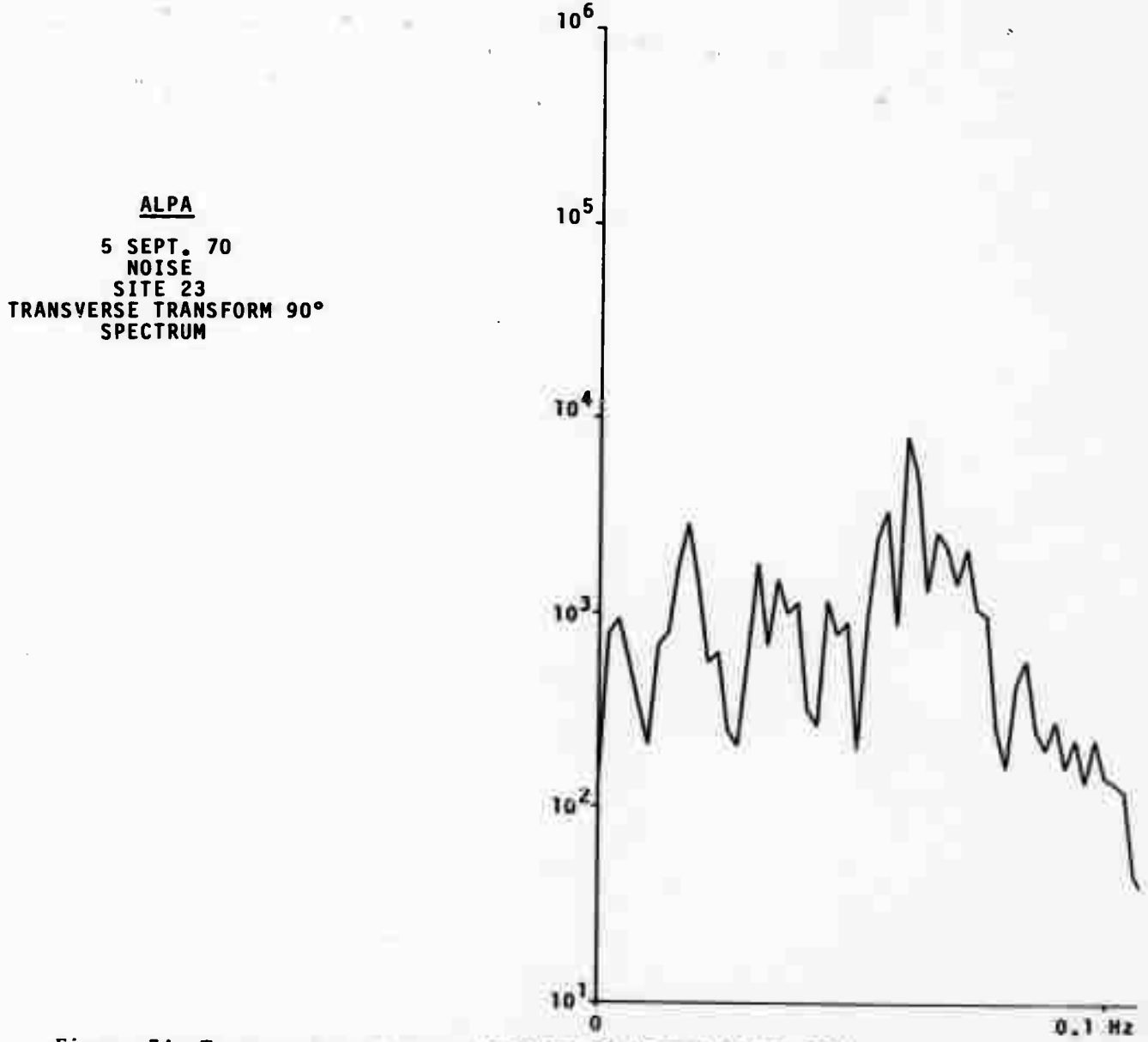

Figure 74. Transverse component spectra of 05 September 1970 noise by site.

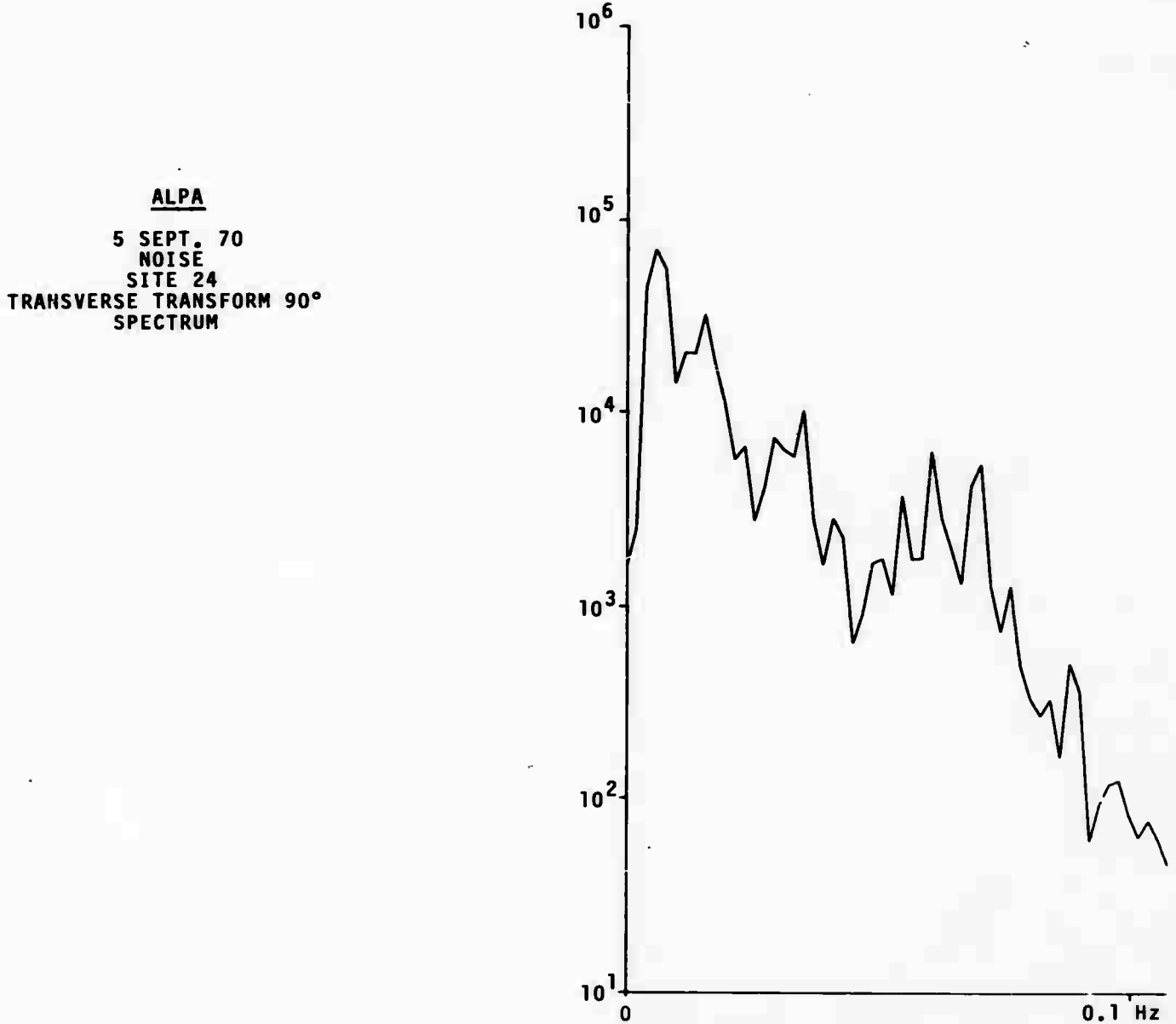

Figure 75. Transverse component spectra of 05 September 1970 noise by site.

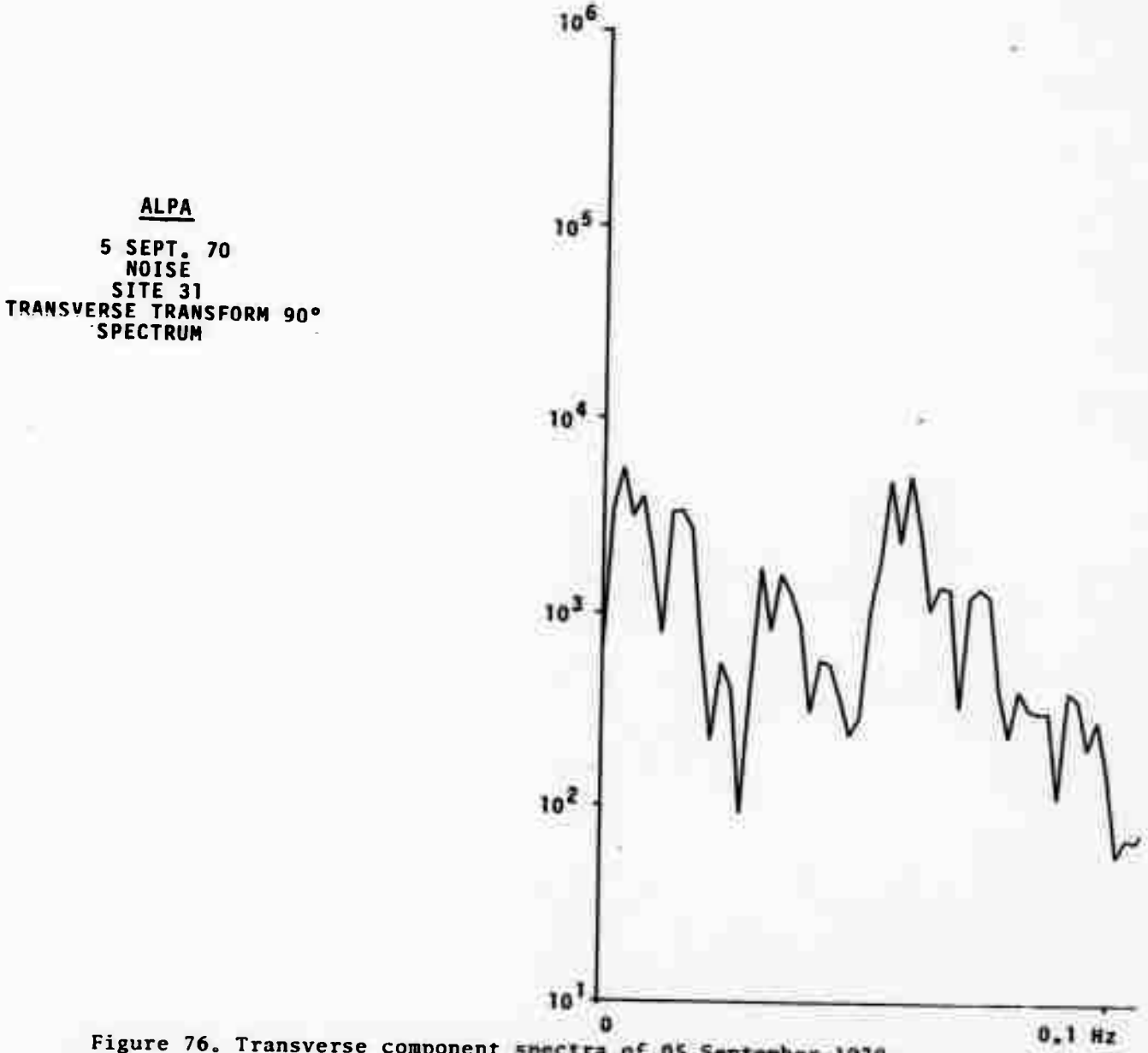

Figure 76. Transverse component spectra of 05 September 1970 noise by site.

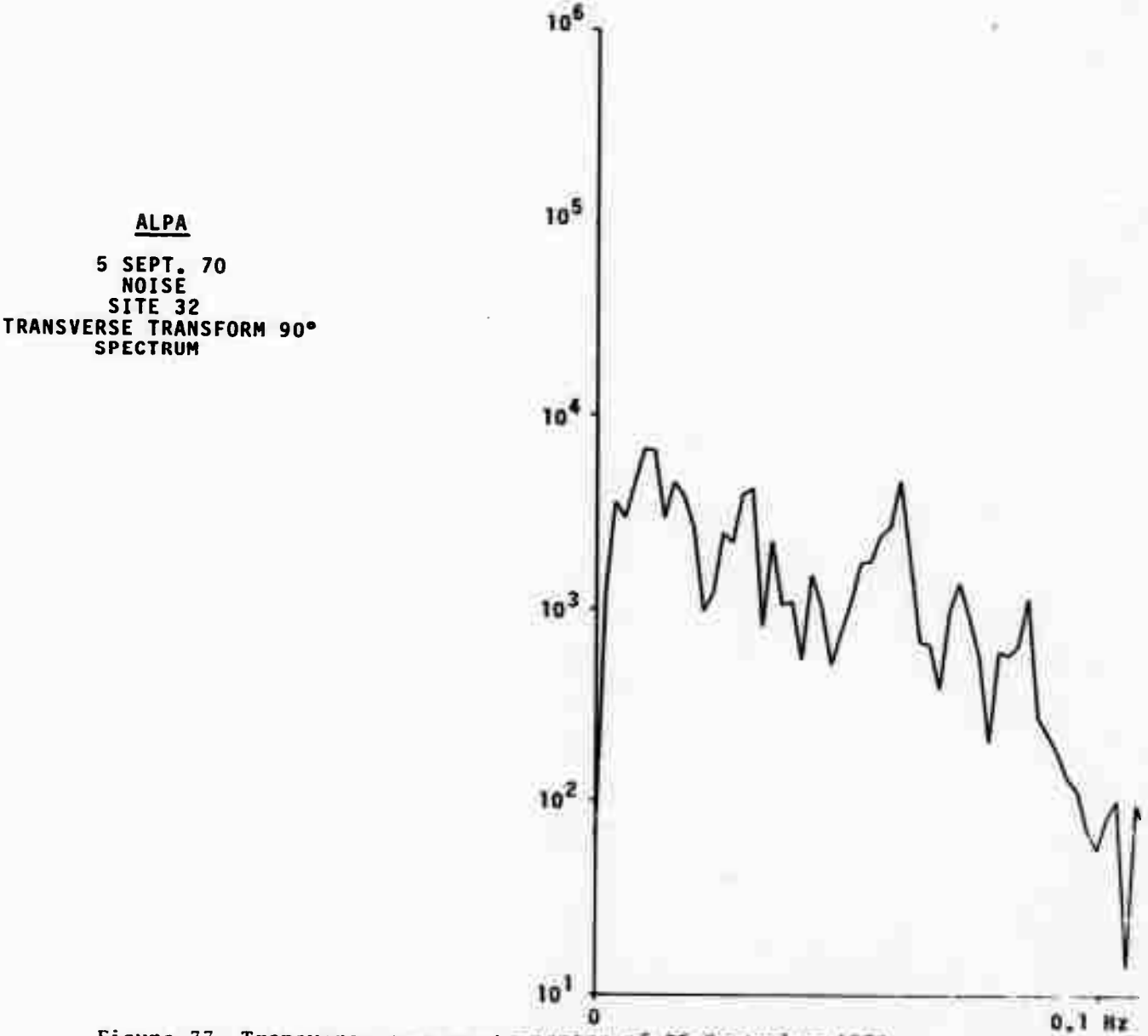

Figure 77. Transverse component spectra of 05 September 1970 noise by site.

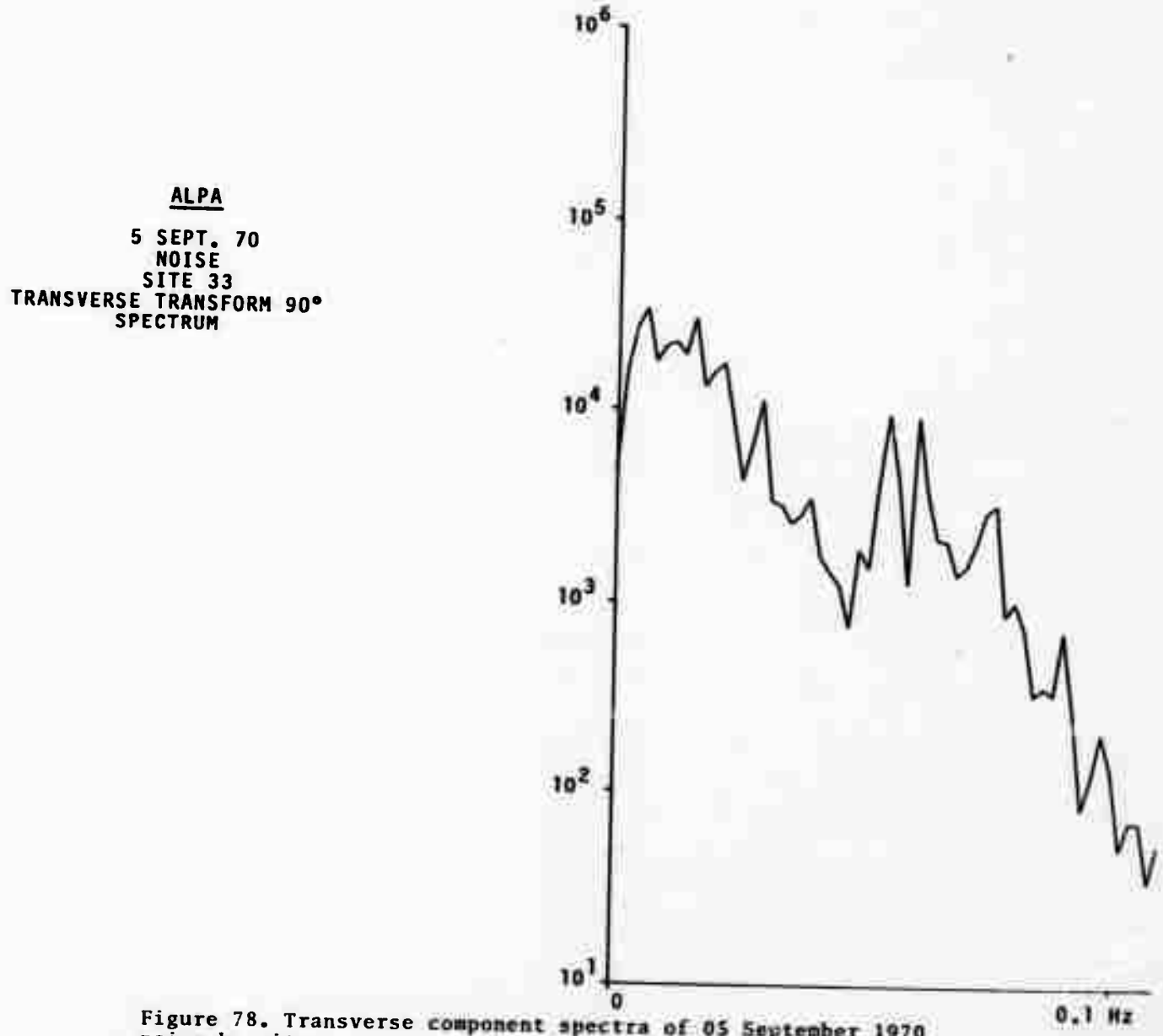

Figure 78. Transverse component spectra of 05 September 1970 noise by site.

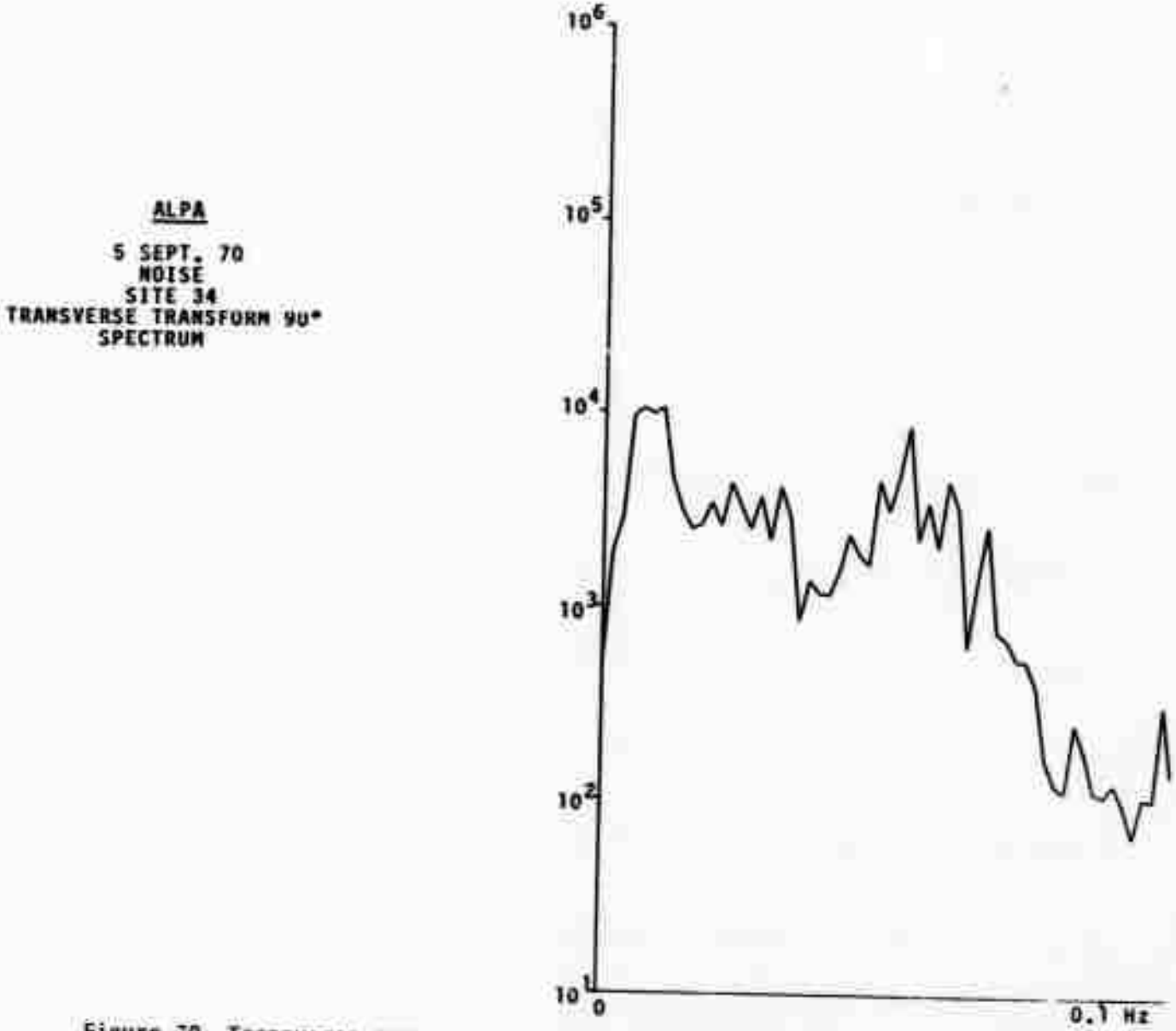

Figure 79. Transverse component spectra of 05 September 1970 noise by site.

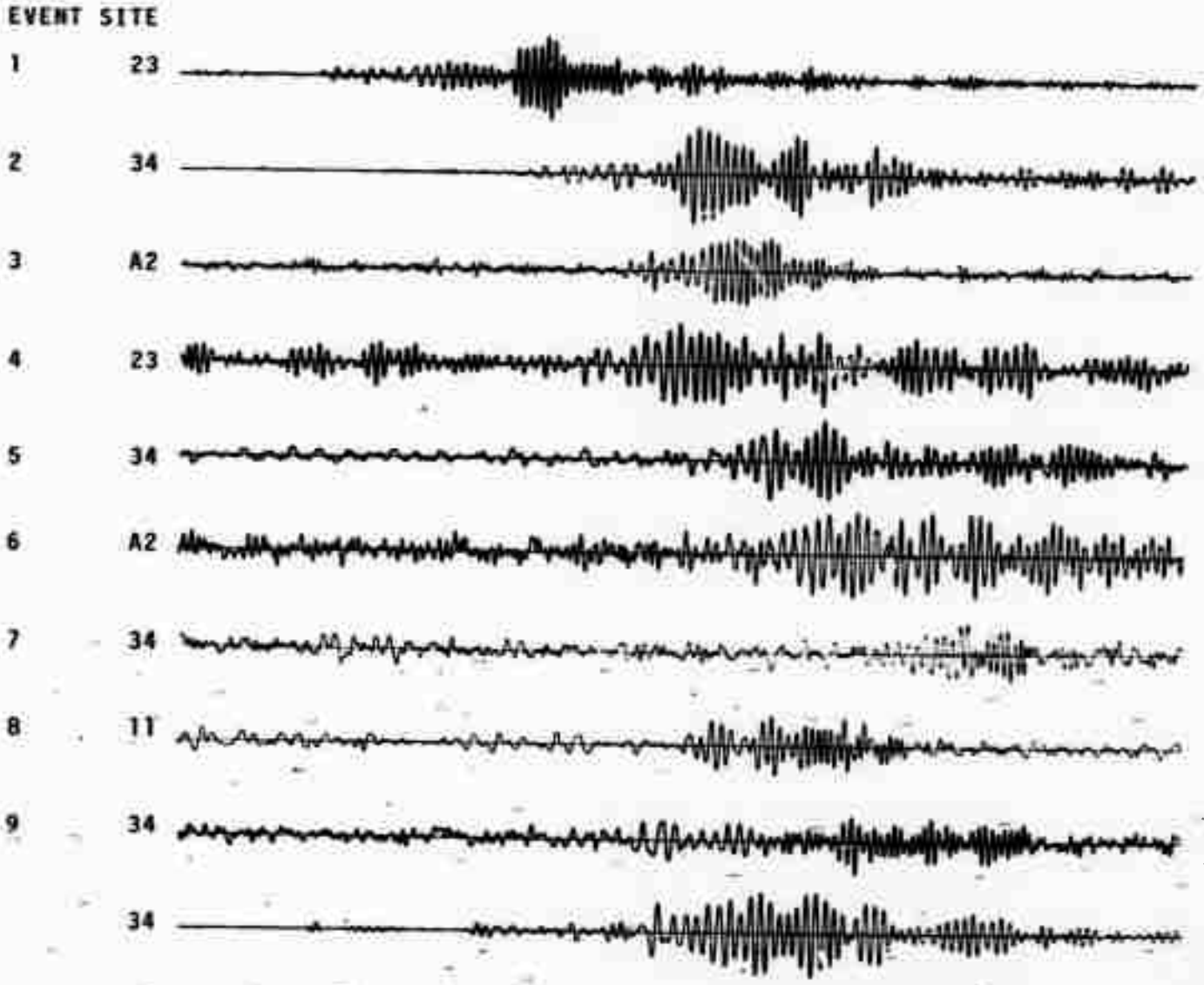

Figure 80. Signals spectral estimated -- vertical transform.

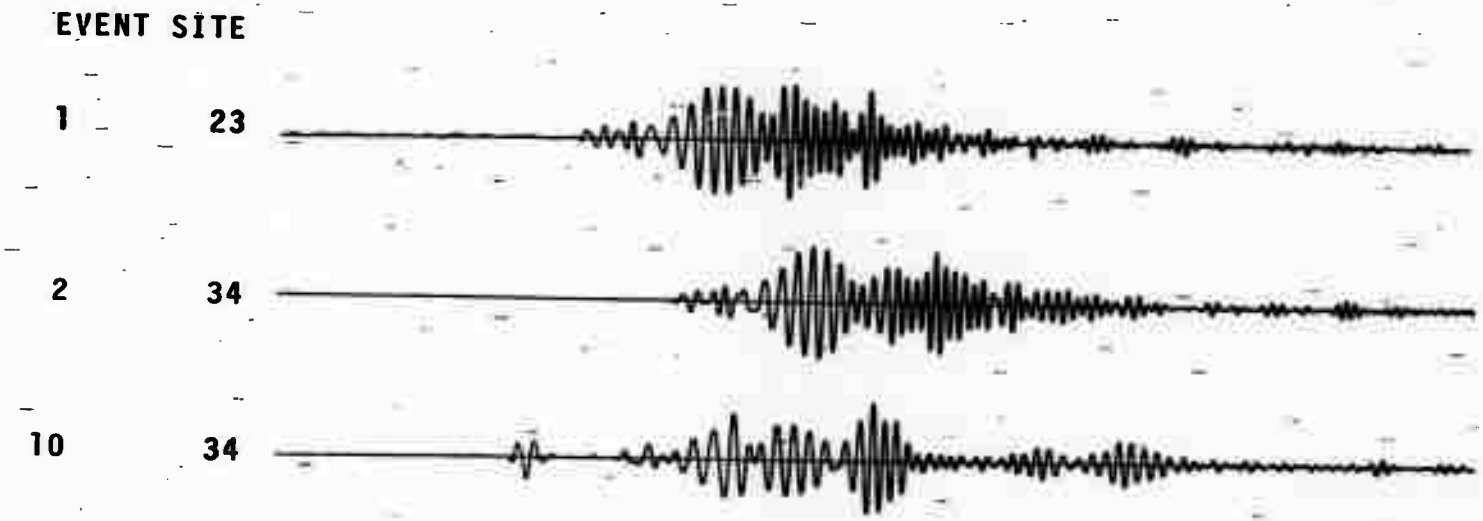

Figure 81. Signals spectral estimates -- transverse transform.

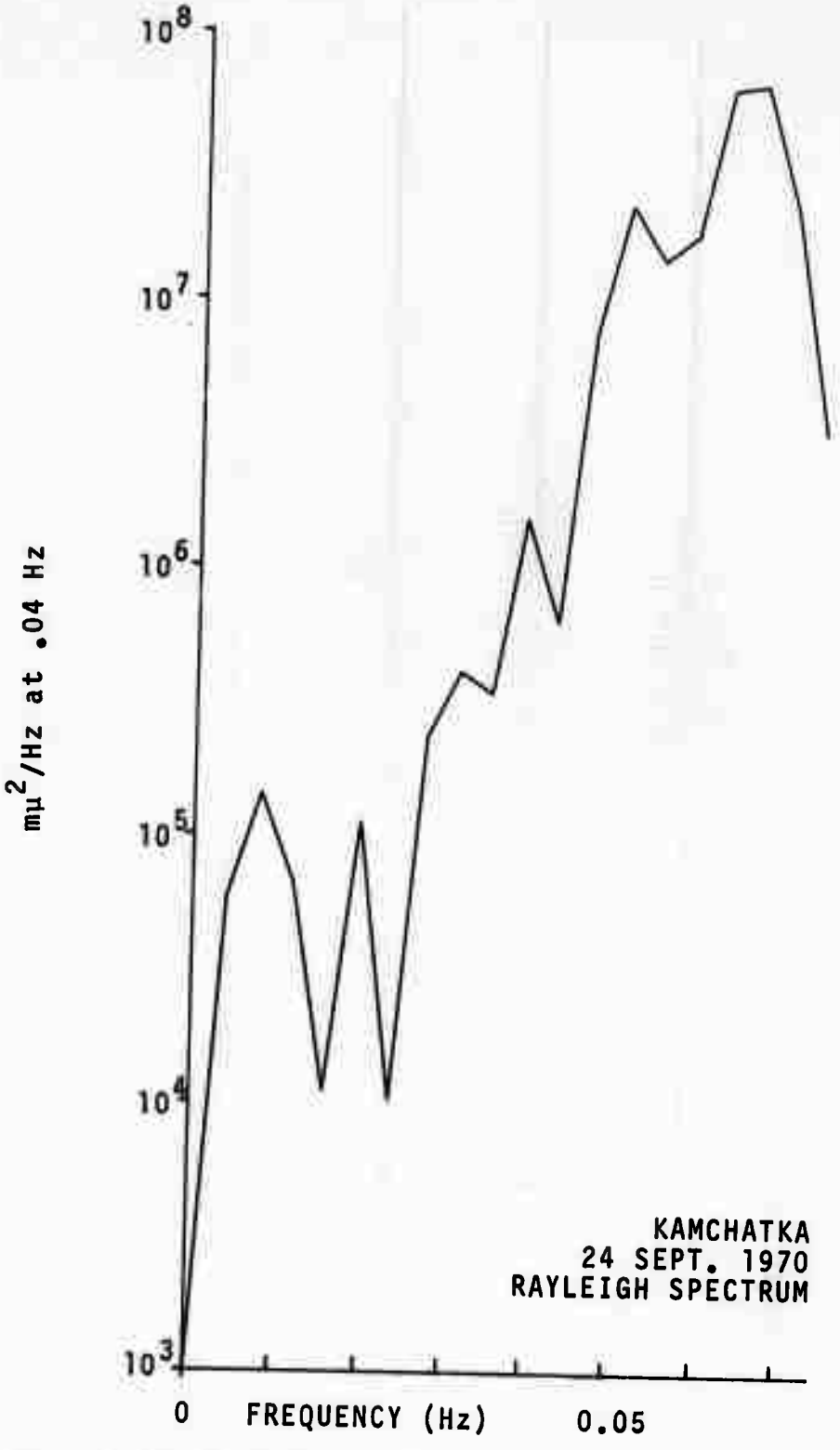

Figure 82. Rayleigh wave spectra of ten events.

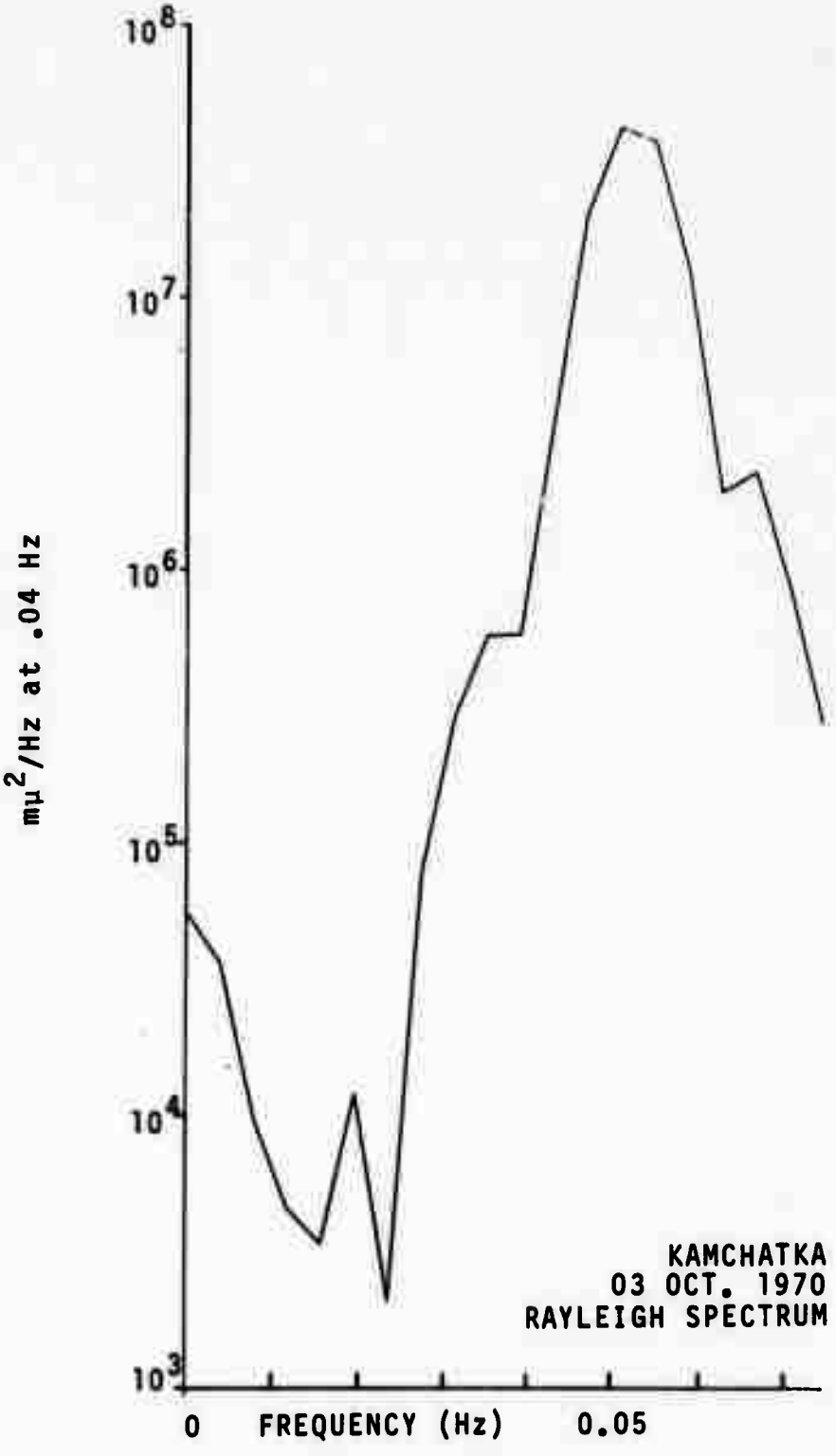

Figure 83. Rayleigh wave spectra of ten events.

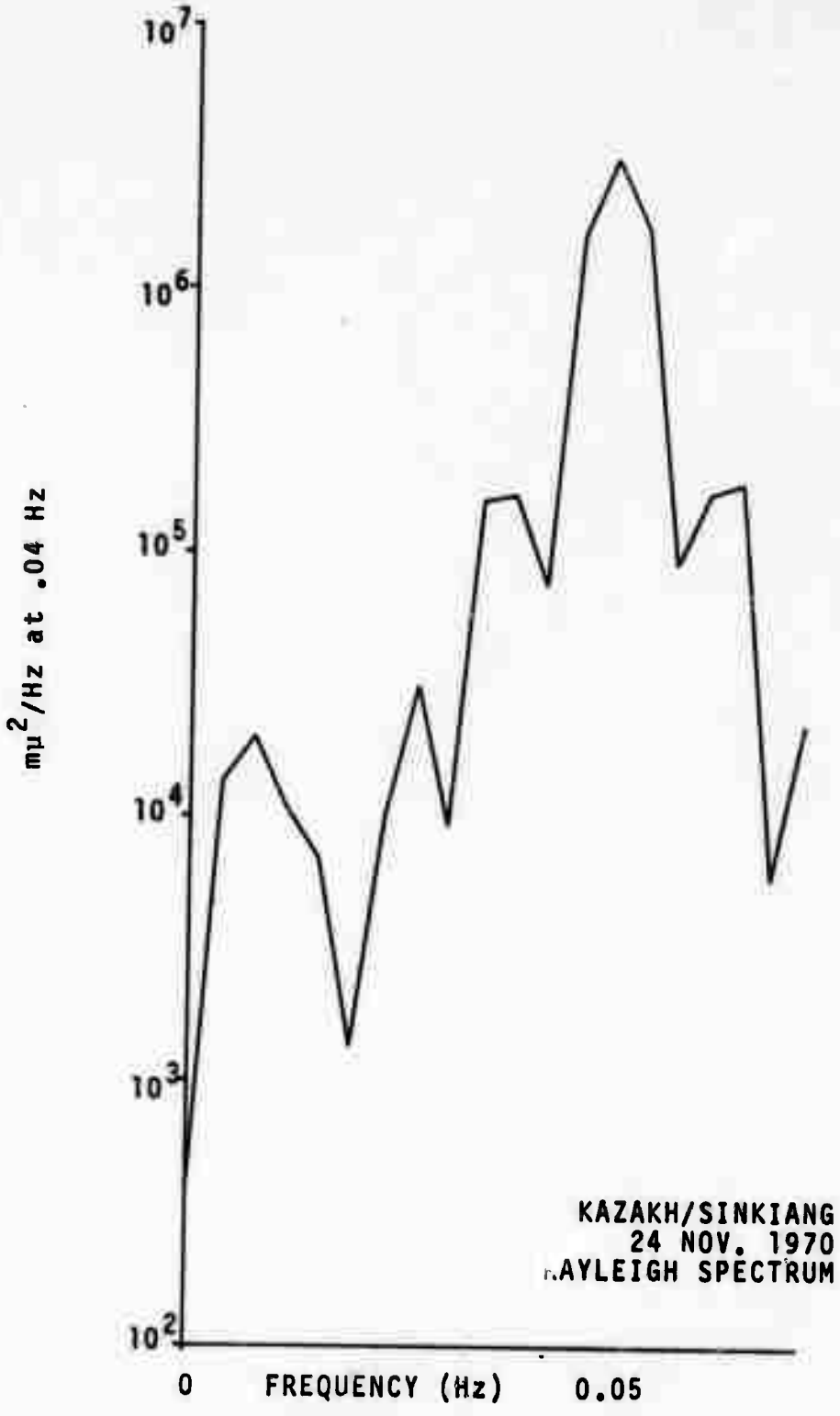

Figure 84. Rayleigh wave spectra of ten events.

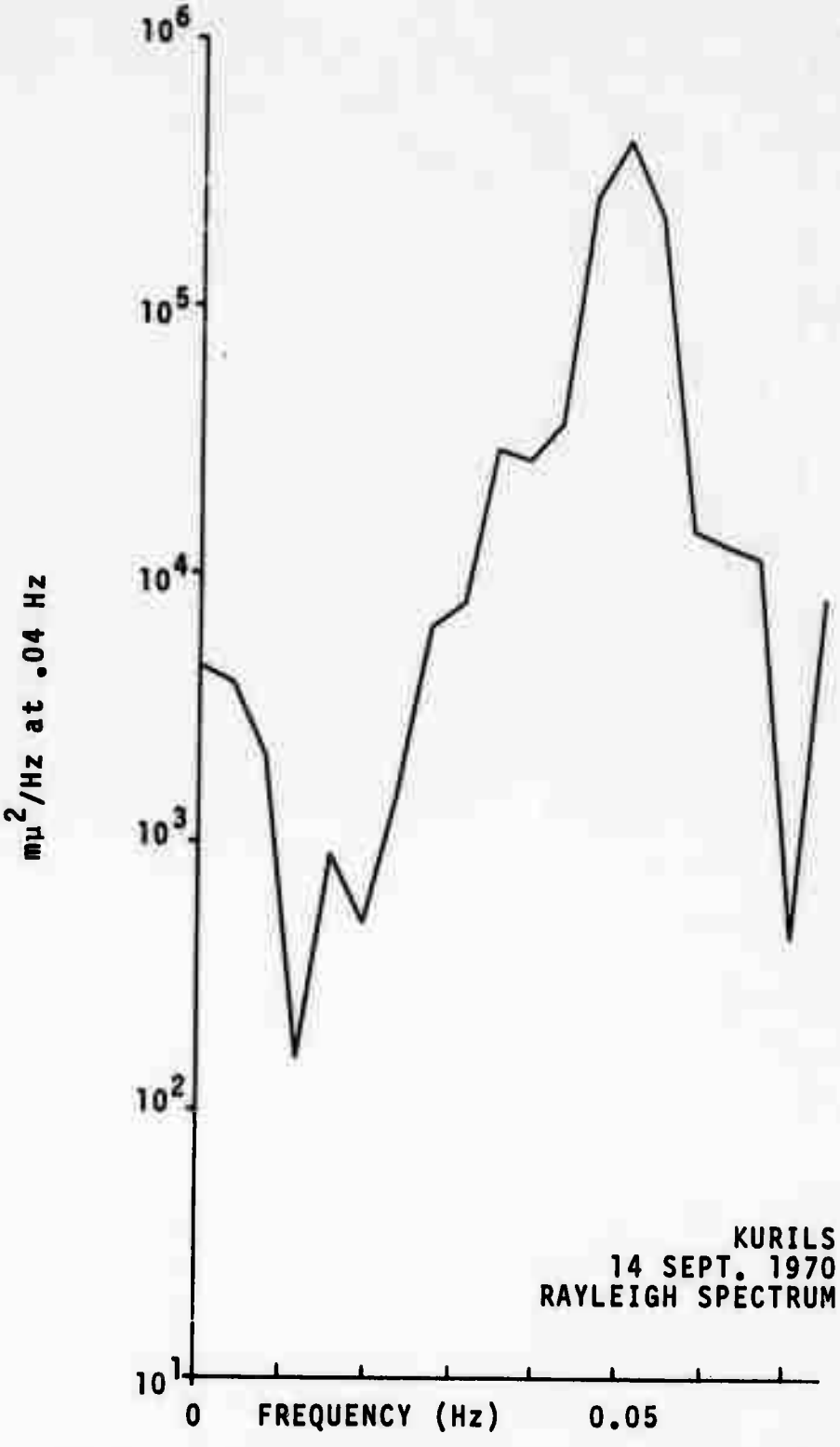

Figure 85. Rayleigh wave spectra of ten events.

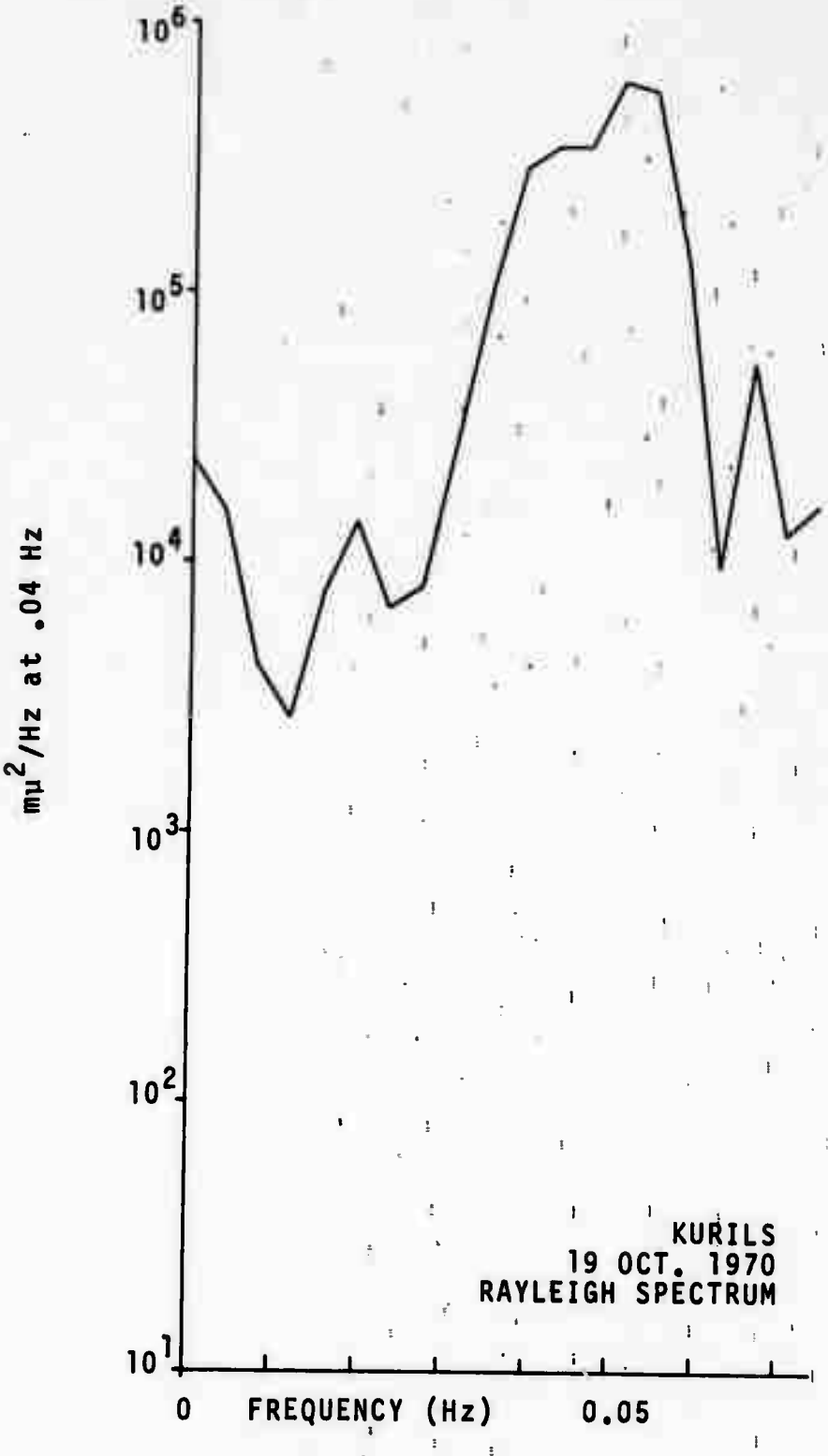

Figure 86. Rayleigh wave spectra of ten events.

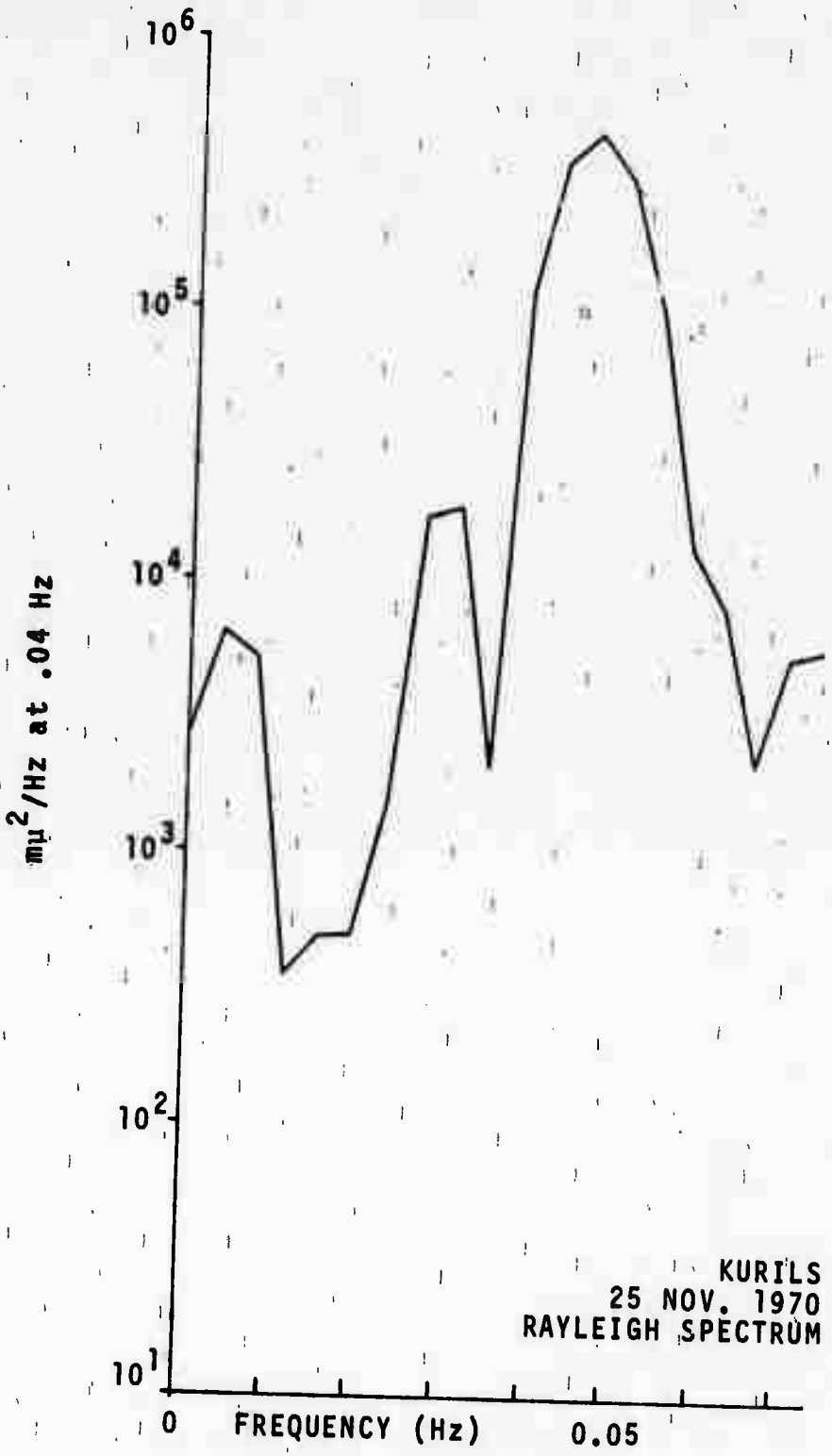

Figure 87. Rayleigh wave spectra of ten events.

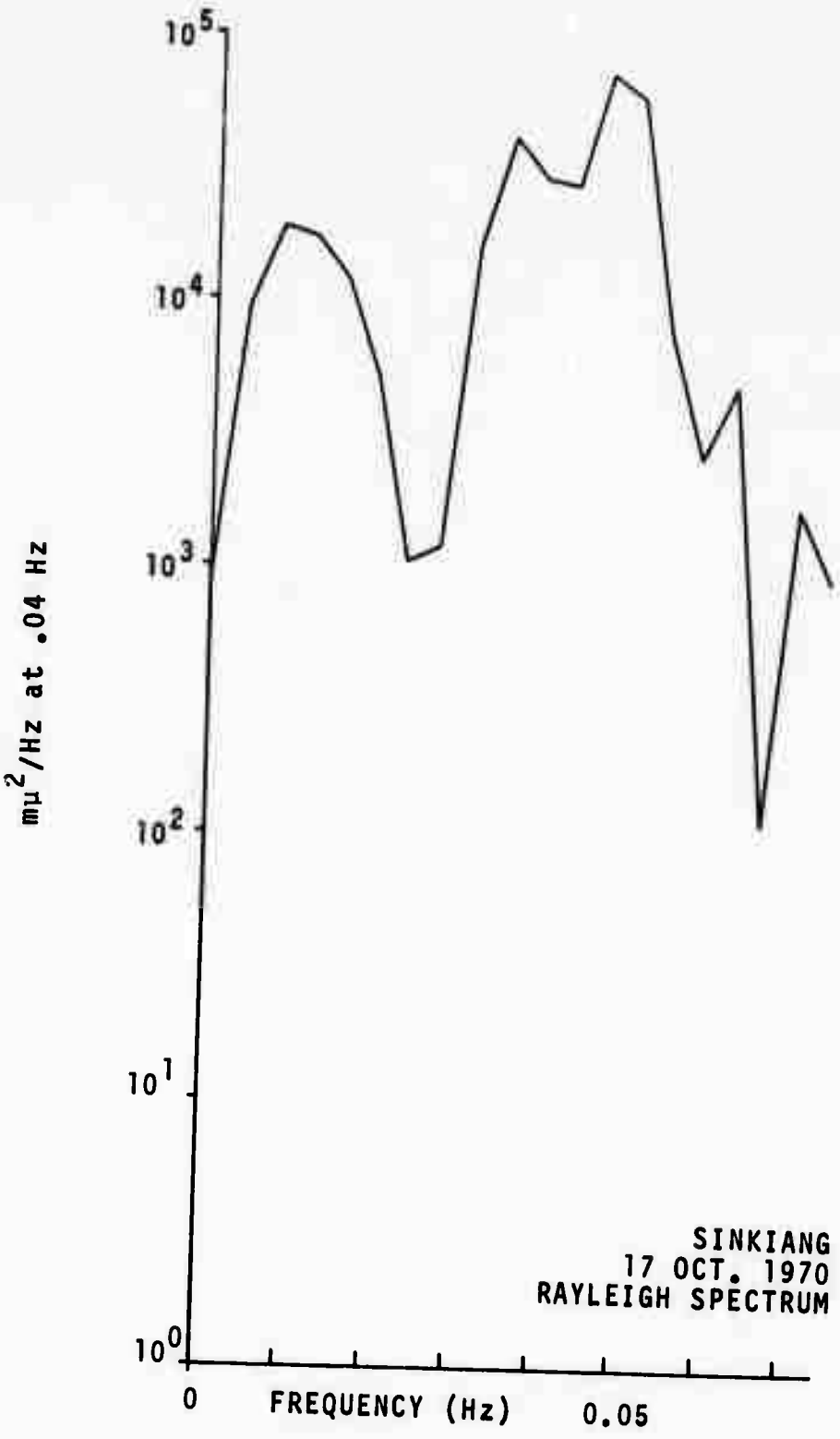

Figure 88. Rayleigh wave spectra of ten events.

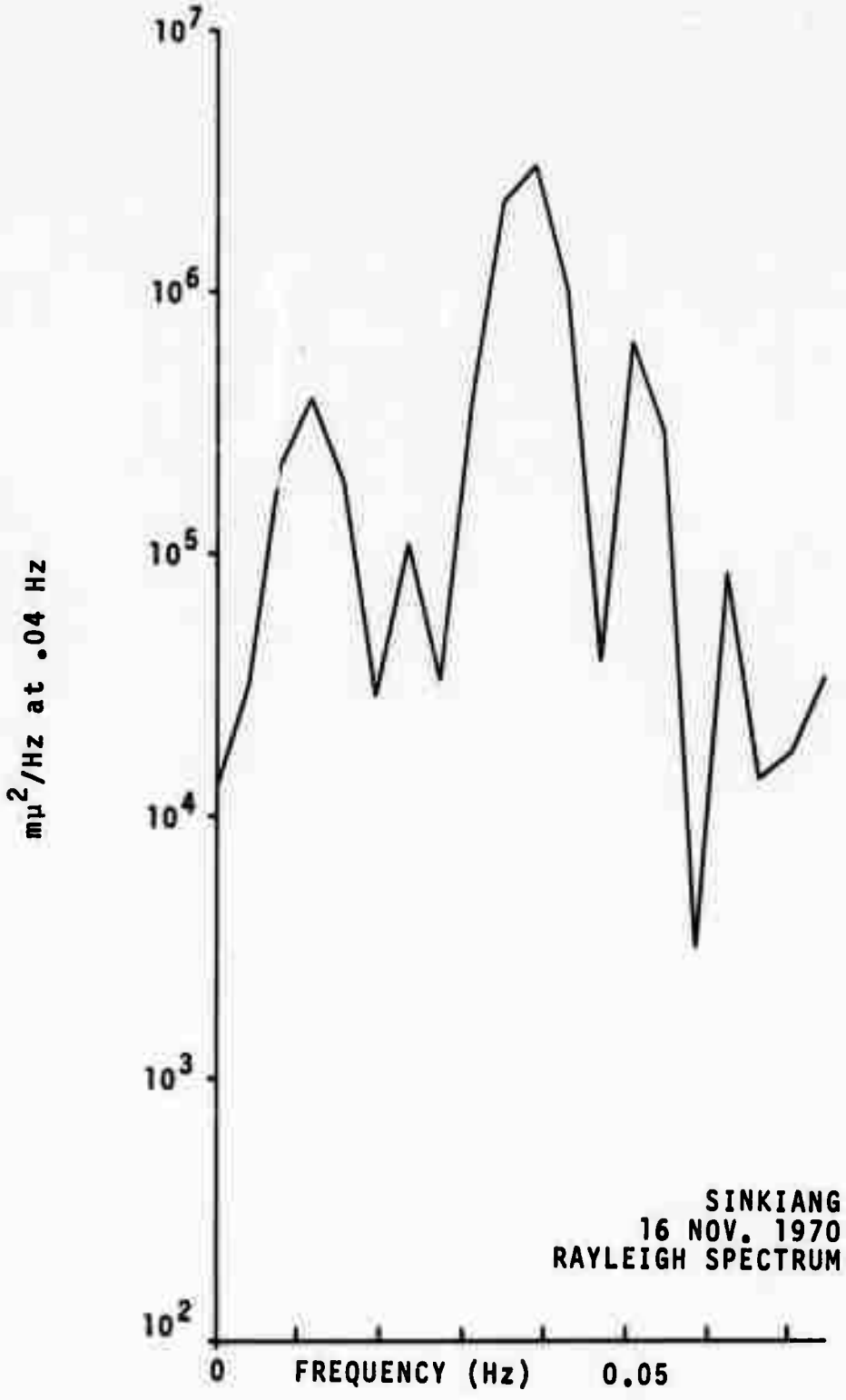

Figure 89. Rayleigh wave spectra of ten events.

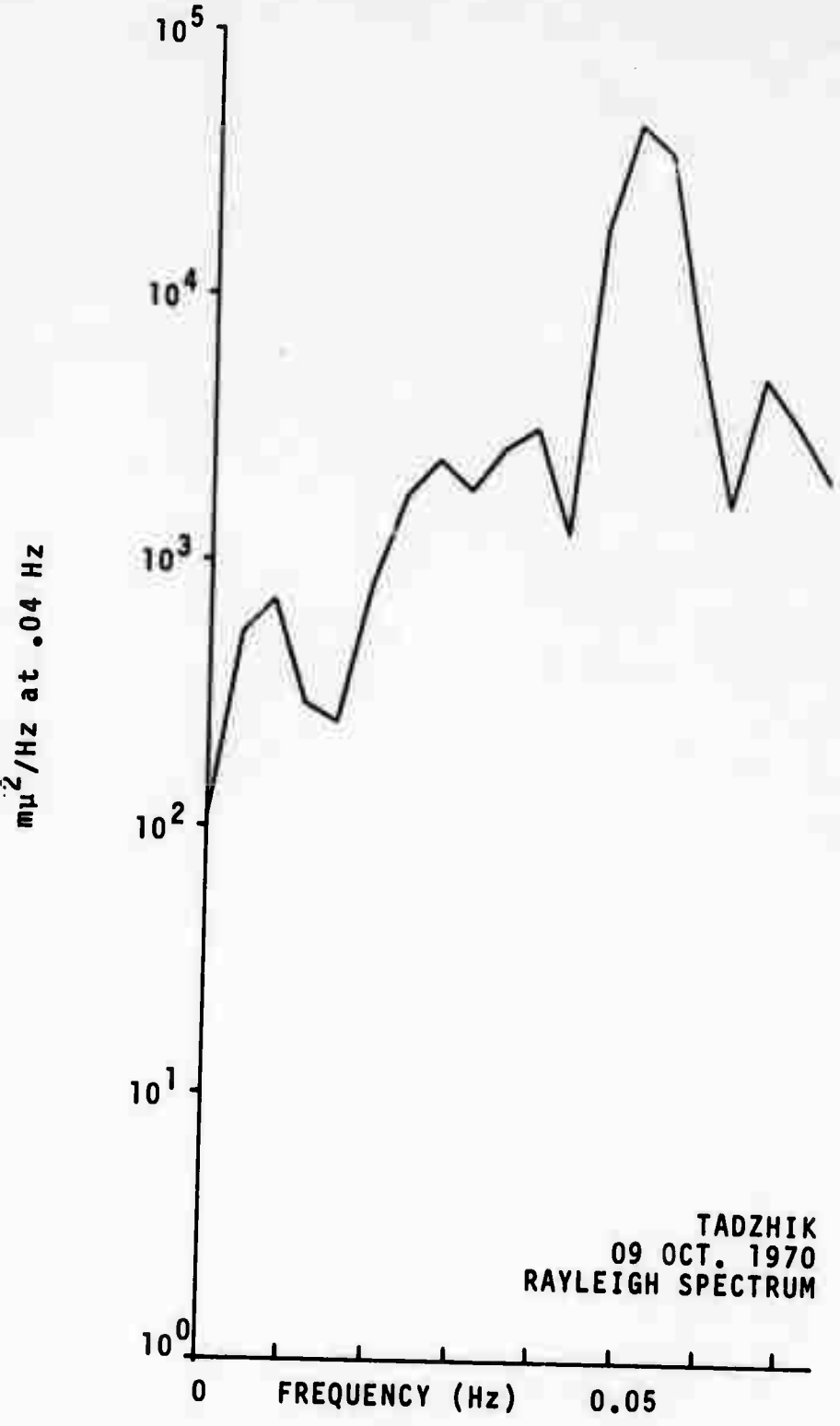

Figure 90. Rayleigh wave spectra of ten events.

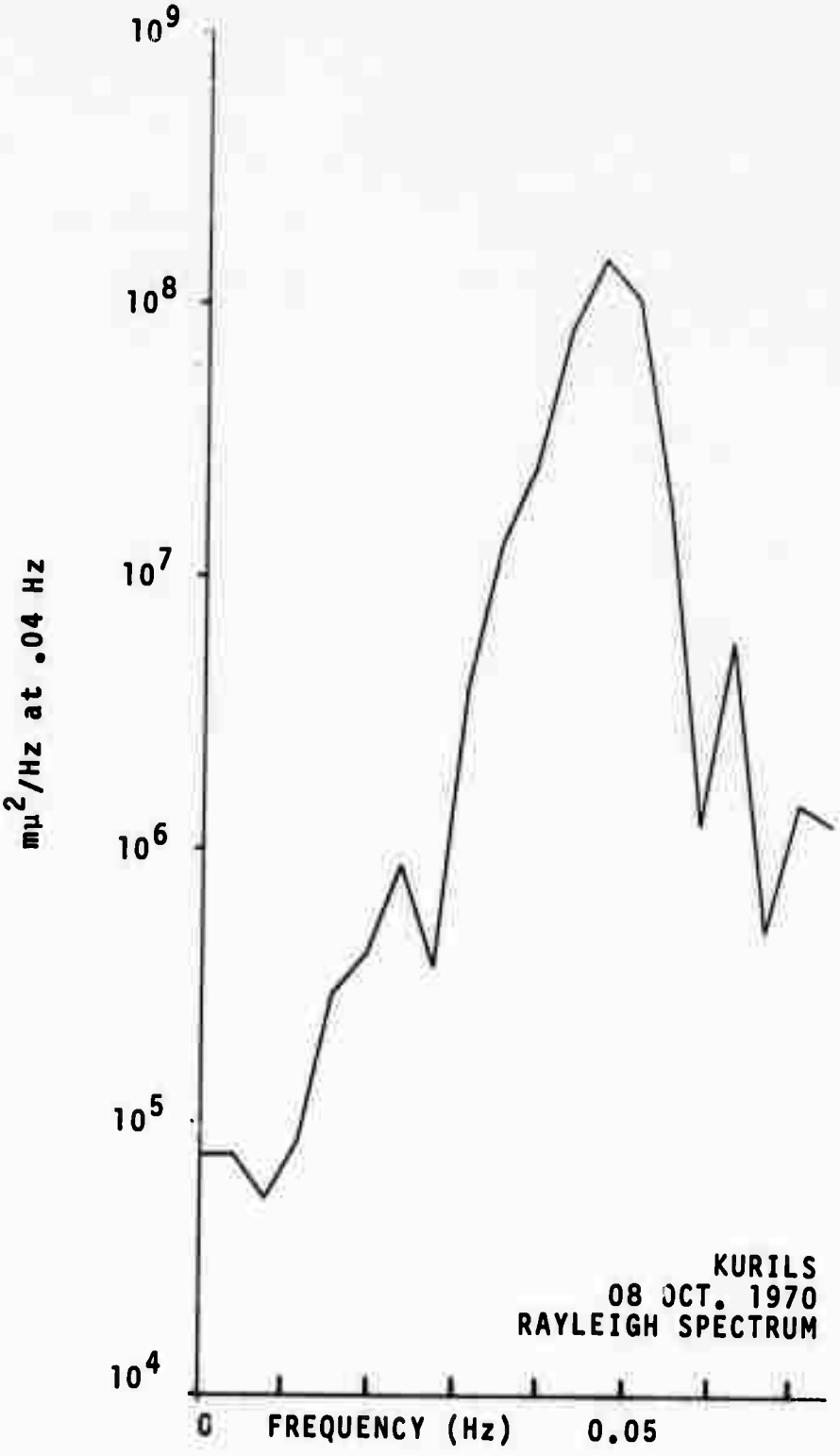

Figure 91. Rayleigh wave spectra of ten events.

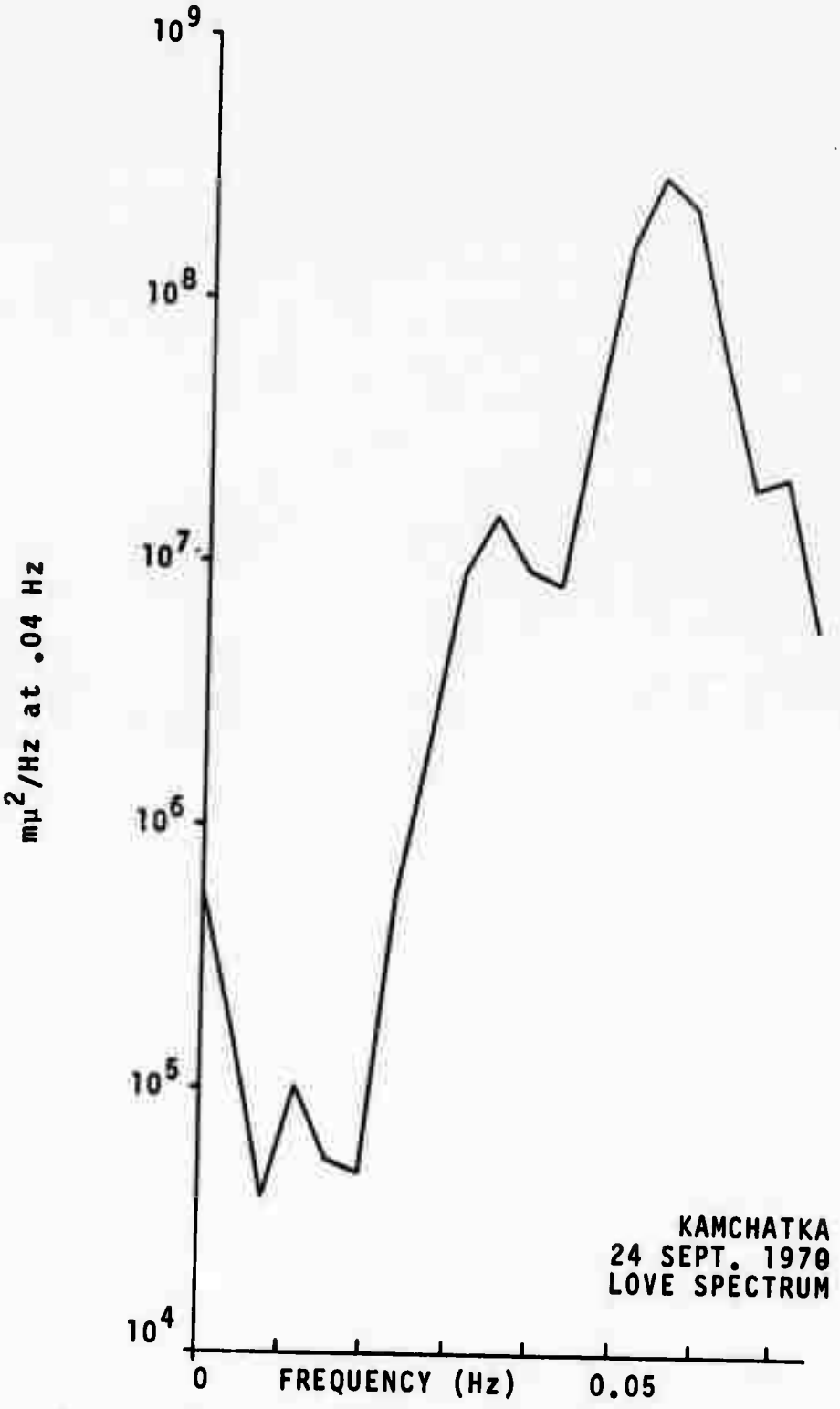

Figure 92. Love wave spectra of three events.

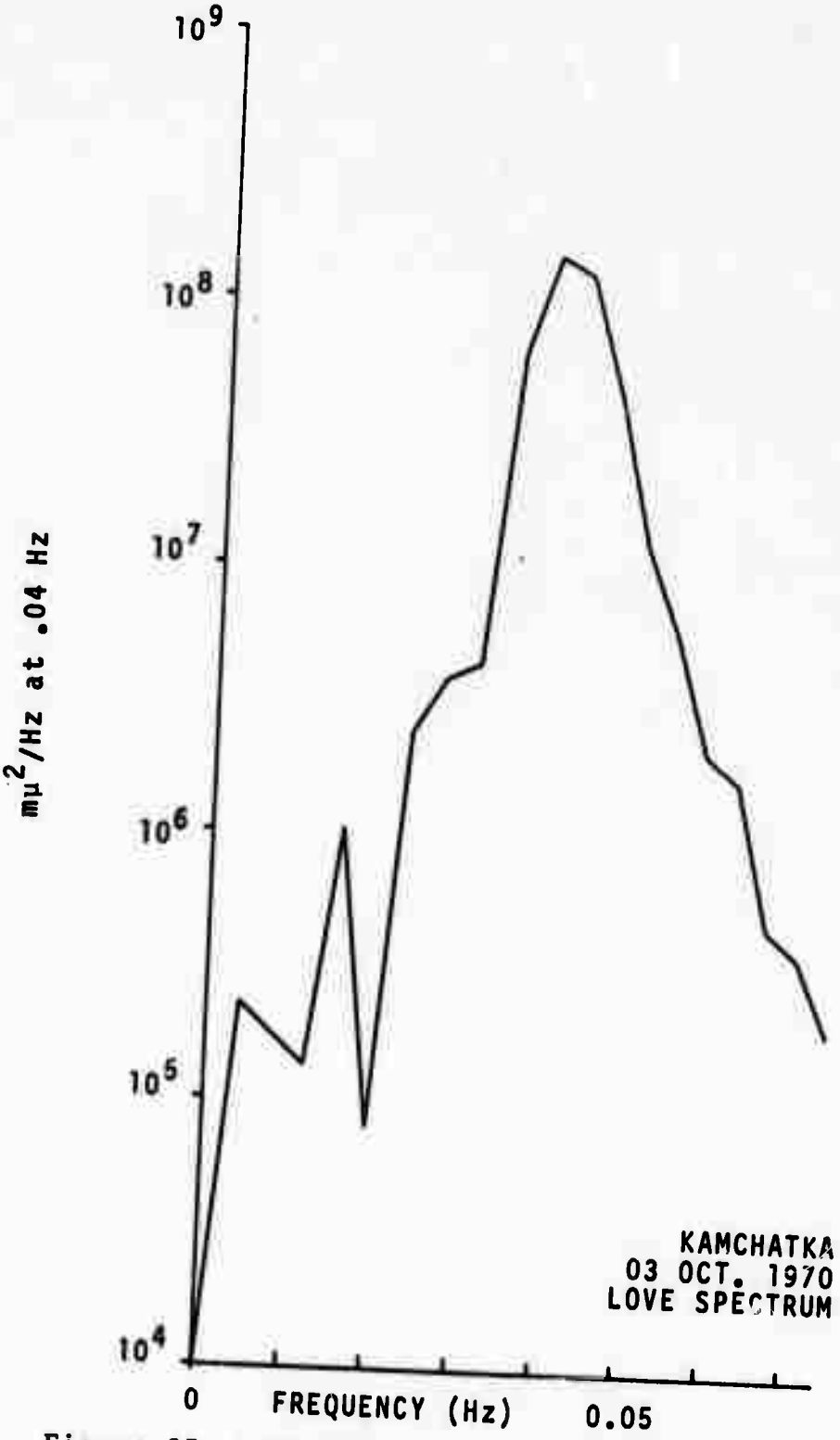

Figure 93. Love wave spectral of three events.

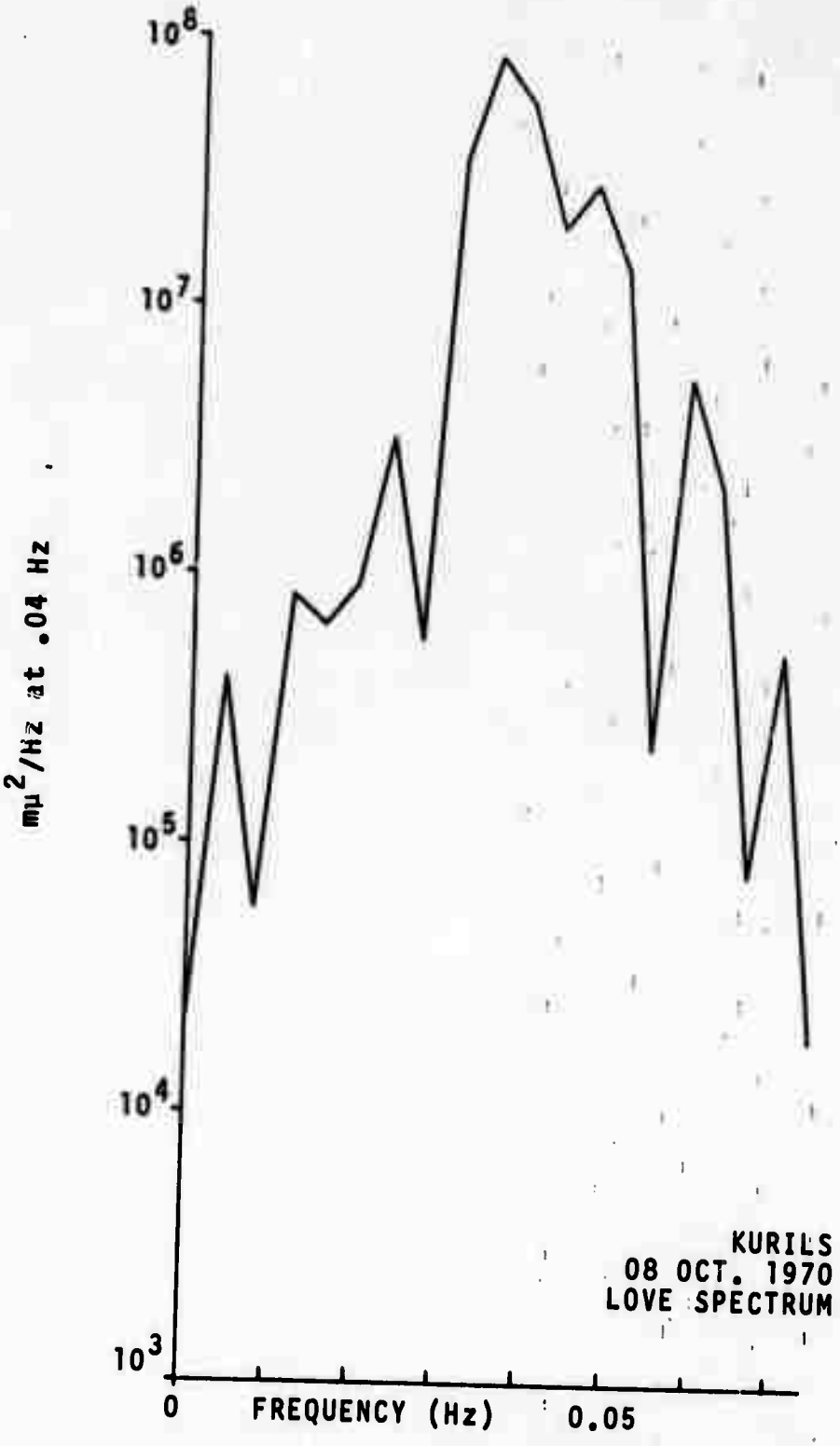

Figure 94. Love wave spectra of three events.

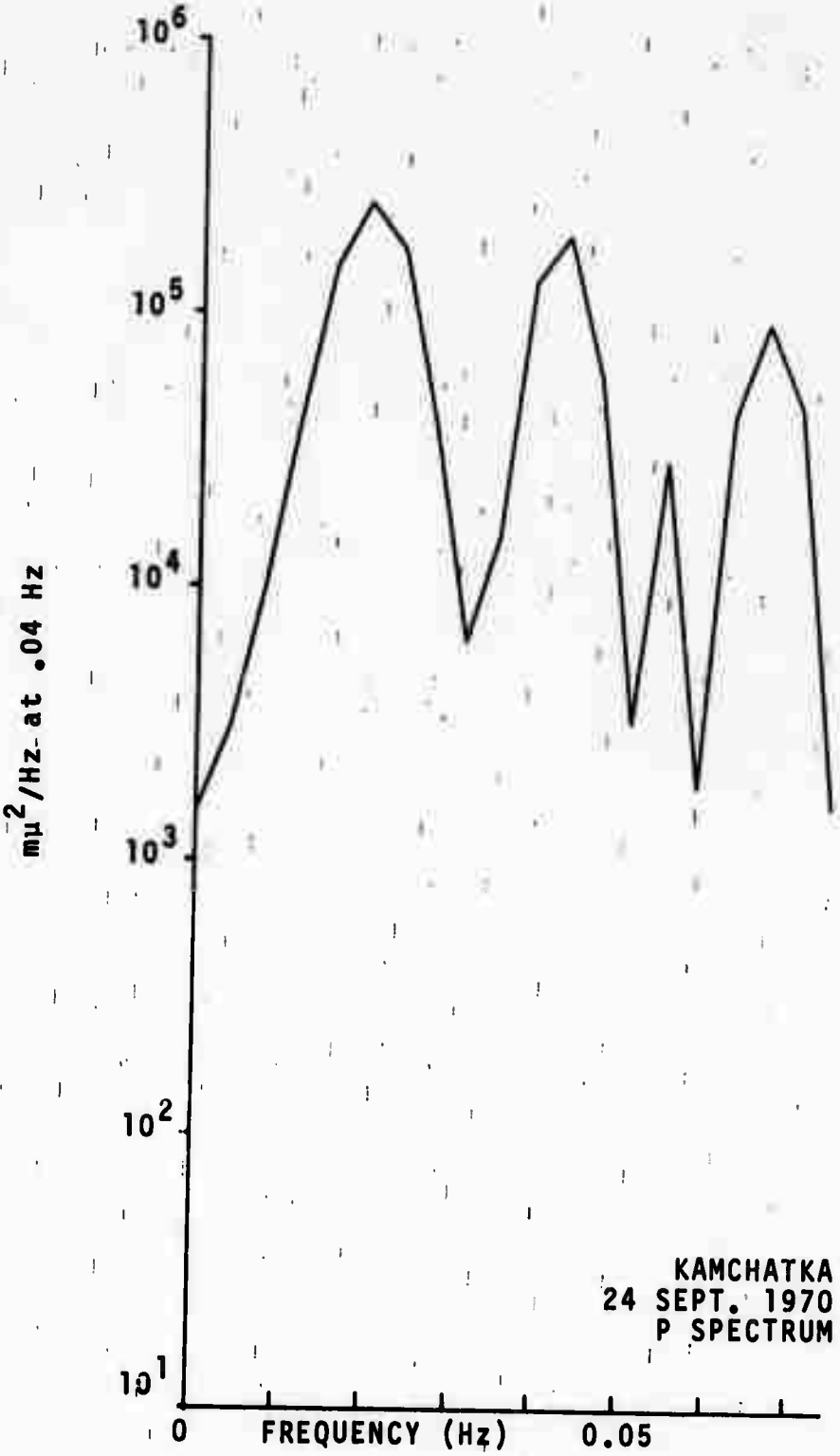

Figure 95. "P" wave spectra of three events.

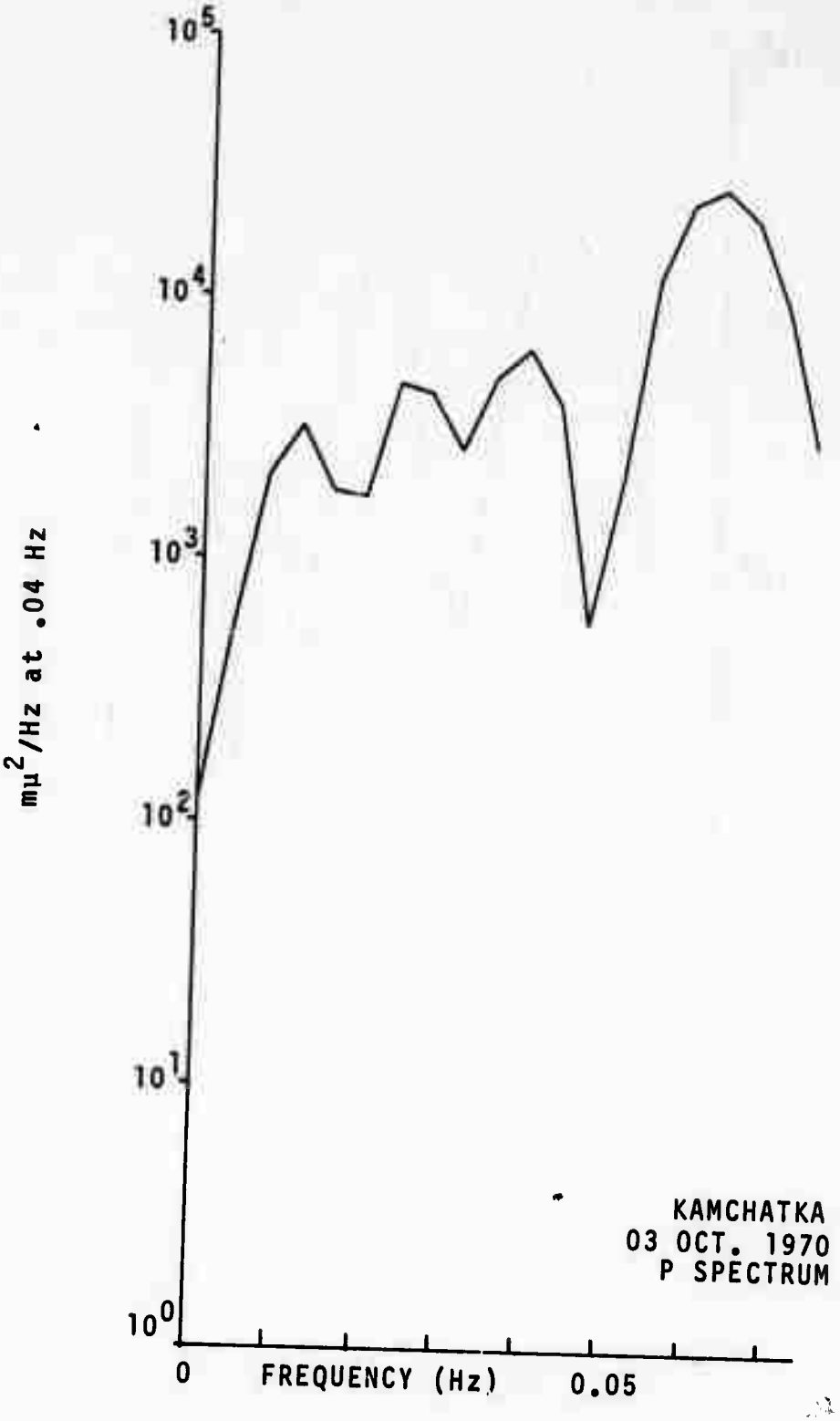

Figure 96. "P" wave spectra of three events.

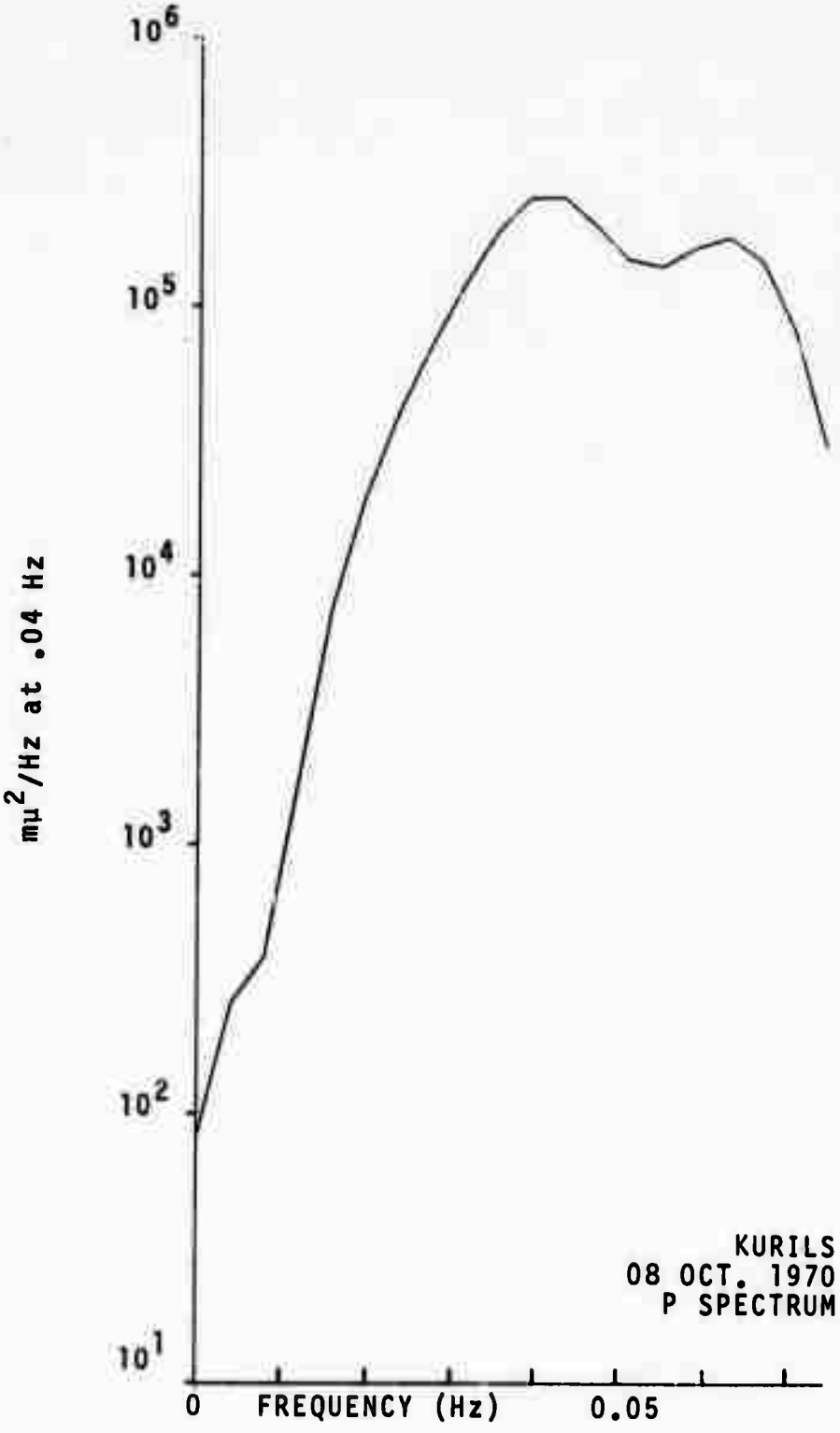

Figure 97. "P" wave spectra of three events.

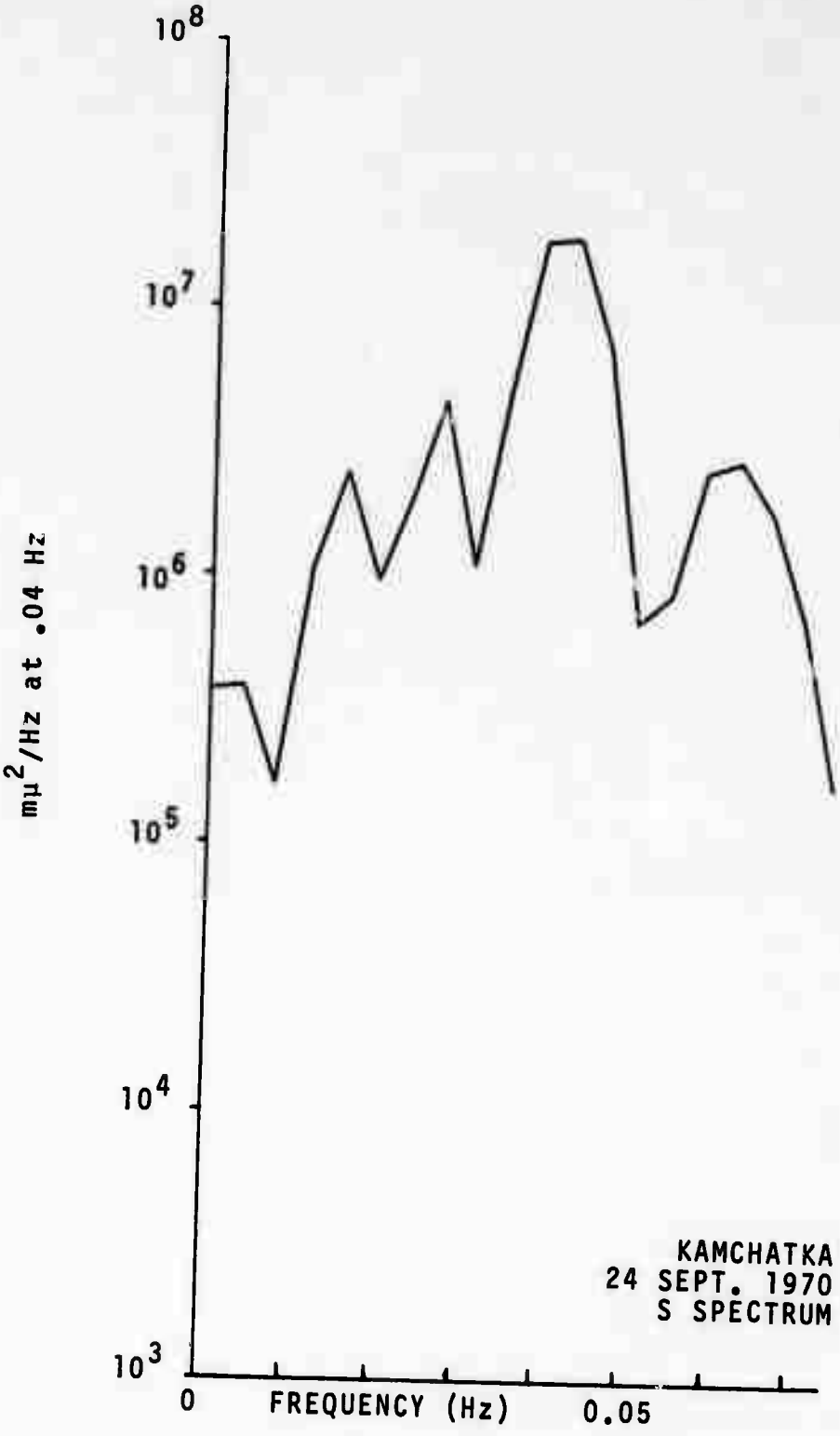

Figure 98. "S" wave spectra of three events.

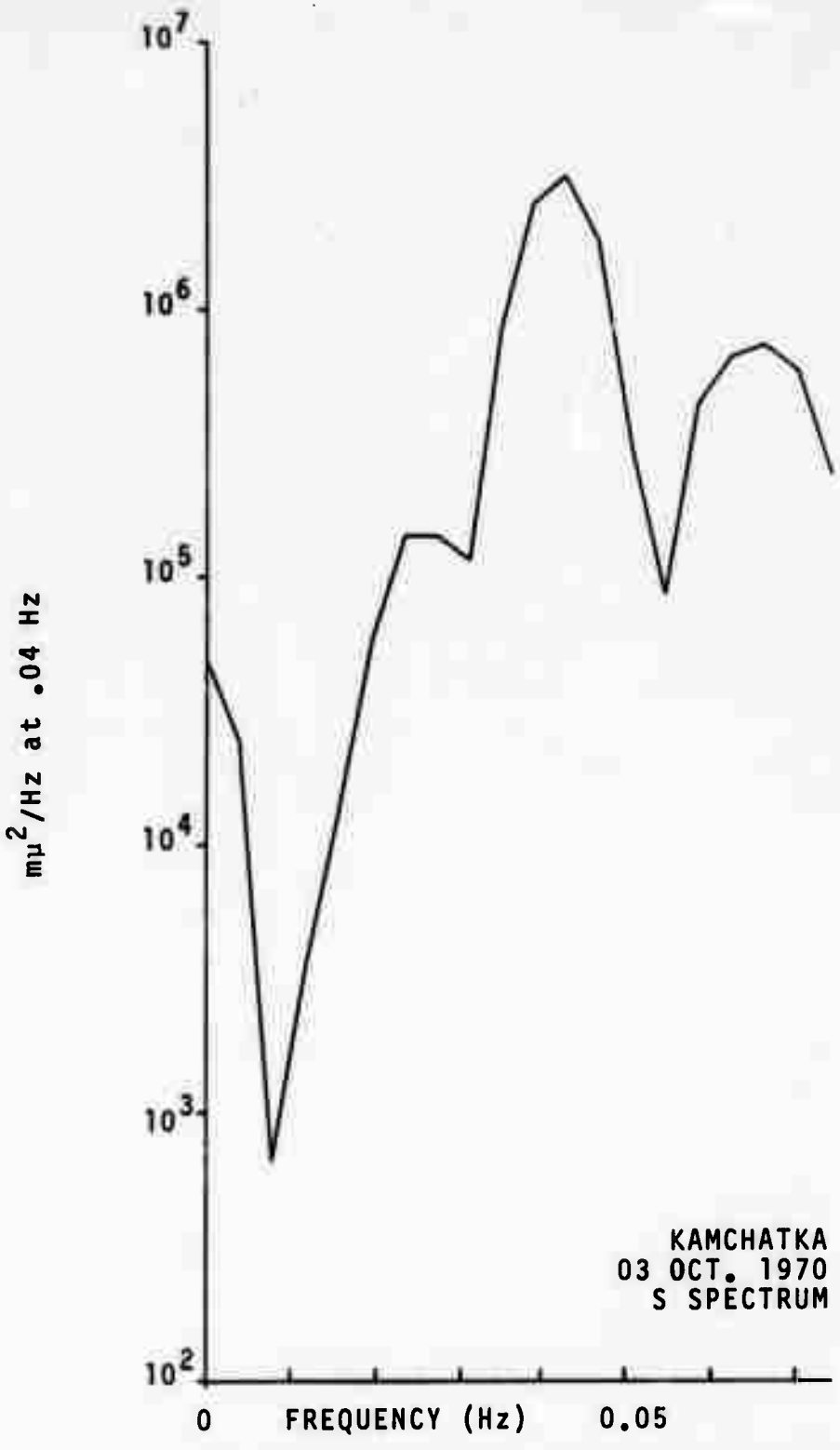

Figure 99. "S" wave spectra of three events.

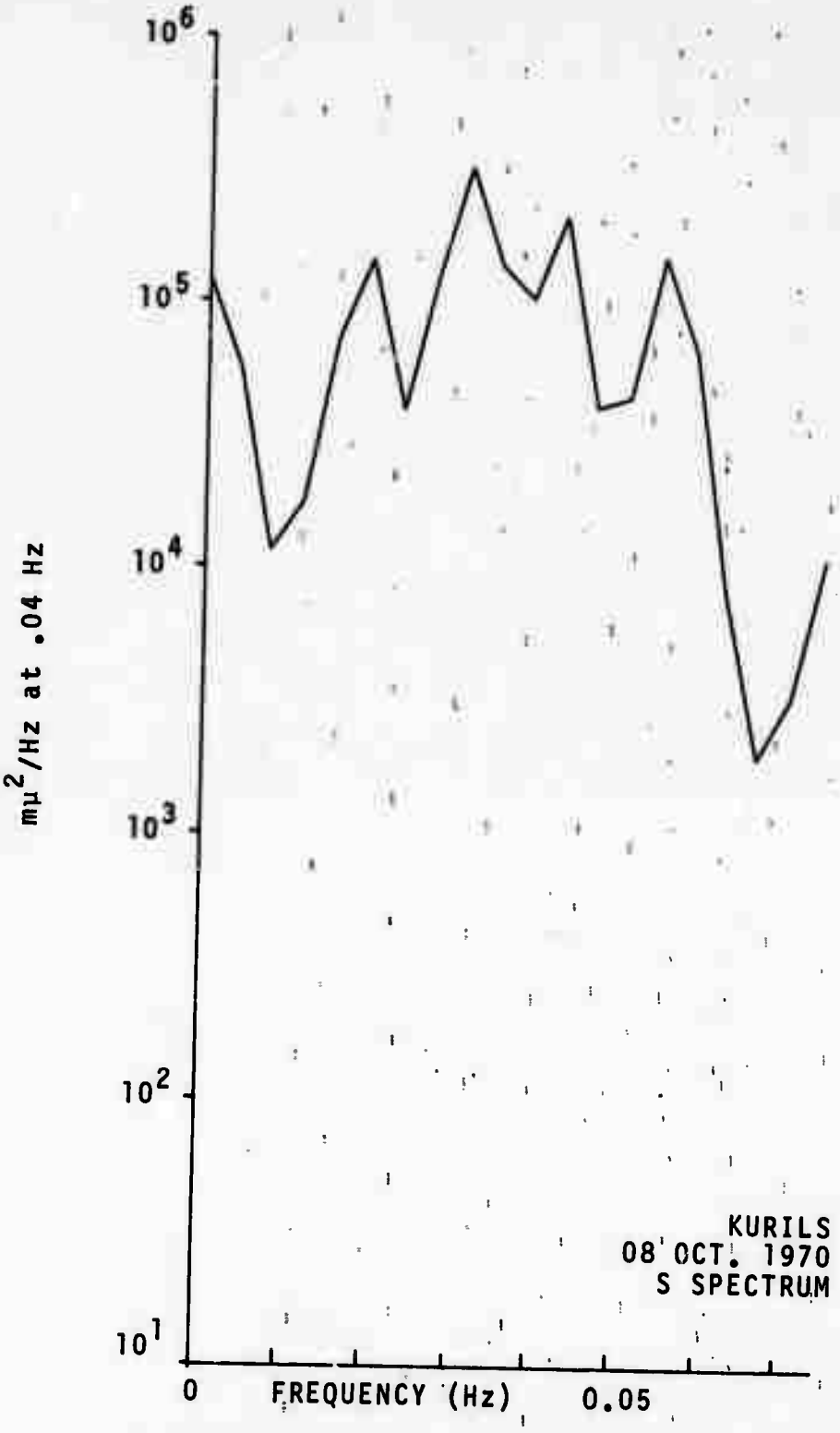

Figure 100. "S" wave spectra of three events.

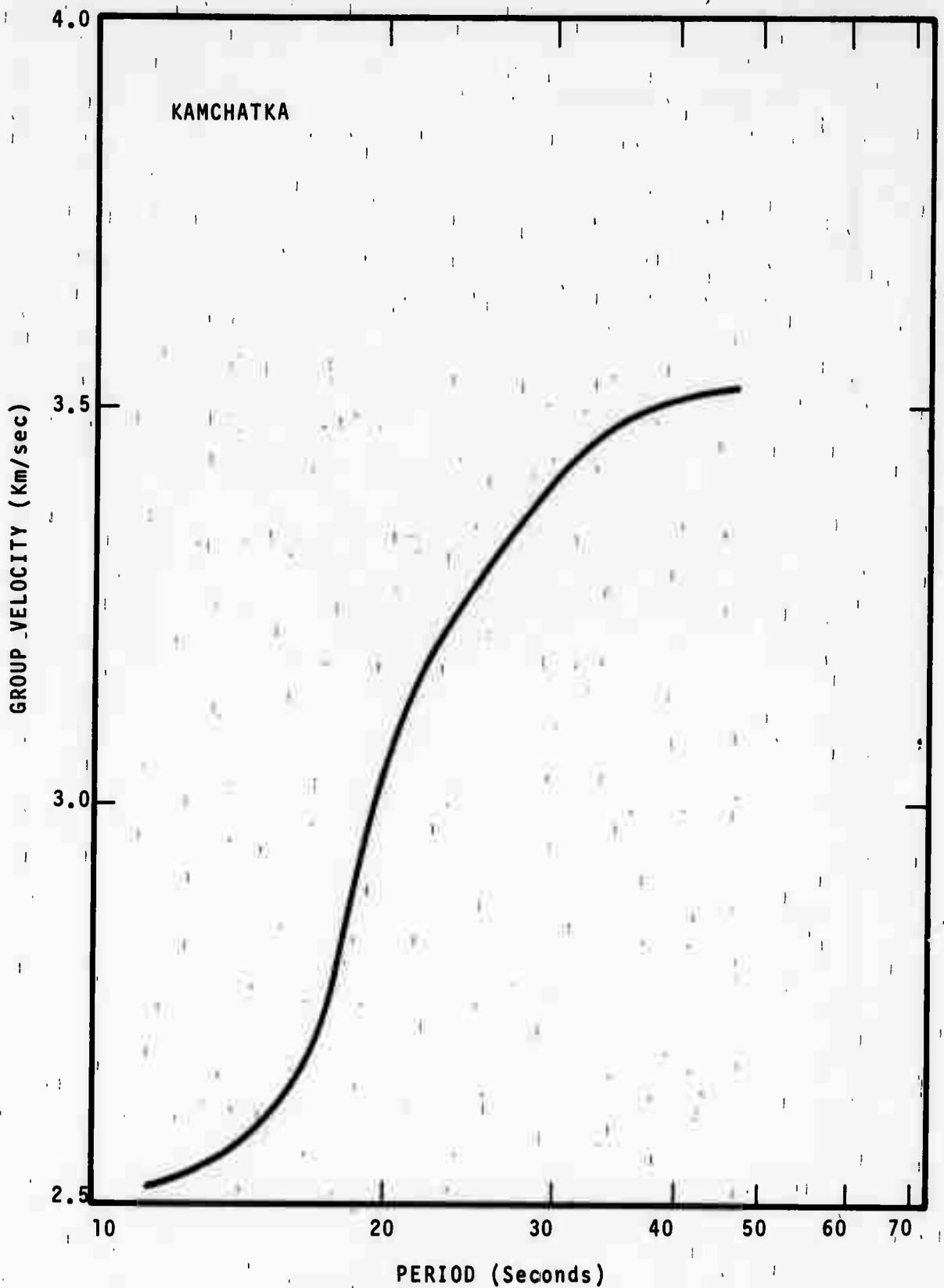

Figure 101. Rayleigh wave dispersion curves for five events.

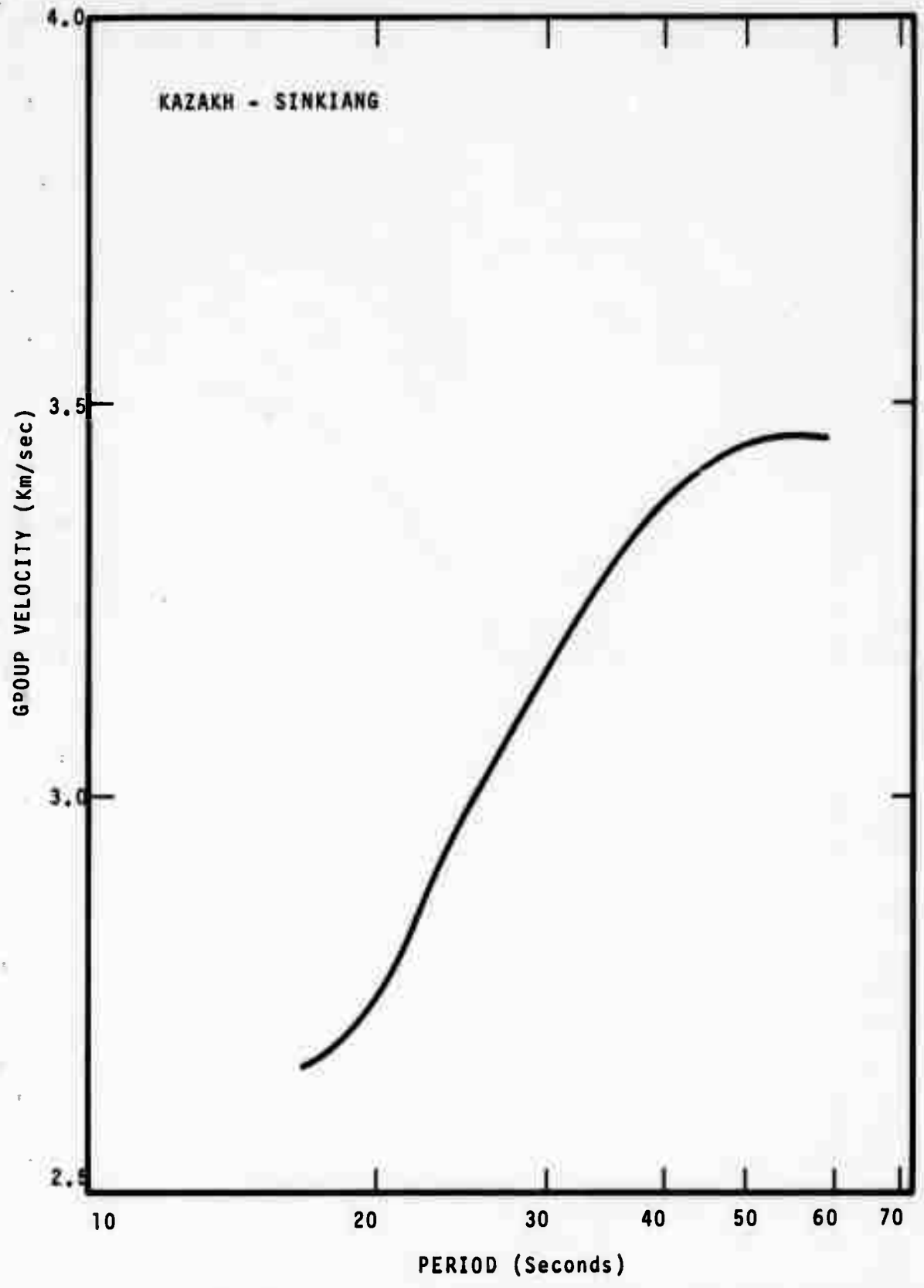

Figure 102. Rayleigh wave dispersion curves for five events.

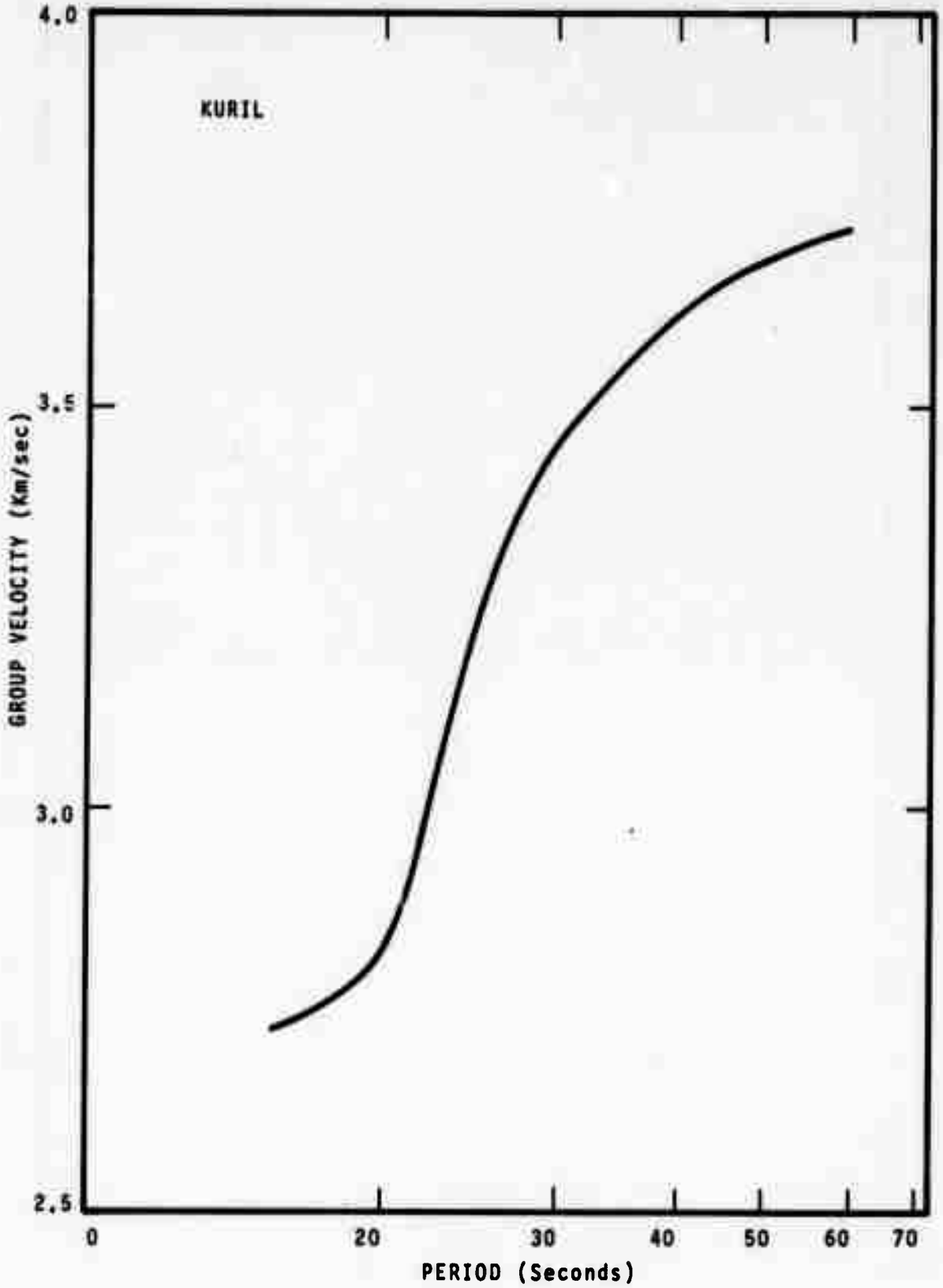

Figure 103. Rayleigh wave dispersion curves for five events.

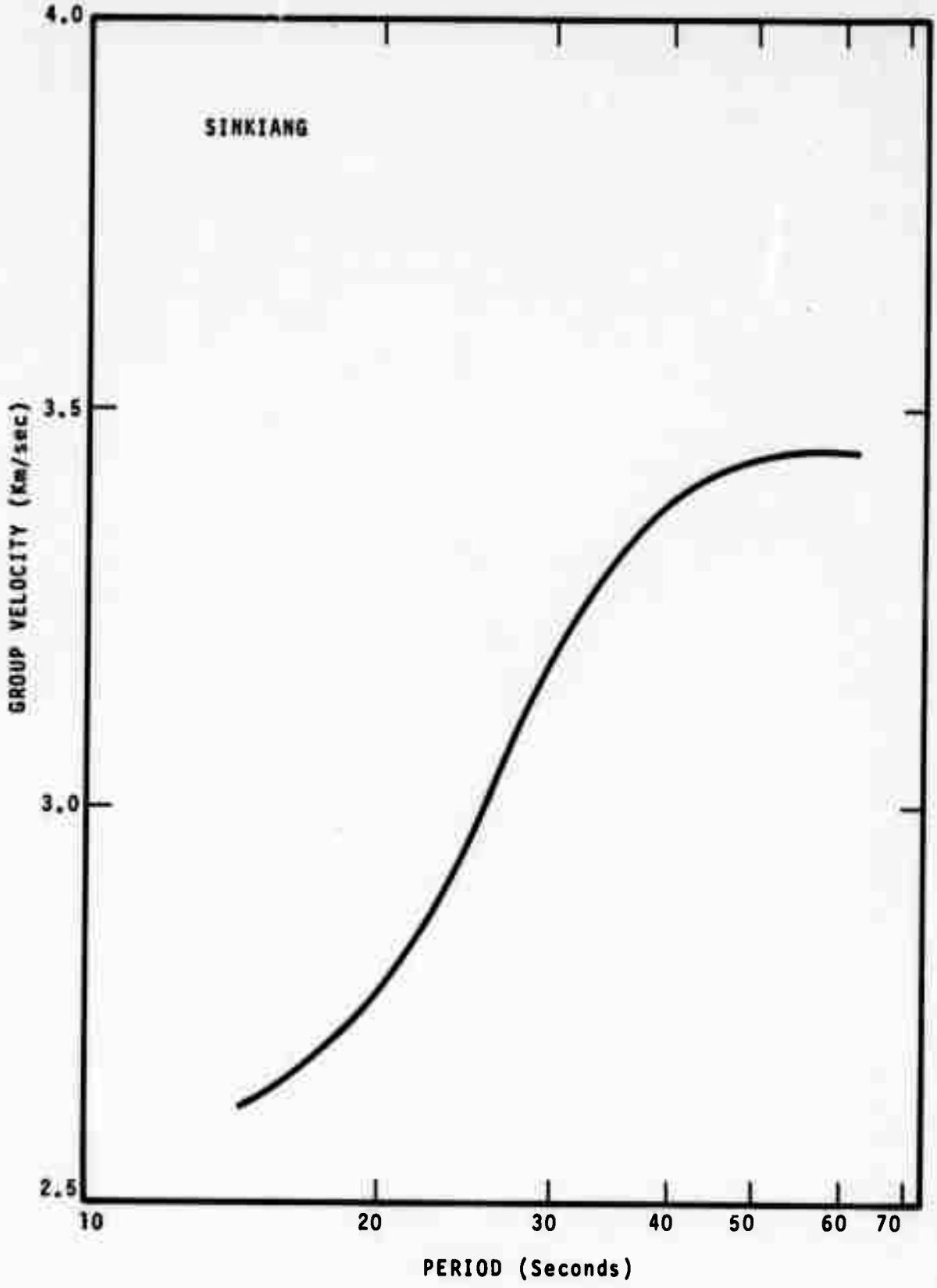

Figure 104. Rayleigh wave dispersion curves for five events.

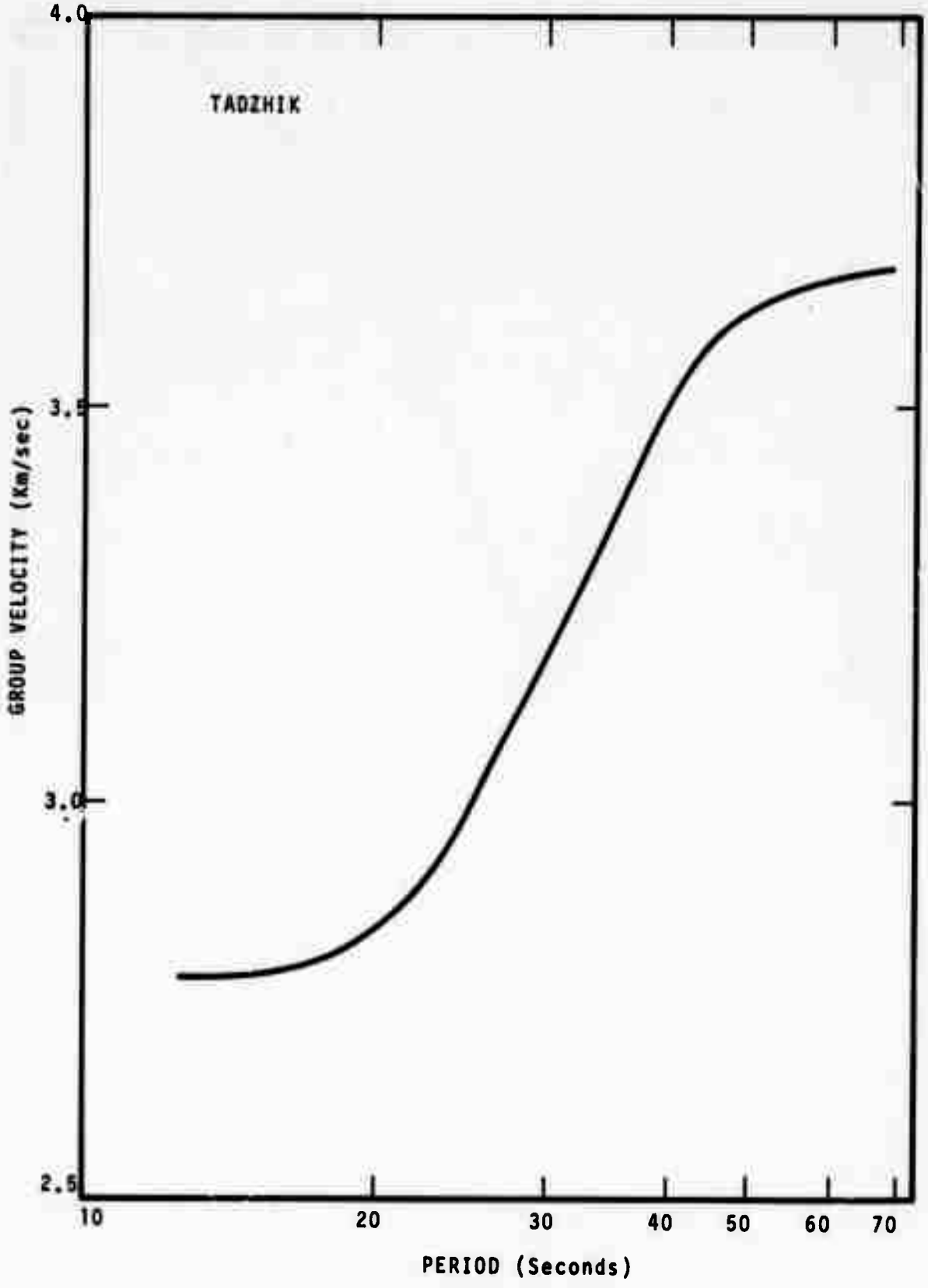

Figure 105. Rayleigh wave dispersion curves for five events.

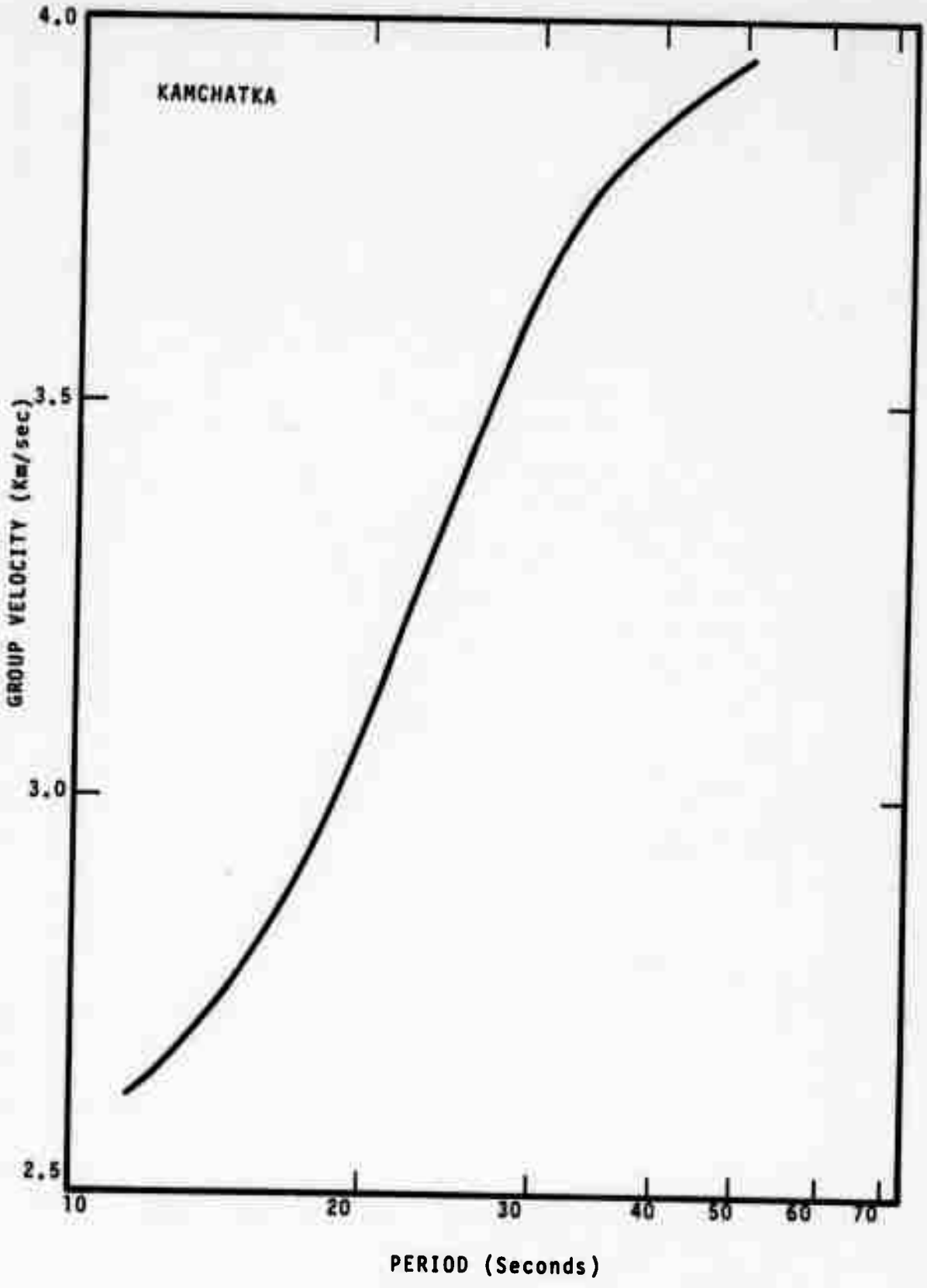

Figure 106. Love wave dispersion curves for five events.

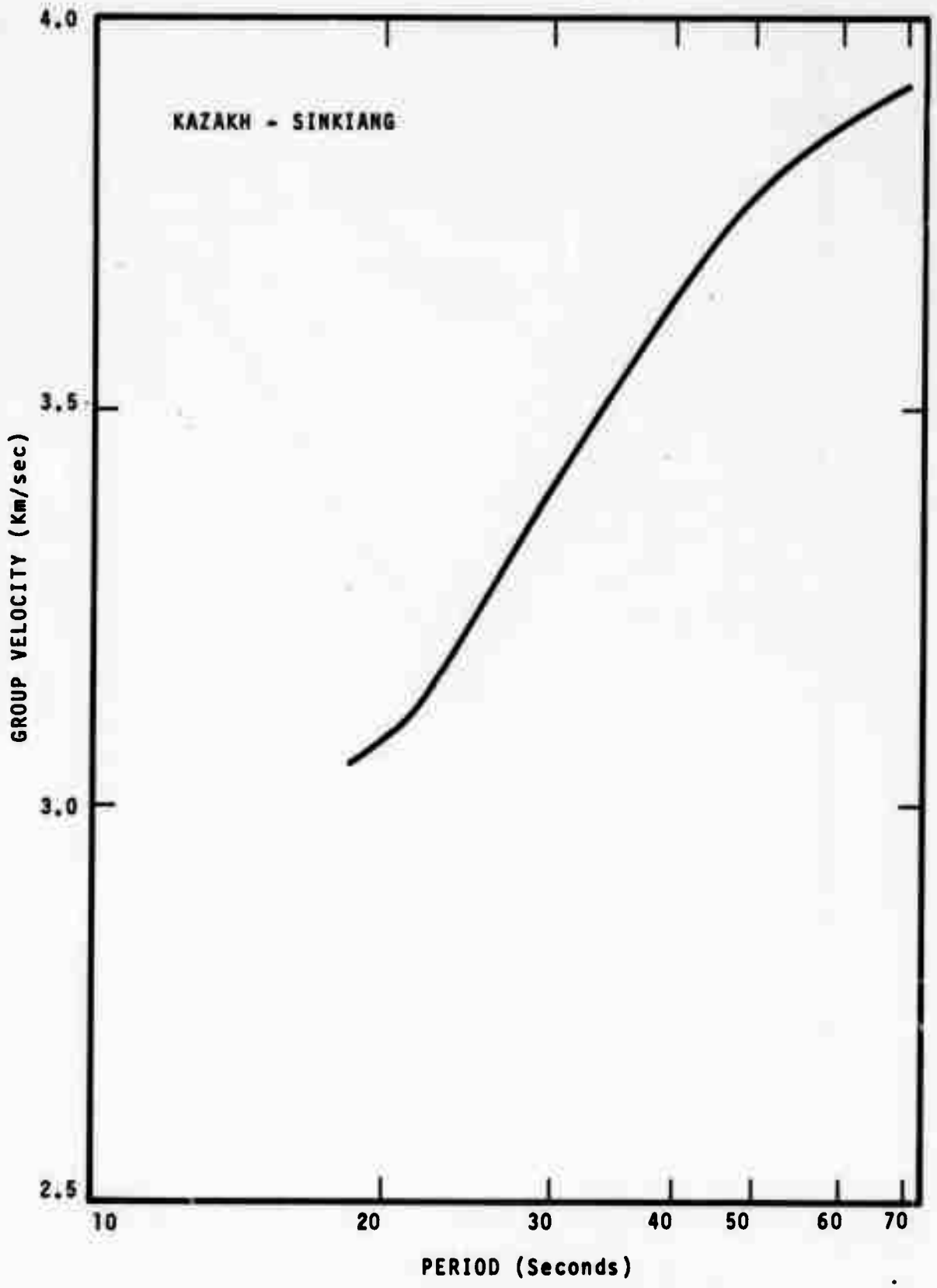

Figure 107. Love wave dispersion curves for five events.

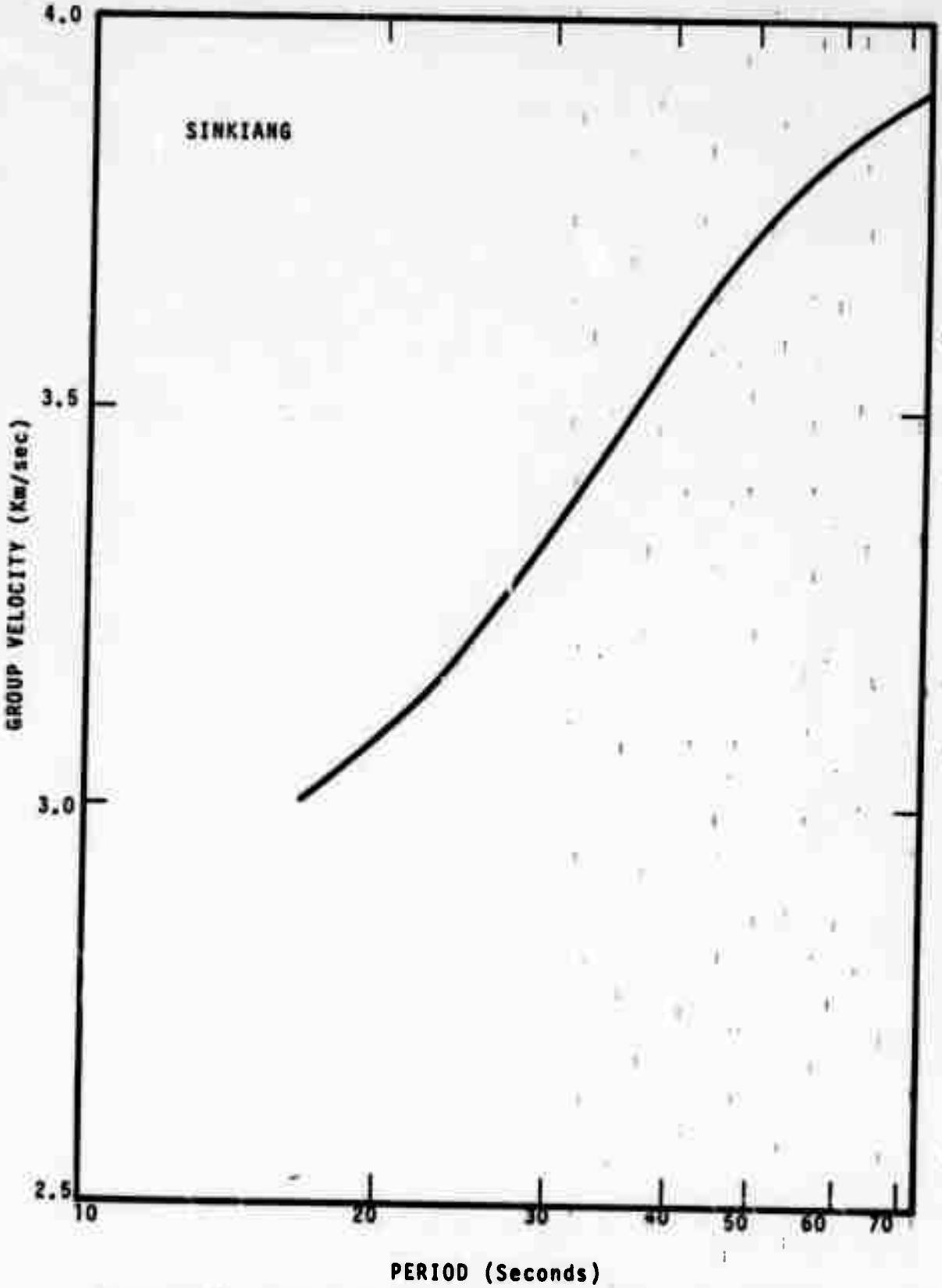

Figure 108. Love wave dispersion curves for five events.

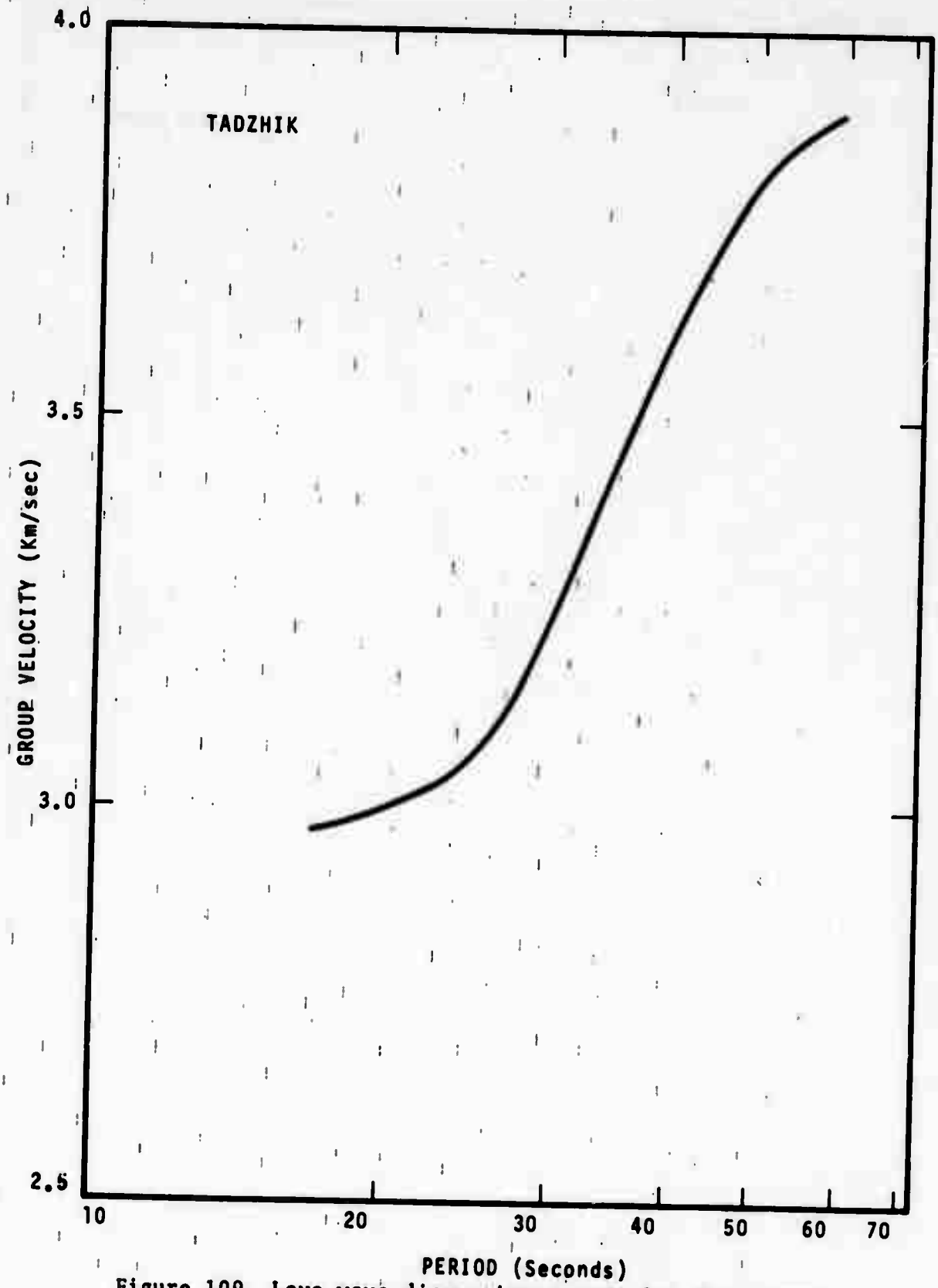

Figure 109. Love wave dispersion curves for five events.

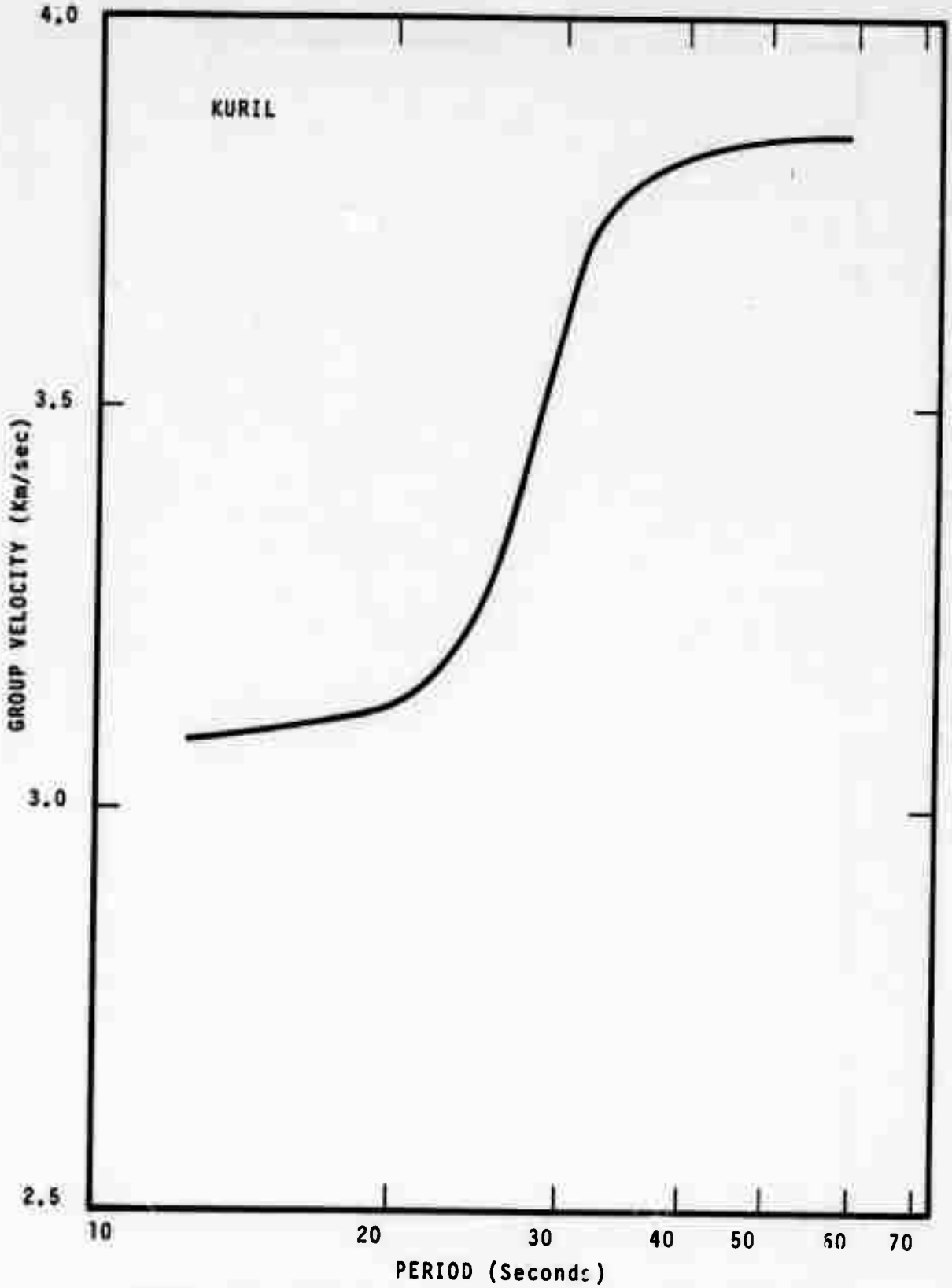

Figure 110. Love wave dispersion curves for five events.

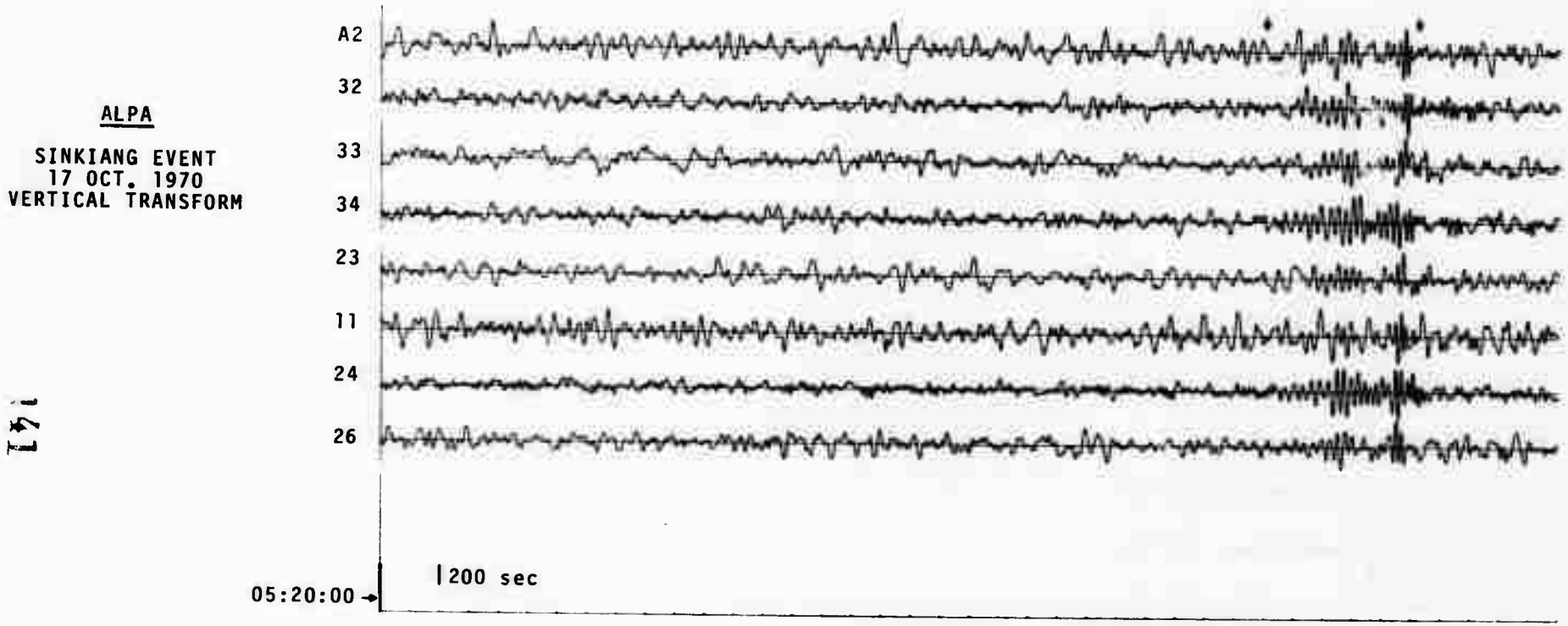

Figure 111. Vertical transform of three Sinkiang events used in matched filtering.

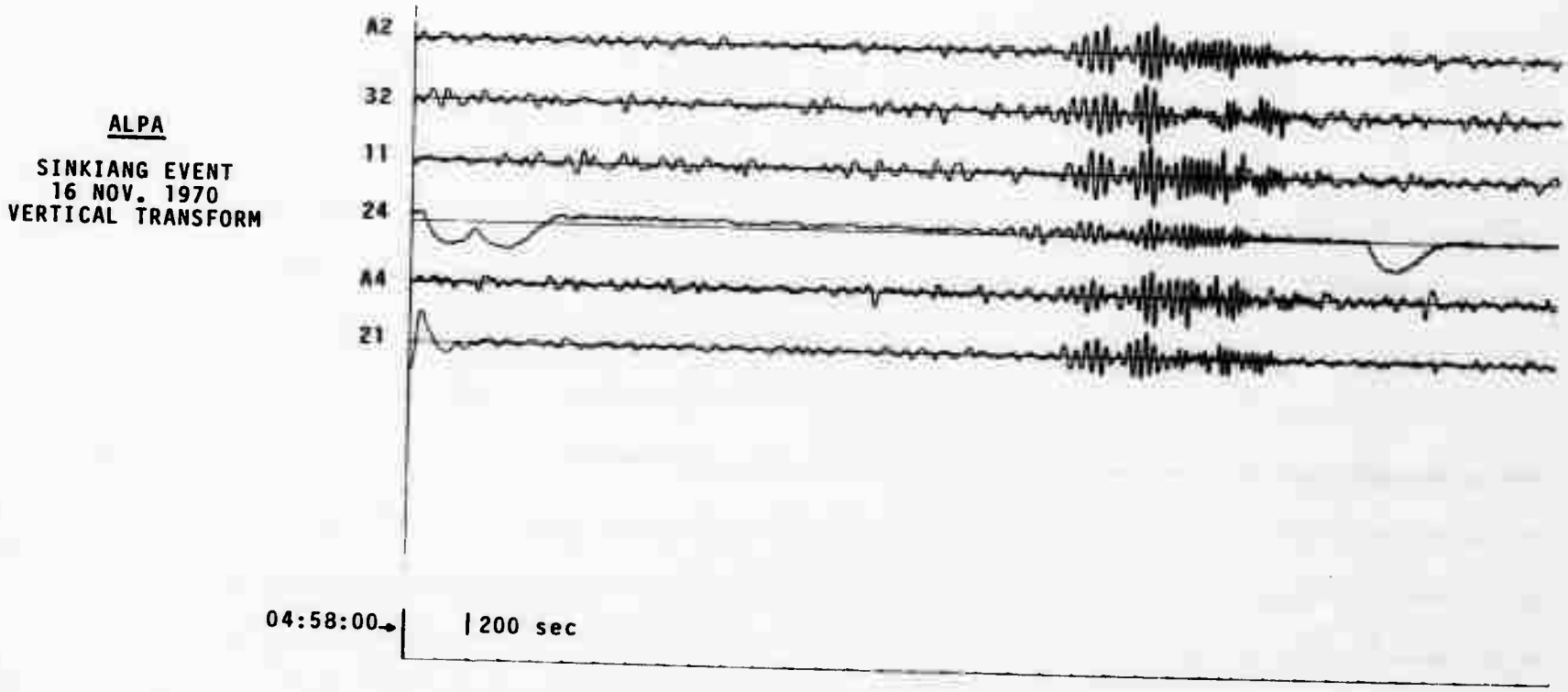

Figure 112. Vertical transform of three Sinkiang events used in matched filtering.

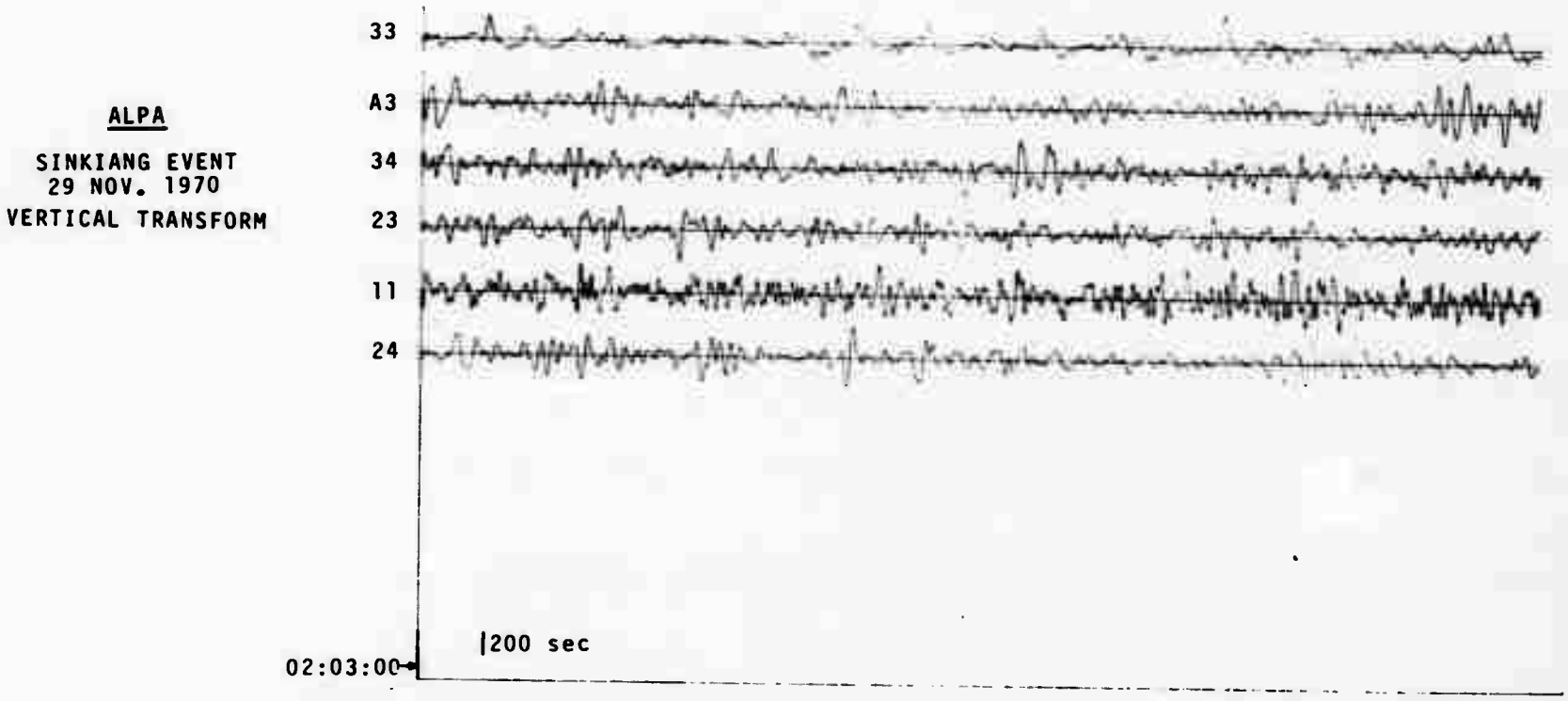

Figure 113. Vertical transform of three Sinkiang events used in matched filtering.

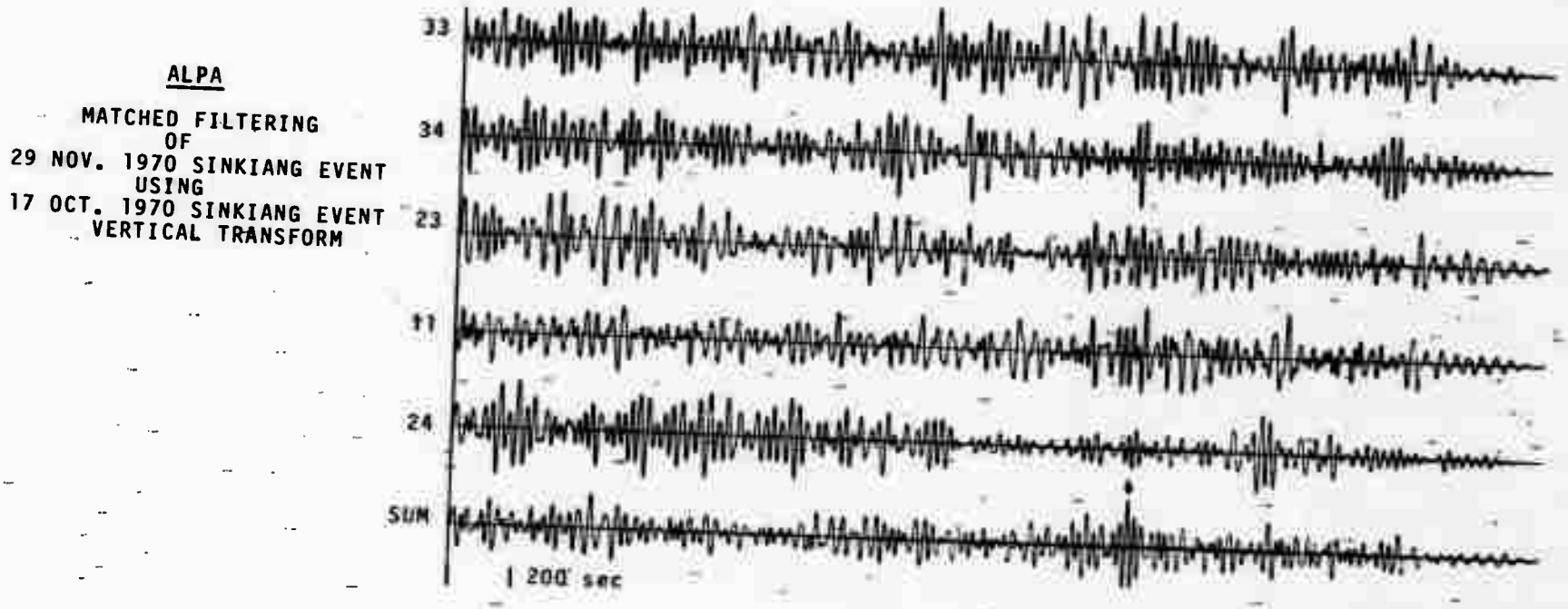

Figure 114. Matched filter results of three Sinkiang events.

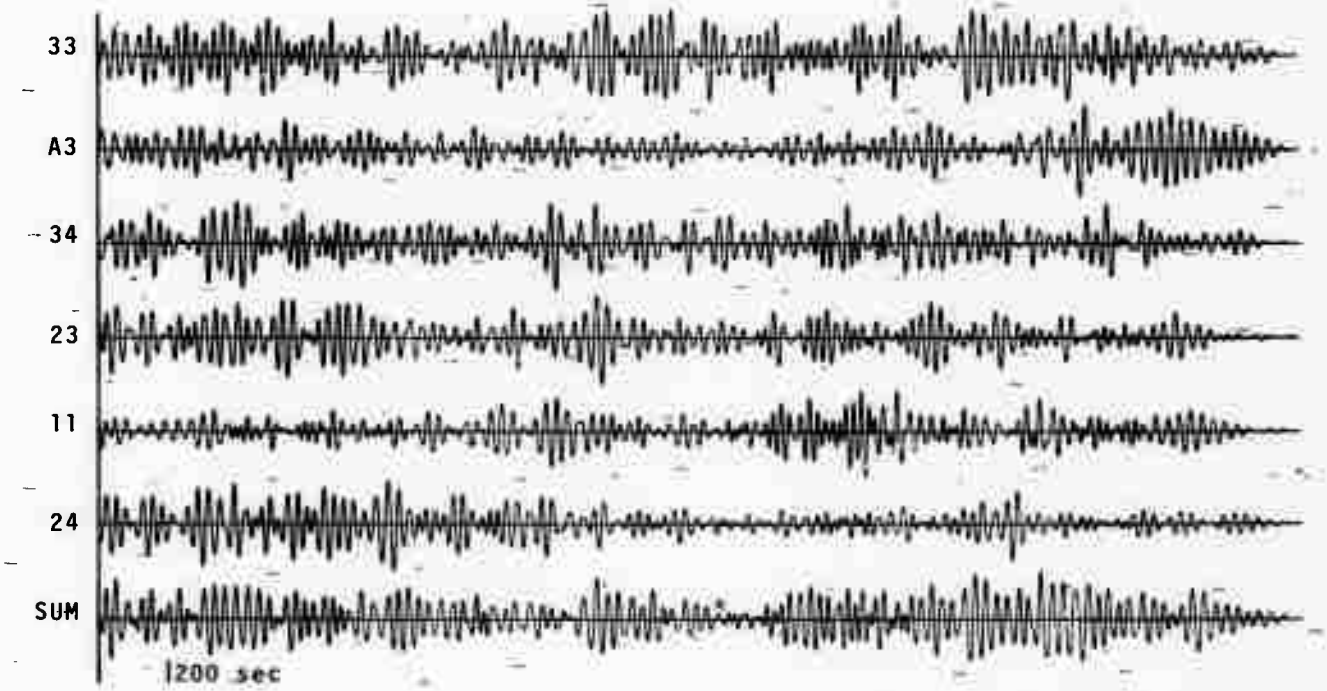

Figure 115. Matched filter results of three Sinkiang events.

ALPA

MATCHED FILTERING
OF
17 OCT. 1970 SINKIANG EVENT
USING
16 NOV. 1970 SINKIANG EVENT
VERTICAL TRANSFORM

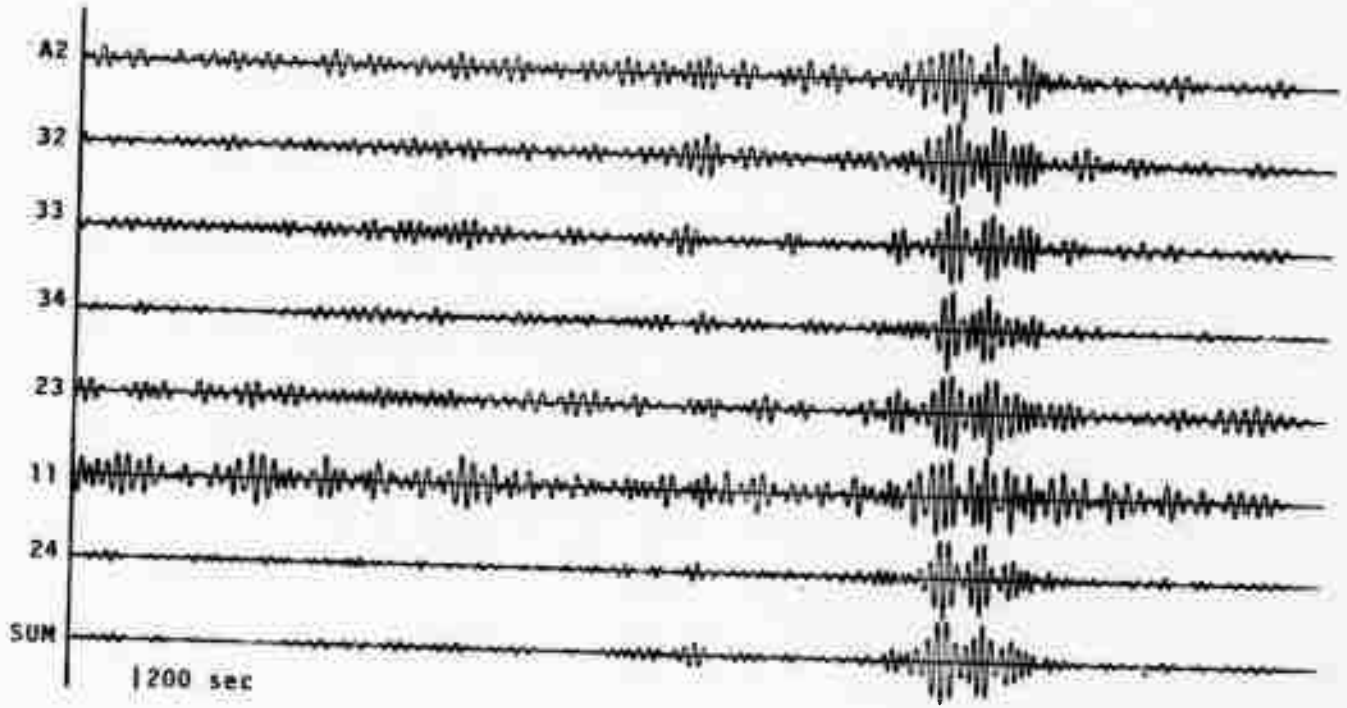

Figure 116. Matched filter results of three Sinkiang events.

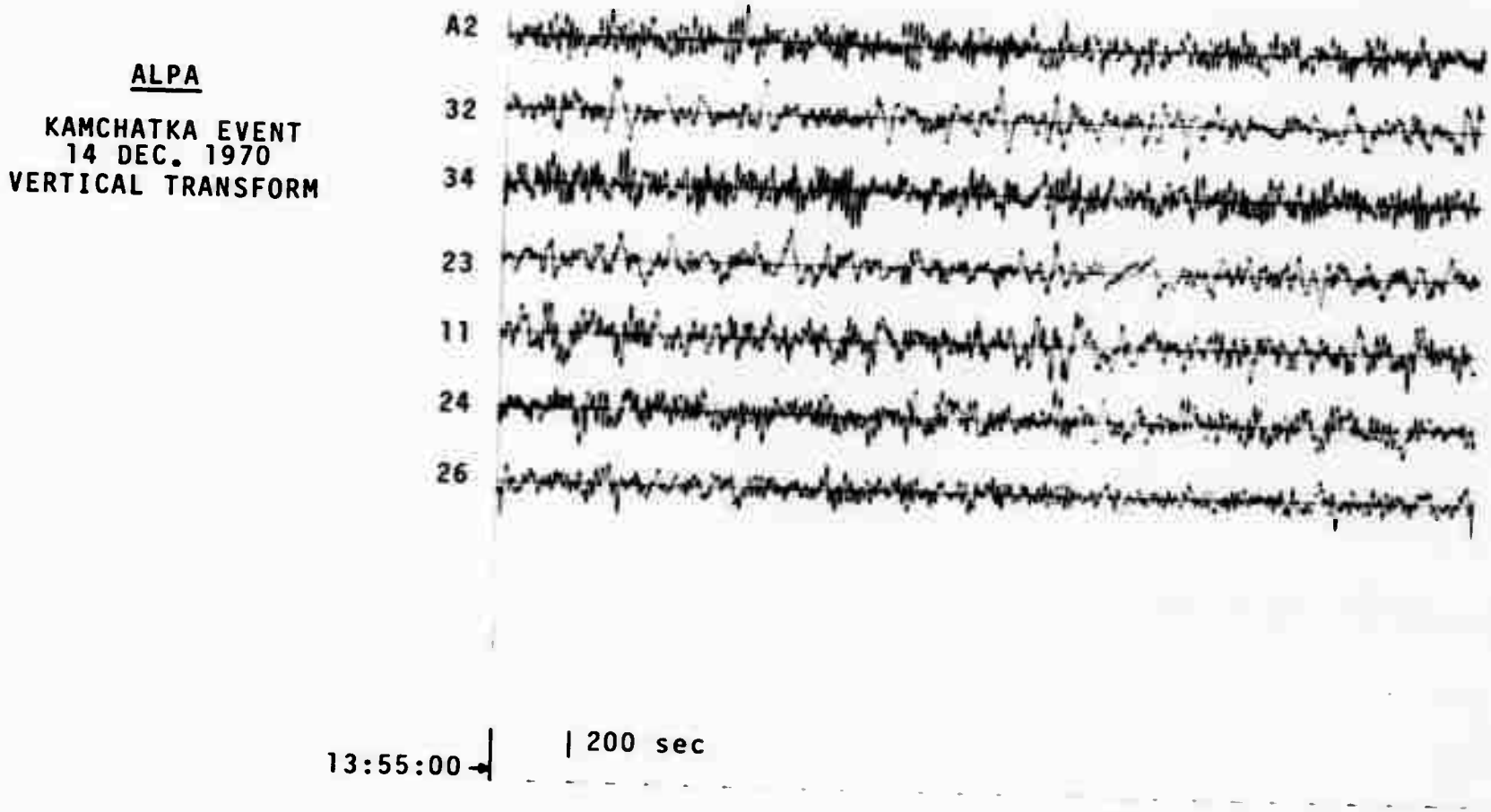

Figure 117. Vertical transform of Kamchatka event of 14 December 1970.

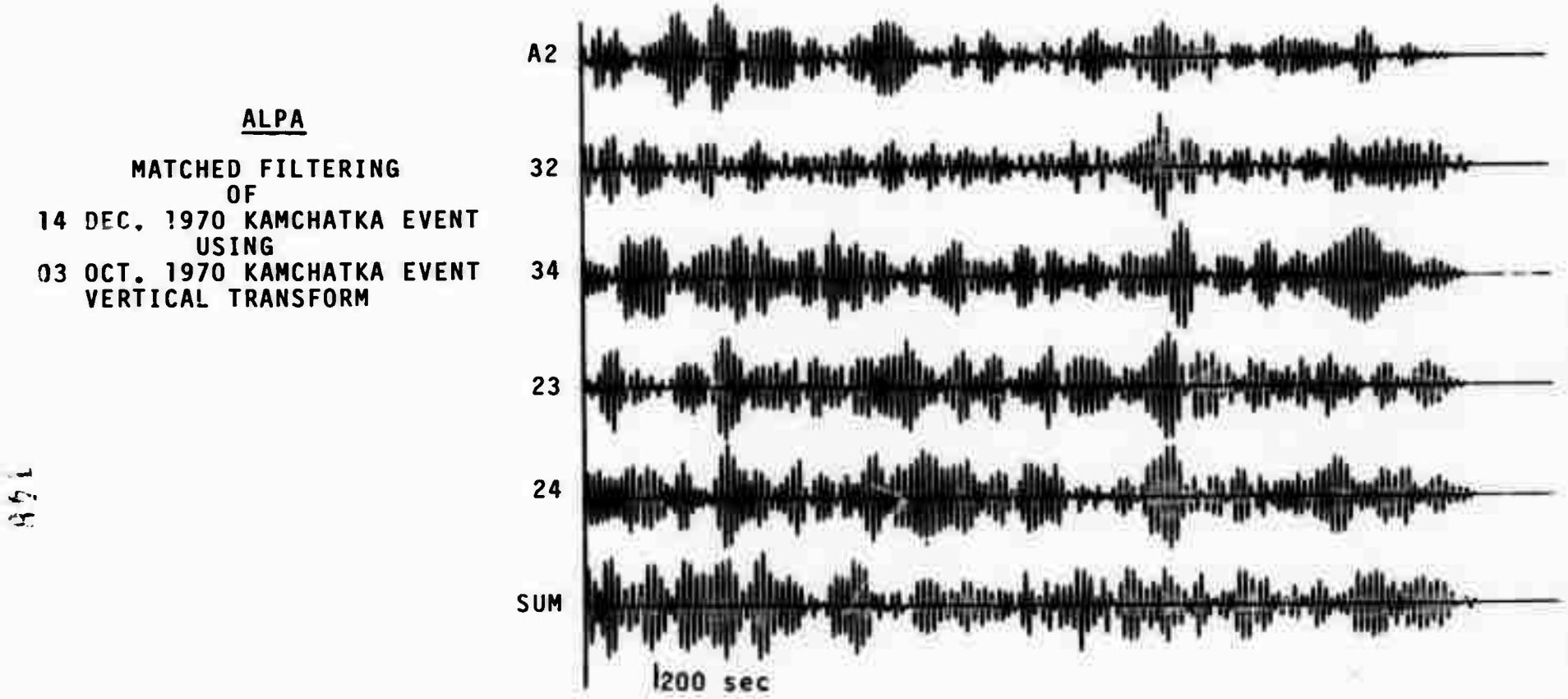

Figure 118. Matched filter results of a Kamchatka event.

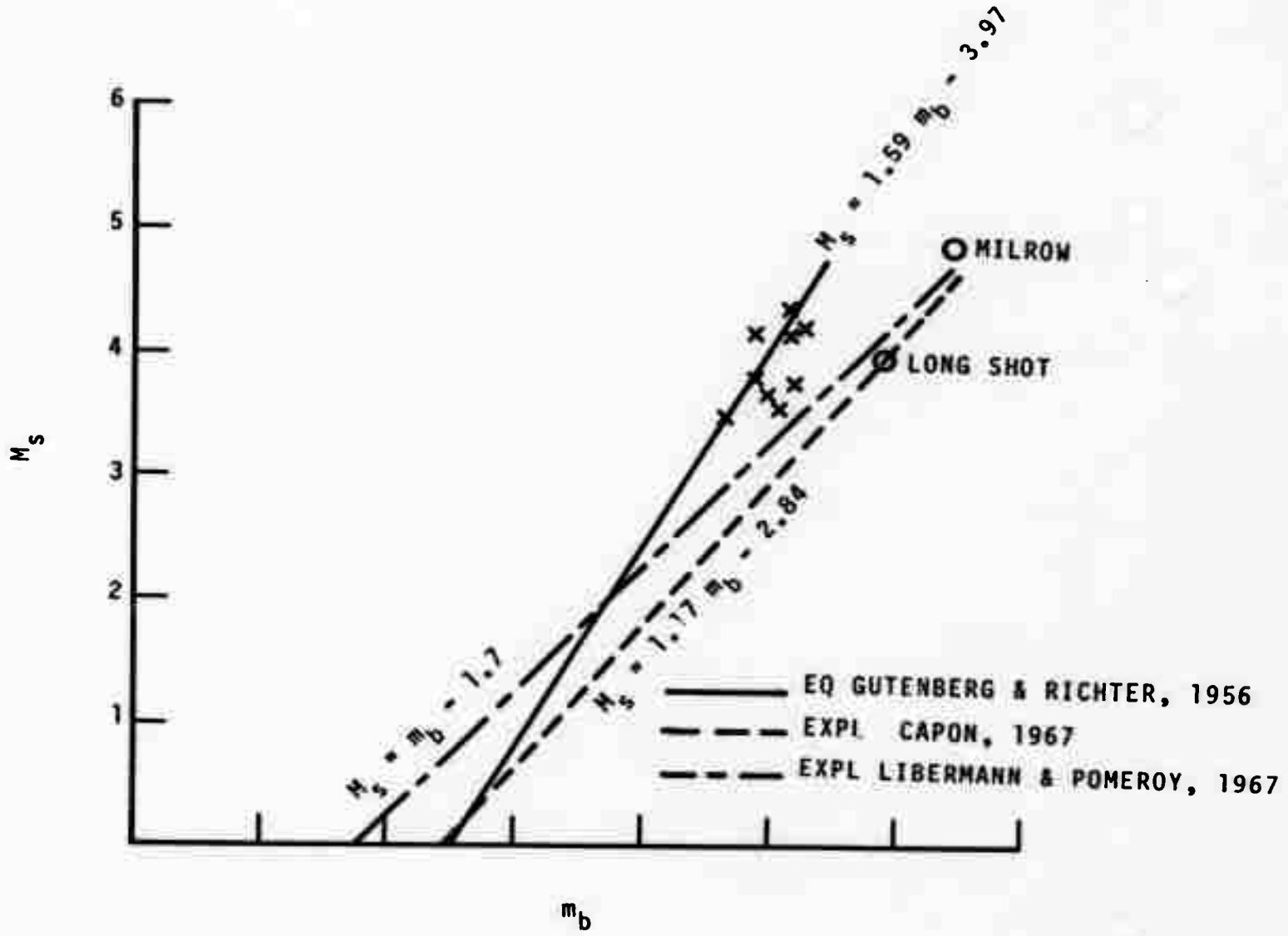

Figure 119. M_s - m_b.